PhD Thesis

2017

# Screening Clinically Relevant Biomarkers in Cancer

**Md. Hakimul Haque**
School of Medicine
Griffith University

**Supervisors:** Prof. Alfred Lam
Dr. Vinod Gopalan
Dr. Muhammad J. A. Shiddiky
Dr. Robert Smith

Submitted in fulfilment of the requirements for the degree of Doctor of Philosophy

March 2017

# Abstract

Oesophageal carcinoma is one of the most aggressive malignancies and the sixth leading cause of cancer-associated mortality worldwide. Being the most prevalent histological subtype, oesophageal squamous cell carcinoma (ESCC) accounts for approximately 90% of oesophageal cancer cases. Both genetic and epigenetic alterations contribute to the pathogenesis of ESCC along with considerable diversity in clinical behaviour and prognosis. In-depth biochemical research on rapid profiling and quantification of potential biomarkers are crucial in the clinical management of patients with cancer for developing effective diagnostic tools along with the accurate prediction of prognosis and therapy response in cancer. Currently, there are many conventional and nanotechnological approaches for screening clinically relevant various genetic and epigenetic biomarkers such as point mutation, DNA methylation, global methylation for the early diagnosis and management of ESCC, resulting in a 10% five-year survival rate for patients. Despite excellent analytical performances of the existing detection methodologies, electrochemical approaches offer a promising alternative for simple, sensitive, specific, rapid, and cost-effective analysis of genetic and epigenetic biomarkers in cancer samples. Therefore, innovative technology using electrochemical approach would be an effective way for the detection of biomarkers in patients with cancer.

*FAM134B* (*Family With Sequence Similarity 134, Member B*), also known as *JK1* is a novel protein-coding gene sited at chromosome 5p15.1 that plays a key role in cancer cell biology and autonomic neurological disorders *via* regulating its expression pattern and cellular autophagy. In this thesis, for the first time, we identified several biomarkers including FAM134B copy number, mRNA and protein expressions along with relationship among different clinical and pathological parameters in ESCC. Initially, 102 matched fresh tissue samples of ESCC, and non-cancer adjacent tissues were recruited after histopathological analysis. The DNA copy number variation and mRNA expression of *FAM134B* in ESCC were studied and analysed by quantitative real-time polymerase chain reaction (qRT-PCR) and ΔΔCt and Ct ratio methods respectively. *FAM134B* DNA and mRNA were detectable in all the samples used in this study. In ESCC, 37% showed increased *FAM134B* copies whereas 35% showed loss of *FAM134B* copies relative to matched non-tumour tissues. The DNA copy number of *FAM134B* in the cancer population was found to have no relationship with the

clinicopathological parameters of the ESCCs. This results implied that this gene might act as both oncogene and tumour suppressor in the progression of ESCC. For profiling of mRNA expression in ESCC tissues, 49% showed overexpression of *FAM134B* while 47% revealed downregulation of *FAM134B* when compared to matched non-neoplastic tissues. For the first time, this study has detected FAM134B protein expression in ESCC cells. Protein quantification was analysed *via* Western blot. Immunofluorescence was performed to examine localisation and expression changes of FAM134B proteins in different ESCC cell lines (HKESC1, HKESC4, KYSE70 and KYSE510) and non-neoplastic squamous epithelial cell line (HACAT). FAM134B protein was localised and expressed in both cytoplasm and nucleus of ESCC cells. The protein expression was noted to be expressed differentially among ESCC cell lines. The altered expression of FAM134B at protein and mRNA levels suggest its fundamental role in the pathogenesis of ESCC.

In addition to profiling of copy number and expression of *FAM134B*, this thesis also reported the novel mutation sites of *FAM134B* in ESCC tissue samples *via* high-resolution melt curve (HRM) and Sanger sequencing analysis. Overall, 37% *FAM134B* mutations were documented in exons 4, 5, 7, 9 as well as introns 2, 4-8 of *FAM134B.* Also, *FAM134B* mutations were detected in all the metastatic ESCC cases and in 14% of the primary ESCC. The altered expression patterns and copy number variations of *FAM134B* in ESCCs might be modulated by these mutation changes. In this study, a significant association of *FAM134B* mutations with metastasis was found in ESCC tissues.

After genomic profiling of *FAM134B,* this thesis reports a new electrochemical method for quantification of the level of point mutation or SNPs in *FAM134B* gene using a single-use and disposable screen-printed electrode. The principle of the method relies on the base dependent affinity interactions of DNA with the gold surface. Since two DNA sequences with different DNA base compositions will have different adsorption affinity towards an unmodified gold electrode, accurate measurement of adsorbed DNA on the electrode surface will give the measure of a point mutation or SNPs present in the DNA sequences. A number of mutation sites in a DNA sequence are quantified by monitoring the Faradaic current generated by the $[Fe(CN)_6]^{3-/4-}$ system present in the electrolyte solution. Using this method, we were able to detect mutations in 50 ng of target PCR-amplified product within 1 hour with high reproducibility (% RSD= <2) and specificity.

Then, we reported a novel method for the detection of regional DNA methylation using base-dependent affinity interaction (*i.e.,* adsorption) of DNA with graphene. Due to the strongest adsorption affinity of guanine bases towards graphene, bisulfite-treated guanine-enriched methylated DNA leads to a larger amount of the adsorbed DNA on the graphene-modified electrodes in comparison to the adenine-enriched unmethylated DNA. The level of the methylation is quantified by monitoring the differential pulse voltammetric current as a function of the adsorbed DNA. Graphene-DNA based assay is sensitive to distinguish methylated and unmethylated DNA sequences at single CpG resolution by differentiating changes in DNA methylation as low as 5%. We anticipated that our assay might be able to detect global hypomethylation.

For the detection of gene-specific DNA methylation, another simple electrochemical method was developed and validated with methylation specific high resolution melting (MS-HRM) curve analysis and Sanger Sequencing. The underlying principle of the method relies on the affinity interaction between DNA bases and the unmodified gold electrode. Since the affinity trend of DNA bases towards the gold surface follows as adenine; (A) > cytosine (C) > guanine (G)> thymine (T), a relatively larger amount of bisulfite-treated adenine-enriched unmethylated DNA adsorbs on the screen-printed gold electrodes (SPE-Au) in comparison to the guanine-enriched methylated sample. The methylation levels were quantified by measuring the saturated amount of charge-compensating $[Ru(NH_3)_6]^{3+}$ molecules in the surface-attached DNAs by chronocoulometry as redox charge of the $[Ru(NH_3)_6]^{3+}$ molecules quantitatively reflects the amount of the adsorbed DNA confined at the electrode surface. Our electrochemical assay can successfully distinguish methylated and unmethylated DNA sequences at single CpG resolution. In addition, our assay showed fairly good reproducibility (% RSD= <3.5%) with greater sensitivity and specificity in detecting different levels of methylations in cell line and tissue samples from patients with ESCC.

Finally, we reported a combined biosensing strategies which integrated simple colorimetric (naked-eye) and electrochemical methods for relatively rapid, sensitive and specific quantification of global methylation levels. Our approach utilises a three-step strategy, (*i*) initial adsorption of the extracted, purified and denatured bisulfite-treated DNA on a screen-printed gold electrode (SPE-Au), *(ii)* immuno-recognition of methylated DNA using HRP-conjugated anti-methylcytosine antibody and (*iii*) subsequent colorimetric and electrochemical detection of global DNA methylation were achieved by the enzymatic oxidation of 3,3′,5,5′-Tetramethylbenzidin (TMB)/$H_2O_2$ which generated a blue-colored complex in the presence of HRP-conjugated

methylated DNA (colorimetric). As $TMB_{(ox)}$ is electroactive, it also produced detectable amperometric current at 150mV vs Ag pseudo-reference electrode (electrochemical detection). The developed methods showed good reproducibility (% RSD= <5%) with fairly good sensitivity (as low as 5% differences in methylation levels) and specificity while analysing various levels of global DNA methylation in synthetic samples and cell lines (n=3). The method has also been tested for analysing methylation level in fresh tissues samples collected from patients (n=8) with ESCC.

In summary, this thesis has provided the genomic profiling for *FAM134B* as a potential novel biomarker for ESCCs followed by the successful development of several electrochemical technologies based on gold-DNA and graphene-DNA affinity interactions for the detection of genetic (point mutation or SNPs) and epigenetic (global and regional DNA methylation) biomarkers. The applicability of the methods developed here was tested in cancer cell lines and clinical samples derived from patients with ESCC. We believe that these proof-of-concept methods will find relevance as alternative diagnostic tools in both clinical diagnostics and research settings allowing more personalized monitoring and better clinical management of patients with ESCC.

# Statement of Originality

The material presented in this report has not previously been submitted for a degree or diploma in any university, and to the best of my knowledge, the thesis contains no materials previously published or written by another person, except where the due acknowledgement is made in the thesis itself.

**Md Hakimul Haque**

# Acknowledgements

I would like to extend my sincere gratitude to my PhD advisors. To Prof. Alfred Lam, Dr. Vinod Gopalan and Dr. Muhammad J. A. Shiddiky, I would like to thank them for their advice, leadership, support and, supervision. Also, I would like to thank Dr Robert Smith for his supervision, advice and support. Without their guidance and assistance, it would not been possible for me to complete the thesis.

I would like to thank the Griffith University for accepting my PhD candidature and their support and assistance throughout my candidature for the last three and half years. I would also like to thank our collaborators Prof. Nam-Trung Nguyen at Queensland Micro- and Nanotechnology centre for his continuous advice and support.

My sincere thanks also go to many fellow staff members and students in Dr. Shiddiky's and Prof. Lam's lab, in particular to my fellow PhD students, Sharda, Kseniia, Suja, Lena, Farhad, Wahab, Masud, Ripon, Munaz for their friendship, technical assistance and suggestions. I would also like to specifically thank Nazmul Islam and Dr. Nassim Saremi for their immense support and advice.

I would like to acknowledge the Institute for Glycomics and staffs for providing me with the training and support in learning protein expression and purification analysis. In particular, I would like to thank Prof. Victoria Kolorik for her supervision and training on basic molecular biology techniques. I would like to thank Dr. Rebecca King for her supervision and training. Also, I also would like to thank Prof. Helen Blanchard for her support during my candidature.

Finally, I must thank my amazingly supportive and loving family. My parents, Rahman and Banu, are my biggest blessings and have unconditional love and support. My brother, Babu and My sister Mousumi have been also incredibly supportive and caring during my PhD. Last but not the least, my infinite gratitude and love for the most invaluable assests of life, my wife Shamima akter and my son Shuaib, whose sacrifice, incomparable love and encouragement have made me come to this far.

**Key words**

*FAM134B*, point mutation, DNA methylation, regional methylation, global methylation, oesophageal cancer, colorimetry, electrochemical detection, gold-DNA base interaction, graphene-DNA base interaction, mC antibody enrichment, disposable screen-printed electrode

**Australian and New Zealand Standard Research Classification (ANZSRC)**

ANZSRC code: 100703, Nanobiotechnology, 50%

ANZSRC code: 100402, Medical Biotechnology Diagnostics (Incl. Biosensors), 50%

**Fields of Research (FoR) Classification**

For code: 1007, Nanotechnology, 50%

For code: 1004, Medical Biotechnology, 50%

# Table of Contents

# List of Abbreviations

| | |
|---|---|
| AP | Alkaline phosphatase |
| 5mC | Methylcytosine |
| AuNPs | Gold nanoparticles |
| AU-SPE | Screen printed gold electrode surface |
| BCH | Basal cell hyperplasia |
| BER | Base excision repair |
| CC | Chronocoulometry |
| CIS | carcinoma *in situ* |
| CTGF | Connective tissue growth factor |
| CV | Cycleic voltammetry |
| DEPC | Diethylpyrocarbonate |
| DMSO | Dimethyl sulfoxide |
| DPV | Differential pulse voltammetry |
| DYS | Dysplasia |
| EADC | Oesophageal adenocarcinoma |
| ESCC | Oesophageal squamous cell carcinoma |
| FAM134B | Family With Sequence Similarity 134, Member B |
| FGF | Fibroblast growth factor |
| FND | Ferrocenylnaphthalene diimide |
| GAPDH | Glyceraldehyde 3-phosphate dehydrogenase |
| g-SPCE | graphene-modified screen-printed carbon electrode |
| H&E | Haematoxylin and eosin |
| HBD | Delta haemoglobin |
| HGF | Hepatocyte growth factor |
| HPV | Human papilloma virus |
| HRM | High resolution melting |
| HSAN IIB | Hereditary sensory and autonomic neuropathy type IIB |
| ICC | Immunocytochemistry |
| IHC | Immunohistochemistry |
| ISS-PCR | Inter-simple sequence repeat-polymerase chain reaction |
| LOH | Loss of heterozygosity |

| | |
|---|---|
| MB | Methylene blue |
| Mdm2 | Murine Double Minute 2 |
| MS-HRM | Methylation specific-high resolution melting |
| NER | Nucleotide excision repair |
| PBS | Phosphate buffered saline |
| PNA | Peptide nucleic acid |
| QD | Quantum dot |
| qRT-PCR | Quantative real-time polymerase chain reaction |
| RuHex | $[Ru(NH_3)_6]^{3+}$ complex |
| SNP | Single nucleotide polymorphism |
| SPSS | Statistical package for social sciences |
| SSC | Saline sodium citrate |
| TGF-α | Transforming growth factor-α |
| TNM | Tumour-Node-Metastasis |
| TSG | Tumour suppressor genes |
| vdW | Van der Wall |
| VEGF | Vascular endothelial growth factor |
| WGA | Whole genome amplification |

# List of Figures

# List of Tables

# Publications arising from this thesis

1. **Haque MH**, Gopalan V, Chan KW, Shiddiky MJA, Smith RA, Lam AK. Identification of Novel FAM134B (JK1) Mutations in Oesophageal Squamous Cell Carcinoma. Sci Rep. 2016 Jul 4;6:29173. **[Impact Factor : 5.228]**

2. **Haque MH**, Gopalan V, Yadav S, Islam MN, Eftekhari E, Li Q, Carrascosa LG, Nguyen NT, Lam AK, Shiddiky MJA. Detection of regional DNA methylation using DNA-graphene affinity interactions. Biosens Bioelectron. 2016 Sep 5;87:615-621. **[Impact Factor: 7.47]**

3. **Haque MH**, Islam MN, Islam F, Gopalan V, A. Lam, Nguyen NT, Lam AK, Shiddiky MJA, Electrochemical Detection of FAM134B Mutations in Oesophageal Cancer Based on DNA-Gold Affinity Interactions. Electroanalysis 2017 February 9, 29(5):1359-1367. **[Impact Factor: 2.471]**

4. **Haque MH**, Gopalan V, Islam MN, Masud MK, Bhattacharjee R, Hossain MSA, A. Lam, Nguyen NT, Lam AK, Shiddiky MJA, Quantification of gene-specific DNA methylation in cancer via electrochemistry. Anal. Chim. Acta 2017 Jul 11 976:84-93. **[Impact Factor: 4.712]**

5. **Haque MH**, Bhattacharjee R, Islam MN, Gopalan V, Nguyen NT, A. Lam, Lam AK, Shiddiky MJA, Colorimetric and electrochemical quantification of global DNA methylation using methylcytosine specific antibody. Analyst. 2017 May 30;142(11):1900-1908. **[Impact Factor: 4.107]**

# Publications tangential to this thesis

1. Islam MN, Yadav S, **Haque MH**, Hossain MS, Gopalan V, Lam AK, Nguyen NT, Shiddiky MJA optical Biosensing Strategies for DNA Methylation Detection. Biosens Bioelectron. 2016 doi: 10.1016/j.bios.2016.10.034. **[Impact Factor: 7.47]**

2. Islam F, **Haque MH**, Yadav S, Islam MN, Gopalan V, Nguyen NT, Lam AK, Shiddiky MJA. A simple and inexpensive electrochemical method for sensitive and rapid detection of FAM134B protein in colon cancer samples. Sci Rep. 2017 Dec;7(1):133. **[Impact Factor: 5.228]**

3. Islam F, Gopalan V, Wahab R, Lee KT, **Haque MH**, Mamoori A, Lu C, smith RA, Lam AK. Novel FAM134B mutations and their clinicopathological significances in colorectal cancer. Hum Genet. 2017 Mar;136(3):321-337. **[Impact Factor: 5.138]**

4. Islam MN, Gopalan V, **Haque MH**, Masud MK, Hossain MS, Yamauchi Y, Nguyen NT, Lam AK, Shiddiky MJA. A PCR-free electrochemical Method for mRNA Detection in Cancer Tissue Samples. [Submitted to Advanced Healthcare Materials.] [**Impact Factor: 5.76]**

# Conference Proceedings

1. **Haque MH**, Gopalan V, Wahab R, Islam F, Smith RA, Lam AK. Natural copy number variations of FAM134B (JK1) in oesophageal squamous cell carcinoma. *Gold Coast Health and Medical Research Conference. Gold Coast, Australia*, 3-4 December 2015.

2. **Haque MH**, Islam F, Shiddiky MJA, Gopalan V, Lam AK. FAM134B (JK1) mRNA and protein expressions in oesophageal squamous cell carcinoma. *Gold Coast Health and Medical Research Conference. Gold Coast, Australia*, 1-2 December 2016.

3. **Haque MH**, Gopalan V, Yadav S, Islam MN, Nguyen NT, Lam AK, Shiddiky MJA. Detection of Regional DNA Methylation Using DNA-Graphene Affinity Interactions. *7th International Nanomedicine Conference. Crowne Plaza Coogee Beach, Sydney, Australia*, 27-29 June 2016.

4. **Haque MH**, Islam MN, Islam F, Gopalan V, Nguyen NT, Lam AK, Shiddiky MJA. Electrochemical Detection of FAM134B Mutations in Oesophageal Cancer Based on DNA-Gold Affinity Interactions. *International Conference on BioSensors, BioElectronics, BioMedical Devices, BioMEMS/NEMS & Applications (Bio4Apps 2016). Gold Coast, QLD, Australia*, 14-16 December 2016.

5. **Haque MH**, Gopalan V, Islam MN, Masud MK, Hossain MSA, Nguyen NT, Lam AK, Shiddiky MJA. Quantification of gene specific DNA methylation in oesophageal cancer via electrochemistry. *International Conference on BioSensors, BioElectronics, BioMedical Devices, BioMEMS/NEMS & Applications (Bio4Apps 2016). Gold Coast, QLD, Australia*, 14-16 December 2016.

6. Islam MN, Gopalan V, Boriachek K, **Haque MH**, Nguyen NT, Lam AK, Shiddiky MJA. Detection of mRNA in Oesophageal Cancer Using mRNA-Gold Affinity Interactions. *International Conference on BioSensors, BioElectronics, BioMedical Devices, BioMEMS/NEMS & Applications (Bio4Apps 2016). Gold Coast, QLD, Australia*, 14-16 December 2016.

7. **Haque MH**, Gopalan V, Shiddiky MJA, Lam AK. FAM134B mutation in oesophageal squamous cell carcinoma: Its clinical significance and quantification by electrochemical methods. *AACR 108th Annual Meeting, Washington DC, USA*. 1-5 April 2017.

# Chapter 1

## General Introduction

## 1.1 Background

This research intends to investigate the mutational effect of a novel gene of unknown function, called *FAM134B* in human cancers. There is some evidence that mutations of *FAM134B* are a cause of human hereditary sensory and autonomic neuropathy type IIB (HSAN IIB) diseases. Generally, the human genome receives exogenous and endogenous attacks that could promote genetic mutations, regional DNA methylation, global methylation, chromosomal rearrangements and finally the development of cancer. Mutations and genetic polymorphisms in coding gene sequences might entail functional alteration of genes. This study is also designed to reveal out the novel gene mutation site in human cancers. Recent studies suggest that *FAM134B* is a growth-related gene which implements a significant role in cancer pathogenesis. Previously, our laboratory showed that it act as tumour suppressor gene in colon cancer whereas other study reveals its role as an oncogene in oesophageal squamous cell carcinoma (ESCC). It signified that down-regulation of the gene might happen as a result of mutation and promoter hypermethylation whereas upregulatory role might depend on the other interacting partners of the gene in cancer metabolism. Evidence suggests that the gene has functions in various normal human tissues. Genes may be copied in cancer, or they may be used in different pathways than in normal tissue. This research will explore any changes of gene behaviour in *FAM134B* and its potential interactions with other cancer-causing genes. Genetic material will be extracted from the cancers as well as the behaviour of the *FAM134B* gene will be detected. The alterations in *FAM134B* will be compared to normal tissue as well as very early cancers. In addition, the research also intends to determine whether this novel gene is a significant contributor to the progression of cancer and if it could be used as a target for therapy as well as early detection marker.

This research will explore the development of novel electrochemical technologies for the detection of clinically relevant biomarkers such as point mutation, gene-specific DNA methylation, and global DNA methylation in oesophageal squamous cell carcinoma based on gold-DNA and graphene-DNA affinity interactions using single disposable screen-printed electrode. Since the affinity interaction (adsorption) trend of DNA bases with gold surface follows as adenine (A) > cytosine (C) > guanine (G)> thymine (T), two DNA sequences with different DNA base compositions will have different adsorption affinity towards an unmodified gold electrode, accurate measurement of adsorbed DNA on the electrode surface will give the quantity of point mutation or SNPs, regional DNA methylation and global DNA methylation present in the DNA sequences. On the other hand, similar to the gold substrate, graphene has been reported as promising substrates

for adsorbing nucleobases and nucleosides. The adsorption of nucleobases onto the graphene surface follows the adsorption trend as guanine (G)> adenine (A)> thymine (T)> cytosine (C). Because this interaction is base (*i.e.*, sequence) dependent and bisulfite conversion generates two DNA sequences with different base compositions, bisulfite-converted two DNA sequences should give different adsorption patterns on the graphene surface. Profiling and quantitative measurement of regional DNA methylation will be performed via accurate measurement of adsorbed DNA on the graphene-modified electrode surface. Growing number of evidence suggests that electrochemistry based techniques offer a promising alternative for biomarkers detection in clinical diagnostics and research purpose due to their high sensitivity and specificity, cost effectiveness, and compatibility with the miniaturisation. A practical advantage of electrochemical detection could have future implications in translating to cheap assays using single-use screen-printed electrodes, which is an ideal tool due to their low cost, disposability and design flexibility as compared to traditional electrode materials. A detailed background and review are given in Chapter 2.

### 1.2 Aims and Hypothesis:

The main aim of this project is to explore the role of *FAM134B (JK1)* in oesophageal squamous cell carcinoma and develop innovative electrochemical technologies for the early detection of various biomarkers of oesophagal squamous cell carcinoma. This research will investigate the mutational effects of *FAM134B* in different tissue samples, and cell lines of oesophageal squamous cell carcinoma (ESCC) at molecular and functional level. This study will also elucidate screening method for *FAM134B* point mutation from different tissue samples of ESCC using molecular biological approach. This study will identify the role of *FAM134B* in the progression and development of ESCC by checking the DNA copy number changes and mRNA expression in different cancer tissues, cell lines and blood samples. Eventually, we will gain a better understanding of the role of *FAM134B* gene in the pathogenesis of oesophageal squamous cell carcinogenesis. At the same time, a novel electrochemical detection method of various biomarkers like point mutation, regional (Targeted *FAM134B* methylation) and global methylation in ESCC will be studied based on gold-DNA and graphene-DNA affinity interaction using single disposable screen-printed electrode. This will be achieved with the following specific research objectives;

**Aim 1**

**Molecular profiling and clinicopathological significance of *FAM134B* in oesophageal squamous cell carcinoma patients.**

Key objectives include

(a) Analyse DNA copy number changes of *FAM134B* in oesophageal squamous cell carcinoma tissues and cell lines

(b) Examine *FAM134B* mRNA expression changes in oesophageal squamous cell carcinoma tissues and cell lines

(c) Identification, cellular localisation and expression pattern at protein level of FAM134B in various cell lines of oesophageal squamous cell carcinoma

**Hypothesis:** Cancer will show genetic alterations of *FAM134B* in comparison to control samples which will be correlated with pathological and physiological characteristics of cancer.

**Aim 2**

**Identification of Novel mutation sites of *FAM134B* and its clinical applications in different tissue samples of oesophageal squamous cell carcinoma.**

**Hypothesis:** Carcinogenesis takes place in somatic mutations of the oncogenes or tumor suppressor genes and the low expression of *FAM134B* might relate to other genetic events such point mutation, and DNA methylation (regional and global methylation).

**Aim 3**

**Development of novel nanotechnological approaches for the detection of genetic and epigenetic biomarker and its clinical applications in oesophageal squamous cell carcinoma.**

Key objectives include

(a) Development of the nanotechnological approaches for *FAM134B* mutation detection and its clinical significance in oesophageal squamous cell carcinoma.

(b) Development of nanotechnological approaches for targeted *FAM134B* promoter methylation and its clinical application in oesophageal squamous cell carcinoma.

(c) Development of nanotechnological approaches for Global methylation and its clinical application in oesophageal squamous cell carcinoma.

**Hypothesis:** Novel nanotechnology approaches will show same or higher sensitivity/specificity for detecting the genetic and epigenetic abberations in ESCC.

## 1.3 Significances

Cancer is one of the leading causes of death in Australia estimating for 3 in every 10 deaths. It has been anticipated that approximately 130,470 new cases are diagnosed in 2016 and more than 44,000 people died from cancer in Australia (Cancer council, NSW, 2015). Approximately 482,300 new cases of oesophageal cancer and 406,800 mortalities from this malignancy are documented each year worldwide and the overall five-year survival rate is below 10 percent (Jemal et al., 2011). In Australia, oesophageal cancer affects about 1450 people in each year (Cancer council, NSW, 2015). Presently, cancer costs in Australia are more than 8.2 billion dollars per year. It is a global health concern as well as a most important health problem in our region. The proposed research projects will investigate the molecular and functional role as well as the clinical significance of *FAM134B* gene in human ESCC pathogenesis which could be an extremely useful tool in both diagnosis and treatment. The initial research indicated that *FAM134B* is upregulated in ESCC whereas it is downregulated in colorectal carcinoma. It suggested that upregulatory role of *FAM134B* might depend on the several other interacting partners of this gene in cancer metabolism whereas it might be down-regulated due to mutation and promoter hypermethylation. The current research project intends to identify the novel mutation sites of *FAM134B* and its clinical significance in ESCC which in turn will broaden the horizon of knowledge in ESCC pathogenesis. Also, the research reveals DNA copy number changes and profiling of *FAM134B* promoter hypermethylation in ESCC. It has also been known that novel *FAM134B* is linked to the pathogenesis of several other diseases such including hereditary sensory and autonomic neuropathy, allergic rhinitis and vascular dementia. So, it is believed that *FAM134B* may associate with a complex biological network. Intensive research based on the molecular and functional mechanism of this novel gene will give us deeper knowledge of their potential role in the pathogenesis of human dieases including cancer. This project will also explore the expression pattern of *FAM134B* in ESCC cells and tissues from different pathological stages. A large number of patient samples will be used for further examination of whether an overexpression of *JK1* in ESCC tumour cells could be a potential prognostic marker for determining regional lymphnode metastatic potential, invasiveness and aggressiveness of tumours. Due to the complexity of cancers, the early detection of ESCC is more important at the moment. If *FAM134B* can be detected as a blood-borne marker, it may enable the development of a simple test that can detect cancer prior to the development of obvious symptoms. This would be of enormous benefit, particularly for cancers without an effective early detection method.

The recent advances in molecular biology have now given rise to a large number of potentially useful genetic, epigenetic and other novel molecular biomarkers for the development of diagnostic methods for many diseases including cancer. It is now widely recognised that investment in innovative, cost-effective diagnostic technologies which can detect cancers early, monitor and personalise their treatment, can potentially provide the greatest social and economic benefits. Over the past several years, a great deal of effort has been devoted towards the development of effective cancer diagnostic technologies, most of these approaches are largely inadequate for inexpensive, simple, and portable readout for the diagnosis of cancer. This PhD project will intend to yield the innovative electrochemical technologies for the detection of biomarkers such as point mutation, regional methylation, global methylation in complex biological samples of ESCC *via* interaction of DNA with gold and graphene using single disposable screen-printed electrode. The method developed from this PhD will potentially be applicable in clinical settings due to their high sensitivity and specificity, cost-effective readout, and compatibility with the miniaturisation (*i.e.,* amenable with the point-of-care devices). Eventually, it will enable practitioners to improve the better clinical management of patients with ESCC.

### 1.4 Structure of the thesis

This thesis includes eight chapters. Chapters 4, 5 and 6 are a collection of journal papers that have been published. Chapter 7 and 8 are research articles submitted to peer-reviewed journals.

**Chapter 1** Introduces the aims, background and significance of this research.

**Chapter 2** depicts a literature review focusing the recent progress made in the investigation of the molecular genetics of oesophageal cancer and the role of *FAM134B* gene in the pathogenesis of chronic diseases including cancer. Also, this chapter highlights the application of various nanotechnological approaches for the detection of genetic and epigenetic biomarkers in cancer.

**Chapter 3** presents the expression and copy number profiling of FAM134B in oesophageal squamous cell carcinoma. DNA copy number and mRNA expression of *FAM134B* gene showed significant variations in ESCC tissues suggesting its potential role in the pathogenesis of ESCC.

**Chapter 4** highlights the detection of novel mutation sites of *FAM134B via* molecular biological methods and its clinical significances in oesophageal squamous cell carcinoma. The detection of novel mutations in different exons and introns of *FAM134B via* HRM and Sanger sequencing analysis is presented.

**Chapter 5** describes the nanotechnological approaches for *FAM134B* mutation detection and its clinical significance in oesophageal squamous cell carcinoma. A relatively simple and inexpensive electrochemical method is showed for detecting point mutation in cancer by using the direct adsorption of purified DNA sequences onto an unmodified gold surface. The method relies on the base dependent affinity interaction of DNA with gold. This method can successfully distinguish single point mutation in DNA from oesophageal cancer.

**Chapter 6** Development of nanotechnological approaches for regional methylation of *FAM134B* gene in ESCC and its clinical application in oesophageal squamous cell carcinoma is highlighted. A new method for the detection of regional DNA methylation using base-dependent affinity interaction (i.e., adsorption) of DNA with graphene is presented. The level of the methylation is quantified by monitoring the differential pulse voltammetric current as a function of the adsorbed DNA. The assay is sensitive to distinguish methylated and unmethylated DNA sequences at single CpG resolution by differentiating changes in DNA methylation as low as 5%.

**Chapter 7** Development of a cost-effective nanotechnological approach for the sensitive and selective detection of gene-specific DNA methylation and its clinical application in oesophageal cancer is presented. The underlying principle of the method relies on the affinity interaction between DNA bases and the unmodified gold electrode. The methylation levels were (*i.e.,* different level of surface-attached DNA molecules) quantified by measuring saturated amount of charge-compensating $[Ru(NH_3)_6]^{3+}$ molecules in the surface-attached DNAs by chronocoulometry as redox charge of the $[Ru(NH_3)_6]^{3+}$ molecules quantitatively reflects the amount of the adsorbed DNA confined at the electrode surface. The assay could successfully distinguish methylated and unmethylated DNA sequences at single CpG resolution and as low as 10% differences in DNA methylation.

**Chapter 8** presented a simple colorimetric (naked-eye) and electrochemical methods for relatively rapid, sensitive and specific quantification of global methylation levels and its clinical significance in oesophageal cancer. Our approach utilises a three-step strategy,

(*i*) initial adsorption of the extracted, purified and denatured bisulfite-treated DNA on a screen-printed gold electrode (SPE-Au), *(ii)* immuno-recognition of methylated DNA using HRP-conjugated anti-methylcytosine antibody and (*iii*) subsequent colorimetric and electrochemical detection of global DNA methylation were achieved by the enzymatic oxidation of 3,3′,5,5′-Tetramethylbenzidin (TMB)/$H_2O_2$ which generated a blue-colored complex in presence of HRP-conjugated methylated DNA (colorimetric). As $TMB_{(ox)}$ is electroactive, it also produced detectable amperometric current at 150mV vs Ag pseudo-reference electrode (electrochemical detection). The assay could successfully distinguish the samples before and after de-methylating drug-treated cells. It showed good reproducibility (% RSD= <5%) with fairly good sensitivity (as low as 5% differences in methylation levels) and specificity while analysing various levels of global DNA methylation in cells and tissue samples from patients with ESCC.

**Chapter 9** Summary and Conclusions are provided.

# Chapter 2

## Literature Review

## Introduction

The aim of this chapter to understand the current knowledge of genetic and epigenetic profile involving in the progression of oesophageal squamous cell carcinoma and focussing their application on the development of novel diagnostic tools for the clinical management of patients with ESCC. We also address the functional mechanism of new genetic players in the development and progress of ESCC. Through literature surveys, the role of *FAM134B* gene in the pathogenesis of chronic diseases including ESCC is highlighted and understood. Then, we critically analysed the current literature in the arena molecular mechanism of *FAM134B* gene in chronic disease including cancer. Also, we thoroughly analyse and address the recent developments of various electrochemistry based approaches and their major technical and biological limitations for the detection of genetic and epigenetic biomarkers in cancer.

## 2.1 Introduction to oesophageal cancer

### 2.1.1 Anatomy of oesophagus

The human oesophagus is a hollow muscular tube about 25 cm long and 2.5 cm diameter. It lies posterior to the trachea and the heart, passing through the mediastinum and penetrating the stomach through the hiatus of the diaphragm. Generally, the oesophagus has three main parts such as the cervical oesophagus, thoracic oesophagus and abdominal oesophagus (Pearson et. al., 2002). The cervical oesophagus begins from the cricopharyngeal muscle junction in pharynx to thoracic inlet and is situated at 15-18 cm long from incisor teeth (Holland et. al., 2000). The thoracic oesophagus starts at the suprasternal notch to the hiatus at the diaphragm which has 3 parts. The upper thoracic portion extends from the thoracic inlet to the level of the tracheal bifurcation and is located at about 18-24 cm from the incisor teeth (Holland et. al., 2000). The midthoracic portion lies between the tracheal bifurcation and the oesophagogastric junction and is positioned at approximately 24-32 cm from the upper incisor teeth (Holland et. al., 2000). The lower thoracic portion sited between the tracheal bifurcation and the oesophagogastric junction and can be found at 32-40 cm from the upper incisor teeth (Holland et. al., 2000). The abdominal oesophagus is located at 40-48 cm from incisor and starts from the esophagogastric junction to the gastric cardia (Pearson et. al., 2002).

### 2.1.2 Tumours of oesophagus

Histologically, oesophageal cancer exists in two main types with distinct etiological and pathological characteristics such as oesophageal squamous cell carcinoma (ESCC) and oesophageal adenocarcinoma (EADC) (Fiugure 1). ESCC is the most common histological subtype (approximately 60%) among all the oesophageal tumours. It has a relatively even distribution in the upper, middle and lower sections of the oesophagus (Gore and Levine, 2000). A sequence of histological changes in the epithelium can be recognised during the progression of ESCC (Lam and Ma, 1997). This sequence comprises basal cell hyperplasia (BCH), dysplasia (DYS), carcinoma *in situ* (CIS) and carcinoma (Mandard et al., 2000). Most of the EADC develops in the distal oesophagus and it may extend into the stomach depend on its position near the gastroesophageal junction. EADC develops in Barrett's oesophagus in a stepwise progression from specialised metaplastic columnar epithelium to dysplasia, followed by the change of early adenocarcinoma to deeply invasive and metastatic disease (Haggitt, 1992). Distinctive gross and histopathological features of ESCC are described below:

**Gross appearance**

Macroscopically, advanced ESCC can be parted into fungating, ulcerating or infiltrative. The fungating type exhibits as polypoidal, irregular and bulky masses of tumours that protrude into the lumen. Tumours of the ulcerating type can be seen as relatively flat masses in which the bulk of the tumour is replaced by ulceration. The infiltrative type is the most frequent type in which the wall of the oesophagus usually becomes thickened, the lumen becomes narrow and turns the texture as rigid.

**Histopathological features**

ESCC can be graded as well, moderately, poorly or undifferentiated types. The well-differentiated tumours have cytological features that closely resemble those of normal oesophagal squamous epithelium. Squamous nests, keratin pearls, intercellular bridges and cells undergoing differentiation can be found. In contrast, poorly-differentiated tumors lose most of the above features and have a high nucleus-cytoplasmic ratio. Although individual cell keratinization may still be present, no keratin pearls are formed. Moderately-differentiated tumors are those with features in between well and poorly differentiated types. Undifferentiated tumors have no glandular or squamous structure or other features to indicate definite differentiation. Pleomorphic nuclei and scanty cytoplasm with many mitotic figures can be found in these tumour cells.

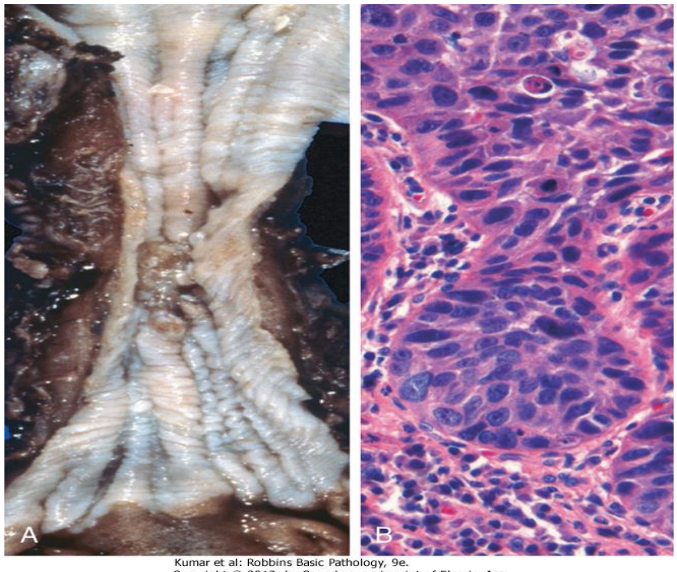


**Figure 1. (A &B) Anatomy and Histology of oesophageal squamous cell carcinoma.** A, Squamous cell carcinoma most frequently is found in the mid-esophagus, where it commonly causes strictures. B, Squamous cell carcinoma composed of nests of malignant cells that partially recapitulate the stratified organization of squamous epithelium.

### 2.1.3 Epidemiology

ESCC is the eighth most aggressive malignancies generated in the upper aerodigestive tract and ranks the sixth leading cause of cancer-associated death in the world (Lam, 2000; Chattopadhyay, 2014). Globally, it categorises as the sixth most common cancer among male and ninth most frequent cancer among female. Approximately 482,300 new cases of oesophageal cancer and 406,800 mortalities from this malignancy are documented each year worldwide and the overall five-year survival rate is below 10 percent (Jemal et al., 2011). In Australia, Oesophageal cancer affects about 1450 people in each year (Cancer council, NSW, 2015). Males are three times more likely to develop oesophageal cancer than females. The risk of oesophageal cancer increases with age. However, the incidence of oesophageal cancer varies significantly between developed and developing countries (Lam et al., 2000). The high-risk areas are known as the oesophageal cancer belt, which extends from north-central China westward through Central Asia to northern Iran. The extremely high incidence of oesophageal cancer has been accounted from certain parts of China, Iran, South Africa, Uruguay, France and Italy (Stoner and Gupta, 2001).

### 2.1.4 Etiology

The aetiology of oesophageal cancer is believed to be complex and consisted of multiple factors, those instigated by the environment being of utmost significance (Figure 2) (Hendricks and Parker, 2002). Tobacco use and alcohol consumptions are a potential threat and a well-known risk factors for ESCC (Yasushi et. al., 2010). A highly processed diet, red meat, certain preservatives (such as lye), and nutrients such as vitamins A, C, E, ß-carotene, folic acid, B12, riboflavin and certain trace elements (such as zinc) deficient fruits and vegetables also possess the risk factors for ESCC (Lam, 2000; Engel et al., 2003; Tran et al., 2005).


**Figure 2. Established risk factors in the etiology of ESCC,** Liyanage et al., 2013.

Exposure to radiation and certain industrial chemicals (such as perchlorethylene, combustion products and asbestos) and the ingestion of hot food and beverages have been occupied as a thermal injury in the pathogenesis of ESCC (Ward, 2005; Islami et al., 2009). Finally, recent findings in molecular biology attribute infectious agents as causal factors in ESCC, either acting directly on oncogenes or by aiding carcinogenic mechanisms. Mycotoxins with carcinogenic properties are identified as to have the potential to produce nitrosamine in food that has been linked to ESCC. While *Helicobacter pylori* have been ascribed as a protective agent against ESCC, other bacteria are supposed to possibly produce carcinogens that able to play role in causing disease (Wu et al., 2005). Recent studies on the molecular biology of ESCC contemplate on the viral etiopathogenesis and cancer susceptible genes to chemical carcinogens.

### 2.1.5 Symptoms

Early stage oesophageal carcinoma is totally asymptomatic with incidental findings at endoscopy or may present with mild nonspecific symptoms such as heartburn, atypical chest pain, or dyspepsia (Watanabe et al., 2014; Elton, 2005). Symptoms of advanced oesophageal carcinoma become noticeable with tumour growth. An initial symptom of the oesophageal cancer is dysphagia (difficulty in swallowing) which may progress from an inability to swallow solids is followed by difficulty in swallowing ground food and finally liquids. Advanced oesophageal carcinomas clinically experienced with mild or intermittent dysphagia, odynophagia or a foreign body sensation, dyspnea, weight loss and anorexia (Elton, 2005). Gastrointestinal reflux, regurgitation, and epigastric pain are the additional symptoms of oesophageal adenocarcinoma (Elton, 2005). Hoarseness is usually associated with recurrent laryngeal nerve paralysis. Hiccups may occur due to the mediastinal or diaphragmatic involvement of the tumour. Anaemia due to gastrointestinal bleeding and weakness may be present if the tumour is ulcerated and friable.

### 2.1.6 Diagnosis and Treatment

Diagnosis can be made for patients with ESCC to confirm and determine the disease stage for initiation of appropriate therapeutic measures. ESCC can be diagnosed by non-invasive methods like Barium contrast radiography or endoscopic methods such as Chest X-ray, Gastrointestinal endoscopy, Endoscopic brush cytology, Endoscopic ultrasonography (EUS) or computed tomography (Watanabe et al., 2014; Pearson et al., 2002). CT scanning can be performed for the 3-dimensional evaluation of the oesophagus in relation to its adjacent structures. Currently, there are several ways used for treatment of ESCC including resection, external beam radiotherapy, chemotherapy, photodynamic therapy depending upon the stage of cancer (Watanabe et al., 2014; Pearson et al., 2002).

## 2.2 Molecular genetics of oesophageal Squamous cell carcinoma

### 2.2.1 Viral etiopathogenesis

Human papilloma virus (HPV) is a closed circular double-stranded DNA virus belongs to the papovavirus family that play a vital role in the progression of ESCC. Among, more than 200 different HPV genotypes, HPV-16 and 18 are the predominant types identified in ESCC (Bernard et al., 2010). Other HPV types detected in ESCC include HPV 6, 11, 26, 30, 31, 33, 35, 39, 45, 51, 52, 53, 56, 57, 58, 66 and 87 (Chang et al., 2000; Lu et al., 2008; Wang et al., 2010; Moradi and Mokhtari-Azad, 2006; Mohseni, 2010; de Villiers et al., 2004; Liyanage et al., 2013).

It has been suggested that higher rates of HPV infection were observed in ESCC of patient from high risk areas such as China, Iran, Japan, India, and South Africa. The incidence of HPV in ESCC ranges from 13% to 46% and the overall incidence is 29%. The variations of environmental, geographic or genetic factors may influence in susceptibility to oesophageal HPV infection for different populations (Lam, 2000). In contrast, Epstein–Barr virus (EBV) is a double-stranded DNA virus belongs to the herpes virus family which is correlated with Hodgkin's disease, Burkitt's lymphoma, gastric and esophageal cancer (Paraskevas and Dimitroulopoulos, 2005). Awerkiew et al. in Germany showed that EBV DNA was detected in 35% of squamous cell carcinomas and 36% of adenocarcinomas by nested polymerase chain reaction (Awerkiew et al., 2003). The negative result was reported in ESCC from 103 Chinese patients by Chang et al., 2000. Hence, the significance of EBV in ESCC carcinogenesis is currently not supported.

### 2.2.2 Susceptible genes to chemicals

A variety of toxic chemicals in the diet or in the environment are associated with the risk of oesophageal cancer. A number of genes encoding carcinogen, alcohol and folate metabolic enzymes plays a significant role in the progression of oesophageal cancer *via* genetic polymorphism (Hiyama et al., 2007). The enzymes produced by these genes comprise cytochromes P450 (CYPs), sulfotransferases (SULT), glutathione S-transferases (GSTs), N-acetyltransferases (NATs), alcohol dehydrogenases (ADHs), aldehyde dehydrogenases (ALDs), Methylenetetrahydrofolate reductase (MTHFR) etc. CYPs variants such as CYP1A1, CYP2E1, CYP2A6 and CYP3A5 have been implicated in the progression of ESCC (Dandara et al., 2006). The combined association between null genotype of GSTT1, GSTP1 and GSTM1 increases oesophageal cancer risk ( Yi and Li, 2012; Moaven et al., 2010). CYP2E1, ALDH2 and ADH1B genotypes are associated with oesophageal cancer risk among moderate-to-heavy drinking males and detection of those genes may become a useful index for early detection of oesophageal cancer (Guo et al., 2008). Wu et al. in China identified several new ESCC susceptible SNPs, including ADH1B rs1042026 and rs17033, ADH1C rs1614972 and rs1789903 as well as ADH7 rs17028973 through a GWAS analysis (Wu et al., 2012). The ADH1B-ADH1CADH7 cluster polymorphisms were associated with risk of ESCC in Chinese populations (Wang et al., 2014). Polymorphisms in folate metabolic genes may also involve in the progression of ESCC. Recent studies in China suggested that MTHFR C677T polymorphism might be associated with a risked of ESCC (Wang et al., 2005; Gao et al., 2004). SNPs in key genes involved in nucleotide excision repair (NER) and base excision repair (BER) pathways are associated with oesophageal cancer (Tse et al., 2008).

### 2.2.3 Keratin

Keratins are a family of nearly 30 different related cytoplasmic proteins which plays a vital role in the ESCC pathogenesis. These keratin polypeptides are the product of various genes and expressed in diverse cells at different stages of cancer progression. Several studies have shown the altered expression of CK protein in the development of ESCC (Jazii et al., 2006; Du et al., 2007; Makino et al., 2009). CK10 was frequently related with well-differentiated ESCC. Recent studies reported that keratin1, keratin 8 and keratin 13 were overexpressed in ESCC, while keratin 4 and keratin 14 were downregulated (Jazii et al., 2006; Chung et al., 2006). CK18 were found of 42.9% positive in oesophageal cancer. Significant differences in expression of CK8, 18, and CK19 were reported between lymph node positive and lymph node negative ESCC (Cintorino et al., 2001). A recent study by Xue et al. observed that CK14 diffusely positive in ESCC whereas the underexpression of CK4 in the ESCC was an early event (Xue et al., 2006). It was reported that CK4 underexpression, and the overexpression of CK5, CK8 and CK14 were useful in differentiating normal epithelium from cancer in the general population while CK4 underexpression and CK14 overexpression were useful to differentiate normal epithelium from ESCC in the high-risk population (Singh et al., 2009).

### 2.2.4 Alteration of cancer-related genes in ESCC

It is known that there are several classes of genes involved in the initiation and development of oesophageal squamous cell carcinoma such as proto-oncogenes, tumor suppressor genes, telomerase activity and genes related to metastasis and apoptosis but to date no gene directly allied to ESCC has been identified (Kwong, 2005). Table 1 illustrates the nomenclature, chromosomal location and mechanisms of the genes that have been studied in oesophageal cancer.

Aberrant regulation of growth factors and their receptors play a significant role in the progression of ESCC (Ekman et al., 2007). Growth factors regulate growth and development of cells which is supposed to be supplied by distant glands and tissues, neighbouring cells, or by tumour cells (Figure 3). They exert their effects by binding to a specific receptor on the cell surface which is stimulated the tyrosine kinase activity and eventually phosphorylation of specific residues occurs in the intracellular domain of receptors. Then, phosphorylated cytoplasmic domains trigger signalling pathways for promoting cellular proliferation and survival (Pawson et al., 2002). Fibroblast growth factor (*FGF*) regulates growth and differentiation of cells. Overexpression and release of

*FGF-2* by stromal fibroblasts correlate with tumour recurrence and short survival in oesophageal cancer patients (Oshima et al., 2010; Barclay et al., 2005). Studies suggest that *FGF-2* is involved in carcinogenesis through degradation of extracellular matrix, secretion of growth factors, stimulation of cancer cell proliferation, induction of angiogenesis, cell mobility, inhibition of cell adhesion, and promotion of epithelial-mesenchymal transition (Zhang et al., 2009).

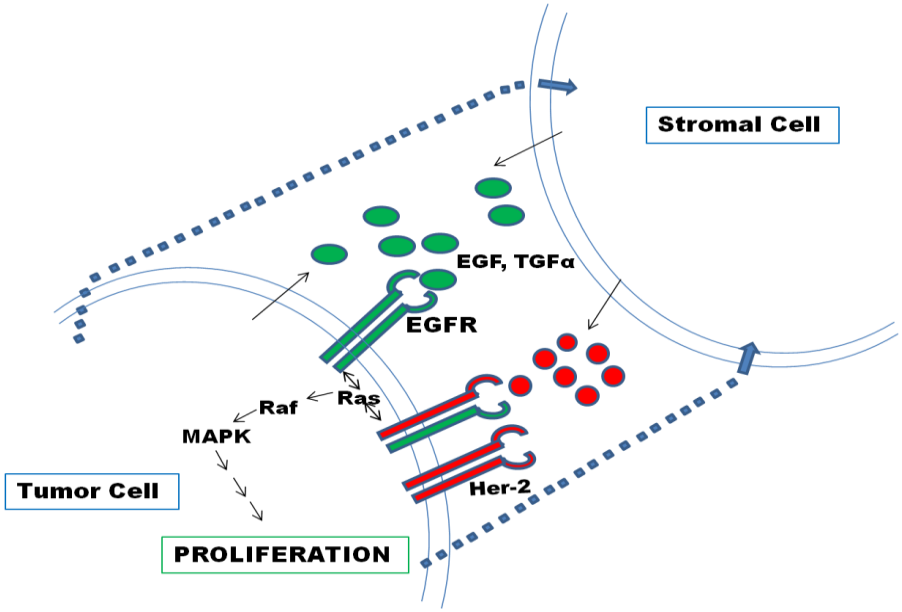


**Figure 3. Molecular signalling pathways of cancer.** *Black arrows* represent the secretion of growth factors by tumor or stromal cells. *Blue arrows* represent the secretion of chemokines by tumor cells to induce stromal cells to secrete growth factors. Stimulation of growth factor receptors leads to the activation of tyrosine kinases that in turn activate internal pathways (ras, raf, and mitogen activated protein [MAP] kinase) to promote cell proliferation. Both *epidermal growth factor* (*EGF*) and *transforming growth factor-α* (*TGF-α*) can stimulate the *epidermal growth factor receptor* (*EGFR*). Although the *Her-2* receptor can homodimerize, no known ligand for the homodimeric receptor has been defined. *Her-2* can heterodimerize to signal with *EGFR* (as shown) or with other *EGFR* family members (not shown). (MAPK = MAP kinase)

*Transforming growth factor-α* (*TGF-α*) binds to *EGFR* which activates the signalling pathway for cell proliferation, differentiation and development. Altered expression of *TGF-α* and *Heparin-binding growth factor* (*Midkine*) plays an important role in the progression of ESCC (Li et al., 2000; Ren and Zhang, 2006). Midkine is also associated with tumour size, immunoreactivity, and poor survival of patients (Oshima et al., 2010; Shimada et al., 2003). Overexpression of the *PDGFR-β* receptor has been shown in ESSC tissues (Zhang et al., 2006). *Hepatocyte growth factor* (*HGF*) acts in a paracrine way to promote ESCC through activation of *VEGF* and IL8 expression (Ren et al., 2005).

Moreover, increased expression of *c-Met* tyrosine kinase receptor is significantly correlated with the reduced survival rate, distant metastasis, and local recurrence of cancer in ESCC patients (Ren et al., 2005; Tuynman et al., 2008). Among all closely related members of *vascular endothelial growth factor* (*VEGF*), *VEGF-A* is one of the most important prognostic factors of ESCC (Gu et al., 2006; Matsumoto et al., 2006). *VEGF* provides the vascular permeability, proliferation and interference of apoptosis. Overexpression of *VEGF* has been found in 30-60% of ESCC cases which is significantly linked with an early stage of disease, distant metastasis, and poor survival rate in patients (Shih et al., 2000). *Connective tissue growth factor* (*CTGF*) paly a vital role in the progression of ESCC *via* involving various cell regulatory process such cell adhesion, cell proliferation and angiogenesis (Li et al., 2010). CTGF protein overexpression was found in 82% ESCC tissue samples while underexpression of this protein was reported in 19% using immunohistochemistry (Li et al., 2010). The CTGF protein overexpression was significantly associated with poor survival of ESCC patients (Li et al., 2010). Another study by Deng et al. reported upregulation of *CTGF* gene in 75% ESCC in comparison to the normal non-cancerous epithelial tissue *via* RT-PCR (Deng et al., 2007). *CTGF* promotes carcinogenesis through β-catenin-T-cell factor (TCF)/Lef signalling pathways (Deng et al., 2007). Zhou et al., also reported overexpression of CTGF protein in 49% ESCC tissue samples *via* immunohistochemistry which is linked with poor survival of ESCC patients (Zhou et al., 2009). Overexpression of *EGFRs* has been reported in 29-92% of ESCC samples (Dragovich and Campen, 2009; Takaoka et al., 2004). Immunohistochemical assays confirmed overexpression of the erbB-2 proteins in ESCC (Sunpaweravong et al., 2005). Another study by Mimura et al. reported that 30% ESCC were positive for erbB-2 which was coupled with a poor prognosis (Mimura et al., 2005).

The three Ras isoforms include *H-Ras*, *K-Ras*, and *N-Ras* are crucial components in normal cell division and differentiation (Shields et al., 2000). Ras proteins act as signal transducing molecule from membrane receptor to the cell cytoplasm. It was established that RAS proteins became activated by binding to GTP. Activation of the Ras oncogene frequently exists in gastrointestinal tract cancers. Shigaki et al. examined 203 ESCC samples for screening the frequency of *KRAS* mutations using a high-throughput pyrosequencing assay and found 0.5 % *KRAS* Mutation (Shigaki et al., 2013). Wang et al. have shown that *K-Ras* gene is abnormally expressed in oesophageal cancer tissues (Wang et al., 2012).

*cyclin D1* and *mdm2* (*Murine Double Minute 2*) are members of the nuclear factors in ESCC. Altered expression of the *cyclin D1* and *Rb* genes play a role in esophageal cancer. In the clinical arena, *CCND1* was overexpressed in 22% to 71% of ESCCs (Sunpaweravong et al., 2005; Shamma et al., 2000). Increased expression of *cyclin D1* was found in 61% oesophageal carcinomas and 35%the adjacent epithelia cases (Xiao et al., 2006). Mdm2 encodes a 90-kDa protein with a p53 binding domain at the N-terminus and a RING domain at the C-terminus acting as an E3 ligase responsible for p53 ubiquitylation. When wild-type p53 is activated by various stimuli such as DNA damage; it binds to *p53* at the N-terminus to inactivate the transcriptional activity of *p53* and promote the degradation of p53 via the ubiquitin-proteasome pathway. It results in the deregulation of cell overgrowth leading to tumour development (Dong et al., 2005; Lev et al., 2000; Saito et al., 2002). Takahashi et al. suggested that the overexpression of *Akt1* and *Mdm2* may be linked to oesophageal carcinogenesis (Takahashi et al., 2009). Akt1 overexpression induces *Mdm2* mRNA over-expression in ESCC.

*FRAT1* is a protein-coding gene belongs to the GSK (Glycogen synthase kinase)-3-binding protein family mapped at 10q24.1. It has been suggested that *FRAT1* gene promoted carcinogenesis through activation of the WNT-β-catenin-TCF signalling pathway (Benassi et al., 2006). Saitoh and colleagues observed that FRAT1 expression was relatively high in ESCC cell lines in 2002 (Saitoh et al., 2002). Furthermore, Wang showed overexpression of *FRAT1* in 74% of ESCC tissues using RT-PCR when compared to match noncancerous tissue (Wang et al., 2008). Also, expression of *c-Myc* in ESCC cells lines was noted to be necessary for upholding of the growth state in cells expressing *FRAT1* entailing that *c-Myc* may be a vital factor in oncogenesis induced by FRAT1 (Wang et al., 2008). Therefore, overexpression of *FRAT1* gene might play a vital role in activating β-catenin/TCF signalling pathway and c-Myc-induced by *FRAT1* may be a critical factor in the pathogenesis of ESCC.

*p53* is a cancer suppressor gene that terminates advancement in both the G1 and G2 phase of the cell cycle to evaluate DNA damage. The *p53* tumour suppressor gene regulates cell cycle progression, apoptosis and DNA repair. It also inhibits vascular endothelial growth factor. Indeed, Cell cycle is controlled via two main regulatory pathways such as the p53 (p14-MDM2-p53-p21) and pRb (p16-cyclinD1-pRb) (Xu, 2007). Deregulation of both mechanisms shows crucial role in the progression of most human cancers including oesophageal cancer via alteration its expression pattern. *p53* is the most common mutated gene in all human malignancies comprising 50-80% in oesophageal cancer. Until now, more than 100 mutations of ESCC have been compiled

in the IRAC TP53 mutation database (Olivier et al., 2002). More than 92% of these mutations are placed in the four conserved domains of the p53 gene such as exon 5 to exon 8 with hot spots at Arg175, Cys176, Arg248, Arg273 and Arg282. Among them, 80% mutations are point including 46% transition and 36% transversion (Xu, 2007). Measurement of circulating anti p53 antibody in serum of ESCC patients is helpful for detection of *p53* mutations which could be used as a tumour marker or prognostic marker (Shimada et al., 2002).

The *p21* gene is a cyclin-dependent kinase inhibitor-induced by wild-type p53. It reconciles G1 arrest following to DNA damage via the accumulation of hypo phosphorylated *pRB*. Polymorphisms at codon 31 and codon 149 in exon 2 of the p21 gene play a significant role in oesophageal carcinogenesis (Bahl et al., 2000). Moreover, inductions of *p21* may occur through *p73* that also regulates *p21* expression in oesophageal cancer (Masuda et al., 2003). *p21* overexpression is correlated with a poorer prognosis (Lam et al., 1999. Wild-type *p53* affiliated with *p21* expression is a predictor of a good response to chemotherapy or chemoradiotherapy in ESCC in vivo (Michel et al., 2002).

*p16* is a member of cyclin-dependent kinase inhibitors that is positioned on chromosome 9p21. Inactivation of the *p16* gene is a common event occurring through homozygous deletion, point mutation, or aberrant DNA methylation. Homozygous deletion and promoter methylation are the main causes of *p16* gene silencing in ESCC (Fong et al., 2000). A high frequency of homozygous deletion has been observed in oesophageal cancer cell lines. Methylation or LOH of *p16* gene occurs in the early stages of ESCC progression while homozygous deletion of its locus is a late event (Fong et al., 2000; Tokugawa et al., 2002). Therefore, *p16* could be used an epigenetic biomarker for the screening of ESCC (Nie et al., 2002; Hibi et al., 2001).

p27 is one of the cyclin-dependent kinase inhibitory proteins that shows genetic aberrations in ESCC. Low levels of *p27* expression affect tumour progression or indicate a poor prognosis in ESCC (Shamma et al., 2000). Also, it was reported that the increased expression of *p27* by 61% of oesophageal carcinomas was correlated with tumour invasion, lymph node metastasis and poor patient prognosis (Kagawa et al., 2000). High expression of *p27* may inhibit more likely cyclin E than cyclin D1 which promotes tumour growth of ESCC (Anayama et al., 2001). In addition, Fukuchi et al. in Japan suggest that S-phase kinase-interacting protein 2 (Skp2) is inversely correlated with p27 which is probably the main target substrate in primary ESCC (Fukuchi et al., 2004).

Retinoblastoma (Rb) is a nuclear phosphoprotein that plays a vital role in the regulation of cell cycle. Loss of heterozygosity of the retinoblastoma locus plays an essential role in the inactivation of *Rb* gene and is associated with *p53* alterations in oesophageal cancer. Association of *Rb* with *p53* inactivation may be the major event in the progression of oesophageal cancer. Loss of *RB* is one of the main genetic alterations accompanying the progression through dysplasia to adenocarcinoma of the oesophagus (Jenkins et al., 2002). The transcription factor E2F-1 is a downstream regulator of the RB pathway that is required for cell cycle progression and has been found to be overexpressed in related to poor prognosis in ESCC (Ebihara et al., 2004).

*Oesophageal cancer-related gene 4* (*ECRG4*) was cloned and identified from the normal oesophageal epithelium which is located at chromosome 2q14.1-14.3 (Bi et al., 2001). Yue et al. observed that *ECRG4* mRNA level was down-regulated in 80% of ESCC tissues and 3 of the 4 oesophageal cancer cell lines *via* promoter hypermethylation in 2003 (Yue et al., 2003). Also, Li and colleagues reported that ECRG4 protein expression was downregulated in 68.5% of ESCCs by using tissue microarray which was significantly linked with the size of cancer, regional lymph node metastasis and pathological stages in ESCC (Li et al., 2009). In addition, high expression of the ECRG4 protein was allied with the prolonged overall survival of patients with ESCC (Li et al., 2009). Besides, ECRG4 overexpression hinders cell proliferation through the G1/S transition block of the cell cycle, increase of p21 along with p53 protein expression (Li et al., 2009; Li et al., 2010; Li et al., 2011). In vivo study in mice proved that the inhibition of proliferation leading to slower growth of cancer (Li et al., 2009). The inhibition of cell migration and invasion in cell lines of ESCC are another in vitro effect of ECRG4 overexpression (Li et al., 2011). Furthermore, *ECRG4* inhibits cancer growth in ESCC cells by inducing COX-2 down-regulation through NF-kB pathway (Li et al., 2009).

The *ING* (*Inhibitor of growth gene*) family is a tumour suppressor genes implicated in multiple types of cancers including ESCC (Chen et al., 2001). It plays a crucial role in cell cycle regulation, senescence, apoptosis, chromatin remodelling and DNA repair (Guérillon et al., 2013). In ESCC, loss of the terminal regions of chromosome 13q has been reported by Chen and colleagues in 2001 (Chen et al., 2001). As a result, the genetic alterations of *ING1* gene in this region along with the impairment of 13q might play a significant role in the progression of ESCC. Also, the authors identified allelic loss of ING1 in 58.9% tissue samples in ESCC (Chen et al., 2001). Four missense mutations of *ING1* gene have been found from tissue samples of ESCC patients *via* direct sequencing of RT-PCR products. Furthermore, loss of ING1 protein expression using

immunohistochemistry has been noted in ESCC tissues (Chen et al., 2001). Therefore the low level of ING1 protein expression and a missense mutation of ING1 gene could be a critical factor in the development of ESCC.

The tetraspanin cell surface receptor Uroplakin 1A (UPK1A) is an integral protein that belongs to transmembrane 4 superfamilies (TM4SF). It was identified as a novel potential tumour suppressor gene at 19q13.13 chromosome in ESCC in 2010 (Kong et al, 2010). Kong and colleagues found negative expression of *UPK1A* gene in 68% of primary ESCC tissues and 55% ESCC cell lines *via* semi-quantitative RT-PCR (Kong et al, 2010). They also showed no expression of UPKIA in 56% ESCC tissues *via* immunohistochemical analysis (Kong et al., 2010). Furthermore, they suggested that the down-regulation of *UPK1A* gene mainly occurred in primary ESCC tissues *via* promoter hypermethylation. Thus it can be hypothesised that the promoter hypermethylation could be the main driving force for inactivation of *UPK1A* gene in ESCC. Besides, the down-regulation of *UPK1A* is positively correlated with lymph node metastasis, advanced tumour stages, and poorer patient's survival (Kong et al., 2010). The authors also demonstrated the suppressive properties of *UPK1A* gene in ESCC using in vitro and in vivo analysis (Kong et al., 2010). Besides, the tumour-suppressive effect of *UPK1A* was closely allied with its role in cell cycle arrest at the G1-S checkpoint (Kong et al., 2010). Furthermore, *UPK1A* gene may be performed a fundamental role in signalling pathways by the inhibition of *β-catenin* and inactivation of its downstream targets such as *cyclin-D1*, *c-jun*, *c-myc*, *E-cadherin*, *CDK4* and matrix metalloproteinase 7 (MMP7) (Lu et al., 2003; Noort et al., 2002; Kong et al., 2010). These results strongly support the critical roles of *UPK1A* gene in regulating the cellular biology and pathogenesis of ESCC.

T-lymphocyte maturation associated protein (MAL) is positioned on chromosome 2q11.1. MAL belongs to the MAL proteolipids family encoding an integral membrane protein which plays a role in membrane trafficking and signalling in T-lymphocytes (Alonso and Millan, 2001). It has also a peptidase modulator function involving in apoptotic process in cancer. Mimori and colleagues first reported that *MAL* mRNA expression was remarkably downregulated in 35 ESCCs by reverse transcriptase-polymerase chain reaction (RT-PCR) in 2003 (Mimori et al., 2003). Kazemi-Noureini and colleagues also noted down-regulation in all the ESCC studied by RT-PCR. In addition, MAL protein expression in rat model was noted to be associated with the histological grades of oesophageal dysplasia (Mimori et al., 2007).

**Table 1**

**Location, Function and Mechanism of genetic alterations that have been studied in oesophageal carcinoma**

| *Gene* | Chromosome | Alternative Names | Function | Mechanism |
|---|---|---|---|---|
| *hst-1* | 11q13 | *bFGF, HSTF1, Fibroblast growth factor gene* | Growth factor | Amplification |
| *int-2* | 11q13 | *Heparin-binding growth factor gene* | Growth factor | Amplification |
| *TGF-α* | | *Transforming growth factor-α* | Growth factor | Amplification |
| *PDGFa* | 7p22 | *Platelet-derived growth factor a* | Growth factor | Over expression |
| *PDGFb* | 22q13 | *c-sis, Platelet-derived growth factor b* | Growth factor | Over expression |
| *HGF* | | *Hepatocyte growth factor* | Growth factor | Over expression |
| *EXP1* | 11q13 | | | |
| *VEGF* | 6p12 | *Vascular endothelial growth factor* | Endothelial cell growth factor | Over expression |
| *c-erbB1* | 7p12-13 | *HER-1, Epidermal growth factor receptor (EGFR)* | Growth factor receptor, signal transduction (membrane tyr kinase) | Amplification, Over expression |
| *c-erbB2* | 17q21 | *HER-2, NGL, neu, EGFR2,* p185, p185neu, ERBB2 | Growth factor receptor | Amplification, Over expression |
| *c-myc* | 8q24 | | transcription factor | Amplification, Over expression |
| *Cyclin D1* | 11q13 | *bcl-1, PRAD1, EXP2, CCND1* | Promotes transition from G1 to S phase, cell cycle control | Amplification, Over expression |
| *Mdm2* | 12q13-14 | *Murine double minute 2* | | Amplification |
| *FRAT1* | 10q24 | | activation of the WNT-beta-catenin-TCF signalling pathway | Over expression |
| *p53* | 17p13 | | Tumor suppressor, G1 arrest, apoptosis, genetic stability | Mutation, LOH, Over expression |
| *p73* | 1p36.3 | | apoptosis | Over expression |
| *p21* | 6p21 | *WAF1, CIP1, CAP20, PIC1, SDI1* | Tumor suppressor | Over expression |
| *p16* | 9p21 | *MTS1, CDK4I, INK4a, CDKN2, CDKN2A* | Tumor suppressor, CDK inhibitor (cell cycle control) | Mutation, LOH, Hpermethylation |
| *p15* | 9p21 | *MTS2, INK4b, CDKN2B* | Tumor suppressor CDK inhibitor (cell cycle control) | Mutation, LOH, Hpermethylation |
| *p27* | 12p13 | *KIP1* | Tumor suppressor | Over expression |
| *Rb* | 13q14 | *Retinoblastoma* | Inhibits entry into S phase, cell cycle control (EF2 sequestering) | LOH, Mutation |
| *DCC* | 18q21 | *Deleted in colorectal cancer gene, CRC18; CRCR1; IGDCC1* | Cellular adhesion | LOH |
| *MCC* | 5q21 | *Mutated in colorectal cancer gene* | Tumor suppressor | LOH |
| *APC* | 5q21 | *FAP ( familial adenomatous polypis coli) gene* | Tumor suppressor | LOH |
| *BRCA1* | 17q21 | | Tumor suppressor | LOH |
| *FHIT* | 3p14.2 | | Negative regulation of progression via cell cycle | Hpermethylation |
| *DEC1* | 9q32 | *Deleted in esophageal cancer 1* | Tumor suppressor | Under expression |
| *ECRG4* | 2q14.1–14.3 | *Esophageal cancer related gene 4* | Tumor suppressor | Methylation |
| *ING* | 13q33-34 | *ING1 to ING5,* | cell cycle control and apoptosis | Over expression |
| *UPK1A* | 19q13.13 | *uroplakin 1A,* TSPAN21 | Tumor suppressor | Methylation |
| *MAL* | 2q11.1 | *T-lymphocyte maturation associated protein* | Tumor suppressor | Methylation |
| *DLC1* | 3p21.3 | *Deleted in lung cancer 1* | Tumor suppressor, growth inhibition | LOH |
| *WWOX* | 16q23.3–24.1 | *WW domain containing oxireductase* | Tumor suppressor | Mutation, LOH |
| *Annexin1* | | *lipocortin 1, ANX-I, p35* | Tumor suppressor | Under expression |
| *β-TM* | | *Tropomyosins, (TM1)* | Tumor suppressor | Down regulation |
| *FAS* | | *TNFSF6, CD95, or APO-1* | Apoptotic signal receptor | Under expression |
| *nm23* | 17*q*21 | *NME1, NME2* | Act inside the cell in a regulatory pathway | Under expression |
| *bcl-2* | 18q21 | | Blocks apoptosis | Under expression |
| *Bax* | 19q13 | *bcl-2 -associated X* | Apoptosis gene | Under expression |
| *Bcl-xL* | | | Antiapoptotic | Over expression |
| *PCNA* | | *Proliferating cell nuclear antigen* | DNA damage repair | Over expression |
| *Survivin* | | | inhibitor of apoptotic proteins | Over expression |
| *MMP-7* | | *Matrilysin, Matrix metalloproteinase-7* | To degrade elastin, proteoglycans, fibronectin and type IV collagen. | Over expression |
| *MT* | | *Metallothionein* | inhibiting apoptosis | Over expression |
| *E2F-1* | | | induce apoptosis | Over expression |
| *DcR3* | | *M68* | blockade of FasL-induced cell death | Over expression |
| *MLH1* | 3p21 | *h MLH-1* | DNA repair | LOH |
| *GASC1* | 9p23-24 | *gene amplified in squamous cell carcinoma 1* | chromatin-mediated transcriptional regulation | Amplification Over expression |
| *FEZ1* | 8p22 | | Transcription factor | Mutation |
| *CTSB* | 8p22 | *Cathepsin B* | Degrade extracellular matrix components | Amplification Over expression |
| *ODC* | | *Ornithine decarboxylase* | Biosynthesis of polyamines | Over expression |
| *FzE3* | | | Negative regulator of APC function | Up regulation |
| *MSH2* | 2p21 | *hMSH-2* | DNA repair | LOH |
| *β-Catenin* | 3p21 | *CTNNB1* | Cellular adhesion, gene transcription | Low expression |
| *E-cadherin* | 16q22 | *CDH1* | Cellular adhesion | Low or Un expression |
| *DPC4* | 18q21 | | TGF- β pathway | LOH |
| *Periplakin* | | | Keratinization | Under expression |
| *Clusterin* | | | Promotion or inhibition of apoptosis | Under expression |

In oesophageal cancer cell lines, under expression of *MAL* gene was found which may be due to the promoter hypermethylation (Mimori et al., 2003). Furthermore, *MAL* gene expression reduced cellular motility, G1/S transition block, invasion and tumorigenicity as well as increased apoptosis *via* the Fas signalling pathway in MAL-expressing ESCC cells using in vitro and in vivo analysis (Mimori et al., 2003). Overall, epigenetic inactivation of *MAL* gene may act as a critical factor during the initiation and progression of ESCC.

The *WW domain containing oxidoreductase* gene (*WWOX*) is a tumour suppressor gene located on the common fragile site of chromosome 16q23.3-24 in ESCC (Paige et al., 2001; Bednarek et al., 2001; Kuroki et al., 2002). Aberrant genomic alteration of the *WWOX* gene might play a critical role in the progression of ESCC (Kuroki et al., 2002). Kuroki et al. first detected the LOH in *WWOX* in 39% of ESCC tissues *via* an RT-PCR approach in 2002 (Kuroki et al., 2002). In addition, missense mutation and allele missing in WWOX were also noted in this study. This is also known as a two-hit mechanism including allelic loss and point mutation (Bednarek et al., 2001). Furthermore, the aberrant absence of exons or the whole transcript in *WWOX* was detected by nested RT-PCR analysis in ESCC (Kuroki et al., 2002). The data suggest that *WWOX* could act as a tumour suppressor in ESCC through genomic alteration and inactivation.

*Annexin1* is a member of annexin family which are calcium and phospholipid-binding proteins (Xia et al., 2002). The involvement of the gene in ESCC was first reported by Paweletz and colleagues in 2000 (Paweletz et al., 2000). They detected the loss or reduction of expression of Annexin I protein expression in 25 cases of ESCC using immunohistochemistry and Western blot. Also, Xia and colleagues showed that reduced expression of three annexin 1 isoforms was a common phenomenon in the progression of ESCCs (Xia et al., 2002). They documented *annexin 1* mRNA levels significantly downregulated in 71% of ESCC tissues via RT-PCR analysis. Low annexin 1 protein expression levels were seen mostly in high grades (grades 2 or 3) ESCCs using immunohistochemical analysis. This finding might be influenced by its post-translational modification in ESCC (Xia et al., 2002). Also, there is a change in subcellular location of Annexin 1 protein in ESCC when compared to non-neoplastic epithelial cells (Liu et al., 2003).

*Deleted in colorectal cancer* (*DCC*) gene is located on chromosome 18q21.1 regions encoding a netrin receptor (Arakawa, 2004). Decreased or loss of *DCC* expression through promoter hypermethylation as well as point mutations and LOH which are correlated with the degree of lymph node metastasis and differentiation have been shown

in esophageal cancer (Jenkins et al., 2002). Park et al. have demonstrated that *DCC* methylation is a frequent and cancer-specific event in primary ESCCs suggesting that *DCC* and associated pathways may represent a new diagnostical therapeutic target (Park et al., 2008). They also advised that *DCC* promoter methylation deserves further attention as a biomarker in the early detection of human ESCC.

Tropomyosin (TM) isoforms are a family of cytoskeletal proteins. Zare et al. showed that TM1, TM2, and TM3 were downregulated at the protein level in ESCC cell line in 2012 (Zare et al., 2012). Moreover, at the transcription level, TPM1 and TPM2 were noticeably reduced by 93% and 96% respectively in ESCC cells when compared to non-neoplastic oesophageal epithelial cells (Zare et al., 2012). Jazii and colleagues also reported a loss of β tropomyosin protein expression in ESCC *via* two-dimensional electrophoresis with mass spectrometry in 2006 (Jazii et al., 2006). Down-regulation of various isoforms of TMs in ESCC is mainly occurred due to promoter hypermethylation as inhibition of methyltransferase considerably overexpressed TM1 (Zare et al., 2012). This study also noted that TMs suppression can lead to the inhibition MEK/ERK and PI3K/Akt pathways. Therefore, the down-regulation of TMs by promoter hypermethylation and activation of MEK/ERK and PI3K/Akt pathways might play a role in the development of ESCC.

The *fragile histidine triad* (*FHIT*) is at a chromosomal fragile site at 3p14.2. Chromosomal fragile sites are specific heritable points of genomic regions that may tend to break and eventually affect for structural chromosome aberrations such as translocations, duplications or deletions in carcinogenesis (Dillon et al., 2010). FHIT allelic deletion and reduced /absent FHIT protein expression followed by alteration of p16, p53 proteins has been observed in multiple cancers including ESCC in 2002 (Pekarsky et al., 2002). In 2001, Kitamura and colleagues first studied the expression of FHIT protein in 75 cases of ESCC as well as 19 epithelia with carcinoma in situ in the oesophagus by immunohistochemistry. Significant reduction of FHIT expression in 89.3% was noted in ESCC and the loss of expression was associated with the severity of histological changes (Kitamura et al., 2001). Noguchi and co-workers first reported FHIT promoter hypermethylation in 69.4% of patients with ESCC and it was significantly linked with low FHIT protein expression (Noguchi et al., 2003). The study concluded that loss of heterozygosity or hypermethylation of FHIT might be a mechanism for FHIT protein expression regulation and could play a crucial role in early stage of progression of ESCC (Noguchi et al., 2003). In other studies, hypermethylation of CpG Island in the FHIT promoter region was also linked with the loss of FHIT protein expression in ESCC

(Nie et al., 2002; Guo et al., 2005; Kuroki et al., 2003). Ishii and co-workers first reported adenoviral-FHIT expression guided growth inhibition at G2/M and S phases and caspase-dependent apoptosis (Ishii et al., 2001). Thus, *FHIT* inactivation by chromosomal deletions and promoter hypermethylation could be a vital tool for assessing the status of FHIT expression and inactivation of FHIT might be a cause of downstream effect of DNA repair aberrations.

Repetitive telomere sequences (TTAAGGG) are found at the ends of eukaryotic chromosomes to protect the ends from damage and rearrangement. Bergqvist et al. detected a broad range of telomerase activity levels in EC cell lines (Bergqvist et al., 2006). Li et al. found that increased telomerase activity was associated with the progression of ESCC (Li et al., 2003). Grade I (metaplasia) stage showed a 60% telomerase activity and Grades II (dysplasia) and III (highgrade dysplasia) showed 90% and 91% telomerase activity respectively. This result supported other reports of telomerase activity being correlated with ESCC differentiation and lymphatic metastasis. The poorer the differentiation, the higher the telomerase activity occurred, and also patients with lymphatic metastasis showed a higher telomerase activity than those without lymphatic metastasis (Bergqvist et al., 2006). Microarray analysis indicated telomerase activity as a possible candidate for prognostic and prediction factors in esophageal cancer (Li et al., 2003).

The major causes of treatment failure in ESCC usually involve recurrence and metastasis. They are two classes of gene products in relation to metastasis such as *Nm23* that act inside the cell in a regulatory pathway and cathepsin-D that act outside the cell to block dissect the metastasis pathway (Mona et al., 2000). In fact, *Nm23-H1* and *Nm23-H2* are the two most abundantly expressed *Nm23* genes in human tissues. Studies suggested that loss of *nm23* expression has been found to associate with shorter survival in ESCC patients with lymph node metastasis (Tomita et al., 2001). Ligang et al. in China found that low expression of Nm23-H1 and high expression of p53 play significant role in the progression of ESCC (Liu et al., 2002). Li et al. revealed that SEI1 can upregulate SET expression which induces NM23H1 translocation from cytoplasm to nucleus resulting in increased chromosome instability (Li et al., 2010). Screening for nm23-H1 expression in tumour cells may be a potential therapeutic strategy in ESCC patients (Wang et al., 2004).

Survivin is a unique inhibitor of apoptotic proteins (IAP) family and was noted to play roles in ESCC in 2013 (Ikeguchi et al, 2003). Ikeguchi et al state that survivin exhibits anti-apoptotic function by binding to microtubules of the mitotic spindles

resulting in inactivation of caspase-3 and caspase-7 activity (Ikeguchi et al., 2003). Increased survivin expression can have a cancerous effect on the cell as it routes the G2/M phase checkpoint advancing into mitosis (Ikeguchi et al., 2003). Also, survivin encourages cell proliferation by interacting with CDK4 and displacing p21 (McCabe and Dlamini, 2005). In ESCC tissue, the nuclear expression of survivin was found to correlate with poor prognosis of the patients (Grabowski et al., 2003). It appears that localisation of survivin expression is critical for activity in tumour cells and its negative effect in dysregulating cell cycle definitely plays a role in the progression of cancer (Grabowski et al., 2003). Mega et al also showed that the overexpression of survivin was linked with the poor prognosis in patients with ESCC (Mega et al., 2006). In addition, Beardsmore et al. found survivin immunostaining in 95% of oesophageal carcinomas and noted a strong positive correlation between levels of survivin expression and the number of proliferating cells in the neoplastic tissue (Beardsmore et al., 2003). Expression of survivin and other IAPs (cIAP1, cIAP2, NAIP, and XIAP) was elevated in ESCC (Nemoto et al., 2004). These findings implied that survivin expression along with its anti-apoptotic role plays a fundamental role in the pathogenesis of ESCC.

*Fas* is a cell surface receptor that plays a major role in apoptotic signalling in many cell types (Sharma et al., 2000). Alterations in expression of *Fas* and *FasL* favours malignant transformation and progression (Muschen et al., 2000). Moreover, mutations in the *FAS* and *FASL* gene that impair apoptotic signal transduction are linked with a high risk of cancer. Thus, the FAS/FASL system appears to have a role in the development and progression of cancer. In human ESCC, expression of FAS is lower and FASL expression is higher than in normal tissue indicating a linked between the aberrant expression of FAS and FASL (Kase et al., 2002). In addition, aberrant expression of FAS and FASL occurs early in dysplasia and in carcinoma *in situ* and has been related with differentiation, invasiveness, and metastasis of cancer cells and with patients' survival (Kase et al., 2002; Younes et al., 2000). These findings suggest that FAS and FASL are likely to be involved in the initiation and development of ESCC. Chan et al. in China detected Fas expression in 89.7% of ESCCs and suggested higher Fas expression was associated with longer survival of patients (Chan et al., 2006). Sun et al. in China stated that genetic polymorphisms in the death pathway genes FAS and FASL appeared to be associated with an increased risk of developing ESCC (Sun et al., 2004).

Dysregulation of normal cell-cell adhesion and cell-matrix interactions are mediated by a distinct protein known as cell adhesion molecules (CAMs). Cell adhesion molecules can be classified as cadherins, β-catenin, CD44 receptor, integrin receptors

family, the immunoglobulin superfamily (IgCAMs), lectin-like cell adhesion molecules such as selectins, lamin-binding protein, EpCAM, Periostin, Rho-associated protein kinase (ROCK) and Migfilin (Figure 4). Altered expression of cell adhesion molecules has a significant impact in the pathogenesis of ESCC. In ESCC, reduced E-cadherin expression are correlated with tumour differentiation, metastasis and prognosis (Lin et al., 2004). Also, low or absence of E-cadherin expression is related with infiltration and metastasis of ESCC (Uchikado et al., 2005). In addition, methylation and the subsequent reduced expression CDH1 has been reported in 61% of ESCC cases (Takeno et al., 2004). It was also showed that downregulation of E-cadherin and up-regulation of N-cadherin may be involved in the genesis of ESCC (Li et al., 2009). The study suggests that accumulation of nuclear β–catenin in oesophagus squamous epithelium might be the crucial step for the carcinogenesis of ESCC (Veeramachaneni et al., 2004). A meta-analysis conducted by Zeng et al found that aberrant expression of β-catenin was linked with a significant increase in mortality risk of EC patients (Zeng et al., 2014). Well-differentiated ESCCs showed greater CD44 expression than moderately or poorly differentiated ones (Gotoda et al., 2000). In an immunohistochemical study conducted on 233 patients with ESCC found that CD44v2 was downregulated in the cancer cells (Nair et al., 2005). Downregulation of CD44v2 expression is associated with a poor prognosis in patients with ESCC (Nair et al., 2005). Another study by Vay et al. suggests that alterations in both pattern and magnitude of integrin expression may play a major role in the disease progression of ESCC patients (Vay et al., 2014). Stromal carcinoembryonic antigen (CEA) expression has also been reported to play a role in the lymphatic invasion of ESCC (Kijima et al., 2000). EpCAM is a 40 KD type I transmembrane glycoprotein at chromosome 2p21 which is strongly positive in ESCC (Philip et al., 2008). Stoecklein et al. observed 79% EpCAM neo-expression with three expression levels such as 1+ (26%), 2+ (11%) and 3+ (41%) in ESCC (Stoecklein et al., 2006). In addition, Periostin was noted in 2010 to play a role in the progression of ESCC *via* regulating expression pattern (Kashyap et al., 2010; Michaylira et al., 2010). Kashyap et al. showed increased expression of periostin in 100% of ESCC while 6% of non-cancer oesophageal epithelia demonstrated periostin expression (Kashyap et al., 2010). Moreover, Michaylira and colleagues noted overexpression of periostin in ESCC which was correlated with tumour progression (Michaylira et al., 2010).

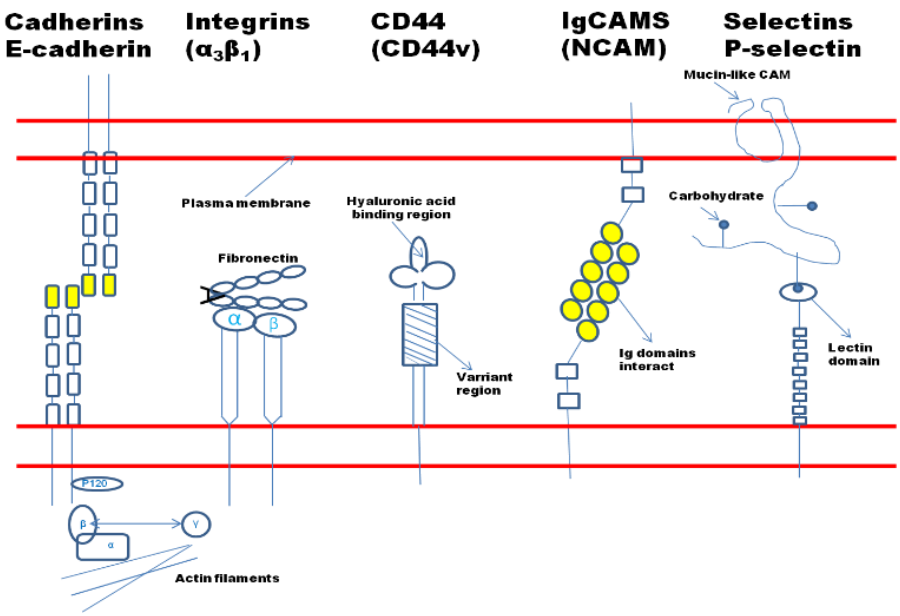


**Figure 4. Diagrammatic representation of five families of cell adhesion molecules (CAMS).** cadherins, integrins, CD44, immunoglobulin (Ig) CAMs, and selectins. Cadherin dimers engage in calcium dependent homotypic binding to dimers from an adjacent cell. The cytoplasmic domain of E-cadherin is complexed with β/γ catenin, which in turn is linked with the actin cytoskeleton via a catenin. Integrins are heterodimers consisting of α and β subunits that bind to extracellular molecules. The CD44 standard isoform binds to hyaluronic acid; however, the inclusion of combinations of variant (v) exons alters its binding affinity for this molecule. IgCAMs are characterised by their extracellular Ig-like domains. Selectins possess an N-terminal lectin domain that binds fucosylated and sialylated carbohydrates. NCAM, neural cell adhesion molecule.

Also, Wong et al. in 2013 reported that *periostin* reduced the growth of tumour through a knockdown manipulation of this gene in ESCC (Wong et al., 2013). *Periostin* was also found to cooperate with P53 mutant to enhance invasion *via* the activation of signal transducer and activator of transcription 1 (STAT1) in ESCC (Wong et al., 2013). Furthermore, altered expression of LIM domain-containing protein is involved in the pathogenesis of ESCC (Zhao et al., 2009; Kashyap et al., 2012; Lo et al., 2012; Takeshita et al., 2012; Tao et al., 2012). Another study by He et al. exhibited expression of migfilin was significantly upregulated in ESCC in concomitance with a nuclear-cytoplasm translocation compared to normal adjacent tissue (He et al., 2012).

### 2.3 Molecular epigenetics of oesophageal squamous cell carcinoma

Epigenetics means the study of heritable changes in gene expression without changes in gene sequence. Indeed, Carcinogenesis is a stepwise process driven by the accumulation of heritable changes in the regulation and information content of proto-oncogenes and tumour suppressor genes. It has been known for decades that a variety of genetic alterations including p53-Rb pathway with gene amplification, loss of

heterozygosity, point mutations and chromosomal rearrangements contribute to tumorigenesis (Kwong, 2005). In addition to genetic alteration, epigenetic modifications also act equally as driving force in the pathogenesis of ESCC by transcriptional inactivation and silencing of gene function (Ma et al., 2016).

### 2.3.1 DNA methylation

DNA methylation is the covalent addition of a methyl group to the 5-carbon ($c^5$) position of cytosine bases that are located 5′ to a guanosine base in a CpG dinucleotide. DNA methylation is the best studied epigenetic mechanism which mainly occurs at promotor region leads to transcriptional silencing of the methylated gene with the loss of protein function (Klose et al., 2006). DNA methylation is one of the clinically relevant epigenetic biomarkers which represents the highest translation potential because of its stable nature and reliable detection technologies. DNMT1, DNMT3A and DNMT3B have been recognised as DNA methyltransferases in eukaryotic cells which catalyse the DNA methylation process (Figure 5). DNMT1 plays a role in maintaining DNA methylation whereas DNMT3A and DNMT3B are responsible for de novo methylation. Over expressions of these DNMTs were described to be involved in different cancers including oesophageal cancer (Klose et al., 2006). DNMT3L and DNMT2 were reported recently related to DNA methylation (Chen et al., 2005). DNMT3L is required for the methylation of imprinted genes in germ cells and interacts with DNMT3A and 3B in de novo methyltransferase activity (Chen et al., 2005). The function of DNMT2 remains unclear but its strong binding to DNA suggests that it may mark specific sequences in the genome.

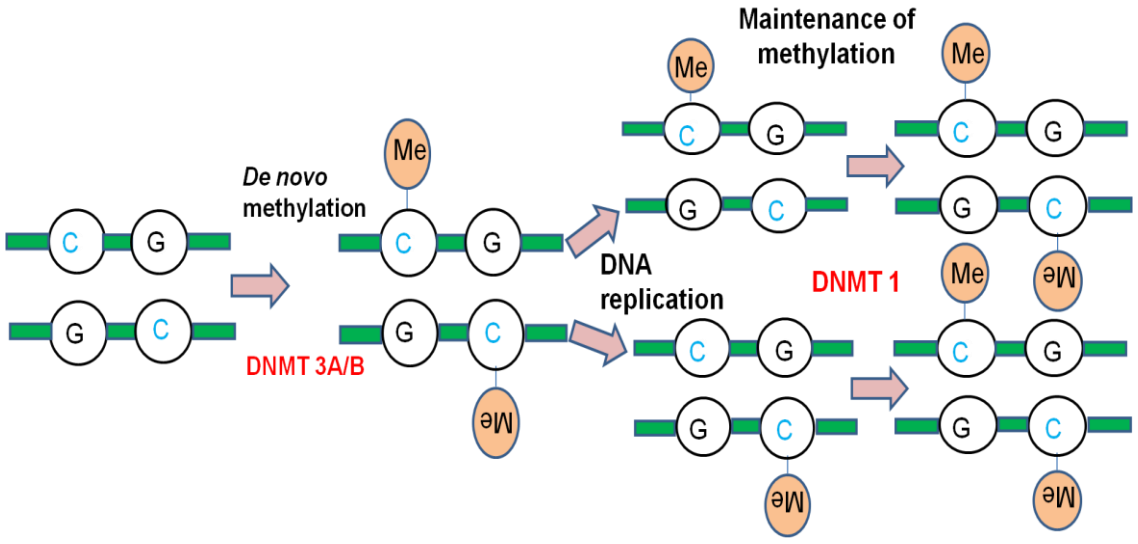


**Figure 5.** DNA methylation, the covalent addition of a methyl group to the cytosine base in DNA, may be set up de novo (by DNA methyltransferase DNMT3A and DNMT3B) and maintained (by DNMT1) after DNA replication.

Over the past few decades, growing number of evidence suggest that aberrant epigenetic changes play critical role in the progression of ESCC *via* affecting genes involved in cell cycle, DNA damage repair and cancer associated signalling pathways (Ma et al., 2016). DNA methylation has progression tendency in the pathogenesis of ESCC indicating that it is an early event. It was reported that p16 is a cell cycle related gene that frequently methylated in ESCC (Guo et al., 2006). Another study by Hibi et al. provided the strong evidence of aberrant methylation of p16 gene in 80% serum samples from patients with ESCC (Hibi et al., 2001). In addition, other cell cycle related gene such as *RASSF1A* and *CHFR* are frequently methylated in 44.3% and 45% of ESCC, respectively (Kuroki et al., 2003; Yun et al., 2015). Furthermore, Promoter methylation of *FHIT* gene is involved with early stage of cancer and associated with poor prognosis. Recently, it was reported that *DACT2* and *NKD2* are frequently methylated in ESCC which is correlated with advanced pathological stage and lymph node metastasis (Ma et al., 2016). *RARβ2* methylation was detected in normal oesophagus but increased methylation of this gene was noted to be play critical role in the progression of ESCC (Kuroki et al., 2003). It was showed that cigarette smoking is a cause of *SSBP2* promoter methylation and that *SSBP2* harbors a tumour suppressive role in ESCC through inhibition of Wnt signalling pathway (Huang et al., 2011). A previous study demonstrated that duration of tobacco smoking is associated significantly with DNA methylation of *HOXA9, MT1M, NEFH, RSPO4*, and *UCHL1* in the background oesophageal mucosa of oesophageal cancer patients (Oka et al., 2009). Till now, promoter methylation of many gene have been discussed as biomarkers for early detection, prognosis, therapeutic responsiveness, and therapeutic targets in various cancer including ESCC (Heyn and Esteller, 2012; Toh et al., 2013). Despite, several important genes have been found to be frequently methylated in ESCC, the landscape of the ESCC epigenome are still need to be completed for the development of epigenetic biomarkers for early detection, tumour recurrence and prognosis in ESCC.

### 2.3.2 Histone modification

Post-transtional marking of chromatin proteins (Histones) is a major epigenetic mechanism that plays a critical role in neoplastic processes by the regulation of cellular processes such as heterochromatin formation, X-chromosome inactivation and transcriptional regulation (Loizou et al., 2006). Acetylation, methylation, phosphorylation and ubiquitylation are major histone modifications which may constitute the histone code that extends and modulates the genetic code (Loizou et al., 2006). It was reported that Histone arginine methylation is stated on the residues 2, 8, 17 and 26 of

histone H3 and residue 3 of histone H4 in mammals. Also, Histone lysine methylation occurs in histones H3 and H4 and can be mono-, di- or trimethylated. Like histone lysine methylation, arginine methylation occurs in monomethyl, symmetrical di-methyl or asymmetrical di-methyl state, and contributes to both active and repressive effects on chromatin function (Martin and Zhang, 2005). Though there is no evidence that lysine methylation directly affects chromatin dynamics, acetylation of lysine residues in histones is reported to antagonize folding of chromatin in vitro (Hansen, 2002). The main sites of lysine methylation is associated with gene activity include *K4, K36* and *K79* of histone H3. Trimethylation of lysine 27 on histone H3 (H3K27me3) is a silencing epigenetic marker. Acetylation neutralizes the positive charge of lysine. It has been suggested that this modification might operate through an electrostatic mechanism and histone acetylation is associated with active gene transcription. Methylation of histone H3 lysine 9 was triggered by DNA methylation. DNA methyltransferases have been shown to interact with histone deacetylases (HDAC), histone methyltransferases, and methyl-cytosine-binding proteins in a complex network (Fuks et al., 2000). Langer et al reported that H3K18Ac and H3K27triMe were associated with worse survival of ESCC particularly in early stages patients (Langer et al., 2009). Zester homolog 2 (EZH2) is reported to be overexpressed and correlates with poor prognosis in human cancers. The expression frequency of H3K27me3 was significantly higher in ESCCs than in normal tissues by immunohistochemistry. Expression of H3K27me3 was significantly related with WHO grade, tumour size, T status, locoregional progression and EZH2 expression. High expression level of H3K27me3 was significantly associated with poor locoregional progression-free survival (LPFS) in ESCC (He et al., 2009). A study of 237 ESCC patients showed that histone modifications have significant effects on recurrence-free survival (RFS) after oesophagectomy in ESCC, such as acetylation of histone H3 lysine9 (H3K9Ac), histone H3 lysine 18 (H3K18Ac), and histone H4 lysine 12 (H4K12Ac), and the demethylation of histone H3 lysine 9 (H3K9diMe) and histone H4 arginine 3 (H4R3diMe).

### 2.3.3 Non-coding RNA (ncRNAs)

Non-coding RNA are functional RNA molecules that do not code for proteins. ncRNAs play a vital role in the pathogenesis of many cancers including ESCC by regulating gene expression at the transcriptional and post-transcriptional level. They are classified into three categories according to size such as (i) small ncRNAs with size of 15-30 nucleotides (nts) including small interfering RNAs (siRNAs), Piwi-interacting RNAs (piRNAs), microRNAs (miRNAs), and transcription initiation RNAs (ii) medium-

size ncRNAs with size of 30-200 nts and (iii) long ncRNAs (lncRNAs) with the length of 200 nts and more (Brosnan and Voinnet, 2009; Lin and Xu, 2015). Among all the ncRNAs, miRNA is one of the well-studied ncRNAs in different cancer including oesophageal cancer (Feber et al., 2011). It was reported that miRNAs are associated with the development, progression and prognosis of oesophageal cancers *via* their negative regulation of gene expression (Feber et al., 2011). Also, altered expression of miRNA modulates oncogenes and tumour suppressor genes expression by regulation of proliferation, apoptosis, motility and invasibility in gastrointestinal cancer including ESCC (Harada et al., 2016). It was observed that *miR-25, miR-151* and *miR-424* were up-regulated whereas *miR-29c, miR-99a* and *miR-100* were reduced in oesophageal cancer (Fassan et al., 2011). Another study by Guo et al stated that low levels of *miR-103/107* provide a strong correlation with high overall and disease-free survival periods for patients with ESCC (Guo et al., 2008). Expression levels of mature *miR-21* and mature *miR-145* were significantly higher in ESCC when compared to the normal epithelium and were significantly linked with lymph node positive, recurrence and metastasis in ESCC (Akagi et al., 2011; Kano et al., 2010; Maru et al., 2009). Like protein-coding genes, promoter hypermethylation of miRNAs exhibited a greater role in the regulation of *miRNA* in cancers. For instance, *miR-375, miR-34a, miR-34b/c* and *miR-129-2* were down-regulated by hypermethylation in oesophageal cancer (Chen et al., 2012; Li et al., 2011). In recent years, it is evident that long non-coding RNAs play a significant role in the pathogenesis of ESCC by regulating gene expression (Lin and Xu, 2015). For example, *HOTAIR* was overexpressed in ESCC which was correlated to the advanced pathological stage and poorer prognosis with the patients with ESCC (Chen et al., 2013).

## 2.4 *FAM134B (JK1)* gene

### 2.4.1 Introduction of *FAM134B* gene

*FAM134B* (*Family With Sequence Similarity 134, Member B*) also known as *JK1* is a novel protein-coding gene which is placed at 5p15.1 chromosome downstream to δ-catenin (Tang et al., 2007). This gene encodes a cis-Golgi transmembrane protein that may be necessary for the long-term survival of nociceptive and autonomic ganglion neurons (Kurth et al., 2009). Recent studies suggest that *FAM134B* is a growth-related gene which executes a significant role in cancer pathogenesis (Tang et al., 2007; Kasem et al., 2014b). However, much of the molecular biology and functional study of it are still need to be understood.

### 2.4.2 *FAM134B* gene location

The *FAM134B* gene is situated on the short (p) arm of chromosome 5 at position 15.1, from base pair 16,473,146 to base pair 16,617,117 on chromosome 5. It is sited 3' downstream to the delta-catenin gene (*CTNND2*; 604275). The gene location is illustrated in Figure 6. Alternative given names for the gene are *FLJ20152*, *FLJ22155*, *FLJ22179* and *HSAN2B* (www.genecards.org).

### 2.4.3 Gene description of *FAM134B*

*FAM134B* gene belongs to a family of 3 genes, namely *FAM134A*, *FAM134B* and *FAM134C*. All the 3 genes are protein coding. The gene has 2 isoforms formed by alternative splicing. All earlier studies on *FAM134B* refer to isoform 1 which represents the longer transcript (3234 base pairs compared to the length of 3083 from isoform 2) and encodes the longer isoform (Kurth et al., 2009). The gene comprises 9 exons, has a start and end codon and encodes a 497-amino acid, 54681 Dalton proteins with 2 hydrophobic long segments, in addition to a C-terminal coiled-coil domain. FAM134B protein isoform 2 differs in the 5' UTR coding sequence compared to variant 1 (http://ghr.nlm.nih.gov). The resulting isoform 2 has a shorter (356 amino acids) and distinct N-terminus compared to isoform 1. There is 1-141 amino-acid missing and substitution of 142-152: RGAQLWRSLSE → MPEGEDFGPGK) (Kurth et al., 2009).

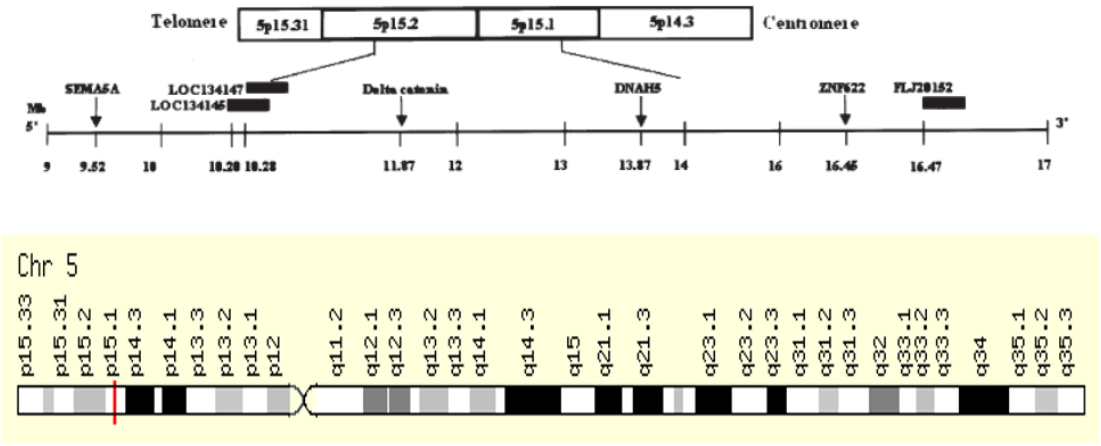


**Figure 6. The upper image shows the position of *JK1* (*FAM134B*) gene in relation to delta-catenin. The image below it illustrates the gene's location in relation to the chromosome 5.**

### 2.4.4 FAM134B in Human tissues

FAM134B is expressed in many human normal tissues including esophageal and gastrointestinal organs (Figure 7). The highest FAM134B expression is found in brain, kidney,hypothalamus, pancreas, lung, hippocampus, pooled germ cell tumours. Precise role and function of FAM134B in human cancer still remain unclear (Kurth et al., 2009).

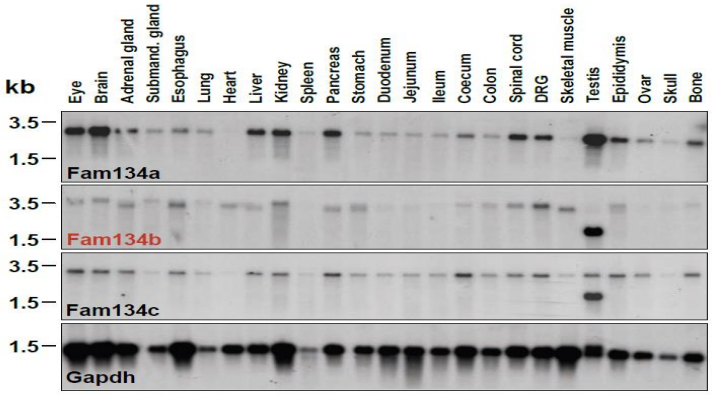


**Figure 7. Expression of the *FAM134B* gene family, Kurth *et al*., 2009**

### 2.4.5 *FAM134B* gene and Mutation

Kurth and colleagues in 2009 stated that the human FAM134B protein contains 497 amino acids (Kurth et al., 2009). Structure analysis showed that the N-terminal half of FAM134B has 2 unusually long hydrophobic segments of about 35 amino acids each that are separated by a hydrophilic loop of about 60 amino acids. This structure is similar to that of reticulon proteins that shape the curvature of endoplasmic reticulum membranes. The C-terminus of FAM134B contains a coiled-coil domain. Northern blot analysis of adult mouse tissues detected at least 4 JK1 transcripts. High expression of an approximately 1.5-kb transcript was detected in testis only. Transcripts of about 3.5 kb were more weakly expressed in dorsal root ganglia, oesophagus, skeletal muscle, and kidney, and many other tissues showed much weaker FAM134B expression. In situ hybridization of day-14.5 mouse embryos showed prominent staining of sensory and autonomic ganglia. In cultured mouse dorsal root ganglia, FAM134B colocalised with a cis-Golgi marker and partly colocalized with a trans-Golgi marker (Kurth et al., 2009). Loss-of-function mutations in *FAM134B* are the cause of hereditary sensory and autonomic neuropathy type 2B (HSAN2B). The onset of hereditary sensory and autonomic neuropathy type II (HSANII) in a Somalian family occurred due to a homozygous nonsense mutation in FAM134B (Murphy et al., 2012). The similar finding reported in a Saudi-Arabian family (Kurth et al., 2009). The mechanism by which mutations in *FAM134B* cause HSNII is unknown. They suggested that a structural change in the Golgi apparatus may occur affecting trafficking of neurotrophins which are critical for the survival of sensory and autonomic ganglia neurones. They also reported that considerable motor involvement rather that autonomic involvement in the patient providing further evidence for the pathogenicity of mutations in *FAM134B*. Kong et al. showed that *FAM134B* and *tumour necrosis factor receptor* superfamily member 19 have a strong synergistic effect in exposure to vascular dementia (Kong et al., 2011).

It indicates that *FAM134B* is associated with the different complex network of the biological system. Another study by Scheubert et al. reported that *FAM134B* is the best biomarker for pluripotent stem cells using a wrapper of genetic algorithm and support vector machine (GA/SVM) approach (Scheubert et al., 2011). They mentioned that the sets of pluripotency markers returned by the GA include the *FAM134B* gene in 35% of the selected gene sets (174 times out of 500) making it the most important feature for selection marker. In the neural context, Golgi-mediated processing and/or transport of neurotrophin precursors and their receptors may be impaired as FAM134B mutation produces new cis-Golgi-protein. In the Embryonic Stem cell perspective, *FAM134B* mutation can lead to Golgi-mediated post-translational processing (glycosylation, methylation etc.) and/or transport of two markers of unknown function in pluripotency, SSEA1 (stage-specific embryonic antigen 1) and AP (alkaline phosphatase) may be impaired since both of these protein localised in the Golgi-apparatus. Davidson et al., (2012) also reported a homozygous nonsense mutation in *FAM134B* (p.Gln145X), in an in a UK cohort patient with HSAN II (Davidson et al., 2012). Another study also found *FAM134B* mutation in the patients of HSAN II with spasticity (Ilgaz et al., 2013). These results represent that *FAM134B* genetic alteration linked to the pathogenesis of neurodegenerative disease. Melchiotti et al. exhibited that *FAM134B* up-regulation is connected with allergic rhinitis patients. An up-regulation of *FAM134B* gene expression at mRNA level is occurred by exposure of monocytes to extracellular ATP (Melchiotti et al., 2014). Extracellular ATP is a pro-inflammatory molecule released by damaged cells and regulatory T cell. It can suppress inflammation by hydrolysis these molecules through the production of ecto-nucleoside triphosphate diphosphohydrolase1 (known as CD39). This study also revealed a negative correlation of CD39 expression with FAM134B expression in whole blood from their cohort analysis (Melchiotti et al., 2014). By this way, the FAM134B molecule may likely to play a key role in host immune protection and inflammatory responses. So, the FAM134B protein could potentially be involved in vesicle trafficking as it is located in the cis-Golgi compartment and may also influence cytokine secretion by monocytes in response to external stimuli including ATP.

### 2.4.6 *FAM134B* in colon cancers

In colorectal cancer, we have reported that *FAM134B* is a growth related gene which acts as a driver player in the cancer progression via presenting its tumour suppressor properties (Kasem et al., 2014a; Kasem et al., 2014b; Kasem et al., 2014c; Islam et al., 2016). It was reported that *FAM134B* DNA copy number deletion was noted in 57% patients with colorectal cancer while compared to non-neoplastic tissue (Kasem

et al., 2014a). Lower copy number were also associated with the advanced pathological staging (TNM) of the colorectal adenocarcinomas (Kasem et al., 2014a). Also, more DNA copy number amplification of *JK-1* gene was found in adenomas when compared to non-tumor tissues and cancers (Figure 8). So, *FAM134B* copy number alterations were found as a frequent incident in colorectal adenoma and adenocarcinoma (Kasem et al., 2014a). Survival analysis by the authors also suggested that lower survival rates were found in patients with copy number deletion when compared to patients with amplification or no change in DNA copy numbers (Kasem et al., 2014a).

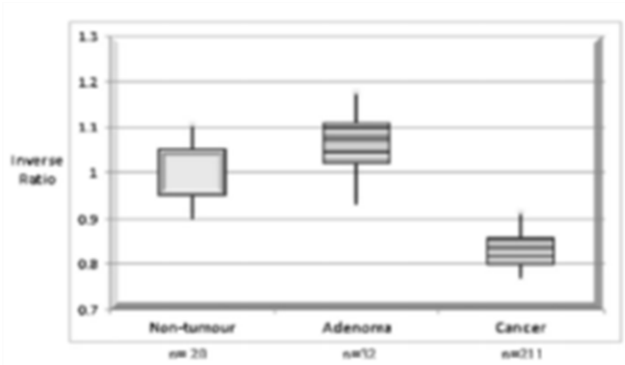


**Figure 8. *JK1* amplification levels in different colorectal tissues.** Lower level of amplification ratio (shown as inverse ratio) was obtained for cancer samples compared to the colorectal adenoma or non-cancer samples ($p$=0.029), Kasem *et al*., 2014a

Our group have also examined the mRNA expression of *FAM134B* on a large number of tissue samples from patients with colorectal tumours. The results showed that mRNA was notably lower in colorectal cancer than in normal and benign tumour groups (Kasem and Lam, 2010). Significantly lower levels of *FAM134B* mRNA expression was reported in colon cancer cell line when compared to non cancer colonic epithelial cell line (Kasem et al., 2014b).

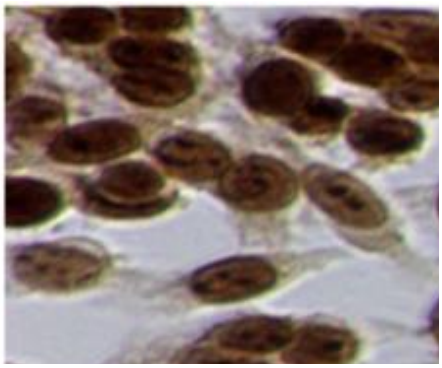

**Figure 9. Immunocytochemistry for JK1 protein in colon cancer cell line (SW480).** The sub cellular localization of JK1 protein is highlighted by the strong nuclear staining. **Kasem *et al*., 2014c**

The low expression levels of *FAM134B* implies that *FAM134B* acts as a tumour suppressor gene in colorectal adenocarcinoma (Kasem et al., 2014c). It was also reported that FAM134B protein expression was significantly underexpressed in comparison to non-neoplastic tissues and colorectal adenoma via immunocytochemistry and immunohistochemistry ( Figure 9 and 10) (Kasem et al., 2014b). A functional study by our team suggested that *FAM134B* inhibits the invasion and migration of colon cancer cells (Kasem et al., 2014c). The findings to date indicate that *FAM134B* play an important role in the pathogenesis of colorectal adenocarcinoma. Furthermore, the stage-dependent expression of FAM134B in colorectal cancer has been recently reported and it suppresses the growth and proliferation of colon cancer in vivo and in-vitro (Islam et al., 2016). A more recent study reported the novel mutations of FAM134B in colorectal cancer which was significantly associated with several clinical and pathological parameters (Islam et al., 2017).

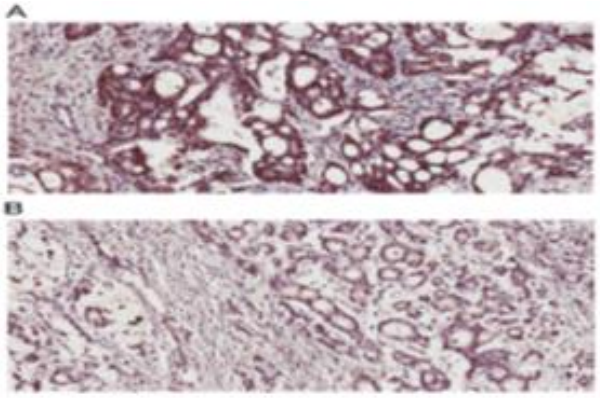


**Figure 10. JK1 protein staining on immunohistochemistry across different grades of colorectal cancer.** A. Strong nuclear staining was noted in well /moderately differentiated ADC. B. Weak nuclear staining was noted in poorly differentiated (mucinous) adenocarcinoma. **Kasem *et al*., 2014c**

### 2.4.7 *FAM134B* in oesophageal squamous cell carcinoma

The genes in the p-arm region of chromosome 5 play crucial roles in the pathogenesis of ESCC. In the early investigation, our group discovered several novel genes in chromosome 5p by inter-simple sequence repeat PCR, a DNA fingerprinting approach (Tang et al., 2001). Also, chromosomal gains in chromosome 5p were noted in approximately 50% of the ESCC patients *via* comparative genomic hybridization (Kwong et al., 2004). By searching a region of chromosome 5p amplified in ESCC in a Chinese population, Tang et al. 2007 identified *JK1* also known as *FAM134B*. The deduced 39.3-kD protein has an EGF-like domain, 3 N-glycosylation sites, 3 N-myristoylation sites, and numerous possible phosphorylation sites. It was reported that JK1 was overexpressed in a significant number of ESCC cell lines and tumours compared with normal

oesophageal cells and tissues by multiplex RT-PCR (Figure 11) (Tang et al., 2007). Overexpression of JK1 in NIH-3T3 mouse fibroblasts and HEK293 cells caused an increase in growth rate, colony formation in soft agar, and foci formation in confluent cultures. In vivo study revealed that high-grade sarcomas were formed in athymic nude mice following subcutaneous injection of JK1 overexpressing NIH-3T3 cells (Tang et al., 2007).

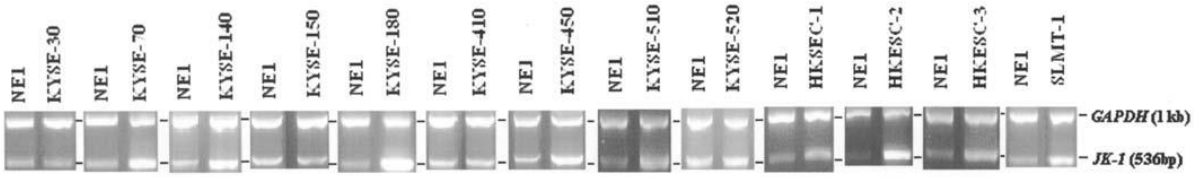


**Figure 11. Multiplex RT-PCR analysis for FAM134B expression in ESCC cell lines and NE1, a non-tumour epithelial cell line.** GAPDH expression was used as an internal control. ESCC cell lines of KYSE 70, 140, 180, 450, 510, HKESC-1, HKESC-2, HKESC-3 and SLMT-1 showed overexpression of JK1, while KYSE 30, 150, 410 and 520 showed underexpression.

## 2.5 Detection of genetic and epigenetic biomarkers

### 2.5.1 Optical strategies for detection of genetic and epigenetic biomarkers

Over the last few decades, a large number of optical techniques have been extensively developed for the analysis of various cancer associated genetic (e.g., gene mutations) and epigenetic biomarkers (e.g., DNA methylation, non-coding RNAs etc.) (Carrascosa et al., 2016; Islam et al., 2017). These techniques are mostly confined to fluorescence, surface plasmon resonance (SPR), Raman spectroscopy, electrochemiluminescence and colorimetric readouts (Islam et al., 2017).

Fluorescence resonance energy transfer (FRET) is the most commonly used fluorescence method for the detection of cancer biomarkers. In FRET, when a donor chromophore is in an excited state, it can transfers energy to an acceptor chromophore through the non-radiative process, resulting in a change in the fluorescence intensity. The electronic energy transfer between chromophores is the result of the dipole-dipole interactions between a donor and an acceptor chromophore, where the FRET intensity is inversely proportional to the sixth power of the distance between donor and acceptor (Freeman and Willner 2012). When donors are excited, energy is transferred to the acceptor molecules which result in a significant fluorescence amplification enabling the detection. Over the past several years, several FRET techniques for DNA methylation analysis have been developed where different types of chromophore including cationic conjugated polymers (CCPs) (Feng et al., 2008) quantum dots (QDs) (Ma et al., 2016) and up-conversion nanoparticles (UCNPs) (Kim et al., 2016a) were used. Apart from the epigenetic biomarker screening, FRET has also been widely used to interrogate genetic

biomarkers (Shi et al., 2015). For instance, Kitano et al. (Kitano et al., 2011) developed a method referred to as fluorescence resonance energy transfer-based preferential homoduplex formation assay (FRET-PHFA) for detecting somatic mutations. FRET-PHFA method enabled the rapid (15 min) identification of multiallelic *KRAS* mutations in codons 12 and 13 with high sensitivity and reproducibility.

SPR is considered as one of the effective optical detection approaches due to its unique capability of real-time and label-free monitoring of disease-related biomolecules. Upon adsorption of the biomolecules on the metallic sensor surface of SPR, it can specifically analyse the binding event of biomarkers in real time (Homola 2008). Depending on the presence of target molecules on the metallic SPR sensor, the refractive index of the metal substrate changes allowing the detection (Homola 2008; Sipova et al., 2010). In recent years, diverse type of SPR based DNA methylation detection approaches has been introduced (Pan et al., 2010; Sina et al., 2014a). In these appraoches, either an SPR sensor surface bound capture probes specific for methylated target region or methylation specific recognition elements (e.g., MBD protein or 5mC antibody) have been used to recognise the methylation sites (Pan et al., 2010). However, the direct detection of methylated DNA by SPR has also been reported which avoids any type of capture or recognition elements as evident by the method developed by Sina et al. (Sina et al., 2014a). In this assay, methylated DNA is directly adsorbed on the SPR sensor surface which results in a measurable refractive index changes compared to that of the unmethylated control. Bisulfite-treated methylated and unmethylated DNA sequences possess a distinct level of adsorption pattern on the gold surface of SPR sensor due to the different affinity interaction of DNA bases towards gold, which facilitates distinguishable refractive index changes in methylated and unmethylated DNA. Similarly, SPR has also been used to design several novel biosensors for the detection of gene mutations (Fiche et al., 2008; Jiang et al., 2005).

Other optical methods such as Raman spectroscopy especially surface-enhanced Raman scattering (SERS), elecelectrochemiluminescence (ECL) and colorimetric readouts have been extensively used for identification of various genetic and epigenetic biomarkers (Ge et al., 2012; Hu and Zhang 2012; Kim et al., 2016b; Kurita et al., 2012; Li et al., 2005; Zhu et al., 2004). Although the recent developments in imaging processing technologies have led to the development of many integrated optical biosensors for the quantification and detection of biomarkers, most of the methods rely on complex and expensive instrumentations (Islam et al., 2017). Despite the high analytical performance of optical sensors compared to the conventional biomarker detection methods, portable,

easy to use and inexpensive methods are still required to be developed for biomarker analysis. In this regard, electrochemical methods offer relatively inexpensive and simple platform for biomarker detection and analysis. Electrochemistry is a surface bound technique, which mainly relays an interaction between the surface and target analyte either directly or through a mediator, and it requires very small sample volumes can be used for measurement (Labib et al., 2016). Additionally, electrochemical methods are highly amenable to miniaturisation and have the potential to be multiplexed.

### 2.5.2 Electrochemical detection techniques

In electrochemical methods, target biomolecules can be detected by converting the biological event to an easily processed electronic signal (D'Orazio 2003; Ronkainen et al., 2010). Over the past several decades, many electrochemical sensing approaches have been widely developed to interrogate clinically relevant biomolecules (Grieshaber et al., 2008; Labib et al., 2016). In electrochemical detection, a variety of recognition elements (e.g. antibodies, enzymes, oligonucleotide probes etc.) are used to interact with the target to selectively recognise the biomarker. Then, an electroactive signal transducer is incorporated in the sensor to obtain a measurable electrochemical signal (Figure 12). This signal obtained could be the amount of current measured as a function of time via amperometric (e.g., chronoamperommetry) and voltammetric techniques (i.e., cyclic voltammetry (CV), linear sweep voltammetry, differential pulse voltammetry (DPV), square wave voltammetry (SWV) and stripping voltammetry). The measurable amount of charge accumulation or potential as a function of time can also be obtained as an electrochemical signal in different potentiometric and coulometry (e.g., chronocoumometry) methods (Chaubey and Malhotra 2002).

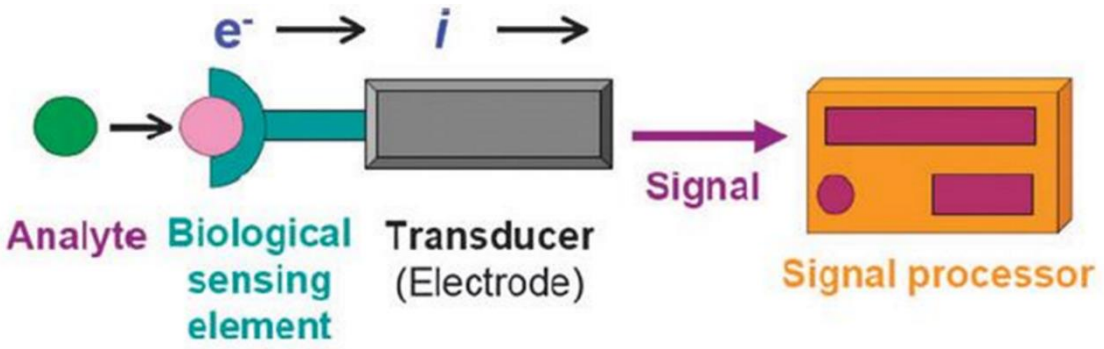


**Figure 12. Schematic presentation of a biosensor with electrochemical transducer**.

## Amperometry

Amperometric biosensors generally measure the current changes, resulting from the redox process (biochemical reaction) of an electroactive species on the electrode (working) surface (Thevenot et al., 2001). A number of current changes is directly proportional to the concentration of the target analyte which facilitates the quantitative detection of biolchemical events (Chaubey and Malhotra, 2002). The most notable examples of amperometric sensors are glucose biosensor (based on the detection of hydrogen peroxide) and pregnancy kit (amperometry works in combination with immunue sensors for measuring the levels of the human chorionic gonadotropin subunit) (Grieshaber et al., 2008).

**Chronoamperometry** is one of the widely used amperometric techniques, where a potential is stepped to the working electrode for calculating the steady state current with respect to time (Grieshaber et al., 2008). Current changes are occurred due to the oxidation or reduction of the diffusion layer at the electrode. The longer the electrode remains at this reducing potential, the region away from electrodes gains more variable concentration creating an area which is known as the *diffusion layer*. Diffusion layer, which is the region near electrodes having different concentrations of the analyte compared to the bulk solution, was first introduced by Nernst which confirms the presence of a stationary thin layer of solution in the vicinity of the electrode surface. The local analyte concentration thereby reduced to zero at the electrode surface and as per the concept of the diffusion layer, analytes in the bulk solution gain higher concentration to the electrode resulting in a concentration gradient away from the electrode surface. In the bulk solution, the concentration of the analyte is sustained at a value of $C_0$ by convective transfer (Figure 13).

**Chronoamperometry** readout consists of either a single potential step (current results only from the forward step) or double potential step (potential is returned to a final point after a given time). The principle of this technique can be described by the Cottrell equation (Nahir and Buck, 1992) (Equation 1), which defines the observed current (planar electrode) at any time following a large forward potential step in a reversible redox reaction (or too large overpotential) as a function of $t^{-1/2}$

$$i_t = \frac{nFAC_0D_0^{1/2}}{\pi^{1/2}t^{1/2}} \quad \ldots\ldots\ldots (1)$$

Here, $n$ = stoichiometric number of electrons involved in the reaction; $F$ = Faraday's constant (96,485 C/equivalent), $A$ = electrode area (cm2), $C_0$ = concentration of analytes (mol/cm$^3$), and $D_0$ = diffusion coefficient (cm$^2$/s).

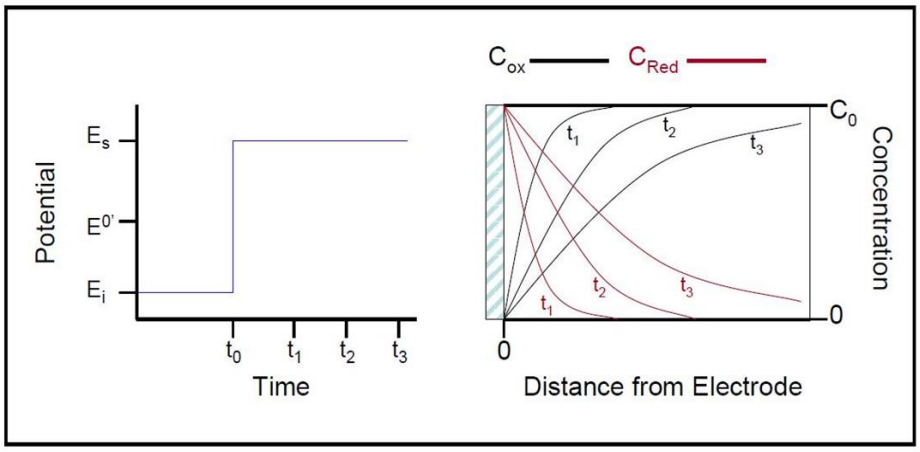


**Figure 13 Schematic presentation of Chronoamperometry**, Bard and Faulkner, 1980.

Amperometric detection is highly suitable for biocatalytic and affinity sensors as it offers very low detection limit (Halsall and Heineman, 1990). Additionally, the constant potential during the detection results in a negligible charging current thereby reducing the background signal (Ronkainen et al., 2010).

**Voltammetry**

As discussed in the previous section, in amperometry a constant potential is maintained while measuring the current, however, in voltammetric technique, the current readout is observed where the potential varies in a definite manner (Grieshaber et al., 2008; Ronkainen et al., 2010). The current measured describes the diffusion of analytes from the solution to the electrode for further oxidation or reduction where the current obtained is linearly proportional to the concentration of target analyte (Grieshaber et al., 2008). Since the potential of the voltametric sensor can be changed in different ways, there are also many reported forms of voltammetry such as differential pulse voltammetry, square-wave voltammetry, linear sweep voltammetry, cyclic voltammetry, hydrodynamic voltammetry, polarography, and stripping voltammetry (Ronkainen et al., 2010).

**Cyclic voltammetry (CV)** is the most widely used forms in voltametric sensors where the potential is scanned between two values (i.e., V1, V2) at a fixed rate. When the voltage reaches V2, the potential scan is reversed back to V1, as shown in Figure 18 (Grieshaber et al., 2008). The scan rate of CV is crucial as the adequate duration of a scan is required to facilitate the chemical reaction to occur. The voltage is measured between the reference and working electrode whereas the current is calculated between the working and counter electrode. The readout is plotted as current *vs.* voltage which is known as voltammogram (Figure 14).

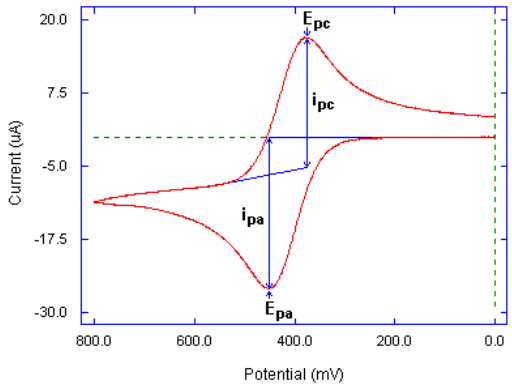


**Figure 14.** A typical cyclic voltammogram recorded for a reversible one electron transfer reaction.

In a cyclic voltammogram, the important parameters are the peak potentials (*E*pc, *E*pa) and peak currents (*i*pc, *i*pa) of the cathodic and anodic peaks, respectively. If the electron transfer process is fast compared with other processes (such as diffusion), the reaction is said to be electrochemically reversible, and the peak separation is

$$\Delta Ep = | Epa - Epc | = 2.303 \frac{RT}{nF} \dots\dots\dots\dots\dots\dots\dots (2)$$

The formal reduction potential ($E^o$) for a reversible couple is given by

$$E^o = \frac{Epc + Epa}{2} \dots\dots\dots\dots\dots\dots\dots\dots\dots\dots\dots\dots\dots\dots (3)$$

In linear Sweep Voltammetry (LSV), the observed peak current, ip, for a reversible electron transfer is given by the Randles-Sevcik equation,

$$i_p = (2.69\text{x}10^5)\, n^{\frac{3}{2}} \text{A}\, \text{D}^{\frac{1}{2}} \text{Ci}\, v^{\frac{1}{2}} \dots\dots\dots\dots\dots\dots\dots (4)$$

It should be mentioned that in CV both faradaic and non-faradaic processes take place while in **Differential pulse voltammetry,** the charging current resulted in non-faradaic process is minimized making them one of the highly sensitive voltametric techniques. DPV involves a range of successive pulses of voltage superimposed on the potential linear sweep or stairsteps. The current is measured instantly before each potential step, and the current changes are plotted as a function of potential to enable the detection (Aoki et al., 1984; Lovrić and Osteryoung, 1982) (Fig. 15).

However, when the equivalent time is used at the potential of the ramped baseline and superimposed pulse, the pulse voltammetry is known as **square wave voltammetry (SWV)** (Chen and Shah, 2013). Gupta et al. stated that the sensitivity of SWV is relatively

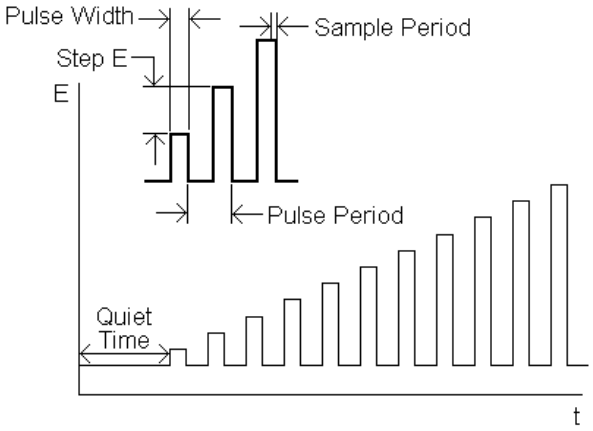


**Figure 15.** Schematic diagram of a potential wave form for normal pulse voltammetry, Bard and Faulkner, 1980.

better than that of DPV (Gupta et al. 2011). In their study, 4 times higher SWV peak current was observed than that of DPV. The principle of SWV has been shown in figure 16. SWV possesses staircase potential ramp combined with square-shaped potential pulses (Figure 16A) while the potential cycle composed of two neighbouring pulses (Figure 1B). The SW amplitude is the height of the pulses ( *E*sw) and the SW frequency (*f*), defined as $f = 1/t$, where t is the duration of a potential cycle. In terms of the duration of the single potential pulse *t*p (t = 2*t*p), the frequency could be defined as $f = 1/(2t\text{p})$. The potential cycle is repeated at each step of the staircase ramp with a forward and reverse pulse.

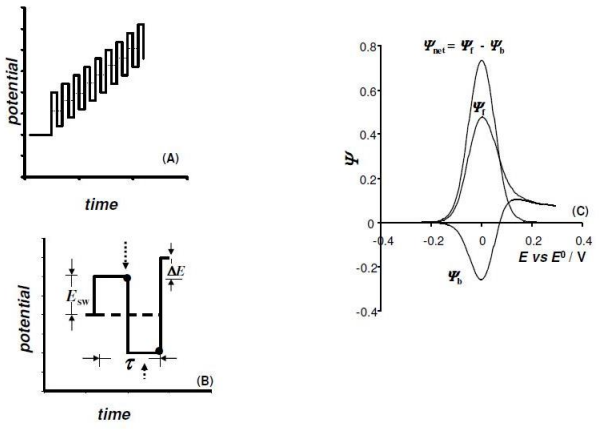


**Figure 16.** (A) A typical potential waveform, (B) one potential cycle, and (C) a typical voltammogram in SWV, Bard and Faulkner, 1980.

SWV biosensors offer high selectivity and sensitivity and thus have been extensively used to develop a biosensor for numerous genetic and epigenetic biomarkers (Chen and Shah, 2013).

In another electrochemical technique, **chronocoulometry (CC)**, the total charge (Q) transfer following a potential step is measured as a function of time. Q is obtained by from the integration of the current, i, during the potential step. For a diffusion only standard electrochemical system, measured Q upon a potential step towards more negative of the can be explained by the Anson equation;

$$Q_r = \frac{2nFAC_0D_0^{1/2}}{\pi^{1/2}}\left[\tau^{1/2} + (t-\tau)^{1/2} - t^{1/2}\right] \ldots\ldots\ldots\ldots (5)$$

Figure 17 depicts the chronocoulometry experiment with a double potential step. Compared to the amperometric and voltametric approaches where the current is measured as the readout signal, The most obvious advantage of recording CC is the improvements of signal-to-noise ratio. Additionally, the enhanced signal observed in CC also can explain the kinetics of chemical reactions following electron transfer.

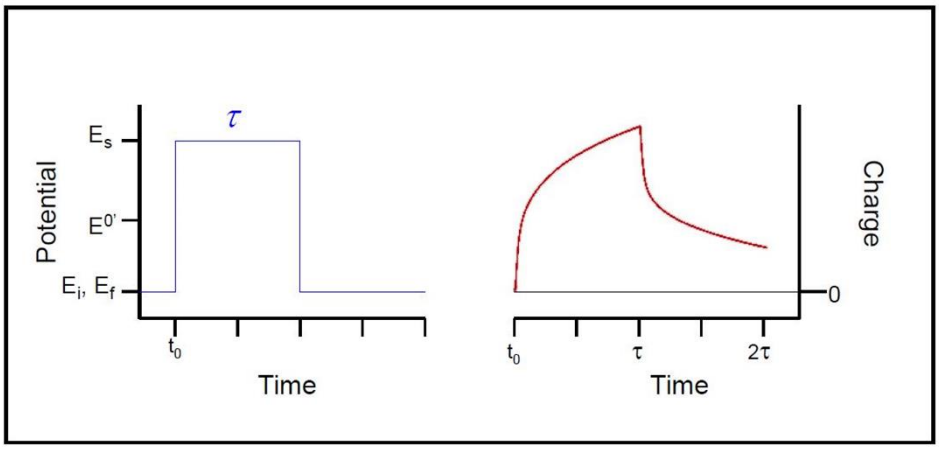


**Figure 17.** A typical potential wave form and charge-time response for a double-potential step for chronocoulometry, Bard and Faulkner, 1980.

## DNA-gold affinity interaction for biosensing

Over the past several decades, an impressive number of biosensing approaches based on coupling DNA receptors onto gold surfaces have been developed (Drummond et al., 2003; Song et al., 2008). In these biosensors, the gold sensor surface is coupled with selective DNA probes for designing the biorecognition and transduction layers to capture and detect the varying number of targets including disease-associated DNA, RNA, proteins, and other biomolecules (Song et al., 2008). Generally, covalent surface chemistries such as gold-thiol interactions have been employed to attach the DNA probes with the gold surfaces (Mirkin et al., 1996; Steel et al., 2000). In the past decades, intense attention was given to avoid the underlying complex chemistry (e.g., gold thiol interaction) involved in DNA-gold sensors and to develop the easiest way to directly

adsorb DNA on the gold surfaces (Koo et al., 2015). In that time, it was a common perception that the direct adsorption of native DNA onto the gold surface is theoretically not possible as it is 'complex', 'non-specific' and 'difficult to control' (Koo et al., 2015; Lao et al., 2005). However, over the past 15 years, there was an exemplary development in the field of DNA-gold direct interaction by the Mirkin (Demers et al., 2002; Ostblom et al., 2005), Tarlov (Kimura-Suda et al., 2003; Opdahl et al., 2007), and Rothberg (Nelson and Rothberg, 2011) research group. Several fundamental studies from these groups showed that DNA-gold interactions can be tuned for specific and controlled adsorption which further indicated that the adsorption of DNA onto gold happens in a sequence dependent manner follows a definite adsorption trend of adenine (A) > cytosine (C) > guanine (G) > thymine (T) (Fig. 18) (Kimura-Suda et al. 2003; Koo et al. 2015). Till then, the distinct affinity interactions of DNA bases towards gold have been used as an advantage to develop a number of cost-effective and exceptionally simplified biosensors (via avoiding underlying complicated chemistries of attaching DNA to gold surface) including electrochemical and colorimetric sensors (Hossain et al. 2017; Li and Rothberg 2004a; Islam et al. 2017; Opdahl et al. 2007; Zhang et al. 2012; Zhang et al. 2013).

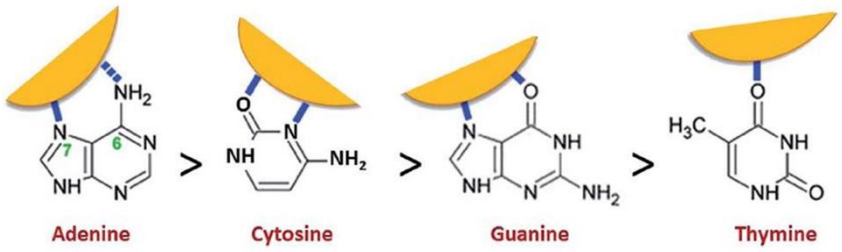


**Figure 18.** The relative affinities of DNA nucleobases towards gold surface follow the trend A> C> G> T.

The affinity interaction between DNA and gold is finely controlled by various interrelated non-covalent forces (e.g., electrostatic interactions, hydrophobic forces etc) and factors (e.g., sequence-dependency and DNA conformation) (Koo et al., 2015). The underlying principles of the DNA-gold affinity interaction and the interplays between the associated influencing factors are crucial for the development of suitable DNA-gold based biosensors. It has also been well understood that these factors are commonly influenced by external conditions including pH, time and buffer composition (Koo et al., 2015). The most important non-covalent force involved here is the electrostatic interactions between DNA and gold. This is due to the fact that, electrostatic repulsion occurs between negatively charged phosphate backbones of DNA and positively charged gold surfaces especially gold nanoparticles (AuNPs) (Koo et al., 2015). Therefore, to attain the

successful adsorption of DNA onto the gold surfaces, the experimental conditions such as pH and salt concentrations in the electrolytes should be optimized in such way that the adsorption process can overcome the repulsive forces between oppositely charged DNA and gold. In addition to the electrostatic forces, hydrophobic forces can also influence the DNA-gold interactions (Nelson and Rothberg 2011).

Tarlov and colleagues (Steel et al. 1998) were the first to provide the empirical evidence of the affinity interaction of DNA and gold. They detected the lower affinity of dT-rich oligonucleotide onto gold surface compared to random DNA sequences and thereby hypothesised the possibility of sequence dependent adsorption DNA onto a gold surface. This observation was further confirmed by several studies from Mirkin and co-workers (Demers et al. 2000; Storhoff et al. 2002). They have also proposed a specific affinity trends of DNA bases (guanine (G) > adenine (A) > cytosine (C) > thymine (T)) (Demers et al. 2002; Ostblom et al. 2005). However, in 2003, this observation was contested by a landmark study developed by Kimura-Suda et al (Kimura-Suda et al. 2003) and a very different type of adsorption trend of A > C $ G > T was demonstrated (Fig). This specific sequence dependent trend was confirmed by a series of further studies using both planar gold surfaces (Koo et al. 2014; Opdahl et al. 2007; Sina et al. 2014a; Sina et al. 2014b) and AuNPs systems (Zhang et al. 2012; Zhang et al. 2013).

**Applications of DNA-gold affinity in electrochemical detection**

Typical DNA biosensors rely on the immobilisation of thiol-modified ssDNA probes on the sensor surface (i.e. gold) to generate self-assembled monolayer for hybridizing the specific sequences of biomarkers (Drummond et al. 2003). However, development of thiol-modified ssDNA capture probes along with various sensor fabrication steps increase the complexity and cost of the assay. Since DNA–gold interaction maintained specific sequence-dependency under optimised conditions, it has the high potential for the direct detection of biomolecules *via* adsorbing unmodified DNA on the gold surfaces. This could avoid the complicated surface chemistry involved in the surface modification of the electrode while developing relatively inexpensive, rapid and simple alternative for biosensing (Hossain et al. 2017). Consequently, base-dependent DNA adsorption has been found to be an effective way to control the immobilization of unmodified DNA probes onto gold surfaces. This definite trend of nucleobases adsorption on gold can be used to distinguish two different DNA sequences (e.g., bisulfite-treated methylated and unmethylated DNA sequences, mutations). Until recently, very few methods have been reportedly developed for DNA methylation detection using this phenomen (Koo et al. 2014; Sina et al. 2014b).

To the best of our knowledge, Sina et al. (2014b) reported the first demonstration of an electrochemical method (referred to as eMethylsorb) for 5mC quantification that is based on the different affinity interactions between DNA bases and unmodified gold electrodes (Figure 19). In eMethylsorb, initial bisulfite treatment of extracted DNA converts unmethylated cytosines into uracils but methylated cytosine remains unchanged. Subsequent asymmetric PCR amplification steps convert uracils of antisense strands into adenines whereas guanines are generated from mC and C. Thus the target methylated DNAs become guanine-enriched leaving the unmethylated samples adenine-enriched. These base differences in the methylated and unmethylated DNA sequences result in two distinct adsorption behaviour towards gold.

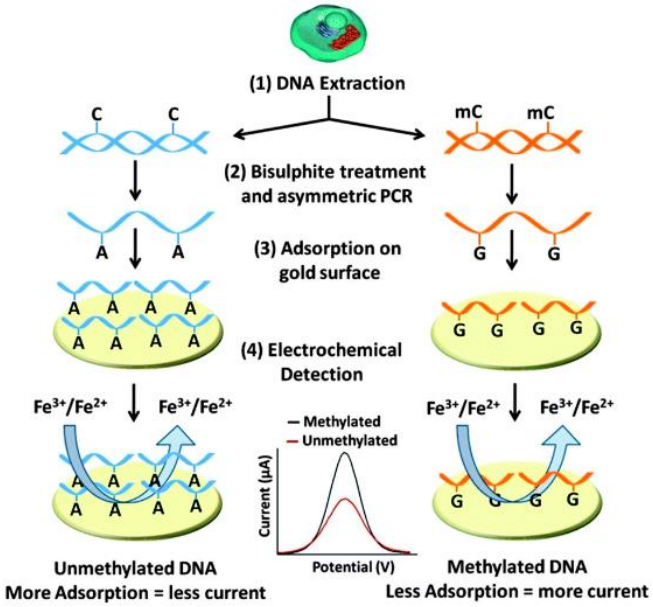


**Figure 19.** Schematic representation of the eMethylsorb approach for DNA methylation detection. As DNA-gold affinity interaction follows the trend, A> C> G> T, the adenine-enriched unmethylated DNA adsorbed more on the electrode compared to the guanine-enriched methylated DNA. Due to the strong coulombic repulsion between $[Fe(CN)6]^{3-}$ ions and negatively charged adenine or guanine enriched DNA strands, a detectable amount of Faradaic current is produced. Sina et al. 2014b.

ssDNA- AuNPs adsorption has been used in many optical sensors for detecting single nucleotide polymorphisms (SNPs) or gene mutations (Li and Rothberg 2004a; Li and Rothberg 2004b). Among these methods, the colorimetric method involving the salt induced aggregation of AuNps is the most common and effective way to visualise the mutations (Li and Rothberg 2004a).

## Electrochemical detection of gene mutations

Gene mutations play an important role in multiple alterations in protein structure, expression levels and gene regulations in many diseases including cancer (Sidransky 2002). Increasing number of research has shown their active role diagnosis and prognosis of cancer (Greenman et al. 2007; Sidransky 2002). Over the past several years, many conventional methods mostly based on gene sequencing and optical readouts have been developed for the detection of mutations and single nucleotide polymorphisms (SNPs) alleles (Alioto et al. 2015; Grompe 1993). Despite their good performance, they are not always suitable for mutation screening in under-resourced settings due to the potential cost barrier of using sophisticated instruments and longer assay time. To meet the increasing demand for an alternative detection method, a number of electrochemical DNA sensors have been developed which are relatively inexpensive, rapid and sensitive (Boon et al. 2000; Drummond et al. 2003; Johnson et al. 2012; Kelley et al. 1999). In the past decade, Barton group has contributed significantly in the electrochemical biosensing of point mutations and DNA-base lesions based on unique DNA charge transfer phenomena (Boon et al. 2000; Kelley et al. 1999). Generally, in these methods, a mutation specific DNA probe is initially attached to the electrode surface *via* covalent conjugation or self-assembly monolayer formation. A redox-active label that attached either intercalatively to the hybridised target or covalently to the label is then used to detect and quantify the mutations. For instance, Boon et al (Boon et al. 2000) developed a DNA charge transport based mutation detection method using the redox active methylene blue. In this method, gold electrodes were initially modified with preassembled DNA duplexes for further monitoring electrocatalytic signal of methylene blue in the presence of $[Fe(CN)_6]^{3-}$. The presence of a mutation (base mismatch) or DNA damage considerably reduced the electrocatalytic signal. The applicability of the method was successfully tested to detect eight possible single-base DNA mismatches and mutation hotspots of p53 gene. The underlying principle of this assay is based on the catalytic charge transport through the DNA films where the electrons are transferred from the electrode surface to intercalated MB in a DNA-mediated reaction. When methylene blue is reduced to leucomethylene blue (LB), ferricyanide present in the solution is also reduced allowing more electron transport to methylene blue. This helps to maintain a continuous catalytic signal. However, when the target sequence is hybridised with surface bound capture probe, the double-stranded duplexes mutational sites, there is less number of methylene blue molecules are available for being electrochemically reduced resulting in a significant reduction in the catalytic signal.

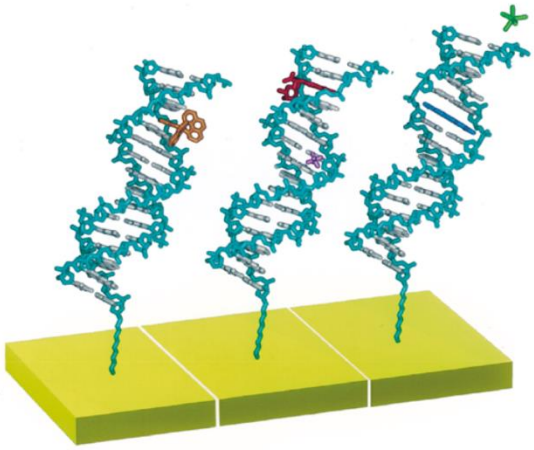

**Figure 20.** A typical representation of biosensor based on DNA duplexes (cyan and white) immobilized on a gold surface, Kelley et al. 1999

A similar type of method has also been developed by the group for a high-throughput screening of mutations (Kelley et al. 1999). The method employed various redox active indicators including Ir(bpy)(phen)(phi)3+ (orange), DM (red) and methylene blue (blue). Figure 20 shows that the groove-binder $Ru(NH_3)5Cl2+$ (purple) and $[Fe(CN)_6]^{4-}$(green) cannot bind the hybridized sequences on the electrode surface due to its negative charge. Since then, a range of electrochemical methods has been described for the sensitive and selective detection of mutations in duplex DNA (Cash et al. 2009; Wakai et al. 2004; Xiao et al. 2006). Despite such progress, a simple, rapid yet sensitive electrochemical sensor is still highly amenable for the routine mutation screening in resource-limited settings which can avoid the multistep fabrication of the sensors (i.e., the lack of a robust protocol for electrode modification). As discussed in the previous section, the specific trend of base-dependent affinity interaction (*i.e.*, adsorption) of DNA bases on the bare gold surface (i.e., A > C > G> T) can be a possible option to achieve this goal. This is due to the fact that mutated and unmutated (wild-type) DNA sequences have their distinct ability to interact with gold surfaces as a consequence of their different mutation status (different bases). Thus apart from the simplification of the sensor, the direct adsorption of DNA onto an unmodified gold electrode could also provide the accurate measurement of the adsorbed DNA onto an unmodified gold electrode for quantifying gene mutations.

## References

Ahn SH, Sawada H, Ro JY, Nicolson GL. Differential expression of annexin I in human mammary ductal epithelial cells in normal and benign and malignant breast tissues. Clin Exp Metastasis. 1997;15:151-156.

Akagi I, Miyashita M, Ishibashi O, Mishima T, Kikuchi K, Makino H, Nomura T, Hagiwara N, Uchida E, Takizawa T. Relationship between altered expression levels of MIR21, MIR143, MIR145, and MIR205 and clinicopathologic features of esophageal squamous cell carcinoma. Dis Esophagus. 2011;24:523-530.

Alioto TS, Buchhalter I, Derdak S, Hutter B, Eldridge MD, Hovig, E, et. al. A comprehensive assessment of somatic mutation detection in cancer using whole-genome sequencing. Nat.Commun. 2015; 6:10001.

Alonso MA, Millán J. The role of lipid rafts in signalling and membrane trafficking in T lymphocytes. J Cell Sci. 2001; 114:3957-3965.

Anayama T, Furihata M, Takeuchi T, Sonobe H, Sasaguri S, Matsumoto M, Ohtsuki Y. Insufficient effect of p27(KIP1) to inhibit cyclin D1 in human esophageal cancer in vitro. Int J Oncol. 2001;18:151-155.

Aoki K, Tokuda K, Matsuda H. Theory of differential pulse voltammetry at stationary planar electrodes. J. Electroanal. Chem. Interfacial Electrochem. 1984; 175(1):1-13.

Arakawa H. Netrin-1 and its receptors in tumorigenesis. Nature 2004;4:978-987.

Awerkiew S, Bollschweiler E, Metzger R, Schneider PM, Hölscher AH, Pfister H. Esophageal cancer in Germany is associated with Epstein–Barr-virus but not with papillomaviruses. Med Microbiol Immunol. 2003;192:137-140.

Bahl R, Arora S, Nath N, Mathur M, Shukla NK, Ralhan R. Novel polymorphism in p21(waf1/cip1) cyclin dependent kinase inhibitor gene: association with human esophageal cancer. Oncogene. 2000;19:323-328.

Barclay C, Li AW, Geldenhuys L, Baguma-Nibasheka M, Porter GA, Veugelers PJ, Murphy PR, Casson AG. Basic fibroblast growth factor (FGF-2) overexpression is a risk factor for esophageal cancer recurrence and reduced survival, which is ameliorated by coexpression of the FGF-2 antisense gene. Clin Cancer Res. 2005;11:7683-7691.

Bard, A. J. and Faulkner, L. R. *Electrochemical Methods.* New York: Wiley, 1980.

Baril P, Gangeswaran R, Mahon PC, Caulee K, Kocher HM, Harada T, Zhu M, Kalthoff H, Crnogorac-Jurcevic T, Lemoine NR. Periostin promotes invasiveness and resistance of pancreatic cancer cells to hypoxia-induced cell death: role of the beta4 integrin and the PI3k pathway. Oncogene. 2007;26:2082-2094.

Beardsmore DM, Verbeke CS, Davies CL, Guillou PJ, Clark GW. Apoptotic and proliferative indexes in esophageal cancer: predictors of response to neoadjuvant therapy [corrected]. J Gastrointest Surg. 2003;7:77-86.

Bednarek AK, Keck-Waggoner CL, Daniel RL, Laflin KJ, Bergsagel PL, Kiguchi K, Brenner AJ, Aldaz CM. WWOX, the FRA16D gene, behaves as a suppressor of tumor growth. Cancer Res. 2001;61:8068-8075.
Benassi B, Fanciulli M, Fiorentino F, Porrello A, Chiorino G, Loda M, Zupi G,Biroccio A. c-Myc phosphorylation is required for cellular response to oxidative stress. Mol Cell. 2006 ;21:509-519.

Bergqvist M, Brattstrom D, Brodin D, Lindkvist A, Dahlman-Wright K, Dreilich M, Wagenius G, Paulsson-Karlsson Y. Genes associated with telomerase activity levels in esophageal carcinoma cell lines. Dis Esophagus. 2006;19:20-23.

Bernard HU, Burk RD, Chen Z, van Doorslaer K, Hausen H, de Villiers EM: Classification of papillomaviruses (PVs) based on 189 PV types and proposal of taxonomic amendments. Virol. 2010;401:70-79.

Bi MX, Han WD, Lu SX. Using Lab On-line to Clone and Identify the Esophageal Cancer Related Gene 4. Sheng Wu Hua Xue Yu Sheng Wu Wu Li Xue Bao (Shanghai). 2001;33: 257-261.

Boon EM, Ceres DM, Drummond TG, Hill MG, Barton JK. Mutation detection by electrocatalysis at DNA-modified electrodes. Nat. Biotechnol. 2000; 18(10):1096-1100.

Brosnan CA, Voinnet O. The long and the short of noncoding RNAs. Curr Opin Cell Biol. 2009 Jun;21(3):416-425.

Carrascosa LG, Huertas CS, Lechuga LM. Prospects of optical biosensors for emerging label-free RNA analysis. Trends Analyt. Chem. 2016; 80:177-189.

Cash KJ, Heeger AJ, Plaxco KW, Xiao Y. Optimization of a Reusable, DNA Pseudoknot-Based Electrochemical Sensor for Sequence-Specific DNA Detection in Blood Serum. Anal. Chem. 2009; 81(2):656-661.

Chan KW, Lee PY, Lam AK, Law S, Wong J, Srivastava G. Clinical relevance of Fas expression in oesophageal squamous cell carcinoma. J Clin Pathol. 2006;59:101-104.

Chang F, Syrjanen S, Shen Q, et al. Evaluation of HPV, CMV, HSV and EBV in esophageal squamous cell carcinomas from a high-incidence area of China. Anticancer Res. 2000; 20:3935-3940.

Chattopadhyay I. A Brief overview of Genetics of Esophageal Squamous Cell Carcinoma. J Cell Sci Molecul Biol. 2014;1:103.

Chaubey A, Malhotra BD. Mediated biosensors. Biosens. Bioelectron. 2002;17(6-7):441-456.

Chen A, Shah B. Electrochemical sensing and biosensing based on square wave voltammetry. Anal. Methods. 2013; 5(9):2158-2173.

Chen FJ, Sun M, Li SQ, Wu QQ, Ji L, Liu ZL, Zhou GZ, Cao G, Jin L, Xie HW, Wang CM, Lv J, De W, Wu M, Cao XF. Upregulation of the long non-coding RNA HOTAIR promotes esophageal squamous cell carcinoma metastasis and poor prognosis. Mol Carcinog. 2013;52(11):908-915.

Chen L, Matsubara N, Yoshino T, Nagasaka T, Hoshizima N, Shirakawa Y, Naomoto Y, Isozaki H, Riabowol K, Tanaka N. Genetic alterations of candidate tumor suppressor ING1 in human esophageal squamous cell cancer. Cancer Res. 2001;61:4345-4349.

Chen X, Hu H, Guan X, Xiong G, Wang Y, Wang K, Li J, Xu X, Yang K, Bai Y. CpG island methylation status of miRNAs in esophageal squamous cell carcinoma. Int J Cancer. 2012;130:1607-1613.

Chen ZX, Mann JR, Hsieh CL, Riggs AD, Chédin F. Physical and functional interactions between the human DNMT3L protein and members of the de novo methyltransferase family. J Cell Biochem. 2005;95:902-917.

Chen-Yu Lin, Han-Mei Xu; Novel perspectives of long non-coding RNAs in esophageal carcinoma. Carcinogenesis 2015; 36 (11): 1255-1262.

Chung JY, Braunschweig T, Hu N, Roth M, Traicoff JL, Wang QH, Knezevic V, Taylor PR, Hewitt SM. A multiplex tissue immunoblotting assay for proteomic profiling: a pilot study of the normal to tumor transition of esophageal squamous cell carcinoma. Cancer Epidemiology Biomarkers and Prev. 2006;15:1403.

Cintorino M, Tripod SA, Santopietro R, Antonio P, Lutfi A, Chang F, Syrjänen S, Shen Q, Tosi P, Syrjänen K. Cytokeratin expression patterns as an indicator of tumour progression in oesophageal squamous cell carcinoma. Anticancer Res. 2001;21:4195-4201.

Dandara C, Li D-P, Walther G, Parker MI. Gene-environment interaction: the role of SULT1A1 and CYP3A5 polymorphisms as risk modifiers for squamous cell carcinoma of the esophagus. J Carcinog. 2006;27:791-797.

Davidson G, Murphy S, Polke J, Laura M, Salih M, Muntoni F, Blake J, Brandner S, Davies N, Horvath R, Price S, Donaghy M, Roberts M, Foulds N, Ramdharry G, Soler D, Lunn M, Manji H, Davis M, Houlden H, Reilly M. Frequency of mutations in the genes associated with hereditary sensory and autonomic neuropathy in a UK cohort. J Neurol. 2012 ;259:1673-8165.

de Villiers E, Gunst K, Stein H, Scherübl H. Esophageal squamous cell cancer in patients with head and neck cancer: prevalence of human papillomavirus DNA sequences. Int J Cancer. 2004;109:253-258.

Demers LM, Mirkin CA, Mucic RC, Reynolds RA, Letsinger RL, Elghanian R, Viswanadham G. A Fluorescence-Based Method for Determining the Surface Coverage and Hybridization Efficiency of Thiol-Capped Oligonucleotides Bound to Gold Thin Films and Nanoparticles. Anal. Chem. 2000; 72(22):5535-5541.

Demers LM, Östblom M, Zhang H, Jang N-H, Liedberg B, Mirkin CA. Thermal Desorption Behaviour and Binding Properties of DNA Bases and Nucleosides on Gold. J. Am. Chem. Soc. 2002; 124(38):11248-11249.

Deng YZ, Chen PP, Wang Y, Yin D, Koeffler HP, Li B, Tong XJ, Xie D. Connective tissue growth factor is overexpressed in esophageal squamous cell carcinoma and promotes tumorigenicity through beta-catenin-T-cell factor/Lef signaling. J Biol Chem. 2007;282(50):36571-36581.

Dillon LW, Burrow AA, Wang YH. DNA instability at chromosomal fragile sites in cancer. Curr Genomics. 2010;11(5):326-337.

Dong M, Ma G, Tu W, Guo KJ, Tian YL, Dong YT. Clinicopathological significance of p53 and mdm2 protein expression in human pancreatic cancer**.** World J Gastroenterol. 2005;11:2162-2165.

D'Orazio P. Biosensors in clinical chemistry. Clin. Chim. Acta. 2003; 334(1-2):41-69.
Dragovich T, Campen C. Anti-EGFR-Targeted Therapy for Esophageal and Gastric Cancers: An Evolving Concept. J Oncol. 2009;2009:804108.

Drummond TG, Hill MG, Barton JK. Electrochemical DNA sensors. Nat. Biotechnol. 2003; 21(10):1192-1199.

Du XL, Hu H, Lin DC, et al. Proteomic profiling of proteins dysregulted in Chinese esophageal squamous cell carcinoma. J Mol Med. 2007;l.85: 863-875.

Duffy MJ. Carcinoembryonic antigen as a marker for colorectal cancer: is it clinically useful? Clin Chem. 2000;47:624-630.

Ebihara Y, Miyamoto M, Shichinohe T, Kawarada Y, Cho Y, Fukunaga A, Murakami S, Uehara H, Kaneko H, Hashimoto H, Murakami Y, Itoh T, Okushiba S, Kondo S, Katoh H. Over-expression of E2F-1 in esophageal squamous cell carcinoma correlates with tumor progression. Dis Esophagus. 2004;17:150-154.

Ekman S, Bergqvist M, Heldin CH, Lennartsson J. Activation of growth factor receptors in esophageal cancer--implications for therapy. Oncologist. 2007;12:1165-77.
Elton E. Esophageal Cancer. Dis Mon. 2005;51:664-684.

Engel LS, Chow WH, Vaughan TL, Gammon MD, Risch HA, Stanford JL, et al. Population attributable risks of esophageal and gastric cancers. J Natl Cancer Inst. 2003;95:1404-1413.

Enzinger PC, Mayer RJ. Esophageal cancer. N Engl J Med. 2003;349:2241-2252.

Fassan M, Volinia S, Palatini J, Pizzi M, Baffa R, De Bernard M, Battaglia G, Parente P, Croce CM, Zaninotto G, Ancona E, Rugge M. MicroRNA expression profiling in human Barrett's carcinogenesis. Int J Cancer. 2011 Oct 1;129(7):1661-1670.

Feber A, Xi L, Pennathur A, Gooding WE, Bandla S, Wu M, Luketich JD, Godfrey TE, Litle VR. MicroRNA prognostic signature for nodal metastases and survival in esophageal adenocarcinoma. Ann Thorac Surg. 2011;91:1523-1530.

Feng F, Wang, H, Han L, Wang S. Fluorescent Conjugated Polyelectrolyte as an Indicator for Convenient Detection of DNA Methylation. J Am. Chem. Soc. 2008; 130(34):11338-11343.

Fiche JB, Fuchs J, Buhot A, Calemczuk R, Livache T. Point mutation detection by surface plasmon resonance imaging coupled with a temperature scan method in a model system. Anal. Chem. 2008; 80(4):1049-1057.

Fong LY, Nguyen VT, Farber JL, Huebner K, Magee PN. Early deregulation of the p16ink4a-cyclin D1/cyclin-dependent kinase4-retinoblastoma pathway in cell proliferation-driven esophageal tumorigenesis in zinc-deficient rats. Cancer Res. 2000;60:4589-4595.

Freeman, R., Willner, I. Optical molecular sensing with semiconductor quantum dots (QDs). Chem. Soc. Rev. 2012; 41(10):4067-4085.

Fuks F, Burgers WA, Brehm A, Hughes-Davies L, Kouzarides T. DNA methyltransferase Dnmt1 associates with histone deacetylase activity. Nat Genet. 2000 ;24:88-91.

Fukuchi M, Masuda N, Nakajima M, Fukai Y, Miyazaki T, Kato H, Kuwano H. Inverse correlation between expression levels of p27 and the ubiquitin ligase subunit Skp2 in early esophageal squamous cell carcinoma. Anticancer Res. 2004;24:777-783.

Gao CM, Takezaki T, Wu JZ, Liu YT, Ding JH, Li SP, Su P, Hu X, Kai HT, Li ZY, Matsuo K, Hamajima N, et al. Polymorphisms in thymidylate synthase and methylenetetrahydrofolate reductase genes and the susceptibility to esophageal and stomach cancer with smoking. Asian Pac J Cancer Prev. 2004;5:133-138.

Ge C, Fang Z, Chen J, Liu J, Lu X, Zeng L. A simple colorimetric detection of DNA methylation. Analyst. 2012; 137(9):2032-2035.

Gore MR, Levine MS. Textbook of gastrointestinal radiology, 2nd ed. Philadelphia: WB Saunders 2000

Gotoda T, Matsumura Y, Kondo H, Ono H, Kanamoto A, Kato H, Watanabe H, Tachimori Y, Nakanishi Y, Kakizoe T. Expression of CD44 variants and prognosis in oesophageal squamous cell carcinoma. Gut. 2000;46:14-19.

Grabowski P, Kühnel T, Mühr-Wilkenshoff F, Heine B, Stein H, Höpfner M, Germer CT, Scherübl H. Prognostic value of nuclear survivin expression in oesophageal squamous cell carcinoma. Br J Cancer. 2003;88:115-119.

Greenman C, Stephens P, Smith R, Dalgliesh GL, Hunter C, Bignell G, Davies H. et. al. Patterns of somatic mutation in human cancer genomes. Nature. 2007; 446(7132):153-158.

Grieshaber D, MacKenzie R, Vörös J, Reimhult E. Electrochemical Biosensors - Sensor Principles and Architectures. Sensors. 2008; 8(3):1400-1458.

Grompe, M. The rapid detection of unknown mutations in nucleic acids. Nat. Genet. 1993; 5(2):111-117.

Gu Y, Swisher SG, Ajani JA, Correa AM, Hofstetter WL, Liao Z, Komaki RR,Rashid A, Hamilton SR, Wu TT. The number of lymph nodes with metastasis predicts survival in patients with esophageal or esophagogastric junction adenocarcinoma who receive preoperative chemoradiation. Cancer. 2006;106:1017-1025.

Guérillon C, Larrieu D, Pedeux R. ING1 and ING2: multifaceted tumor suppressor genes. Cell Mol Life Sci. 2013;70:3753-3772.

Guo M, Ren J, Brock MV, Herman JG, Carraway HE. Promoter methylation of HIN-1 in the progression to esophageal squamous cancer. Epigenetics. 2008;3:336-341.

Guo M, Ren J, House MG, Qi Y, Brock MV, Herman JG. Accumulation of promoter methylation suggests epigenetic progression in squamous cell carcinoma of the esophagus. Clin Cancer Res. 2006;12(15):4515-4522.

Guo XQ, Wang SJ, Zhang JH, et al. CpG island methylation of p16 and FHIT gene in tissues of the esophageal precancerous lesions. Chin Clin Cancer 2005; 32: 554-557.

Guo Y, Chen Z, Zhang L, Zhou F, Shi S, Feng X, Li B, Meng X, Ma X, Luo M, Shao K, Li N, Qiu B, Mitchelson K, Cheng J, He J. Distinctive microRNA profiles relating to patient survival in esophageal squamous cell carcinoma. Cancer Res. 2008; 68(1):26-33.

Gupta VK, Jain R, Radhapyari K, Jadon N, Agarwal S. Voltammetric techniques for the assay of pharmaceuticals—A review. Anal. Biochem. 2011; 408(2):179-196.

Haggitt RC. Adenocarcinoma in Barrett's esophagus: a new epidemic? Hum Pathol. 1992;23:475-476.

Halsall, HB, Heineman, WR. Electrochemical immunoassay: an ultrasensitive method. Journal of the International Federation of Clinical Chemistry. 1990; 2(4):179-187.

Hansen JC. Conformational dynamics of the chromatin fiber in solution: determinants, mechanisms, and functions. Annu Rev Biophys Biomol Struct. 2002;31:361-392.

Harada K, Baba Y, Ishimoto T, Shigaki H, Kosumi K, Yoshida N, Watanabe M, Baba H. The role of microRNA in esophageal squamous cell carcinoma. J Gastroenterol. 2016; 51(6):520-530.

He B, Yin B, Wang B, Chen C, Xia Z, Tang J, Yuan Y, Feng X, Yin N. Overexpression of LASP1 is associated with proliferation, migration and invasion in esophageal squamous cell carcinoma. Oncol Rep. 2013;29:1115-1123.

He H, Ding F, Li Y, Luo A, Chen H, Wu C, Liu Z. Migfilin regulates esophageal cancer cell motility through promoting GSK-3beta-mediated degradation of beta-catenin. Mol Cancer Res. 2012;10:273-281.

He LR, Liu MZ, Li BK, Rao HL, Liao YJ, Guan XY, Zeng YX, Xie D. Prognostic impact of H3K27me3 expression on locoregional progression after chemoradiotherapy in esophageal squamous cell carcinoma. BMC Cancer. 2009;9:461.

Hendricks D, Parker MI. Oesophageal cancer in Africa. IUBMB Life. 2002;53:263-268.

Heyn H, Esteller M. DNA methylation profiling in the clinic: applications and challenges. Nat Rev Genet. 2012;13(10):679-692.

Hibi K, Taguchi M, Nakayama H, Takase T, Kasai Y, Ito K, Akiyama S, Nakao A.Molecular detection of p16 promoter methylation in the serum of patients with esophageal squamous cell carcinoma. Clin Cancer Res. 2001;7:3135-3138.

Hiyama T, Yoshihara M, Tanaka S, Chayama K. Genetic polymorphisms and esophageal cancer risk. Int J Cancer. 2007;121:1643-1658.

Holland, James F, Bast, Robert C. Cancer medicine-5 review : a companion to Holland-Frei Cancer medicine-5 Hamilton, Ont. ; Lewiston, NY : B.C. Decker, 2000. pp 156-157.

Homola, J. Surface Plasmon Resonance Sensors for Detection of Chemical and Biological Species. Chem. Rev. 2008; 108(2):462-493.

Hossain, T, Mahmudunnabi, G, Masud, MK, Islam, MN, Ooi, L, Konstantinov, K, Hossain, MSA., Martinac, B, Alici, G, Nguyen, N-T., Shiddiky, MJA. Electrochemical biosensing strategies for DNA methylation analysis. Biosens. Bioelectron. 2017; 94:63-73.

Hu J, Zhang CY. Single base extension reaction-based surface enhanced Raman spectroscopy for DNA methylation assay. Biosens. Bioelectron. 2012; 31(1):451-457.

Huang Y, Chang X, Lee J, Cho Y, Zhong X, Park I, Liu J, Califano J, Ratovitski E, Sidransky D, Kim M. (). Cigarette smoke induces promoter methylation of single-stranded DNA-binding protein 2 in human esophageal squamous cell carcinoma. Int J Cancer 2011;128: 2261-2273.

Ikeguchi M, Yamaguchi K, Kaibara N. Survivin gene expression positively correlates with proliferative activity of cancer cells in esophageal cancer. Tumour Biol. 2003;24(1):40-45.

Ilgaz Aydinlar E, Rolfs A, Serteser M, Parman Y. Mutation in FAM134B causing hereditary sensory neuropathy with spasticity in a Turkish family. Muscle Nerve. 2014;49:774-775.

Ishii H, Dumon KR, Vecchione A, Trapasso F, Mimori K, Alder H, Mori M, Sozzi G, Baffa R, Huebner K, Croce CM. Effect of adenoviral transduction of the fragile histidine triad gene into esophageal cancer cells. Cancer Res. 2001;61:1578-1584.

Islam F, Gopalan V, Wahab R, Lee KT, Haque MH, Mamoori A, Lu CT, Smith RA, Lam AK. Novel FAM134B mutations and their clinicopathological significance in colorectal cancer. Hum Genet. 2017;136(3):321-337.

Islam F, Gopalan V, Wahab R, Smith RA, Qiao B, Lam AK. Stage dependent expression and tumor suppressive function of FAM134B (JK1) in colon cancer. Mol Carcinog. 2017;56(1):238-249.

Islam MN, Yadav S, Haque MH, Munaz A, Islam F, Al Hossain MS, Gopalan V, Lam AK, Nguyen NT, Shiddiky MJ. Optical biosensing strategies for DNA methylation analysis. Biosens. Bioelectron. 2017;92:668-678.

Islami F, Boffetta P, Ren J-S, Pedoeim L, Khatib D, Kamangar F. High-temperature beverages and foods and esophageal cancer risk - a systematic review. Int J Cancer. 2009;125:491-524.

Jazii, FR, Najafi Z, Malekzadeh R, et al. Identification of squamous cell carcinoma associated proteins by proteomics and loss of beta tropomyosin expression in esophageal cancer. World J Gastroenterol. 2006;12:7104-12. ISSN 1007-9327.

Jemal A, Bray F, Center MM, Ferlay J, Ward E, Forman D. Global cancer statistics. CA Cancer J Clin. 2011; 61: 69-90.

Jenkins GJ, Doak SH, Parry JM, D'Souza FR, Griffiths AP, Baxter JN. Genetic pathways involved in the progression of Barrett's metaplasia to adenocarcinoma. Br J Surg. 2002;89:824-837.

Jiang T, Minunni M, Wilson P, Zhang J, Turner AP, Mascini M. Detection of TP53 mutation using a portable surface plasmon resonance DNA-based biosensor. Biosens. Bioelectron. 2005; 20(10):1939-1945.

Johnson RP, Richardson JA, Brown T, Bartlett PN. A Label-Free, Electrochemical SERS-Based Assay for Detection of DNA Hybridization and Discrimination of Mutations. J. Am. Chem. Soc. 2012; 134(34):14099-14107.

Kagawa Y, Yoshida K, Hirai T and Toge T. Significance of the expression of p27Kip1 in esophageal cell carcinomas. Dis Esophagus. 2000;13:179-184.

Kano M, Seki N, Kikkawa N, Fujimura L, Hoshino I, Akutsu Y, Chiyomaru T,Enokida H, Nakagawa M, Matsubara H. miR-145, miR-133a and miR-133b: Tumor-suppressive miRNAs target FSCN1 in esophageal squamous cell carcinoma. Int J Cancer. 2010;127:2804-2814.

Kase S, Osaki M, Adachi H, Kaibara N, Ito H. Expression of Fas and Fas ligand in esophageal tissue mucosa and carcinomas. Int J Oncol. 2002;20:291-297.

Kasem K, Gopalan V, Salajegheh A, Lu CT, Smith RA, Lam AK. JK1 (FAM134B) gene and colorectal cancer: a pilot study on the gene copy number alterations and correlations with clinicopathological parameters. Exp Mol Pathol. 2014a;97:31-36.

Kasem K, Gopalan V, Salajegheh A, Lu CT, Smith RA, Lam AK. The roles of JK-1 (FAM134B) expressions in colorectal cancer. Exp Cell Res. 2014b;326:166-173.

Kasem K, Lam A. Analysis of a novel JK-1 gene expression in benign and malignant colorectal tumors. Virchows Arch. 2010;457:165.

Kasem K, Sullivan E, Gopalan V, Salajegheh A, Smith RA, Lam AK. JK1 (FAM134B) represses cell migration in colon cancer: a functional study of a novel gene. Exp Mol Pathol. 2014c;97:99-104.

Kashyap MK, Marimuthu A, Peri S, Kumar GS, Jacob HK, Prasad TS, Mahmood R, Kumar KV, Kumar MV, Meltzer SJ, Montgomery EA, Kumar RV, Pandey A. Overexpression of periostin and lumican in esophageal squamous cell carcinoma. Cancers (Basel). 2010; 2: 133-142.

Kashyap MK, Pawar HA, Keerthikumar S, Sharma J, Goel R, Mahmood R, Kumar MV, Kumar KV, Pandey A, Kumar RV, Prasad TS and Harsha HC. Evaluation of protein expression pattern of stanniocalcin 2, insulin-like growth factor-binding protein 7, inhibin beta A and four and a half LIM domains 1 in esophageal squamous cell carcinoma. Cancer Biomark. 2012;12:1-9.

Kelley SO, Boon EM, Barton JK, Jackson NM, Hill MG. Single-base mismatch detection based on charge transduction through DNA. Nucleic Acids Res. 1999; 27(24):4830-4837.

Kijima H, Oshiba G, Kenmochi T, Kise Y, Tanaka H, Chino O, Shimada H, Ueyama Y, Tanaka M, Makuuchi H. Stromal CEA immunoreactivity is correlated with lymphatic invasion of human esophageal carcinoma. Int J Oncol. 2000;16:677-682.

Kim S, Hwang SH, Im SG, Lee MK, Lee CH, Son SJ, Oh HB. Upconversion nanoparticle-based förster resonance energy transfer for detecting DNA methylation. Sensors. 2016; 16(8):1259.

Kim S, Jeong S-N, Bae S, Chung H, Yoo SY. Sensitive Surface Enhanced Raman Scattering-Based Detection of a BIGH3 Point Mutation Associated with Avellino Corneal Dystrophy. Anal. Chem. 2016b; 88(23):11288-11292.

Kimura-Suda H, Petrovykh DY, Tarlov MJ, Whitman LJ. Base-Dependent Competitive Adsorption of Single-Stranded DNA on Gold. J. Am. Chem. Soc. 2003; 125(30):9014-9015.

Kitamura A, Yashima K, Okamoto E, Andachi H, Hosoda A, Kishimoto Y, Shiota G, Ito H, Kaibara N, Kawasaki H. Reduced Fhit expression occurs in the early stage of esophageal tumorigenesis: no correlation with p53 expression and apoptosis. Oncology. 2001;61(3):205-211.

Kitano S, Nakayama M, Yamane A, Tsukahara Y, Amano M. Detection of DNA mutations by fluorescence resonance energy transfer-based preferential homoduplex formation assay. Anal. Biochem. 2011; 408(2):197-205.

Klose RJ, Bird AP. Genomic DNA methylation: the mark and its mediators. Trends Biochem Sci. 2006;31:89-97.

Kong KL, Kwong DL, Fu L, Chan TH, Chen L, Liu H, Li Y, Zhu YH, Bi J, Qin YR, Law SY, Guan XY. Characterization of a candidate tumor suppressor gene uroplakin 1A in esophageal squamous cell carcinoma. Cancer Res. 2010;70:8832-8841.

Kong M, Kim Y, Lee C. A strong synergistic epistasis between FAM134B and TNFRSF19 on the susceptibility to vascular dementia. Psychiatr Genet. 2011;21:37-41.

Koo KM, Sina AA, Carrascosa LG, Shiddiky MJ, Trau M. eMethylsorb: rapid quantification of DNA methylation in cancer cells on screen-printed gold electrodes. Analyst. 2014; 139(23):6178-6184.

Koo KM, Sina, AAI, Carrascosa LG, Shiddiky MJA, Trau M. DNA-bare gold affinity interactions: mechanism and applications in biosensing. Anal. Methods. 2015; 7(17):7042-7054.

Kurita R, Arai K, Nakamoto K, Kato D, Niwa O. Determination of DNA Methylation Using Electrochemiluminescence with Surface Accumulable Coreactant. Anal. Chem. 2012; 84(4):1799-1803.

Kuroki T, Trapasso F, Shiraishi T, Alder H, Mimori K, Mori M, Croce CM. Genetic alterations of the tumor suppressor gene WWOX in esophageal squamous cellcarcinoma. Cancer Res. 2002;62:2258-2260.

Kuroki T, Trapasso F, Yendamuri S, Matsuyama A, Alder H, Mori M, Croce CM. Allele loss and promoter hypermethylation of VHL, RAR-beta, RASSF1A, and FHIT tumor suppressor genes on chromosome 3p in esophageal squamous cell carcinoma. Cancer Res. 2003;63:3724-3728.

Kuroki T, Trapasso F, Yendamuri S, Matsuyama A, Alder H, Mori M, Croce CM. Promoter hypermethylation of RASSF1A in esophageal squamous cell carcinoma. Clin Cancer Res. 2003;9(4):1441-1445.

Kuroki T, Trapasso F, Yendamuri S, Matsuyama A, Alder H, Mori M, Croce CM. Allele loss and promoter hypermethylation of VHL, RAR-beta, RASSF1A, and FHIT tumor suppressor genes on chromosome 3p in esophageal squamous cell carcinoma. Cancer Res. 2003;63(13):3724-3728.

Kurth I, Pamminger T, Hennings JC, Soehendra D, Huebner AK, Rotthier A, Baets J, Senderek J, Topaloglu H, Farrell SA, Nürnberg G, Nürnberg P, De Jonghe P, Gal A, Kaether C, Timmerman V, Hübner CA. Mutations in FAM134B, encoding a newly identified Golgi protein, cause severe sensory and autonomic neuropathy. Nat Genet. 2009;41:1179-1181.

Kwong D, Lam A, Guan X, Law S, Tai A, Wong J, Sham J. Chromosomal aberrations in esophageal squamous cell carcinoma among Chinese: gain of 12p predicts poor prognosis after surgery. Hum Pathol. 2004;35:309-316.

Kwong KF. Molecular biology of esophageal cancer in the genomics era. Surg Clin North Am. 2005;85:539- 553.

Liyanage SS, Segelov E, Garland SM, Tabrizi SN, Seale H, Crowe PJ, Dwyer DE, Barbour A, Newall AT, Malik A, Macintyre CR. Role of human papillomaviruses in esophageal squamous cell carcinoma. Asia Pac. J. Clin. Oncol. 2013; 9: 12–28.

Labib M, Sargent EH, Kelley SO. Electrochemical methods for the analysis of clinically relevant biomolecules. Chem. Rev. 2016;116(16):9001-9090.

Lam AK. Molecular biology of esophageal squamous cell carcinoma. Crit Rev Oncol Hematol. 2000;33:71-90.

Lam KY, Law S, Tin L, Tung PH, Wong J. The clinicopathological significance of p21 and p53 expression in esophageal squamous cell carcinoma: an analysis of 153 patients. Am J Gastroenterol. 1999; 94:2060–2068.

Lam KY, Law S, Tung PH, Wong J. Esophageal small cell carcinomas: clinicopathologic parameters, p53 over expression, proliferation marker, and their impact on pathogenesis. Arch Pathol Lab Med. 2000;124:228-233.

Lam KY, Ma L. Pathology of esophageal cancers: local experience and current insights. Chin Med J (Engl). 1997;110:459-464.

Langer R, Ott K, Feith M, Lordick F, Siewert JR, Becker K. Prognostic significance of histopathological tumor regression after neoadjuvant chemotherapy in esophageal adenocarcinomas. Mod Pathol. 2009;22:1555-1563.

Lao R, Song S, Wu H, Wang L, Zhang Z, He L, Fan C. Electrochemical interrogation of DNA monolayers on gold surfaces. Anal. Chem. 2005; 77(19):6475-6480.

Lev Bar-Or R, Maya R, Segel LA, Alon U, Levine AJ, Oren M. Generation of oscillations by the p53-Mdm2 feedback loop: a theoretical and experimental study**.** Proc Natl Acad Sci USA. 2000; 97:11250-11255.

Li C, Wu MY, Liang YR, Wu XY. Correlation between expressions of human telomerase activity in 90 esophageal squamous cell carcinoma. World J Gastroenterol. 2003;9:2395-2399.

Li DP, Dandara C, Parker MI. Association of cytochrome P450 2E1 genetic polymorphisms with squamous cell carcinoma of the oesophagus. Clin Chem Lab Med. 2005;43:370-375.

Li H, Rothberg L. Colorimetric detection of DNA sequences based on electrostatic interactions with unmodified gold nanoparticles. Proc. Natl. Acad. Sci. U.S.A. 2004a; 101(39):14036-14039.

Li H, Rothberg LJ. Label-free colorimetric detection of specific sequences in genomic DNA amplified by the polymerase chain reaction. J. Am. Chem. Soc. 2004b; 126(35):10958-10961.

Li J, Chu X, Liu Y, Jiang J-H, He Z, Zhang Z, Shen G, Yu R-Q. A colorimetric method for point mutation detection using high-fidelity DNA ligase. Nucleic Acids Res. 2005; 33(19):e168-e168.

Li K, Wang X, He W, Lin N, Fan QX. Expression of N-cadherin in esophageal squamous cell carcinoma and silencing expression of N-cadherin using RNA interference on invasiveness of EC9706 cells. Ai Zheng. 2009;28:8-13.

Li LW, Li YY, Li XY, Zhang CP, Zhou Y, Lu SH. A novel tumor suppressor gene ECRG4 interacts directly with TMPRSS11A (ECRG1) to inhibit cancer cell growth in esophageal carcinoma. BMC Cancer. 2011;11:52.

Li LW, Yu XY, Yang Y, Zhang CP, Guo LP, Lu SH. Expression of esophageal cancer related gene 4 (ECRG4), a novel tumor suppressor gene, in esophageal cancer and its inhibitory effect on the tumor growth in vitro and in vivo. Int J Cancer. 2009;125:1505-1513.

Li LY et al. Connective tissue growth factor expression in precancerous lesions of human esophageal epithelium and prognostic significance in esophageal squamous cell carcinoma. Dis Esophagus. 2010;24: 337-345.

Li W, Liu X, Zhang B, Qi D, Zhang L, Jin Y, Yang H. Overexpression of candidate tumor suppressor ECRG4 inhibits glioma proliferation and invasion. J Exp Clin Cancer Res. 2010; 29:89.

Li X, Lin R, Li J. Epigenetic silencing of microRNA-375 regulates PDK1 expression in esophageal cancer. Dig Dis Sci. 2011;56:2849-2856.

Li Y, Nie CJ, Hu L, Qin Y, Liu HB, Zeng TT, Chen L, Fu L, Deng W, Chen SP, Jia WH, Zhang C, Xie D, Guan XY. Characterization of a novel mechanism of genomic instability involving the SEI1/SET/NM23H1 pathway in esophageal cancers. Cancer Res. 2010;70:5695-5705.

Li Z, Shimada Y, Uchida S, Maeda M, Kawabe A, Mori A, Itami A, Kano M, Watanabe G, Imamura M. TGF-alpha as well as VEGF, PD-ECGF and bFGF contribute to angiogenesis of esophageal squamous cell carcinoma. Int J Oncol. 2000;17:453-460.

Lin CY, Xu HM. Novel perspectives of long non-coding RNAs in esophageal carcinoma. Carcinogenesis. 2015; 36(11):1255-1262.

Lin YC, Wu MY, Li DR, Wu XY, Zheng RM. Prognostic and clinicopathological features of E-cadherin, alpha-catenin, betacatenin, gamma-catenin and cyclin D1 expression in human esophageal squamous cell carcinoma. World J Gastroenterol. 2004;10:3235-3239.

Liu L, Pan T, Li J, Zhang N, Song D, Hu M. The correlation of p53 and nm23-H1 expression with invasiveness and metastasis in esophageal carcinoma. The Chinese-German J of Cli Oncology. 2002;1:194-198.

Liu Y, Wang HX, Lu N, Mao YS, Liu F, Wang Y, Zhang HR, Wang K, Wu M, Zhao XH. Translocation of annexin I from cellular membrane to the nuclear membrane in human esophageal squamous cell carcinoma. World J Gastroenterol. 2003;9:645-649.

Liyanage SS, Segelov E, Garland SM, Tabrizi SN, Seale H, Crowe PJ, Dwyer DE, Barbour A, Newall AT, Malik A, Macintyre CR. Role of human papillomaviruses in esophageal squamous cell carcinoma. Asia Pac J Clin Oncol. 2013; 9:12-28.

Lo PH, Ko JM, Yu ZY, Law S, Wang LD, Li JL, Srivastava G, Tsao SW, Stanbridge EJ, Lung ML. The LIM domain protein, CRIP2, promotes apoptosis in esophageal squamous cell carcinoma. Cancer Lett. 2012;316(1):39-45.

Loizou JI, Murr R, Finkbeiner MG, Sawan C, Wang ZQ, Herceg Z. Epigenetic information in chromatin: the code of entry for DNA repair. Cell Cycle. 2006;5:696-701.

Lovrić M, Osteryoung J. Theory of differential normal pulse voltammetry. Electrochim. Acta 1982; 27(7):963-968.

Lu XM, Monnier-Benoit S, Mo LZ, Xu SY, Prétet JL, Liu Z, Vuitton DA, Mougin C. Human papillomavirus in esophageal squamous cell carcinoma of the high-risk Kazakh ethnic group in Xinjiang, China. Eur J Surg Oncol. 2008;34:765-770.

Lu Z, Ghosh S, Wang Z, Hunter T. Downregulation of caveolin-1 function by EGF leads to the loss of E-cadherin, increased transcriptional activity of β-catenin, and enhanced tumor cell invasion. Cancer Cell. 2003;4:499-515.

Ma K, Cao B, Guo M. The detective, prognostic, and predictive value of DNA methylation in human esophageal squamous cell carcinoma. Clin Epigenetics. 2016;8:43.

Ma Y, Bai Y, Mao H, Hong Q, Yang D, Zhang H, et. al. A panel of promoter methylation markers for invasive and noninvasive early detection of NSCLC using a quantum dots-based FRET approach. Biosens. Bioelectron. 2016; 85:641-648.

Makino T, Yamasaki M, Takeno A, Shirakawa M, Miyata H, Takiguchi S, Nakajima K, Fujiwara Y, Nishida T, Matsuura N, Mori M, Doki Y. Cytokeratins 18 and 8 are poor prognostic markers in patients with squamous cell carcinoma of the oesophagus. Br J Cancer. 2009;101:1298-1306.

Mandard AM, Hainaut P, Hollstein M. Genetic steps in the development of squamous cell carcinoma of the esophagus. Mutat Res. 2000;462:335-342.

Martin C, Zhang Y. The diverse functions of histone lysine methylation. Nat Rev Mol Cell Biol. 2005 ;6:838-849.

Maru DM, Singh RR, Hannah C, Albarracin CT, Li YX, Abraham R, Romans AM, Yao H, Luthra MG, Anandasabapathy S, Swisher SG, Hofstetter WL, Rashid A, Luthra R. MicroRNA-196a is a potential marker of progression during Barrett's metaplasia-dysplasia-invasive adenocarcinoma sequence in esophagus. Am J Pathol. 2009;174:1940-1948.

Masuda N, Kato H, Nakajima T, Sano T, Kashiwabara K, Oyama T, Kuwano H. Synergistic decline in expressions of p73 and p21 with invasion in esophageal cancers. Cancer Sci. 2003;94:612-617.

Matsumoto M, Natsugoe S, Okumura H, Arima H, Yanagita S, Uchikado Y, Yokomakura N, Setoyama T, Ishigami S, Takao S, Aikou T. Overexpression of vascular endothelial growth factor-C correlates with lymph node micrometastasis in submucosal esophageal cancer. J Gastrointest Surg. 2006;10:1016-1022.

McCabe ML, Dlamini Z. The molecular mechanisms of oesophageal cancer. Int Immunopharmacol. 2005; 5: 1113-1130.

Mega S, Miyamoto M, Li L, Kadoya M, Takahashi R, Hase R, Kaneko H, Shichinohe T, Kawarada Y, Itoh T, Morikawa T, Kondo S. Immunohistochemical analysis of nuclear survivin expression in esophageal squamous cell carcinoma. Dis Esophagus. 2006;19:355-359.

Melchiotti R, Puan KJ, Andiappan AK, Poh TY, Starke M, Zhuang L, Petsch K, Lai TS, Chew FT, Larbi A, Wang de Y, Poidinger M, Rotzschke O. Genetic analysis of an allergic rhinitis cohort reveals an intercellular epistasis between FAM134B and CD39. BMC Med Genet. 2014;15:73.

Michaylira CZ, Wong GS, Miller CG, Gutierrez CM, Nakagawa H, Hammond R,Klein-Szanto AJ, Lee JS, Kim SB, Herlyn M, Diehl JA, Gimotty P, Rustgi AK. Periostin, a cell adhesion molecule, facilitates invasion in the tumor microenvironment and annotates a novel tumor-invasive signature in esophageal cancer. Cancer Res. 2010;70:5281-5292.

Michel P, Magois K, Robert V, Chiron A, Lepessot F, Bodenant C, Roque I, Seng SK, Frebourg T, Paillot B. Prognostic value of TP53 transcriptional activity on p21 and bax in patients with esophageal squamous cell carcinomas treated by definitive chemoradiotherapy. Int J Radiat Oncol Biol Phys. 2002;54:379-385.

Mimori K, Nishida K, Nakamura Y, Ieta K, Yoshikawa Y, Sasaki A, Ishii H,Alonso MA, Mori M. Loss of MAL expression in precancerous lesions of the esophagus. Ann Surg Oncol. 2007;14:1670-1677.

Mimori K, Shiraishi T, Mashino K, Sonoda H, Yamashita K, Yoshinaga K, Masuda T, Utsunomiya T, Alonso MA, Inoue H, Mori M. MAL gene expression in esophageal cancer suppresses motility, invasion and tumorigenicity and enhances apoptosis through the Fas pathway. Oncogene. 2003;22:3463-3471.

Mimura K, Kono K, Hanawa M, Mitsui F, Sugai H, Miyagawa N, Ooi A, Fujii H. Frequencies of HER-2/neu expression and gene amplification in patients with oesophageal squamous cell carcinoma. Br J Cancer. 2005;92:1253-1260.

Mirkin CA, Letsinger RL, Mucic RC, Storhoff JJ. A DNA-based method for rationally assembling nanoparticles into macroscopic materials. Nature. 1996; 382(6592):607-609.

Moaven O, Raziee HR, Sima HR, et al. Interactions between Glutathione-S-Transferase M1, T1 and P1 polymorphisms and smoking, and increased susceptibility to esophageal squamous cell carcinoma. Cancer Epidemiol. 2010;34:285-290.

Mohseni MSM. Detection of human papilloma virus in esophageal squamous cell carcinoma in Guilan province. J Clin Diagnost Res. 2010;4:2373-1377.

Mona A, Kandil MD, Monshira M, ABD El-Wahed MD. The significance of metastasis related-factor nm23-Hi and cathepsin D in prostrate cancer. J Egyptian Nat Cancer Inst. 2000;12**:**199-210.

Moradi A, Mokhtari-Azad T. Detection of HPV in cancerous and non-cancerous esophageal tissues from Turkmen-Sahra, Iran. Int J Cancer Res. 2006;2:113-118.

Murphy SM, Davidson GL, Brandner S, Houlden H, Reilly MM. Mutation in FAM134B causing severe hereditary sensory neuropathy. J Neurol Neurosurg Psychiatry. 2012;83:119-120.

Muschen M, Warskulat U, Beckmann MW. Defining CD95 as a tumor suppressor gene. J Mol Med. 2000; 78:312-325.

Nahir TM, Buck RP. Modified Cottrell behavior in thin layers: Applied voltage steps under diffusion control for constant-resistance systems. J. Electroanal. Chem. 1992; 341(1):1-14.

Nair KS, Naidoo R, Chetty R. Expression of cell adhesion molecules in oesophageal carcinoma and its prognostic value. J Clin Pathol. 2005;58:343-351.

Nelson EM, Rothberg LJ. Kinetics and mechanism of single-stranded DNA adsorption onto citrate-stabilized gold nanoparticles in colloidal solution. Langmuir. 2011; 27(5):1770-1777.

Nemoto T, Kitagawa M, Hasegawa M, Ikeda S, Akashi T, Takizawa T, Hirokawa K, Koike M. Expression of IAP family proteins in esophageal cancer. Exp Mol Pathol. 2004;76:253-259.

Nie Y, Liao J, Zhao X, Song Y, Yang GY, Wang LD, Yang CS. Detection of multiple gene hypermethylation in the development of esophageal squamous cell carcinoma. Carcinogenesis. 2002;23:1713-1720.

Noguchi T, Takeno S, Kimura Y, Uchida Y, Daa T, Yokoyama S, Gabbert HE, Mueller W. FHIT expression and hypermethylation in esophageal squamous cell carcinoma. Int J Mol Med. 2003;11:441-447.

Noort M, Meeldijk J, van der Zee R, Destree O, Clevers H. Wnt signaling controls the phosphorylation status of β-catenin. J Biol Chem. 2002;277:17901–17905.

Oka D, Yamashita S, Tomioka T, Nakanishi Y, Kato H, Kaminishi M, Ushijima T. The presence of aberrant DNA methylation in noncancerous esophageal mucosae in association with smoking history: a target for risk diagnosis and prevention of esophageal cancers. Cancer. 2009;115:3412-3426.

Olivier M, Eeles R, Hollstein M, Khan MA, Harris CC, Hainaut P. The IARC TP53 database: new online mutation analysis and recommendations to users. Hum Mutat. 2002 ;19:607-614.

Opdahl A, Petrovykh DY, Kimura-Suda H, Tarlov MJ, Whitman LJ. Independent control of grafting density and conformation of single-stranded DNA brushes. Proc. Natl. Acad. Sci. U.S.A. 2007; 104(1):9-14.

Oshima Y, Yajima S, Yamazaki K, Matsushita K, Tagawa M, Shimada H. Angiogenesis-related factors are molecular targets for diagnosis and treatment of patients with esophageal carcinoma. Ann Thorac Cardiovasc Surg. 2010;16:389-393.

Ostblom M, Liedberg B, Demers LM, Mirkin CA. On the structure and desorption dynamics of DNA bases adsorbed on gold: a temperature-programmed study. J. Phys. Chem. B. 2005; 109(31):15150-15160.

Paige AJ, Taylor KJ, Taylor C, Hillier SG, Farrington S, Scott D, Porteous DJ, Smyth JF, Gabra H, Watson JE. WWOX: a candidate tumor suppressor gene involved in multiple tumor types. Proc Natl Acad U S A. 2001;98:11417-11422.

Pan S, Xu J, Shu Y, Wang F, Xia W, Ding Q, Xu T, Zhao C, Zhang M, Huang P, Lu S. Double recognition of oligonucleotide and protein in the detection of DNA methylation with surface plasmon resonance biosensors. Biosens. Bioelectron. 2010; 26(2):850-853.

Paraskevas E, Dimitroulopoulos D. Epstein-Barr virus infection and gastrointestinal diseases. Annals of Gastroenterol. 2005;18:386-390.

Park HL, Kim MS, Yamashita K, Westra W, Carvalho AL, Lee J, Jiang WW, Baek JH,Liu J, Osada M, Moon CS, Califano JA, Mori M, Sidransky D. DCC promoter hypermethylation in esophageal squamous cell carcinoma. Int J Cancer. 2008 ;122:2498-2502.

Paweletz CP, Ornstein DK, Roth MJ, Bichsel VE, Gillespie JW, Calvert VS, Vocke CD, Hewitt SM, Duray PH, Herring J, Wang QH, Hu N, Linehan WM, Taylor PR, Liotta LA, Emmert-Buck MR, Petricoin EF 3rd. Loss of annexin 1 correlates with early onset of tumorigenesis in esophageal and prostate carcinoma. Cancer Res. 2000;60:6293-6297.

Pawson T, Raina M, Nash P. Interaction domains: From simple binding events to complex cellular behavior. FEBS Lett. 2002;513:2-10.

Pearson FG, Cooper JD, Deslaurier J, Ginsberg RJ, Hiebert CA, Pattreson GA, Urschel Jr. *Esophageal Surgery, edition 2, 2002, p. 9 edited by* Pearson FG, Cooper JD, Deslaurier J, Ginsberg RJ, Hiebert CA, Pattreson GA, Urschel HC Jr. Philadelphia; Churchill Livingstone.

Pekarsky Y, Zanesi N, Palamarchuk A, Huebner K, Croce CM. FHIT: from gene discovery to cancer treatment and prevention. Lancet Oncol. 2002;3:748-754.

Philip W, Stephan D, Daniel S, Holger M, Gilbert S. Expression and Prognostic Significance of EpCAM. Journal of Cancer Molecules. 2008;3:169-174.

Ramburan A, Govender D. Cadherins and catenins in pathology. Curr Diagn Pathol. 2002;8:305-317.

Ren Y, Cao B, Law S, Xie Y, Lee PY, Cheung L, Chen Y, Huang X, Chan HM, Zhao P, Luk J, Vande Woude G, Wong J. Hepatocyte growth factor promotes cancer cell migration and angiogenic factors expression: a prognostic marker of human esophageal squamous cell carcinomas. Clin Cancer Res. 2005;11:6190-6197.

Ren YJ, Zhang QY. Expression of midkine and its clinical significance in esophageal squamous cell carcinoma. World J Gastroenterol. 2006;12:2006-2010.

Ronkainen NJ, Halsall HB, Heineman WR. Electrochemical biosensors. Chem. Soc. Rev. 2010; 39(5):1747-1763.

Saito H, Tsujitani S, Oka S, Ikeguchi M, Maeta M, Kaibara N. The expression of murine double minute 2 is a favorable prognostic marker in esophageal squamous cell carcinoma without p53 protein accumulation**.** Ann Surg Oncol. 2002;9:450-456.

Saitoh T, Mine T, Katoh M. Molecular cloning and expression of proto-oncogene FRAT1 in human cancer. Int J Oncol. 2002;20:785-789.

Scheubert L, Schmidt R, Repsilber D, Lustrek M, Fuellen G. Learning biomarkers of pluripotent stem cells in mouse. DNA Res. 2011;18:233-251.

Shamma A, Doki Y, Shiozaki H, Tsujinaka T, Yamamoto M, Inoue M, Yano M, Monden M. Cyclin D1 overexpression in esophageal dysplasia: a possible biomarker for carcinogenesis of esophageal squamous cell carcinoma. Int J Oncol. 2000;16:261-266.

Shamma A, Doki Y, Tsujinaka T, Shiozaki H, Inoue M, Yano M, Kawanishi K,Monden M. Loss of p27(KIP1) expression predicts poor prognosis in patients with esophageal squamous cell carcinoma. Oncology. 2000;58:152-158.

Sharma K, Wang RX, Zhang LY, Yin DL, Luo XY, Solomon JC, Jiang RF, Markos K,Davidson W, Scott DW, Shi YF. Death the Fas way: regulation and pathophysiology of CD95 and its ligand. Pharmacol Ther. 2000;88:333-347.

Shi J, Tian F, Lyu J, Yang M. Nanoparticle based fluorescence resonance energy transfer (FRET) for biosensing applications. J. Mater. Chem. B. 2015; 3(35):6989-7005.

Shields JM, Pruitt K, McFall A, Shaub A, Der CJ. Understanding Ras: 'it ain't over 'til it's over'. Trends Cell Biol. 2000;10:147-154.

Shigaki H, Baba Y, Watanabe M, Miyake K, Murata A, Iwagami S, Ishimoto T, Iwatsuki M, Yoshida N, Baba H. KRAS and BRAF mutations in 203 esophageal squamous cell carcinomas: pyrosequencing technology and literature review. Ann Surg Oncol. 2013; 203:S485-491.

Shih C H, Ozawa S, Ando N, Ueda M, Kitajima M. Vascular endothelial growth factor expression predicts outcome and lymph node metastasis in squamous cell carcinoma of the esophagus. Clin Cancer Res. 2000;6:1161-1168.

Shimada H, Nabeya Y, Okazumi S, Matsubara H, Funami Y, Shiratori T, Hayashi H,Takeda A, Ochiai T. Prognostic significance of serum p53 antibody in patients with esophageal squamous cell carcinoma. Surgery. 2002;132:41-47.

Shimada H, Nabeya Y, Okazumi S, Matsubara H, Kadomatsu K, Muramatsu T, Ikematsu S, Sakuma S, Ochiai T. Increased serum midkine concentration as a possible tumor marker in patients with superficial esophageal cancer. Oncol Rep. 2003;10:411-414.

Sidransky D. Emerging molecular markers of cancer. Nat. Rev. Cancer. 2002; 2(3), 210-219.

Sina AA, Carrascosa LG, Palanisamy R, Rauf S, Shiddiky MJ, Trau M. Methylsorb: a simple method for quantifying DNA methylation using DNA-gold affinity interactions. Anal. Chem. 2014a; 86(20):10179-10185.

Sina AA, Howell S, Carrascosa LG, Rauf S, Shiddiky MJ, Trau M. eMethylsorb: electrochemical quantification of DNA methylation at CpG resolution using DNA-gold affinity interactions. Chem. Commun. 2014b; 50(86):13153-13156.

Singh A, Kapur S, Chattopadhyay I, Purkayastha J, Sharma J, Mishra A, Hewitt SM, Saxena S. Cytokeratin immunoexpression in esophageal squamous cell carcinoma of high-risk population in Northeast India. Appl Immunohistochem Mol Morphol. 2009;17:419-424.

Sipova H, Zhang S, Dudley AM, Galas D, Wang K, Homola J. Surface plasmon resonance biosensor for rapid label-free detection of microribonucleic acid at subfemtomole level. Anal. Chem. 2010; 82(24):10110-10115.

Song S, Wang L, Li J, Fan C, Zhao J. Aptamer-based biosensors. Trends Anal. Chem.; TrAC. 2008;27(2):108-117.

Steel AB, Herne TM, Tarlov MJ. Electrochemical quantitation of DNA immobilized on gold. Anal. Chem. 1998;70(22):4670-4677.

Steel AB, Levicky RL, Herne TM, Tarlov MJ. Immobilization of nucleic acids at solid surfaces: effect of oligonucleotide length on layer assembly. Biophys. J. 2000; 79(2):975-981.

Stoecklein NH, Siegmund A, Scheunemann P, Luebke AM, Erbersdobler A, Verde PE,Eisenberger CF, Peiper M, Rehders A, Esch JS, Knoefel WT, Hosch SB. Ep-CAM expression in squamous cell carcinoma of the esophagus: a potential therapeutic target and prognostic marker. BMC Cancer. 2006;6:165.

Stoner GD, Gupta A. Etiology and chemoprevention of esophageal squamous cell carcinoma. J Carcinog. 2001;22:1737-1746.

Storhoff JJ, Elghanian R, Mirkin, CA, Letsinger RL. Sequence-Dependent Stability of DNA-Modified Gold Nanoparticles. Langmuir. 2002; 18(17):6666-6670.

Su Y, Wang X, Li J, Xu J, Xu L. The clinicopathological significance and drug target potential of FHIT in breast cancer, a meta-analysis and literature review. Drug Des Devel Ther. 2015;9:5439-5445.

Sun T, Miao X, Zhang X, Tan W, Xiong P, Lin D. Polymorphisms of death pathway genes FAS and FASL in esophageal squamous-cell carcinoma. J Natl Cancer Inst. 2004;96:1030-1036.

Sunpaweravong P, Sunpaweravong S, Puttawibul P, Mitarnun W, Zeng C, Baro´n AE, Franklin W, Said S, Varella-Garcia M. Epidermal growth factor receptor and cyclin D1 are independently amplified and overexpressed in esophageal squamous cell carcinoma. J Cancer Res Clin Oncol. 2005;131:111-119.

Takahashi K, Miyashita M, Makino H, Akagi I, Orita H, Hagiwara N, Nomura T, Gabrielson EW, Tajiri T. Expression of Akt and Mdm2 in human esophageal squamous cell carcinoma. Exp Mol Pathol. 2009;87:42-47.

Takaoka M, Harada H, Andl CD, Oyama K, Naomoto Y, Dempsey KL, Klein-Szanto AJ,El-Deiry WS, Grimberg A, Nakagawa H. Epidermal growth factor receptor regulates aberrant expression of insulin-like growth factor-binding protein 3. Cancer Res. 2004;64:7711-7723.

Takeno S, Noguchi T, Fumoto S, Kimura Y, Shibata T, Kawahara K. Ecadherin expression in patients with esophageal squamous cell carcinoma: promoter hypermethylation, snail overexpression, and clinicopathologic implications. Am J Clin Pathol. 2004;122:78-84.

Takeshita N, Mori M, Kano M, Hoshino I, Akutsu Y, Hanari N, Yoneyama Y, Ikeda N, Isozaki Y, Maruyama T, Akanuma N, Miyazawa Y and Matsubara H. miR-203 inhibits the migration and invasion of esophageal squamous cell carcinoma by regulating LASP1. Int J Oncol. 2012;41:1653-1661.

Tang JC, Lam KY, Law S, Wong J, Srivastava G. Detection of genetic alterations in esophageal squamous cell carcinomas and adjacent normal epithelia by comparative DNA fingerprinting using inter-simple sequence repeat PCR. Clin Cancer Res. 2001;7:1539-1545.

Tang WK, Chui CH, Fatima S, Kok SH, Pak KC, Ou TM, Hui KS, Wong MM, Wong J, Law S, Tsao SW, Lam KY, Beh PS, Srivastava G, Chan AS, Ho KP, Tang JC. Oncogenic properties of a novel gene JK-1 located in chromosome 5p and its overexpression in human esophageal squamous cell carcinoma. Int J Mol Med. 2007;19:915-923.

Tao Y, Chai D, Ma L, Zhang T, Feng Z, Cheng Z, Wu S, Qin Y, Lai M. Identification of distinctgene expression profiles between esophageal squamous cell carcinoma and adjacent normal epithelial tissues. Tohoku J Exp Med. 2012;226:301-311.

Thevenot DR, Toth K, Durst RA, Wilson, GS, 2001. Electrochemical biosensors: recommended definitions and classification. Biosens. Bioelectron. 2001;16(1-2):121-131.

Toh Y, Egashira A, Yamamoto M. Epigenetic alterations and their clinical implications in esophageal squamous cell carcinoma. Gen Thorac Cardiovasc Surg. 2013;61(5):262-269.

Tokugawa T, Sugihara H, Tani T, Hattori T. Modes of silencing of p16 in development of esophageal squamous cell carcinoma. Cancer Res. 2002;62:4938-4944.

Tomita M, Ayabe T, Matsuzaki Y, Edagawa M, Maeda M, Shimizu T, Hara M,Onitsuka T. Expression of nm23-H1 gene product in esophageal squamous cell carcinoma and its association with vessel invasion and survival. BMC Cancer. 2001;1:3.

Tran GD, Sun XD, Abnet CC, Fan JH, Dawsey SM, Dong ZW, et al. Prospective study of risk factors for esophageal and gastric cancers in the Linxian general population trial cohort in China. Int J Cancer. 2005;113:456-463.

Tse, D, Zhai R, Zhou W, Heist R, Asomaning K, Su L, Lynch T, Wain J, Christiani D, Liu G. Polymorphisms of the NER pathway genes, ERCC1 and XPD are associated with esophageal adenocarcinoma risk. Cancer causes & control: CCC.2008;19:1077-1083.

Tuynman JB, Lagarde SM, Ten Kate FJ, Richel DJ, van Lanschot JJ. Met expression is an independent prognostic risk factor in patients with oesophageal adenocarcinoma. Br J Cancer. 2008;98:1102-1108.

Uchikado Y, Natsugoe S, Okumura H, Setoyama T, Matsumoto M, Ishigami S, Aikou T. Slug Expression in the E-cadherin preserved tumors is related to prognosis in patients with esophageal squamous cell carcinoma. Clin Cancer Res. 2005;11:1174-1180.

Vay C, Hosch SB, Stoecklein NH, Klein CA, Vallböhmer D, Link BC, Yekebas EF, Izbicki JR, Knoefel WT, Scheunemann P. Integrin expression in esophageal squamous cell carcinoma: loss of the physiological integrin expression pattern correlates with disease progression. PLoS One. 2014;9:e109026.

Veeramachaneni NK, Kubokura H, Lin L, Pippin JA, Patterson GA, Drebin JA, Battafarano RJ. Down-regulation of beta catenin inhibits the growth of esophageal carcinoma cells. J Thorac Cardiovasc Surg. 2004;127:92-98.

Wakai J, Takagi A, Nakayama M, Miya T, Miyahara T, Iwanaga T, Takenaka S, Ikeda Y, Amano, M. A novel method of identifying genetic mutations using an electrochemical DNA array. Nucleic Acids Res. 2004; 32(18),:e141-e141.

Wang J, Wei J, Xu X, Pan W, Ge Y, et al. Replication Study of ESCC Susceptibility Genetic Polymorphisms Locating in the ADH1B-ADH1C-ADH7 Cluster Identified by GWAS. PLoS ONE. 2014;9:e94096.

Wang LD, Guo RF, Fan ZM, He X, Gao SS, Guo HQ, Matsuo K, Yin LM, Li JL. Association of methylenetetrahydrofolate reductase and thymidylate synthase promoter polymorphisms with genetic susceptibility to esophageal and cardia cancer in a Chinese high-risk population. Dis Esophagus. 2005;18:177-184.

Wang LS, Chow KC, Lien YC, Kuo KT, Li WY. Prognostic significance of nm23-H1 expression in esophageal squamous cell carcinoma. Eur J Cardiothorac Surg. 2004;26:419-424.

Wang W, Xue L, Wang P. Prognostic value of β-catenin, c-myc, and cyclin D1 expressions in patients with esophageal squamous cell carcinoma. Med Oncol. 2011 ;28:163-169.

Wang X, Tian X, Liu F, Zhao Y, Sun M, Chen D, Lu C, Wang Z, Shi X, Zhang Q, Zhang D, Shen Z, Li F, Harris CC, Cai H, Ke Y. Detection of HPV DNA in esophageal cancer specimens from different regions and ethnic groups: a descriptive study. BMC Cancer. 2010;10:19.

Wang XJ, Zheng YL, Fan QX, Zhang XD. RNAi-induced K-Ras gene silencing suppresses growth of EC9706 cells and enhances chemotherapy sensitivity of esophageal cancer. Asian Pac J Cancer Prev. 2012;13:6517-6521.

Wang Y, Liu S, Zhu H, Zhang W, Zhang G, Zhou X, Zhou C, Quan L, Bai J, Xue L, Lu N, Xu N. FRAT1 overexpression leads to aberrant activation of beta-catenin/TCF pathway in esophageal squamous cell carcinoma. Int J Cancer. 2008;123:561-568.

Ward E. Occupational diseases and injury - esophageal cancer. In: Levy B, Wagner G, Rest K, Weeks J (eds). Preventing Occupational Disease and Injury, 2nd edn. American Public Health Association, Washington, DC 2005;195-196.

Watanabe N, Shimizu M, Kochi T, Shirakami Y, Tanaka T. Esophageal carcinogenesis. Open Journal of Pathology. 2014; 4:151-170.

Wijnhoven BP, Tilanus HW, Dinjens WN. Molecular biology of Barrett's adenocarcinoma. Ann Surg. 2001;233:322-327.

Wong GS, Lee JS, Park YY, Klein-Szanto AJ, Waldron TJ, Cukierman E, Herlyn M, Gimotty P, Nakagawa H, Rustgi AK. Periostin cooperates with mutant p53 to mediate invasion through the induction of STAT1 signaling in the esophageal tumor microenvironment. Oncogenesis. 2013;2:e59.

Wu C, Kraft P, Zhai K, Chang J, Wang Z, et al. Genome-wide association analyses of esophageal squamous cell carcinoma in Chinese identify multiple susceptibility loci and gene-environment interactions. Nat Genet. 2012;44:1090-1097.

Wu D-C, Wu IC, Lee J-M et al. Helicobacter pylori infection: a protective factor for esophageal squamous cell carcinoma in a Taiwanese population. Am J Gastroenterol. 2005; 100:588-593.

Wu X, Wu G, Yao X, Hou G, Jiang F. The clinicopathological significance and ethnic difference of FHIT hypermethylation in non-small-cell lung carcinoma: a meta-analysis and literature review. Drug Des Devel Ther. 2016;10:699-709.

Wu YL, Jiang XR, Lillington DM, Newland AC, Kelsey SM. Upregulation of lipocortin 1 inhibits tumour necrosis factor-induced apoptosis in human leukaemic cells: a possible mechanism of resistance to immune surveillance. Br J Haematol. 2000;111(3):807-816.

Xia SH, Hu LP, Hu H, Ying WT, Xu X, Cai Y, Han YL, Chen BS, Wei F, Qian XH,Cai YY, Shen Y, Wu M, Wang MR. Three isoforms of annexin I are preferentially expressed in normal esophageal epithelia but down-regulated in esophageal squamous cell carcinomas. Oncogene. 2002;21:6641-6648.

Xiao Y, Lubin AA, Baker BR, Plaxco KW, Heeger AJ. Single-step electronic detection of femtomolar DNA by target-induced strand displacement in an electrode-bound duplex. Proc. Natl. Acad. Sci. U.S.A. 2006; 103(45):16677-16680.

Xiao-Ping H, Tie-Hua R, Peng L, Qiu-Liang W, Guang-Yu Y, Jing-Hui H, Xiao-Dong S, Xiao-Dong L, Bao-Jiang L, Peng-Yuan Z, Kai L, Zhi-Fan H. Cyclin D1 overexpression in esophageal cancer from southern China and its clinical significance. Cancer Lett. 2006 ;231:94-101.

Xu XC. Tumor-suppressive activity of retinoic acid receptor-beta in cancer. Cancer Lett. 2007;253:14-24.

Xue L, Hu N, Song Y, et al. Tissue microarray analysis reveals a tight correlation between protein expression and progression of esophageal squamous cell carcinoma. BMC Cancer. 2006;6:296.

Yasushi T, Eiji O, Kippei O, Yasuo S, Shuhei I, Akinori E, Hiroshi S, Yoshihiro K, Masaru M, Yoshihisa S, Takeshi O, Yoshihiko M. Alcohol drinking, cigarette smoking, and the development of squamous cell carcinoma of the esophagus: molecular mechanisms of carcinogenesis. Int J Clin Oncol. 2010;15:135-144.

Yi SM, Li GY. Null genotype of GSTT1 contributes to esophageal cancer risk in Asian populations: evidence from a meta-analysis. Asian Pac J Cancer Prev. 2012;13:4967-4971.

Younes M, Schwartz MR, Ertan A, Finnie D, Younes A. Fas ligand expression in esophageal carcinomas and their lymph node metastases. Cancer. 2000;88:524-528.

Yue CM, Deng DJ, Bi MX, Guo LP, Lu SH. Expression of ECRG4, a novel esophageal cancer-related gene, down regulated by CpG island hyper methylation in human esophageal squamous cell carcinoma. World J Gastroenterol. 2003;9:1174-1178.

Yun T, Liu Y, Gao D, Linghu E, Brock MV, Yin D, Zhan Q, Herman JG, Guo M. Methylation of CHFR sensitizes esophageal squamous cell cancer to docetaxel and paclitaxel. Genes Cancer. 2015;6(1-2):38-48.

Zare M, Jazii FR, Soheili ZS, Moghanibashi MM. Downregulation of tropomyosin-1 in squamous cell carcinoma of esophagus, the role of Ras signaling and methylation. Mol Carcinog. 2012;51:796-806.

Zeng R, Duan L, Kong YK, Wu XL, Wang Y, Xin G, Yang KH. Prognostic significance of beta-catenin expression in patients with esophageal carcinoma: a meta-analysis. Asian Pac J Cancer Prev. 2014;15:6103-6108.

Zhang C, Fu L, Fu J, Hu L, Yang H, Rong TH, Li Y, Liu H, Fu SB, Zeng YX, Guan XY. Fibroblast growth factor receptor 2-positive fibroblasts provide a suitable microenvironment for tumor development and progression in esophageal carcinoma. Clin Cancer Res. 2009;15:4017-4027

Zhang X, Liu B, Servos MR, Liu J. Polarity control for nonthiolated DNA adsorption onto gold nanoparticles. Langmuir. 2013; 29(20):6091-6098.

Zhang X, Liu, B, Dave N, Servos MR, Liu J. Instantaneous attachment of an ultrahigh density of nonthiolated DNA to gold nanoparticles and its applications. Langmuir. 2012; 28(49):17053-17060.

Zhang X, Rong TH, Zhang Y, Long H, Fu JH, Ling P, Zhang LJ, Yang MT, Zeng CG, Ma GW, Su XD, Li XD, Wang JY, Wen ZS, Zhao JM. Expression and significance of C-kit and platelet-derived growth factor receptor-beta (PDGFRbeta) in esophageal carcinoma. Ai Zheng. 2006;25:92-95.

Zhao J, Zhang Y, Ithychanda SS, Tu Y, Chen K, Qin J, Wu C. Migfilin interacts with Src and contributes to cell-matrix adhesion-mediated survival signaling. J Biol Chem. 2009;284:34308-34320.

Zhou ZQ, Cao WH, Xie JJ, Lin J, Shen ZY, Zhang QY, Shen JH, Xu LY, Li EM. Expression and prognostic significance of THBS1, Cyr61 and CTGF in esophageal squamous cell carcinoma. BMC Cancer. 2009;9:291.

Zhu D, Xing D, Shen X, Liu J, Chen Q. High sensitive approach for point mutation detection based on electrochemiluminescence. Biosens. Bioelectron. 2004; 20(3):448-453.

# Chapter 3

# Expression and copy number profiling of FAM134B in oesophageal squamous cell carcinoma

A detailed explanation of methodology and results on quantification of FAM134B copy number changes are described in chapter 5 as it appears in Scientific reports (2016). Profiling of FAM134B expression data has not published yet as it appears in page at 93-100.

## Introduction

Recent advances in high-throughput technologies have been provided that changes in DNA copy number and overexpressed or underexpressed transcript of a gene may serve as DNA-based and RNA-based biomarkers in cancer, respectively. Growing number of evidence suggest that *FAM134B* gene plays a key role in regulating cancer cell biology and in autonomic neurological disorders via presenting its altered expression pattern and cellular autophagy. Previously, it has been reported that *FAM134B* has oncogenic properties in oesophageal squamous cell carcinoma (ESCC) while in colon adenocarcinoma, it acts as tumour suppressor gene. However, at this moment, there is little fundamental information regarding the molecular roles of *FAM134B* in the pathogenesis of oesophageal squamous cell carcinoma. Also, FAM134B protein has not been quantified in ESCC. In addition, there is no report on *FAM134B* copy number changes and expression in a large cohort of tissue samples from patients with ESCC. A comprehensive study on FAM134B at DNA, mRNA and protein level will elucidate the role of *FAM134B* in the pathogenesis of ESCC. The aim of this study is to detect the *FAM134B* copy number variations and expression in a large cohort of tissue samples from patients with ESCC. Correlation of *FAM134B* copy number variations, expression and their clinicopathological significance in patients with ESCCs were analysed.

# 3 Profiling of FAM134B expression in ESCC

## 3.1 Materials and methods

### 3.1.1 Recruitment of tissue samples with clinicopathological parameter

To explore the expression pattern of *FAM134B*, about 55 fresh tissues samples including primary tumour, adjacent normal and lymph node metastasis from patients diagnosed with oesophageal squamous cell carcinoma were recruited with no selection bias during the period of 1990 to 2005. Tissue samples for this research were collected after esophagotomy from the Department of Surgery, Queen Mary Hospital, Hong Kong. These samples comprised tumour tissues and adjacent normal tissues of same patients with different stages of oesophageal squamous cell carcinoma. Ethical approval has been obtained for the use of these samples. The adjacent non-tumor epithelial tissues which are at least 10 cm away from the tumour were also enlisted. For each tissue sample, the sex, age, exact site, stage, TNM stage and status of tumours were documented. In this study, the parameters such as site (Lower, Middle and Upper part of the oesophagus), stage (Low and High), TNM stage (I, II, III and IV) and status (Alive and Dead) were also recorded for studying significant correlation with *FAM134B* gene copy number alteration. The tissue samples were fixed in 10% formalin and embedded in paraffin in keeping with standard hospital procedures for immunohistochemical staining. For *FAM134B* mRNA expression analysis, fresh frozen tissues were used after snap freezing them in liquid nitrogen. Both formalin-fixed-paraffin-embedded blocks and fresh tissues were sectioned using a tissue microtome (Leica, RM2235, Wetzlar, Germany) and a cryostat (Leica CM 1850 UV, Wetzlar, Germany) respectively. Tissues were sectioned in 5 microns for histopathological analysis via haematoxylin and eosin. The histological slides were examined by an expert hospital pathologist and reviewed by the research supervisor and principal investigator.

### 3.1.2 ESCC cell lines

Four oesophageal cancer cell lines such as HKESC-1, HKESC-4, KYSE-70, KYSE-510 and one skin epithelial cell line such as HACAT keratinocyte were recruited for this study. Two ESCC cell lines (HKESC-1 and HKESC-4) were kindly provided by our research group (Hu et al., 2000; Cheung et al., 2007). Other ESCC cell lines, KYSE-70, KYSE-510, purchased from Leibniz Institute DSMZ (German collection of microorganisms and cell cultures). The ESCC cell lines of HKESC-1, HKESC-4 and KYSE-510 are maintained in minimum essential medium alpha medium with non-essential amino acids (MEMα growth medium, Gibco) supplemented with 10% fetal

bovine serum (FBS, Gibco), 100 µg/ml penicillin (Gibco) and 100 unit/ml streptomycin (Gibco). On the other hand, HACAT keratinocyte and KYSE-70 cell lines are maintained in Dulbecco's minimum essential medium (DMEM growth medium, Gibco) and RPMI medium (Gibco) supplemented with 10% fetal bovine serum (FBS, Gibco), 100 µg/ml penicillin (Gibco) and 100 unit/ml streptomycin (Gibco), respectively. The ESCC and HACAT cell lines are cultivated in a $37^{O}$C humidified cell culture incubator with 5% carbon dioxide ($CO_2$). Depending upon confluences, cells are washed with PBS and split into 1:3 ratio by using 0.25% trypsin in 0.25% EDTA (Gibco) for subculture. The cell pellets are harvested via trypsinization and kept in $-80^{O}$C for used for DNA and RNA extraction. The liquid nitrogen stocks are made by freezing the cells in 70% of their corresponding mediums, 20% of FBS and 10% of dimethyl sulfoxide (DMSO, Sigma) at $-80^{O}$C for 24 hours and followed by the storage in a liquid nitrogen tank.

### 3.1.3 RNA and DNA extraction from tissue samples and cell lines

For assessing the genetic analysis of *FAM134B*, fresh frozen ESCC tissues were sectioned into 10µm slices for DNA and RNA extraction. For each tissue samples, additional sections have been taken for haematoxylin & eosin staining as these are used to differentiate tumour from surrounding morphologically normal tissue. DNA and RNA are extracted from tissue samples and cell lines as well as purified simultaneously using the protocol from all prep DNA/RNA mini kit (Qiagen, Hilden, NRW, Germany). DNA and RNA quantification is accomplished via Nanodrop Spectrophotometer (BioLab, Scoresby, VIC, Australia) and purity is measured using 260/280 ratio. The concentration of DNA and RNA is noted in ng/µl. RNA was used for cDNA conversion and DNA was stored at $-20^{O}$C until assayed.

### 3.1.4 cDNA conversion

Reverse transcription reactions were performed using 1 µg total RNA in a final reaction volume of 20 µl. cDNA conversion was achieved using the manufacturer's instructions from miScript Reverse Transcription kit (Qiagen, Hilden, NRW, Germany). In order to inactivation of reverse transcriptase mix, 1 µg of total RNA and Master Mix were incubated for 60 minutes at 37ºC and then heated up for 5 min at 95ºC. Each cDNA sample was diluted to 30 ng/µl for providing uniformly concentrated samples for RNA qRT-PCR. Samples were stored at -20ºC.

### 3.1.5 Primer design for qRT-PCR

Primers were designed for the target *FAM134B* gene and housekeeping GAPDH genes for mRNA studies. The primer sets for amplification of *FAM134B* (GenBank accession number for variant 1 NM_001034850 and for variant 2 NM_019000) and GAPDH (GenBank accession number NM_002046) genes were selected using Primer3 version 0.4.0 (http://frodo.wi.mit.edu/primer3/). The specificity of the primers was checked using Primer-Blast (http://www.ncbi.nlm.nih.gov/tools/primer-blast) and Primer Premier program version 5 (Premier Biosoft, Palo Alto, California) to check for primer parameters like GC content, Tm and ΔG, in addition, to forecasting any possible mismatching, primer dimmer or hairpin formation. The primers for *FAM134B* gene were designed to amplify both isoforms of the gene. The product of the primers for *FAM134B* gene is located in Exon 7 of the gene at reference sequence of 1092-1180 of variant 1. The primers for *FAM134B* gene were also designed according to exon wise for the screening of mutation. The primer pairs were prepared from Sigma-Aldrich (NSW, Australia). The primers designed particularly for *FAM134B* and control genes (GAPDH) with a view to identifying mRNA expression levels in oesophageal squamous cell carcinoma. The list of chosen primer sets is summarised in Table 2.

**Table 2: List of Primers designed for qRT-PCR**

| Target Genes | primer sequence (Forward and Reverse) | Amplicon size |
|---|---|---|
| JK1(FAM134B) | 5′-TGACCGACCCAGTGAGGA-3′ | 106 bp |
| | 5′-GGGCAAACCAAGGCTTAA-3′ | |
| GAPDH | 5'-TGCACCACCAACTGCTTAGC-3' | 88 bp |
| | 5'-GGCATGGACTGTGGTCATGAG-3' | |

### 3.1.6 Real-time Quantitative PCR

mRNA expression of *FAM134B* gene was accomplished using a rotor Gene Q Real-Time PCR Detection system (Qiagen). cDNA and Housekeeping genes such as Glyceraldehyde 3-phosphate dehydrogenase (GAPDH) was used for mRNA expression of *FAM134B* gene. GAPDH has been used widely as a universal control for gene expression in many cancer studies since its expression remains almost unchanged. qRT-PCR was achieved in a total volume of 10 µl reaction mixture comprising 5 µl of 2XSensiMix SYBR No-ROX master mix (Bioline, London, UK), 1 µl of each10 picomole/ µl primer, 1 µl of cDNA/ genomic DNA at 30 ng/µl and 2 µl of Nuclease-free water. Assays were accomplished in duplicate and a non-template control was included in all the experiment. The results of the quantitative real-time polymerase change reaction were analysed using the comparative threshold cycle (CT) method (Livak and

Schmittgen, 2001). In order to perform data analysis of *FAM134B* mRNA expression, relative quantification was applied to calculate the ratio between the quantity of a target molecule in a sample (*FAM134B* gene) and in the calibrator (the reference housekeeping gene GAPDH). In this study, the comparative ΔΔCt method has been used for relative quantification as the amplification efficiency of the reference gene is roughly the same compared to the target gene. Normalized (ΔCt) values were calculated by the following equations: ΔCt = Ct JK1[sample] - Ct HBD/GAPDH[sample]. For getting the results of quantitative amplification, the fold change in the target gene was also measured for each sample via 2-ΔΔCt method: ΔΔCt= (CtJK1 – Ct GAPDH)CANCER - (Ct JK1 - Ct GAPDH)NORMAL. For the purpose of showing the results, ratios (=Mean Ct JK1[sample]/Ct GAPDH[sample]) were also utilised. With a view to calculating DNA copy number change, a fold change of less than 0.9 was considered as deletion whereas a fold change of more than 1.5 was noted as amplification of DNA in this research. On the contrary, a fold change of more than 1.5 was regarded as a high expression of JK1 mRNA and a fold change less than one considered as a low expression of JK1 mRNA.

### 3.1.7 Immunocytochemistry

Immunocytochemistry studies were performed to assess the physical localisation of *FAM134B* in oesophageal squamous cell carcinoma and normal epithelial oesophageal cell lines. To facilitate this experiment, Cells were seeded at a density of 4 X $10^5$ cells/ well on 24-well plate and cultured for 24 hours. After achieving the desired confluency, cells were fixed in 70% ice-cold ethanol for 10 minutes at room temperature and were permeabilized with 0.1% Triton X-100 for 5 min. Cells were washed with PBS followed by protein block with 5% BSA (bovine serum albumin). Then, the cultured cells were incubated with the anti-rabbit FAM134B antibody (Santa Cruz, Dallas, TX) for overnight at 4ºC. They were incubated with secondary antibody (1:1000; antirabbit IgG-poly-horseradish peroxidase) in 5% BSA for one hour at 37ºC. A brown positive staining was obtained by developing the peroxidase activity with freshly prepared 3, 30-diaminobenzidine (DAB) and substrate chromogen solution (Leica, North Ryde, NSW, Australia). After washing with phosphate-buffered saline (PBS), cells were visualised by light microscopy (Olympus CKX41, Macquarie Park, NSW, Australia). Each staining was run in triplicate on a 24 well plate.

### 3.1.8 Immunofluorescence

Immunofluorescence was used to further ascertain the cellular distribution of *FAM134B*. It will provide exact localisation of *FAM134B* since it is more specific and sensitive. In order to perform this experiment, cells were seeded on the sterile coverslips at a density of approximately 10,000/$cm^2$ and incubated at $37^OC$ for 12 hours. Then the media was discarded and rinsed the cells with ice-cold PBS. After that, the cells were subjected to fixation using 70% cold ethanol for 30 minutes and were permeabilized with 0.1% Triton X-100 for 5 min. The cells were then washed with PBS and blocking with 5% BSA for 1 hour at room temperature. After washing with PBS, with anti-rabbit FAM134B (Santa Cruz) (1:150) and anti-goat giantin, a cis-Golgi marker protein antibody (Santa Cruz) (1:150) at 4ºC overnight. This was followed by 2 h of incubation with secondary antibody labelled with fluorescein isothiocyanate (FITC) and Texas red fluorophore (Sigma-Aldrich, St Louis, MO) at room temperature and was later mounted on glass slides, sealed with nail polish, and then observed under a confocal microscope (Nikon A1Rþ, Nikon Inc., Tokyo, Japan).

### 3.1.9 Western blot analysis

Western blot analysis was carried out to study the expression pattern of FAM134B at the protein level in different stages of cancer patients as well as in various ESCC cell lines. To execute this experiment, total protein was extracted from cells with lysis buffer (Bio-Rad, USA). The extracted protein was quantified using the protocol from protein quantification assay kit (Macherey-nagel inc. Bethlehem, PA, USA). About 30 µg protein was subjected to SDS-PAGE with 4-15% polyacrylamide precast (Bio-Rad, USA) gels and transferred to PVDF membranes (Bio-Rad, USA). The membrane was blocked with 5% non-fat milk at room temperature for 2 hours and incubated with primary antibody at $4^O$ C for overnight. Then, the membrane was washed twice and incubated using Horse-radish peroxidase-conjugated secondary antibody at room temperature for 2 hours. Protein band was diagnosed by enhanced chemiluminescence (ECL) and visualised using Chemidoc-MP imaging system (Bio-Rad, USA). A strong or thick band in the membrane was considered as FAM134B protein high expression and the thin or weak band will be counted as a lower expression of the FAM134B protein.

### 3.1.10 Data analysis

Correlations of *FAM134B* mRNA expression with clinicopathological parameters were done. Comparisons between groups were implemented using the chi-square test, likelihood ratio and Fisher's exact test. All the data was entered into a computer database

and the statistical analysis was executed using the Statistical Package for Social Sciences for Windows (version 22.0, IBM SPSS Inc., New York, NY, USA). The significance level was taken at $p < 0.05$.

## 3.2 Results

### 3.2.1 Quantification of *FAM134B* mRNA expression in ESCC tissue samples

*FAM134B* mRNA was expressed in all tissue samples of ESCC. After performing real-time PCR, agarose gel electrophoresis was revealed that the generated PCR product existed as a DNA fragment of 106 bp for JK1 and 88 bp for GAPDH, shown in Figure 21.

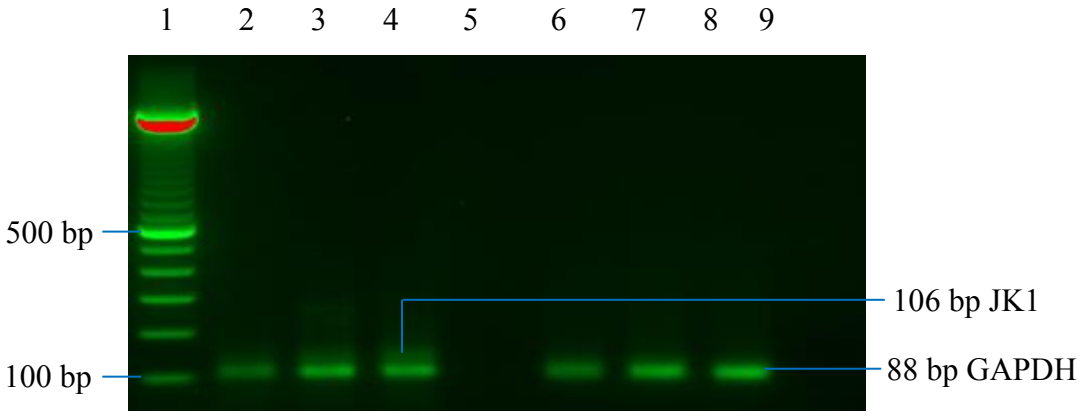


**Figure 21.** *FAM134B* mRNA was expressed in all selected ESCC tissue (2-9) except for the water control (5,9) in 2% agarose gel.

In this study, FAM134B is overexpressed in lymhnode metastasis and down-regulated in cancer in comparison to normal tissue (Figure 22).

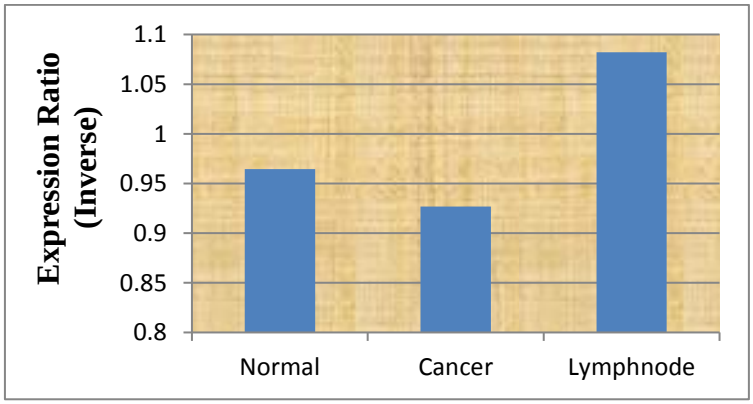


**Figure 22. Altered *FAM134B* mRNA expression levels in normal, cancer and lymphnode tissues**

### 3.2.2 Altered *FAM134B* mRNA expression in ESCC tissues

In ESCC tissues (n=55), 49% (27/55) showed overexpression of *FAM134B* while 47% (26/55) revealed down-regulation of *FAM134B* when compared to matched non-neoplastic tissues (Figure 23). 4% (2/55) of the ESCC tissue did not any change in *FAM134B* mRNA expression compared to the matched non-neoplastic tissues.

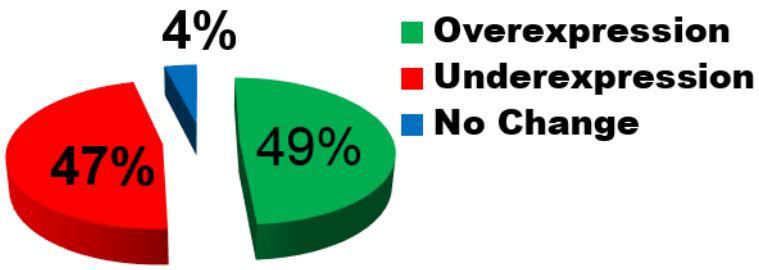


**Figure 23.** FAM134B mRNA expression profiling in oesophageal squamous cell carcinoma.

### 3.2.3 Localisation of FAM134B in ESCC

Immunofluorescence study showed that FAM134B protein was localised and expressed in both cytoplasm and nucleus of ESCC and non-neoplastic squamous epithelial cell line (Figure 24). It was also found that FAM134B co-localized with cis-Golgi marker protein giantin in all cell lines. Immunocytochemistry analyses also revealed cytoplasmic and nuclear expression of the FAM134B protein in the ESCC ESCC and non-neoplastic squamous epithelial cell lines.

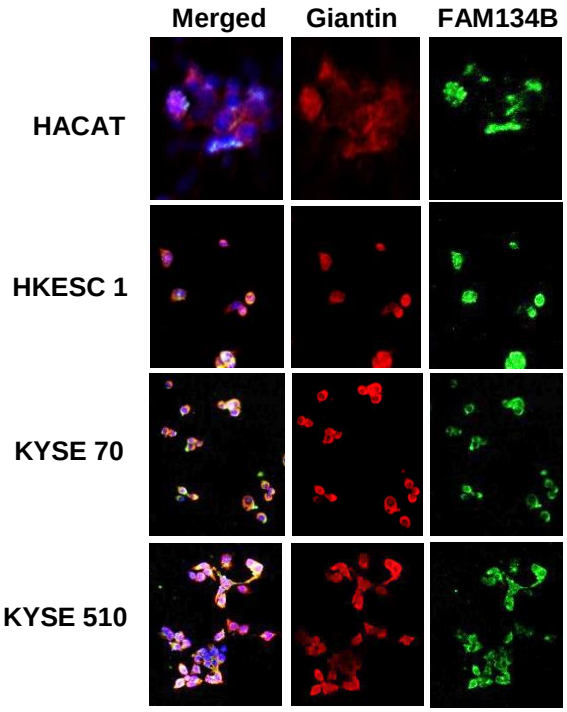


**Figure 24.** Localization of *FAM134B* in ESCC and non-neoplastic squamous epithelial cell line.

### 3.2.4 Expression of FAM134B in ESCC

The expression of FAM134B at protein levels displayed significant changes in the four ESCC cell lines when compared to the non-neoplastic squamous epithelial cell line (HACAT) epithelial cells after normalizing with housekeeping gene (Figure 25). It indicates that alteration of FAM134B protein is a common event in the pathogenesis of ESCC. The FAM134B protein alteration might be happened due to the other genetic (Mutation) or epigenetic event (promoter hypermethylation) of this gene.

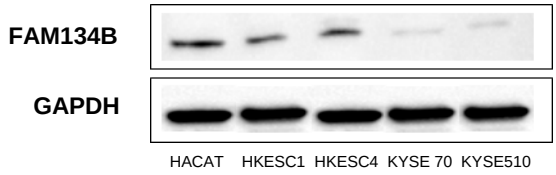


**Figure 25.** Western blot analysis of FAM134B protein (~54 kDa) expression in the different cell lines.

# Chapter 4

# *FAM134B* mutation detection via molecular biological methods and its clinical significances in ESCC

Chapter 4 is included as it appears in Scientific Reports (2016).

## Introduction

Mutations in oncogenes, tumour suppressor genes and mismatch-repair genes are a clinically relevant DNA biomarkers in cancer. Recent studies have confirmed that *FAM134B* is a growth-related gene and it possesses both oncogenic and tumour suppressor properties in oesophageal and colorectal carcinomas, respectively. Our previous reports on DNA copy number changes and altered expression levels of *FAM134B* gene implying its potential role in the progression of ESCC. It has been suggested that genetic alteration of *FAM134B* gene in ESCC might be related with other genetic events such as mutation and promoter hypermethylation which could be used as a biomarker for ESCC. Recent studies have reported *FAM134B* mutations for the first time in hereditary sensory and autonomic neuropathy type IIB (HSAN IIB) and vascular dementia. Despite the mutational data of *FAM134B* in the neurological lesion, till date, there is no current data available on the mutational significance of *FAM134B* in human cancers. Thus, this study aimed to find possible novel *FAM134B* mutation sites and its clinical relevance for the first time in human cancers.

SCIENTIFIC REPORTS

OPEN

# Identification of Novel FAM134B (JK1) Mutations in Oesophageal Squamous Cell Carcinoma

Received: 01 February 2016
Accepted: 09 June 2016
Published: 04 July 2016

Md. Hakimul Haque[1,*], Vinod Gopalan[1,*], Kwok-wah Chan[2], Muhammad J. A. Shiddiky[3], Robert Anthony Smith[1,4] & Alfred King-yin Lam[1,*]

**Mutation of *FAM134B* (*Family with Sequence Similarity 134, Member B*) leading to loss of function of its encoded Golgi protein and has been reported induce apoptosis in neurological disorders. *FAM134B* mutation is still unexplored in cancer. Herein, we studied the DNA copy number variation and novel mutation sites of *FAM134B* in a large cohort of freshly collected oesophageal squamous cell carcinoma (ESCC) tissue samples. In ESCC tissues, 37% (38/102) showed increased *FAM134B* DNA copies whereas 35% (36/102) showed loss of *FAM134B* copies relative to matched non-cancer tissues. Novel mutations were detected in exons 4, 5, 7, 9 as well as introns 2, 4-8 of *FAM134B via* HRM (High-Resolution Melt) and Sanger sequencing analysis. Overall, thirty-seven *FAM134B* mutations were noted in which most (31/37) mutations were homozygous. *FAM134B* mutations were detected in all the cases with metastatic ESCC in the lymph node tested and in 14% (8/57) of the primary ESCC. Genetic alteration of *FAM134B* is a frequent event in the progression of ESCCs. These findings imply that mutation might be the major driving source of *FAM134B* genetic modulation in ESCCs.**

Oesophageal squamous cell carcinoma (ESCC) is the most common histological subtype of oesophageal carcinomas and it has complex molecular pathology compared to other carcinomas[1–3]. Identification of various genetic and epigenetic changes including mutations of key regulatory genes have a significant role in predicting the biological behaviour of ESCC as well as the prognosis of the patients with ESCC[4–13].

Our previous studies using comparative genomic hybridization analysis revealed that genes in the region of chromosome 5p play a vital role in the pathogenesis of ESCC[14,15]. *FAM134B* (*Family with sequence similarity 134, member B*) also known as *JK1*is a novel gene placed at chromosome 5p15.1 downstream of δ-catenin[16]. The oncogenic properties of *FAM134B* (*JK1*) were first reported both in ESCC tissues and cell lines, while ESCC tissues also showed altered *FAM134B* expression[16]. Also, our recent studies have confirmed the growth related properties of *FAM134B* by exhibiting multiple tumour suppressor properties of *FAM134B* (*JK1*) in colorectal cancer tissues and cell lines[17–19].

Recently, other researchers have reported that *FAM134B* encodes a *cis*-Golgi transmembrane protein, and its mutation can regulate cell apoptosis and long-term survival of nociceptive and autonomic ganglion neurons[20–25]. Homozygous loss of function mutations in *FAM134B* was reported for the first time in hereditary sensory and autonomic neuropathy type IIB (HSAN IIB) and in vascular dementia[20,24]. In addition, Khaminets *et al.* have most recently noted that *FAM134B* regulated endoplasmic reticulum turnover by selective autophagy[25]. To the best of our knowledge, at the time of writing, there is no data available on the mutational significance of *FAM134B* in human cancers. Also, the clinicopathological correlation of *FAM134B* mutation and clinicopathological parameters has never been reported in human cancer samples. Thus, the current study aims to detect mutations in different exon and intron regions of *FAM134B* (*JK1*) in ESCC tissue samples. In addition, the correlations of *FAM134B* (*JK1*) mutations with various clinicopathological parameters and natural copy number variations in ESCCs were analysed.

[1]Cancer Molecular Pathology in Menzies Health Institute Queensland, Griffith University, Gold Coast, Australia. [2]Department of Pathology, Li Ka Shing Faculty of Medicine, The University of Hong Kong, Queen Mary Hospital, Hong Kong. [3]School of Natural Sciences, Griffith University, Nathan Campus, Australia. [4]Genomics Research Centre, Institute of Health and Biomedical Innovation, Faculty of Health, Queensland University of Technology, Brisbane, Queensland, Australia. *These authors contributed equally to this work. Correspondence and requests for materials should be addressed to A.K.-Y.L. (email: a.lam@griffith.edu.au)

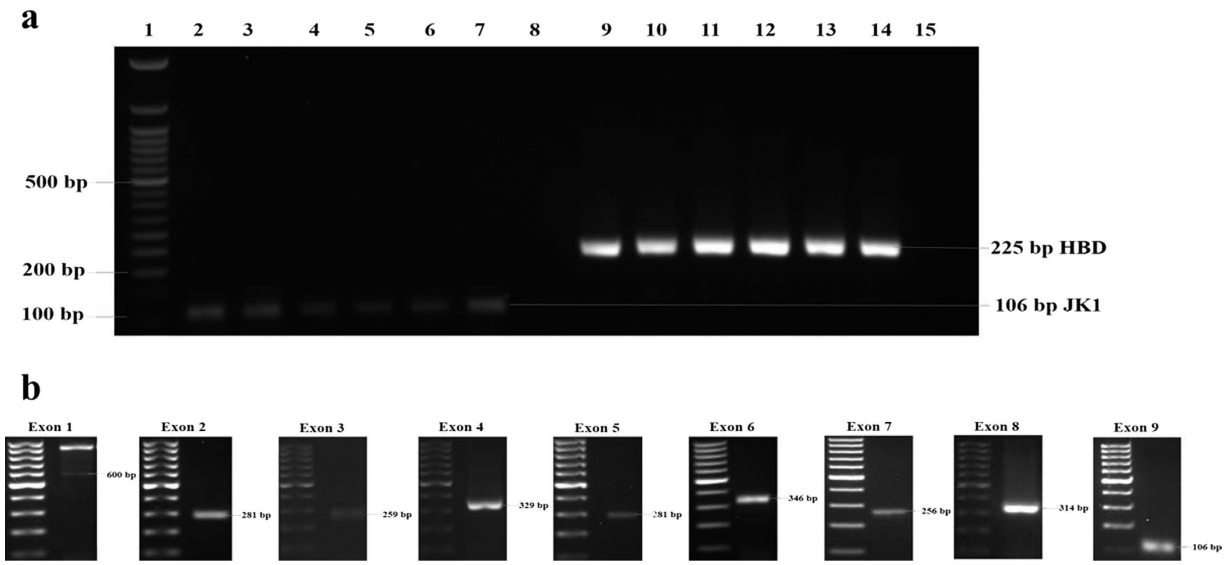


**Figure 1.** ***FAM134B* (*JK1*) gene amplification in oesophageal squamous cell carcinoma. (a)** Amplified PCR products of *FAM134B* (*JK1*) (122bp) and *HBD* (225bp) in 2% agarose gel. *FAM134B* (*JK1*) and *HBD* were present in all the samples (2–14) except for the water control (15). Fifty-base pair DNA ladder was used for comparison. **(b)** Representative amplified PCR products of exon 1, exon 2, exon 3, exon 4, exon 5, exon 6, exon 7, exon 8 and exon 9 of *FAM134B* (*JK1*) in 1.5% agarose gel. Hundred-base pair DNA ladder was used for comparison.

## Results

**Identification of *FAM134B* (*JK1*) DNA in ESCC tissues.** *FAM134B* (*JK1*) DNA was identified in all the studied samples. In these samples, 600-base pairs (bp), 281-bp, 259-bp, 329-bp, 282-bp, 346-bp, 256-bp, 314-bp and 106-bp fragments were amplified for exon 1, exon 2, exon 3, exon 4, exon 5, exon 6, exon 7, exon 8 and exon 9 of *FAM134B* (*JK1*) respectively. Also, a 225-bp fragment was amplified for the control gene, haemoglobin delta (HBD) (Fig. 1a,b).

***FAM134B* (*JK1*) copy number variations.** In ESCC ($n = 102$), 37% ($n = 38$) showed increased *FAM134B* (*JK1*) copies whereas 35% ($n = 36$) showed a loss of *FAM134B* (*JK1*) copies relative to matched non-cancer tissue. Meanwhile, the remaining 22% ($n = 28$) did not show any change in copies. In ESCCs with lymph node metastasis ($n = 64$), 66% ($n = 42$) showed high *FAM134B* (*JK1*) copies whereas 34% ($n = 22$) revealed deletion ($p = 0.80$). The DNA copy number of *FAM134B* (*JK1*) in cancer showed no statistical correlations with the grades and pathological stages of ESCC or with the gender and the age of the patient ($p > 0.05$) (Table 1).

**Mutation screening using high-resolution Melt (HRM) curve and Sanger sequencing.** *FAM134B* (*JK1*) mutations showed no correlation with other clinical and pathological features of ESCC including gender, age of the patient as well as the sites, histological grades and pathological stages of carcinoma ($p > 0.05$) (Table 2). Also, mutations did not show any correlation with the DNA copy number of *FAM134B* (*JK1*) (Tables 3 and 4).

Overall, 37 *FAM134B* (*JK1*) mutations were found in ESCC (Tables 3 and 4). Of these, 36 *FAM134B* (*JK1*) mutations were noted in metastatic ESCC in lymph node and 16 mutations were detected in primary cancer. Of these 37 mutations, 6 were heterozygous mutations and 31 were homozygous mutations. On the other hand, only 14% (8/57) of the primary carcinoma harboured mutations of *FAM134B* (*JK1*). Mutations were noted in both the primary cancer and the lymph node metastasis with ESCC in 2 cases. In these 2 cases (cases 43 and 50), the mutations noted were identical. Also, of the 37 *FAM134B* (*JK1*) mutations, 11 mutations result in alteration of the amino acid sequences in *FAM134B* (*JK1*) protein while 26 mutations were synonymous.

Among the 9 exons of *FAM134B* (*JK1*) examined, mutations were detected in exons 4, 5, 7 and 9 as well as introns 2, 4, 5, 6, 7 and 8 for *FAM134B* (*JK1*) in ESCC (Figs 2 and 3). In exon 9 of *FAM134B* (*JK1*), thirteen substitution and one frameshift (deletion) mutations were documented in ESCCs. The most common substitution variants in exon 9 are c. 1129T > C, c. 1107G > C, c. 1112T > C which alters the codons and subsequently amino acids - TCA > CCA (p. Ser348Pro), GAG > GAC (p. Glu340Asp) and GTT > GCT (p. Val342Ala) respectively. One frameshift (deletion) *FAM134B* (*JK1*) mutation, c. 1137delT, which alters the codon TTT > TTC resulting in no change in amino acid, but altered amino acids following the frameshift (p. Phe379fs) was noted in ESCC. For exon 4 of *FAM134B* (*JK1*), two mutations, c. 546-547CT > GG and c. 660G > A, were detected in ESCC tissues (Table 3). The mutation in c. 546-547CT > GG change the codons in amino acids - AGC > AGG (p. Ser153Arg) and TGG > GGG (p. Trp154Gly). Meanwhile the mutation in c. 660G > A change the codons in amino acids-GAA > AAA (p. Glu163Lys). Furthermore, four polymorphisms were in identified intron 4 *FAM134B* (*JK1*) in ESCC.

Mutations in other exons and introns of *FAM134B* (*JK1*) were less common in ESCC. There was no mutation noted in exon 8 of *FAM134B* (*JK1*) in ESCC. However, two types of variants, c961-33delA and c1087 + 97C > A,

| Characteristics | Number of Patients | DNA copy | | | P value |
|---|---|---|---|---|---|
| | | Amplification | Deletion | No change | |
| Age | | | | | |
| <60 years | 34(33.3%) | 15(44.1%) | 7(20.6%) | 12(35.3%) | 0.07 |
| >60 | 68(66.7%) | 23(33.8%) | 29(42.6%) | 16(23.5%) | |
| Gender | | | | | |
| Male | 84(82.4%) | 32(38.1%) | 28(33.3%) | 24(28.6%) | 0.66 |
| Female | 18(17.6%) | 6(33.3%) | 8(44.4%) | 4(22.2%) | |
| Histological Grade | | | | | |
| Well | 22(21.6%) | 10(45.5%) | 6(27.3%) | 6(27.3%) | 0.61 |
| Moderate | 59(57.8%) | 23(39.0%) | 21(35.6%) | 15(25.4%) | |
| Poor | 21(20.6%) | 5(23.8%) | 9(42.9%) | 7(33.3%) | |
| Site | | | | | |
| Upper | 12(11.8%) | 5(41.7%) | 6(50.0%) | 1(8.3%) | 0.12 |
| Middle | 55(53.9%) | 23(41.8%) | 14(25.5%) | 18(32.7%) | |
| Lower | 35(34.3%) | 10(28.6%) | 16(45.7%) | 9(25.7%) | |
| T Stage | | | | | |
| 1 | 6(5.9%) | 2(33.3%) | 2(33.3%) | 2(33.3%) | 0.85 |
| 2 | 11(10.8%) | 5(45.5%) | 5(45.5%) | 1(9.1%) | |
| 3 | 64(62.7%) | 23(35.9%) | 22(34.4%) | 19(29.7%) | |
| 4 | 21(20.6%) | 8(38.1%) | 7(33.3%) | 6(28.6%) | |
| Lymph node Metastasis | | | | | |
| Negative | 38(37.3%) | 11(28.9%) | 14(36.8%) | 13(34.2%) | 0.33 |
| Positive | 64(62.7%) | 27(42.2%) | 22(34.4%) | 15(23.4%) | |
| Distant metastasis | | | | | |
| Negative | 97(95.1%) | 35(36.1%) | 35(36.1%) | 27(27.8%) | 0.55 |
| Positive | 5(4.9%) | 3(60.0%) | 1(20.0%) | 1(20.0%) | |
| TNM Stage | | | | | |
| Stage I | 6(5.9%) | 4(66.7%) | 0(0.0%) | 2(33.3%) | 0.22 |
| Stage II | 26(25.5%) | 7(26.9%) | 12(46.2%) | 7(26.9%) | |
| Stage III | 65(63.7%) | 24(36.9%) | 23(35.4%) | 18(27.7%) | |
| Stage IV | 5(4.9%) | 3(60.0%) | 1(20.0%) | 1(20.0%) | |

**Table 1. Clinicopathological features of ESCC and *JK1* (*FAM134B*) copy number variation.**

were detected in intron 8. Also, one silent mutation (c. 816C > T) and a mutation (c. 873 + 23T > C) were noted for exon 7 and intron 7 of *FAM134B* (*JK1*) in ESCC respectively. In addition, two synonymous variants (c. 319G > A and c. 352C > T) were noted in exon 5 of *FAM134B* in ESCC. Lastly, five polymorphisms were detected in intron 2 of *FAM134B* (with the most frequent variant being c. 408-27delA).

## Discussion

Chromosomal copy number changes can indicate activation of oncogenes and inactivation of tumour suppressor genes in human cancers[26]. In our previous studies, *FAM134B* (*JK1*) copy number alterations were found as a frequent event in colorectal adenoma and adenocarcinoma[19]. The current study is the first to investigate *FAM134B* (*JK1*) copy number changes in a large cohort of ESCC. Approximately one third of cancers studied revealed amplification and one third revealed deletion of *FAM134B* in ESCC. This altered DNA copy number changes of *FAM134B* indicate its varied modulation potential in different ESCC patients.

This current study is the first systematic study to investigate mutation sites in *FAM134B* (*JK1*) gene in ESCC. Until now, five homozygous mutations of *FAM134B* (*JK1*) were detected in neurological diseases. They are three nonsense mutations, one frame-shift mutation, and one is a splice-site mutation[20–23]. These mutations were located in exon 1 and intron 7 of the gene. In addition, there were 2 heterozygous mutations reported in exon 1. In ESCC, we have noted 37 distinct mutations of *FAM134B* (*JK1*). Thirty-one are homozygous mutations and 6 were heterozygous mutations. These mutations were found in exons 4, 5, 7, 9 and introns 2, 4, 5, 6, 7 and 8 of *FAM134B* (*JK1*). None of these mutation sites are identical to those noted reported in the neurological diseases. Thus, the mutations related to the pathogenesis of ESCC appear to be are unique. The roles of *FAM134B* (*JK1*) mutations in the pathogenesis of the cancer should therefore be different from their roles in neurological diseases. The mechanisms and presence of any downstream effects of the *FAM134B* (*JK1*) mutations need to be further investigated in ESCC to confirm their significance.

Of the 37 novel mutation sites in *FAM134B* (*JK1*) detected in ESCC, 11 mutations changed the amino acid of the resulting protein while 26 mutation sites do not alter the amino acid composition of the protein. The most common mutations are present in exon 9. Amongst the 11 mutations that changed the amino acid structure of JK1 are three relatively common variants in exon 9 (c. 1129T > C, c. 1107G > C, c. 1112T > C). Of these, c. 1129T > C,

| Characteristics | Number of patients | Mutation cases | No mutation cases | p value |
|---|---|---|---|---|
| Age | | | | |
| <60 year | 20 | 11 | 9 | 0.17 |
| >60 year | 37 | 13 | 24 | |
| Gender | | | | |
| Male | 50 | 19 | 31 | 0.12 |
| Female | 7 | 5 | 2 | |
| Site | | | | |
| Upper | 5 | 2 | 3 | 0.44 |
| Middle | 40 | 15 | 25 | |
| Lower | 12 | 7 | 5 | |
| Grade | | | | |
| Well | 20 | 7 | 13 | 0.58 |
| Moderate | 28 | 12 | 16 | |
| Poor | 9 | 5 | 4 | |
| T Stage | | | | |
| 1 | 1 | 0 | 1 | 0.62 |
| 2 | 6 | 3 | 3 | |
| 3 | 38 | 17 | 21 | |
| 4 | 12 | 4 | 8 | |
| Lymph node Metastasis | | | | |
| Negative | 20 | 7 | 13 | 0.58 |
| Positive | 37 | 17 | 20 | |
| Distant metastasis | | | | |
| Negative | 54 | 22 | 32 | 0.57 |
| Positive | 3 | 2 | 1 | |
| TNM Stage | | | | |
| Stage I | 1 | 1 | 0 | 0.55 |
| Stage II | 14 | 5 | 9 | |
| Stage III | 39 | 17 | 22 | |
| Stage IV | 3 | 2 | 1 | |

**Table 2. Clinicopathological features and *JK1* (*FAM134B*) mutations in oesophageal squamous cell carcinoma.**

is predicted by *in silico* methods as being of minimal effect due to lack of conservation of this amino acid in other species while the other two have potentially higher functional significance due to their predicted ability to also cause splice site modification in the protein. In addition, in exon 9 of *FAM134B* (*JK1*), one frame-shift (deletion) mutation, c. 1137delT, is likely to have increased functional significance as it radically alters and can truncate the protein as well as potentially changing exon splicing of the RNA. The other important mutation that lead to an amino acid change was noted in exon 4 resulting in an exon change GAA > AAA (protein change-p.Glu163Lys). The novel mutations detected in this study that alters the amino acid structure of FAM134B (JK1) have potential to affect the function of *FAM134B* (*JK1*).

In the current study, *FAM134B* (*JK1*) mutations were noted predominately in metastatic ESCCs present in lymph nodes, implying that they have a role in the pathogenesis of lymph node metastases in ESCC. Mutation in the majority of metastatic lymph node tissues compared to primary tumours (Table 3) indicates that *FAM134B* (*JK1*) mutation may offer a survival advantage in different tumour microenvironments, or assist in colonisation of those particular microenvironments. Differing *FAM134B* (*JK1*) sequences imply that, the molecular interactions and characteristics would differ between primary and metastatic tumours. Furthermore, the classical model for metastatic processes suggests that the majority of the cancer cells in the primary tumour have low metastatic potential and only a few cells acquire enough somatic mutations to become metastatic[27]. Thus, the absence of *FAM134* (*JK1*) mutation in the bulk of primary ESCC tissues in this study might be due to the harvesting of cancer cells with fewer somatic mutations. Hence, it can be hypothesised that *FAM134B* (*JK1*) might act as a potential target for predicting lymph node metastasis in ESCC patients. Further research with a larger series of ESCC patients with matched metastatic tissues and potentially functional studies on particular mutations are needed to confirm the metastatic potential of *FAM134B* (*JK1*).

In conclusion, we identified for the first time the mutation of FAM134B (*JK1*) in ESCC tissue samples. The altered expression patterns and copy number variations of *FAM134B* in ESCCs might be modulated by these mutation changes in *FAM134B*. In this study, *FAM134B* mutations were frequently observed in metastatic lymph node tissues indicating its use as a potential predictor for metastasis in ESCCs. Multiple different genetic

| Exons | Sample Code | Primary cancer with mutation | Lymph node metastasis with mutation | FAM134B DNA copy number change | | DNA change | Type of mutation | Codon change | Protein change | Comments |
|---|---|---|---|---|---|---|---|---|---|---|
| | | | | Primary cancer | Lymph node metastasis | | | | | |
| Exon 9 | 41 | No | Yes | N | N | c. 1128T > A | Substitution | CTT > CTA | p.Leu347Leu | Potentially functional due to splice site modification |
| | 30 | No | Yes | D | D | c. 1107G > C c. 1129T > C | Substitution | GAG > GAC TCA > CCA | p.Glu340Asp p.Ser348Pro | pGlu340Asp - Likely functional significance pSer348Pro - Probably lesser effect/ polymorphism due to lack of conservation in other species |
| | 14 | Yes | No | A | A | c. 1149A > G | Substitution | GAA > GAG | p.Glu354Glu | Likely functional significance (also affects splice sites) |
| | 19 | No | Yes | D | A | c. 1112T > C c. 1129T > C | Substitution | GTT > GCT TCA > CCA | p.Val342Ala p.Ser348Pro | pVal342Ala - Likely functional significance (also affects splice sites) pSer348Pro - Probably lesser effect/ polymorphism due to lack of conservation in other species |
| | 3 | Yes | No | D | D | c. 1112T > C c. 1149A > G c. 1152T > G c. 1153G > C | Substitution | GTT > GCT GAA > GAG AAT > AAG GGC > CGC | p.Val342Ala p.Glu354Glu p.Asn355Lys p.Gly356Arg | pVal342Ala - Likely functional significance (also affects splice sites) pGlu354Glu - Likely functional significance (also affects splice sites) pAsn355Lys - Likely functional significance pGly356Arg - Likely functional significance (also affects splice sites) |
| | 35 | Yes | No | A | – | c. 1092T > G c. 1093G > C c. 1097GA > AC c. 1107G > T c. 1129T > C | Substitution | CTT > CTG GAC > CAC CGA > CAC GAG > GAC TCA > CCA | p.Leu335Leu p.Asp336His p.Arg337His p.Glu340Asp p.Ser348Pro | pLeu335Leu - Likely functional significance (also affects splice sites) pAsp336His- Likely functional significance (also affects splice sites) pArg337His - Likely functional significance (also affects splice sites) pGlu340Asp - Likely functional significance pSer348Pro - Probably lesser effect/ polymorphism due to lack of conservation in other species |
| | 43 | Yes | Yes | A | N | c. 1112T > C c. 1129T > C c. 1092T > G c. 1093G > C | Substitution | GTT > GCT TCA > CCA CTT > CTG GAC > CAC | p.Val342Ala p.Ser348Pro p.Leu335Leu p.Asp336His | pVal342Ala - Likely functional significance (also affects splice sites) pSer348Pro - Probably lesser effect/ polymorphism due to lack of conservation in other species pLeu335Leu - Likely functional significance (also affects splice sites) pAsp336His- Likely functional significance (also affects splice sites) |
| | 47 | Yes | No | D | – | c. 1107G > C c. 1129T > C | Substitution | GAG > GAC TCA > CCA | p.Glu340Asp p.Ser348Pro | pGlu340Asp - Likely functional significance pSer348Pro - Probably lesser effect/ polymorphism due to lack of conservation in other species |
| | 50 | Yes | Yes | D | A | c. 1107G > T c. 1129T > C c. 1164A > G | Substitution | GAG > GAC TCA > CCA ACA > ACG | p.Glu340Asp p.Ser348Pro p.Thr360Thr | pGlu340Asp - Likely functional significance pSer348Pro - Probably lesser effect/ polymorphism due to lack of conservation in other species pThr360Thr -Likely functional significance (also affects splice sites) |

Continued

| Exons | Sample Code | Primary cancer with mutation | Lymph node metastasis with mutation | FAM134B DNA copy number change | | DNA change | Type of mutation | Codon change | Protein change | Comments |
|---|---|---|---|---|---|---|---|---|---|---|
| | | | | Primary cancer | Lymph node metastasis | | | | | |
| | 51 | Yes | No | N | – | c. 1112T > C c. 1129T > C | Substitution | GTT > GCT TCA > CCA | p.Val342Ala p.Ser348Pro | pVal342Ala - Likely functional significance (also affects splice sites) pSer348Pro - Probably lesser effect/ polymorphism due to lack of conservation in other species |
| | 34 | Yes | No | A | – | c. 1137delT | Deletion | TTT > TTC | p.Phe350Phe | pPhe350Phe- Likely functional significance (frameshift mutation, truncates protein, may change splicing) |
| Exon 7 | 39 | No | Yes | A | N | c. 816C > T or c. 903C > T | Substitution | GAT > GAC | p.Asp272Asp | pAsp272Asp-Likely functional significance (also affects splice sites) |
| | 19 | No | Yes | D | A | c. 816C > T or c. 903C > T | Substitution | GAT > GAC | p.Asp272Asp | pAsp272Asp -Likely functional significance (also affects splice sites) |
| Exon 5 | 14 | Yes | No | A | A | c. 711G > Ac. 744C > T | Substitution Substitution | ACG > ACA CTC > CTT | p.Thr208Thr p.Leu219Leu | Has no functional significance Has no functional significance |
| | 6 | No | Yes | A | A | c. 711G > A | Substitution | ACG > ACA | p.Thr208Thr | Has no functional significance |
| | 12 | No | Yes | N | N | c. 711G > A | Substitution | ACG > ACA | p.Thr208Thr | Has no functional significance |
| | 41 | No | Yes | N | N | c. 711G > A | Substitution | ACG > ACA | p.Thr208Thr | Has no functional significance |
| | 20 | No | Yes | N | N | c. 711G > A | Substitution | ACG > ACA | p.Thr208Thr | Has no functional significance |
| | 11 | No | Yes | A | N | c. 711G > A | Substitution | ACG > ACA | p.Thr208Thr | Has no functional significance |
| | 3 | Yes | No | D | D | c. 711G > A | Substitution | ACG > ACA | p.Thr208Thr | Has no functional significance |
| | 15 | No | Yes | D | N | c. 711G > A | Substitution | ACG > ACA | p.Thr208Thr | Has no functional significance |
| Exon 4 | 6 | No | Yes | A | A | c. 546–547CT > GG c. 660G > A | Substitution Substitution | AGC > AGG and TGG > GGG GAA > AAA | p.Ser153Arg p.Trp154Gly p.Glu163Lys | pSer153Arg and pTrp154Gly-Likely functional significance. (also affects splice sites) pGlu163Lys-Likely functional significance (also affects splice sites). |
| | 38 | No | Yes | N | D | c. 660G > A | Substitution | GAA > AAA | p.Glu163Lys | pGlu163Lys-Likely functional significance (also affects splice sites). |
| | 30 | No | Yes | D | D | c. 660G > A | Substitution | GAA > AAA | p.Glu163Lys | pGlu163Lys-Likely functional significance (also affects splice sites). |
| | 43 | No | Yes | A | N | c. 660G > A | Substitution | GAA > AAA | p.Glu163Lys | pGlu163Lys-Likely functional significance (also affects splice sites). |
| | 59 | No | Yes | N | D | c. 660G > A | Substitution | GAA > AAA | p.Glu163Lys | pGlu163Lys-Likely functional significance (also affects splice sites). |
| | 19 | No | Yes | D | A | c. 660G > A | Substitution | GAA > AAA | p.Glu163Lys | pGlu163Lys-Likely functional significance (also affects splice sites). |

**Table 3. Mutations detected in different exons of *FAM134B* (*JK1*) in ESCC.**

alterations incorporating mutations in coding sequences of *FAM134B* were observed and each might entail either alterations to expression or functional changes of this gene that could play a fundamental role in the progression of ESCCs.

## Methods

**Recruitment of tissue samples and clinicopathological data.** Matched tumour samples and non-cancer tissue (near the surgical resection margin) from the same patient who underwent resection of ESCC were prospectively collected, snapped frozen in liquid nitrogen and stored in minus 80 °C by the author (AKL). Informed consent was obtained from all subjects. In addition, in each case, macroscopically enlarged lymph nodes suspicious for lymph node metastasis were also sampled, snap frozen and stored. After the collection, additional tissues blocks were taken, fixed in formalin and embedded in paraffin for pathological examination. Sections were then cut from these blocks and haematoxylin and eosin stained. They were studied by the author (AKL). The ESCCs were graded according to the World Health Organization (WHO) criteria[27]. The carcinomas

| Introns | Sample Code | Primary cancer | Lymph node metastasis | *FAM134B* DNA copy number change | | DNA change | Type of mutation |
|---|---|---|---|---|---|---|---|
| | | | | Primary cancer | Lymph node metastasis | | |
| Intron 2 | 39 | No | Yes | A | N | c. 514 + 144delA c. 514 + 37 − 38delTT | Deletion Deletion |
| | 41 | No | Yes | N | N | c. 408 − 27delA c. 514 + 37 − 38delTT | Deletion Deletion |
| | 20 | No | Yes | N | N | c. 408 − 27delA c. 514 + 34T > A c. 514 + 37 − 38delTT | Deletion Substitution Deletion |
| | 73 | No | Yes | A | A | c. 408 − 27delA | Deletion |
| Intron 4 | 16 | No | Yes | N | D | c. 408 − 27delA c. 514 + 37 − 38delTT | Deletion Deletion |
| | 39 | No | Yes | A | N | c. 546 − 64delA c. 672 + 46 − 47delTG | Deletion Deletion |
| | 6 | No | Yes | A | A | c. 546 − 64delA c. 546 − 56delA c. 672 + 46 − 47delTG | Deletion Deletion Deletion |
| | 38 | No | Yes | N | D | c. 546 − 56delA c. 672 + 26delT | Deletion Deletion |
| | 30 | No | Yes | D | D | c. 546 − 64delA c. 546 − 56delA | Deletion Deletion |
| Intron 5 | 43 | No | Yes | A | N | c. 546 − 56delA c. 672 + 26delT | Deletion Deletion |
| | 59 | No | Yes | N | D | c. 546 − 56delA c. 672 + 26delT c. 672 + 46 − 47delTG | Deletion Deletion Deletion |
| | 19 | No | Yes | D | A | c. 546 − 56delA | Deletion |
| | 41 | No | Yes | N | N | c. 673 − 54delC | Deletion |
| | 11 | No | Yes | A | N | c. 673 − 54C > A c. 757 + 56G > A | Substitution Substitution |
| | 3 | Yes | No | D | D | c. 673 − 65delA | Deletion |
| | 15 | No | Yes | D | N | c. 757 + 56G > A c. 673 − 52 − 53GA > AG | Substitution Substitution |
| Intron 6 | 38 | No | Yes | N | D | c. 758 − 61 − 62TG > CTc. 758 − 71G > T | Substitution Substitution |
| | 30 | No | Yes | D | D | c. 758 − 71G > T | Substitution |
| Intron 7 | 19 | No | Yes | D | A | c. 873 + 23T > C or c. 960 + 23T > C | Substitution |
| Intron 8 | 14 | Yes | No | A | A | c. 1087 + 97C > A | Substitution |
| | 6 | No | Yes | A | A | c. 1087 + 97C > A | Substitution |
| | 30 | No | Yes | D | D | c. 961 − 33delA c. 1087 + 97C > A | Deletion Substitution |
| | 41 | No | Yes | N | N | c. 961 − 33delA c. 1087 + 97C > A | Deletion Substitution |
| | 31 | No | Yes | A | A | c. 961 − 33delA c. 1087 + 97C > A | Deletion Substitution |

**Table 4. Mutations detected in different introns of *FAM134B* (*JK1*) in ESCC.**

were staged as per the TNM (tumour, lymph node and metastases) classification adopted in the American Joint Committee on Cancer[28]. Overall, tissues from 102 patients with ESCC were recruited. Eighteen patients had lymph nodes with metastatic ESCC sampled. For each patient, clinical and pathological parameters including gender and age of patients as well as the sites, grades, pathological stages of the ESCC were recorded.

**Genomic DNA extraction.** Ethical approval was obtained for the use of these samples (GU Ref No: MED/19/08/HREC) by the Griffith University human research ethics committee. The methods were carried out in accordance with the approved guidelines. .

The selected samples were sectioned using a cryostat (Leica CM 1850 UV, Wetzlar, Germany) and stained by haematoxylin and eosin. Light microscopic examination was performed by author, AKL, to confirm the presence of non-cancer and cancerous tissues for genomic DNA extraction. Five 10 μm slices was sectioned from the frozen tissue samples for DNA extraction. DNA was extracted and purified from frozen tissue samples using all prep DNA/RNA mini kit (Qiagen, Hilder, Germany), following manufacturer's instructions. DNA quantification was accomplished via Nanodrop Spectrophotometer (BioLab, Ipswich, MA, USA) and purity was measured using 260/280 ratio. Concentration of DNA was noted in ng/μl and then stored at −20 °C until use.

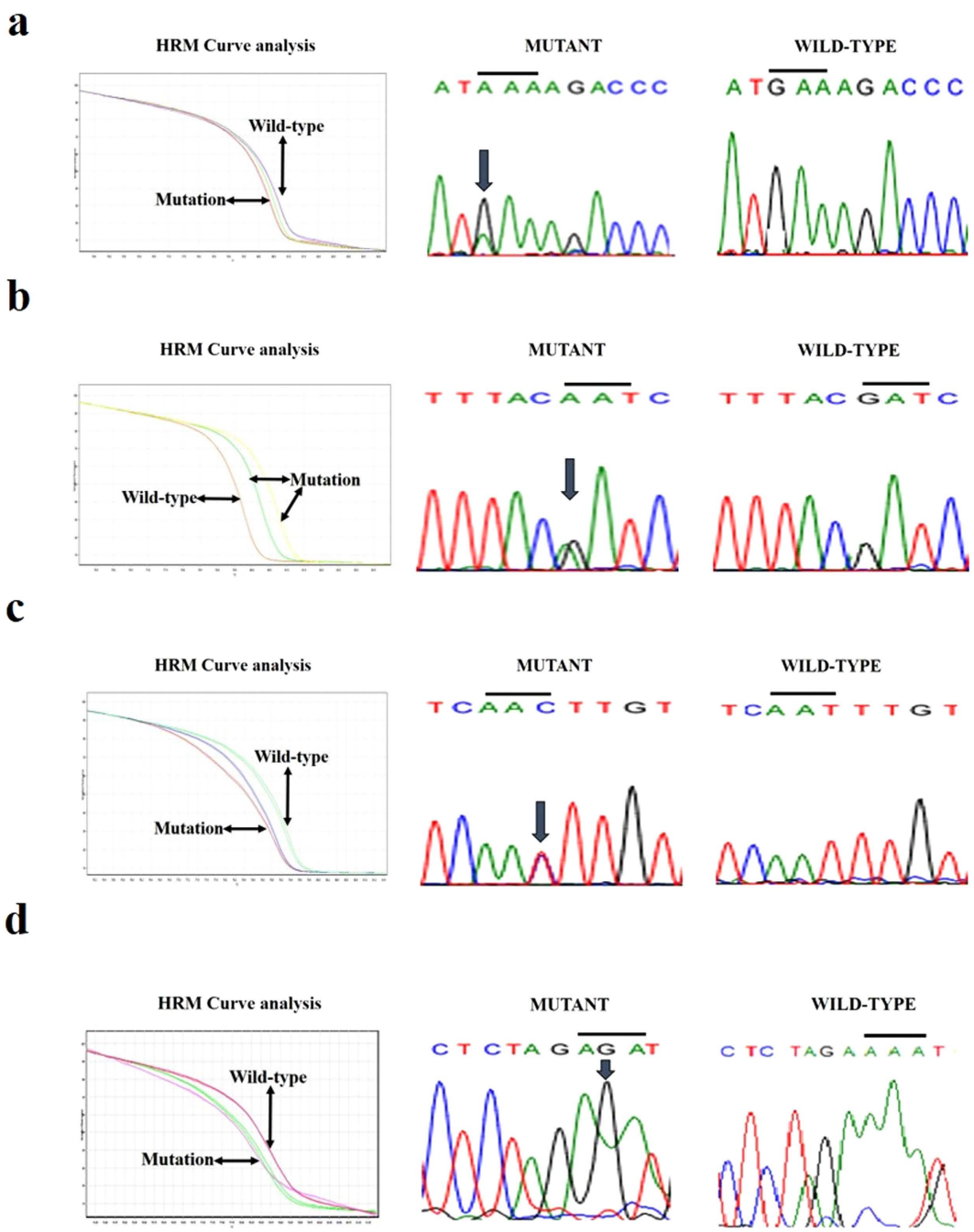


**Figure 2. Validation of *FAM134B* (*JK1*) different exons sequence variant HRM curve analysis results by Sanger sequencing. (a)** The presence of variant (GAA > AAA) in exon 4 of *FAM134B* (*JK1*) is demonstrated via normalized melting curves and sequencing (mutant versus wildtype). **(b)** HRM analysis shows the polymorphism (GAT > AAT) in exon 5 of *FAM134B* (*JK1*) as evident by normalized melting curves and sequencing (mutant versus wide type). **(c)** The presence of variant (AAT > AAC) in exon 7 of *FAM134B* (*JK1*) is confirmed via normalized melting curves and sequencing (mutant versus wide type). **(d)** The evidence of mutant (AAA > AGA) in exon 9 of FAM134B (JK1) is showed using normalized melting curves and sequencing (mutant versus wide type).

**Primer design.** Primers specific for determining *FAM134B* mutation and copy number changes were designed based on GenBank accession number for variant 1 NM_001034850 and for variant 2 NM_019000 as well as for a control gene, *HBD* (GenBank accession number NM_000519) using Primer3 version 0.4.0 (http://frodo.wi.mit.edu/primer3). All primers were analysed for specificity using Primer Blast (http://www.ncbi.nlm.nih.gov/tools/primer-blast) and Primer Premier program version 5 (Premier Biosoft, Palo Alto, CA, USA) to check for primer parameters like GC content, annealing temperature of primer and ΔG (Gibbs free energy change - energy required to break the secondary structure) and to forecast any possible mismatching, primer dimmer or hairpin formation.

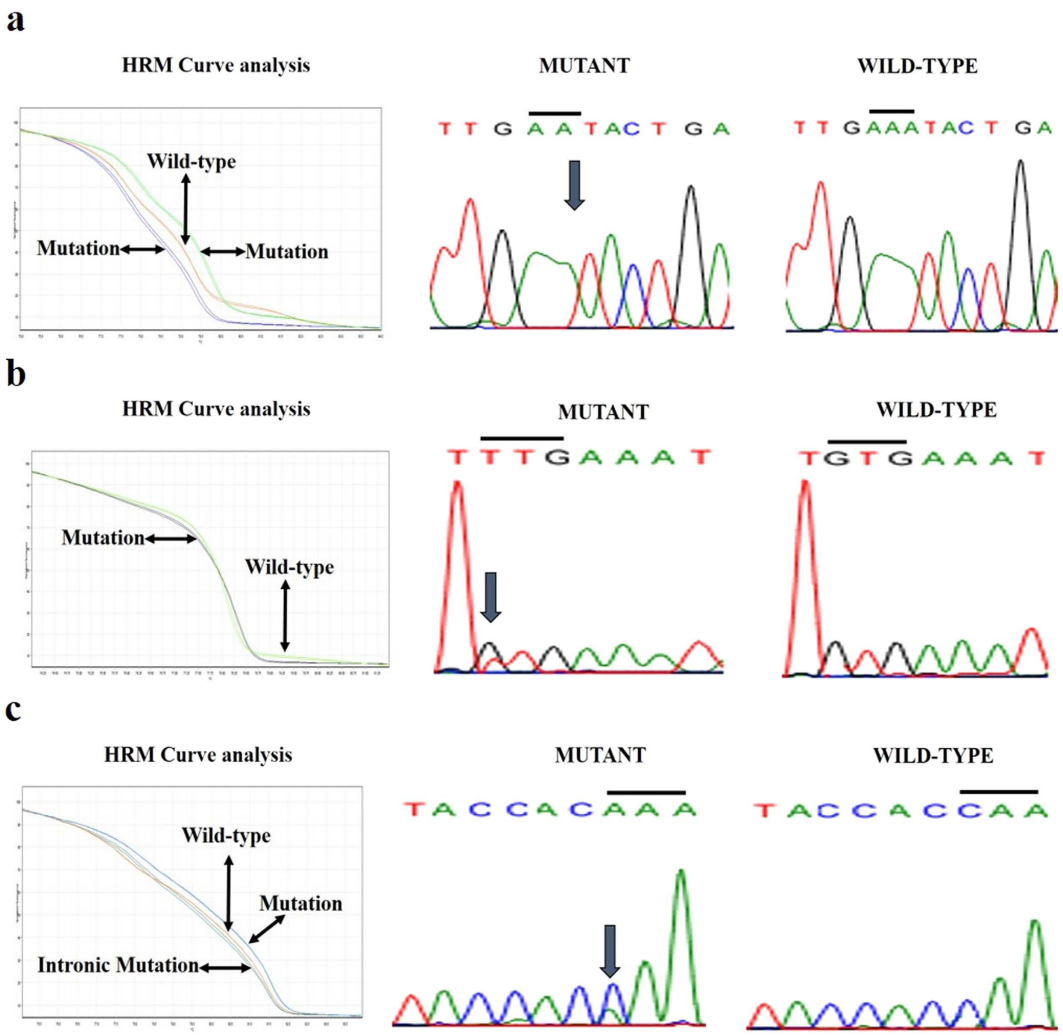


**Figure 3. Confirmation of *FAM134B* (*JK1*) different introns sequence variant HRM curve analysis results via Sanger sequencing. (a)** HRM curve analysis shows characteristic melting pattern of *FAM134B* (*JK1*) intron 2 amplicons using normalized melting curves and Sanger sequencing corroborates the mutation as being c. 14 + 144delA. **(b)** The evidence of mutant (GTG > TTG) in intron 6 of *FAM134B* (*JK1*) is shown using normalized melting curves and sequencing (mutant versus wild type). **(c)** HRM analysis shows the polymorphism (CAA > AAA) in intron 8 of *FAM134B* (*JK1*) as evident by normalized melting curves and sequencing (mutant versus wide type).

Primers for *FAM134B* (*JK1*) gene were designed within the intronic regions on either side of the exon of interest to ensure coverage of the entire exon 1 to exon 9 to amplify and direct sequencing both isoforms of the gene for screening of mutations in ESCC. Primers were also designed for *FAM134B* (*JK1*) and control gene - *haemoglobin delta* (*HBD*) to identify DNA copy number variations in ESCC. The primer pairs were obtained from Sigma-Aldrich (St Louis, MO, USA). The list of chosen primer sets are summarized in Table 5.

**Real-time quantitative polymerase chain reaction (qPCR).** DNA copy number changes of *FAM134B* (*JK1*) were determined using a rotor Gene Q real-time PCR (RT-PCR) Detection system (Qiagen). RT-PCR was achieved in a total volume of 10 μl comprising 5 μl of 2XSensiMix SYBR No-ROX master mix (Bioline, London, UK), 1 μl of each 10 picomole/μl primer, 1 μl of cDNA/ genomic DNA at 20–50 ng/μl and 2 μl of Nuclease-free water. PCR cycling programs encompassed initial denaturation and activated the hot start DNA polymerase in one cycle of 7 minutes at 95 °C followed by 40 cycles of 10 seconds at 95 °C (denaturation), 30 seconds at 60 °C (annealing) and 20 seconds at 72 °C (extension). Melting curve analysis was carried out using 80 cycles of 30 seconds increasing from 55 °C. The melting curves of all final real-time PCR products were analysed for determination of genuine products and contamination by nonspecific products and primer dimers. All samples were also run on 2% agarose gel electrophoresis to ensure that the correct product was amplified in the reaction. To increase the reliability of the results, assays were accomplished in multiple replicates and a non-template control was included in all the experiment. The results of the quantitative real-time polymerase change reaction were analysed using methods published previously[29].

| Target Genes | Primer sequence (Forward and Reverse) | Amplicon size |
|---|---|---|
| *FAM134B* Exon 1 | 5′-CGGCACCCACACCCAGGCGCGCCC-3′ | 600 bp |
| | 5′-GCACTGGGTCCCCGGGGCCCCG-3′ | |
| *FAM134B* Exon 2 | 5′-GTTTCTGTGGCAGGAAGTAAACCC-3′ | 281 bp |
| | 5′-GGACTAATTGGCTAATATGCCTAC-3′ | |
| *FAM134B* Exon 3 | 5′-GTGTTAGAGATCTGAGCATTCCAC-3′ | 259 bp |
| | 5′-CTTGGATTTAGATTCCTGTCAC-3′ | |
| *FAM134B* Exon 4 | 5′-CCAGAGGGTGTGGCCAACAGTAG-3′ | 329 bp |
| | 5′-TGGAGAAATCTGACAAGCTG-3′ | |
| *FAM134B* Exon 5 | 5′-GTCACTTATACCGGTCACTATAG-3′ | 282 bp |
| | 5′-CTCATCCCCCCTCTTCAAAC-3′ | |
| *FAM134B* Exon 6 | 5′-GTGAAATACTGAAATGTACGTAGC-3′ | 346 bp |
| | 5′-CTTTGAGGGAGATTAGCTTC-3′ | |
| *FAM134B* Exon 7 | 5′-GAATATGAGAAATGTGGGGTAAG-3′ | 256 bp |
| | 5′-GGAGTTTATTAGGAAGATCATTCAGC-3′ | |
| *FAM134B* Exon 8 | 5′-CTGTCATTTTGGGGGTTCATATGG-3′ | 314 bp |
| | 5′-TGGTGGTAACATGTTATTTACCC-3′ | 106 bp |
| *FAM134B* Exon 9 | 5′-TGACCGACCCAGTGAGGA-3′ | |
| | 5′-GGGCAAACCAAGGCTTAA-3′ | |
| *Haemoglobin delta* | 5′-TGGATGAAGTTGGTGGTGAG-3′ | 225 bp |
| (HBD) | 5′-CAGCATCAGGAGTGGACAGA-3′ | |

**Table 5. List of Exon primers designed for qRT-PCR and sequencing of *FAM134B*.**

**High-Resolution Melt (HRM) curve analysis.** Fifty-seven matched cancer and non-cancer tissues (including 18 cases with lymph node metastases) were used for HRM analysis. Sections of the lymph nodes were confirmed to have lymph nodes metastases by histological examination as above. HRM curve analysis was accomplished by amplifying target sequences on the Rotor-Gene Q detection system (Qiagen) using the software Rotor-Gene ScreenClust HRM Software. The exon 1, exon 2, exon 3, exon 4, exon 5, exon 6, exon 7, exon 8, exon 9 of *FAM134B* (*JK1*) were PCR amplified in a total reaction volume of 10 μl comprising 5 μl of 2Xsensimix HRM master mix, 1 μl of 30 ng/μl genomic DNA, diethylpyrocarbonate (DEPC, RNase free) treated water 2 μl and 1 μl of 5 μmol/L JK-1 primer. The thermal cycling protocol started with one cycle of 98 °C for 4 minutes. Full activation of the SensiFAST DNA polymerase occurs within 30 seconds at 95 °C. This was followed by 40 cycles of 98 °C for 5 seconds. Then, the reaction mix was at annealed at 60 °C for 15 seconds in exon 2, exon 5, exon 6, exon 7, exon 8, exon 9; 64.5 °C for 15 seconds for exon 3 and exon 4 and at 72 °C for 15 seconds for exon 1. Each PCR run included a negative (no template) control. The melt curve data were generated by increasing the temperature from 65 °C to 85 °C for all assays, with a temperature increase rate of 0.05 °C/seconds and recording fluorescence at each step. All the reactions were done in duplicate to increase the reliability of the results. Each mutant allele had its own distinctive melting curve while compared to the wild-type allele. HRM results were interpreted as mutant when both replicates showed a variant compared to wild type. In cases of uncategorized samples, one replicate showed a variant and the other matched the wild type curve.

**Purification of PCR products and Sanger sequencing analysis.** All the possible mutations detected by HRM analysis were further confirmed by Sanger sequencing. After HRM curve analysis, successful and specific PCR products showing one melting peak were purified according to the manufacturer's protocols from the NucleoSpin Gel and PCR Clean-up kit (Macherey- Nagel, Bethlehem, PA, USA). The purified PCR products were subjected to sequence by corresponding forward and reverse primer using the Big Dye Terminator (BDT) chemistry Version 3.1 (Applied Biosystems, Foster City, CA, USA) under standardised cycling PCR conditions and analysed by the Australian Genome Research Facility (AGRF) using a 3730xl Capillary sequencer (Applied Biosystems). The composition of DNA sequencing reactions was followed according the samples preparation guide from AGRF. Sequence analysis was performed with Chromas 2.31 software.

**Statistical analysis.** Correlations of *FAM134B* (*JK1*) copy number change and mutations with clinicopathological parameters were performed. Comparisons between groups were implemented using the chi-square test, likelihood ratio and Fisher's exact test. All the data was entered into a computer data base and the statistical analysis was executed using the Statistical Package for Social Sciences for Windows (version 22.0, IBM SPSS Inc., New York, NY, USA). Significance level was taken at $p < 0.05$.

## References

1. Lam, K. Y. & Ma, L. Pathology of oesophageal cancers: local experience and current in-sights. *Chin. Med. J.* **110,** 459–464 (1997).
2. Lam, A. K. Molecular biology of esophageal squamous cell carcinoma. *Crit. Rev. Oncol. Hematol.* **33,** 71–90 (2000).
3. Lam, A. K. Cellular and molecular biology of esophageal cancer. In: *Esophageal cancer: prevention, diagnosis and therapy*. (eds Saba N. F. & El-Rayes, B.), Ch. 2, 25–40 (Springer, 2015).
4. Yu, V. Z. *et al.* Nuclear localization of DNAJB6 is associated with survival of patients with esophageal cancer and reduces AKT Signaling and Proliferation of Cancer Cells. *Gastroenterology* **149,** 1825–1836 (2015).

5. Xu, W. W. *et al.* Targeting VEGFR1- and VEGFR2-expressing non-tumor cells is essential for esophageal cancer therapy. *Oncotarget* **6,** 1790–1805 (2015).
6. Chan, D. *et al.* Oncogene GAEC1 regulates CAPN10 expression which predicts survival in esophageal squamous cell carcinoma. *World J. Gastroenterol.* **19,** 2772–2780 (2013).
7. Chung, Y. *et al.* Altered E-cadherin expression and p120 catenin localization in esophageal squamous cell carcinoma. *Ann. Surg. Oncol.* **14,** 3260–3267 (2007).
8. Wong, M. L. *et al.* Aberrant promoter hypermethylation and silencing of the critical 3p21 tumour suppressor gene, RASSF1A, in Chinese oesophageal squamous cell carcinoma. *Int. J. Oncol.* **28,** 767–773 (2006).
9. Fatima. S. *et al.* Transforming capacity of two novel genes JS-1 and JS-2 located in chromosome 5p and their overexpression in human esophageal squamous cell carcinoma. *Int. J. Mol. Med.* **17,** 159–170 (2006).
10. Si, H. X. *et al.* E-cadherin expression is commonly downregulated by CpG island hypermethylation in esophageal carcinoma cells. *Cancer Lett*. **173,** 71–78 (2001).
11. Hu, Y. C., Lam, K. Y., Law. S., Wong, J. & Srivastava, G. Identification of differentially expressed genes in esophageal squamous cell carcinoma (ESCC) by cDNA expression array: overexpression of Fra-1, Neogenin, Id-1, and CDC25B genes in ESCC. *Clin. Cancer Res.* **7,** 2213–2221 (2001).
12. Chow, V., Law, S., Lam, K. Y., Luk, J. M. & Wong, J. Telomerase activity in small cell esophageal carcinoma. *Dis. Esophagus* **14,** 139–142 (2001).
13. Lam, K. Y., Law, S., Tin, L., Tung, P. H. & Wong, J. The clinicopathological significance of p21 and p53 expression in esophageal squamous cell carcinoma: an analysis of 153 patients. *Am. J. Gastroenterol.* **94,** 2060–2068 (1999).
14. Tang, J. C., Lam, K. Y., Law, S., Wong, J. & Srivastava, G. Detection of genetic alterations in esophageal squamous cell carcinomas and adjacent normal epithelia by comparative DNA fingerprinting using inter-simple sequence repeat PCR. *Clin. Cancer Res.* **7,** 1539–1545 (2001).
15. Kwong, D. *et al.* Chromosomal aberrations in esophageal squamous cell carcinoma among Chinese: gain of 12p predicts poor prognosis after surgery. *Hum. Pathol.* **35,** 309–316 (2004).
16. Tang, W. K. *et al.* Oncogenic properties of a novel gene JK-1 located in chromosome 5p and its overexpression in human esophageal squamous cell carcinoma. *Int. J. Mol. Med*. **19,** 915–923 (2007).
17. Kasem, K. *et al.* The roles of JK-1 (FAM134B) expressions in colorectal cancer. *Exp. Cell. Res*. **326,** 166–173 (2014).
18. Kasem, K. *et al.* JK1 (FAM134B) represses cell migration in colon cancer: a functional study of a novel gene. *Exp. Mol. Pathol*. **97,** 99–104 (2014).
19. Kasem, K. *et al.* JK1 (FAM134B) gene and colorectal cancer: a pilot study on the gene copy number alterations and correlations with clinicopathological parameters. *Exp. Mol. Pathol.* **97,** 31–36 (2014).
20. Kurth, I. *et al.* Mutations in FAM134B, encoding a newly identified Golgi protein, cause severe sensory and autonomic neuropathy. *Nat. Genet.* **41,** 1179–1181 (2009).
21. Davidson, G. *et al.* Frequency of mutations in the genes associated with hereditary sensory and autonomic neuropathy in a UK cohort. *J. Neurol.* **259,** 1673–1685 (2012).
22. Murphy, S. M., Davidson, G. L., Brandner, S., Houlden, H. & Reilly, M. M. Mutation in FAM134B causing severe hereditary sensory neuropathy. *J. Neurol. Neurosurg. Psychiatry.* **83,** 119–120 (2012).
23. Ilgaz Aydinlar, E. *et al.* Mutation in FAM134B causing hereditary sensory neuropathy with spasticity in a Turkish family. *Muscle Nerve.* **49,** 774–775(2014).
24. Kong, M., Kim, Y. & Lee, C. A strong synergistic epistasis between FAM134B and TNFRSF19 on the susceptibility to vascular dementia. *Psychiatr Genet*. **2,** 37–41(2011).
25. Khaminets, A. *et al.* Regulation of endoplasmic reticulum turnover by selective autophagy. *Nature*, **522,** 354–358 (2015).
26. Hanahan, D. & Weinberg, R. A. The hallmarks of cancer. *Cell* **100,** 57–70, (2000).
27. Bernards, R. & Weinberg, R. A. A progression puzzle. *Nature*, **418,** 823–810 (2002).
28. Hamilton, S. R. *et al.* Carcinoma of the colon and rectum. (eds Bosman, F. T. *et al.*) *WHO classification of tumours of the digestive system*. IARC Press, Lyon, France, 134–146 (2010).
29. Edge, S. B. *et al.* American Joint Committee on Cancer, American Cancer Society, *7th edn*. AJCC cancer staging manual, III. Springer-Verlag, New York, 143–159 (2010).
30. Gopalan, V. *et al.* GAEC1 and colorectal cancer: a study of the relationships between a novel oncogene and clinicopathologic features. *Hum. Pathol*. **41,** 1009–1015 (2010).


## Acknowledgements

The authors would like to acknowledge the funding from higher degree research student (GUIPRS and GUPRS scholarship) from the Griffith University. The project was also supported by the project funding of Menzies Heath Institute Queensland and joint funding by Griffith University and the Gold Coast University Hospital Foundation.

## Author Contributions

V.G. and A.K.L. developed the idea of novel mutations and supervised the projects. M.H.H. and V.G. designed the experiments; M.H.H. and V.G. conducted the experiments; M.H.H., V.G. and R.A.S. analysed the raw data; K.C. and A.K.L. collected the samples and managed the pathological data. M.H.H., V.G., M.J.A.S. and A.K.L. discussed the results and co-wrote the manuscript.

## Additional Information

**Competing financial interests:** The authors declare no competing financial interests.

**How to cite this article**: Haque, M. H. *et al.* Identification of Novel FAM134B (JK1) Mutations in Oesophageal Squamous Cell Carcinoma. *Sci. Rep.* **6**, 29173; doi: 10.1038/srep29173 (2016).

# Chapter 5

# Nanotechnological approaches for *FAM134B* mutation detection and its clinical significance in ESCC

Chapter 5 is included as it appears in Electrocanalysis (2017).

# Introduction

A simple, rapid and cost-effective new electrochemical method is described for detecting point mutation or SNPs in *FAM134B* gene using gold-DNA affinity interaction phenomenon. Base-dependent affinity interaction (*i.e.*, adsorption) of DNA bases follows the affinity trend of DNA bases as adenine (A) > cytosine (C) > guanine (G)> thymine (T). The mechanism underlying this adsorption process has been well explored in the literature. More recently we have explored this phenomenon in distinguishing two sequentially different DNA molecules (*i.e.*, two DNA sequences with different methylation patterns). Since mutated and unmutated (wild-type) DNA sequences have their distinct ability to interact with gold surfaces as a consequence of their different mutation status, the accurate measurement of the adsorbed DNA onto an unmodified gold electrode could be helpful in quantifying mutation changes in target DNA sequence. In addition, small, inexpensive and portable screen-printed gold electrodes were used to quantify gene mutations in DNA samples from cancer patients. We believe that our assay could potentially lead a low-cost alternative to conventional assays for mutation detection in clinical samples.

Full Paper
Wiley Online Library
ELECTROANALYSIS

DOI: 10.1002/elan.201700039

# Electrochemical Detection of FAM134B Mutations in Oesophageal Cancer Based on DNA-Gold Affinity Interactions

Md. Hakimul Haque,[a, b, c] Md. Nazmul Islam,[b, c] Farhadul Islam,[a] Vinod Gopalan,*[a] Nam-Trung Nguyen,[c] Alfred K. Lam,*[a] and Muhammad J. A. Shiddiky*[b, c]

**Abstract:** Inexpensive, simple and rapid DNA sensors capable of accurate and sensitive detection of cancer specific point mutations in DNA biomarkers are crucial for the routine screening of genetic mutations in cancer. Conventional approaches based on sequencing, mass spectroscopy, and fluorescence are highly effective, but they are tedious, slow and require labels and expensive equipment. Recent electrochemistry based approaches mostly rely on conventional DNA biosensing using recognition and transduction layers, and hence limited by the complicated steps of sensor fabrication associated with surface cleaning, self-assembled monolayer formation, and target hybridization. Herein we report a relatively simple and inexpensive method for detecting point mutation in cancer by using the direct adsorption of purified DNA sequences onto an unmodified gold surface. The method relies on the base dependent affinity interaction of DNA with gold. Since the affinity interaction (adsorption) trend of DNA bases follows as adenine (A) > cytosine (C) > guanine (G) > thymine (T), two DNA sequences with different DNA base compositions (i.e., amplified mutated sequences will be distinctly different than its original sequence) will have different adsorption affinity towards gold. The amount of mutation sites on a DNA sequence is quantified by monitoring the electrochemical current as a function of the relative adsorption level of DNA samples onto a bare gold electrode. This method can successfully distinguish single point mutation in DNA from oesophageal cancer. We demonstrated the clinical utility of this approach by detecting different levels of mutations in tissue samples (n = 9) taken from oesophageal cancer patients. Finally, the method was validated with High Resolution Melt (HRM) curve analysis and Sanger Sequencing.

**Keywords:** FAM134B mutation · Electrochemical detection · Gold-DNA base interaction · Oesophageal cancer · Disposable screen-printed electrode

## 1 Introduction

Point mutations play critical role in multiple alterations in gene sequences, protein structure, expression levels and function of key regulatory genes in human diseases including cancer [1]. Growing evidence in cancer research have suggested that point mutations can also be used in predicting clinical behavior, treatment responses and prognosis in cancer patients [1, 2]. The *FAM134B* gene, one of the best *in-silico* biomarkers for pluripotent stem cell [3], acts as an important player in the progression of oesophageal squamous cell carcinoma (ESCC) [4], colorectal cancer [5,6] and neurological diseases [7] via regulating its expression patterns and regulating apoptosis. More recently, we have reported that *FAM134B* gene is frequently mutated in metastatic lymph node tissues and is correlated with tumour progression in ESCCs [8]. Therefore, simple, inexpensive, accurate, and sensitive method for detecting *FAM134B* gene mutations in ESCC could be potentially useful in future targeted molecular therapies in this carcinoma. Over the past several years, many conventional methods based on sequencing, electrophoresis, fluorescence, and mass spectrometry have been reported for the detection of point mutations or single nucleotide polymorphisms (SNPs) alleles in DNA sequences in cancer patients [9–11]. While these approaches are highly reliable and effective, they are time-consuming and laborious for the use in a clinical setting. These methods might pose a potential cost barrier in low-resource setting due to the need of expensive and sophisticated imaging equipment. These methods are also limited by the use of fluorophores, quenchers or colorants interference, hazard-

[a] M. H. Haque, F. Islam, V. Gopalan, A. K. Lam
Cancer Molecular Pathology Laboratory in School of Medicine, Menzies Health Institute Queensland, Griffith University, Gold Coast Campus, Australia
E-mail: v.gopalan@griffith.edu.au
a.lam@griffith.edu.au
[b] M. H. Haque, M. N. Islam, M. J. A. Shiddiky
School of Natural Sciences, Griffith University, Nathan Campus, QLD 4111, Australia
E-mail: m.shiddiky@griffith.edu.au
[c] M. H. Haque, M. N. Islam, N.-T. Nguyen, M. J. A. Shiddiky
Queensland Micro and Nanotechnology Centre, Griffith University, Nathan Campus, QLD 4111, Australia
Supporting information for this article is available on the WWW under http://dx.doi.org/10.1002/slct.201700039

ous materials such as radioactive isotopes and ethidium bromide. Therefore, there is a demand for an alternative method that can avoid these limitations, and offer conventional methodology - like reliability, accuracy, and sensitivity.

The increasing demand for an alternative detection method has yielded a number of electrochemical DNA sensors, which improve the analytical performances *via* enhancing the speed, sensitivity, portability and accuracy of the point mutations [12] and SNPs [13–20] measurements in complex biological samples. For instance, Barton and co-workers have developed long-range DNA charge transfer based electrochemical sensors for the quantification of point mutations and DNA-base lesions in gene specific sequences [12–13]. In these methods, a capture DNA probe was initially confined to the electrode surface *via* physical adsorption, self-assembly monolayer formation or covalent conjugation. A redox-active label that attached either intercalatively to the hybridized dsDNA or covalently to the reporter probes, was used to read the presence or absence of DNA mutations. Other groups have extended this work to develop several selective and sensitive electrochemical sensors for mutation analysis in duplex DNA [16–20]. Despite the excellent analytical performances in proof-of-concept studies, the applications for analysis of clinical sample have been still limited. This is partly due to the multistep fabrication of the sensors (i.e., the lack of a robust protocol for electrode modification). Additionally, most of these methods are limited by the long analysis time (i.e., typically several hours). This paper describes an electrochemical assay for the detection of point mutation in oesophageal cancer patient samples using the base-dependent affinity interaction of DNA bases toward gold electrode.

Base-dependent affinity interaction (i.e., adsorption) of DNA bases on bare gold surface follows the affinity trend of DNA bases as adenine (A) > cytosine (C) > guanine (G) > thymine (T). The mechanism underlying this adsorption process has been well explored in the literature. Generally, the adsorption of DNA bases to gold surfaces can be described by the conventional physisorption mechanism [21–23], where DNA bases adopt a flat conformation that allow maximum overlapping of electronic densities. The only exception is adenine, where an extra chemical bond between the amino group and a gold atom is formed [21], offering the strongest adsorption strength between them. More recently Sina *et al.* have explored the use of this phenomenon in distinguishing two sequentially different DNA molecules (i.e., two DNA sequences with different methylation patterns) [24–26]. Since mutated and unmutated (wild-type) DNA sequences have their distinct ability to interact with gold surfaces as a consequence of their different mutation status, the accurate measurement of the adsorbed DNA onto an unmodified gold electrode could be helpful in quantifying mutation changes in target DNA sequence. To date, no reports exist on the use of the different adsorption affinity of mutated and unmutated sequences to quantify gene mutations in DNA samples from cancer patients.

Herein, we report a cost-effective and relatively simple proof-of-concept electrochemical approach for detecting point mutation or SNPs in *FAM134B* gene using gold-DNA affinity interaction phenomenon. Target DNA sequences were first extracted from clinical samples and were then PCR amplified and purified prior to adsorption on a single-use screen-printed gold electrode. The amount of adsorbed DNA was detected by monitoring the Faradaic current generated by the $[Fe(CN)_6]^{3-/4-}$ system present in the electrolyte solution. We first applied the method to quantify point mutations or SNPs on synthetic *FAM134B*. Also, the results were validated with High Resolution Melt (HRM) curve Analysis and Sanger sequencing.

## 2 Experimental

### 2.1 Reagents

Unless otherwise stated, all the reagents and chemicals used in this study are of analytical grade and purchased from Sigma-Aldrich (Sydney, NSW, Australia). Reagents and washing solutions used in the experiments were prepared with phosphate buffer saline (PBS, 10 mM, pH 7.4). The primers and synthetic DNA samples were obtained from Integrated DNA technologies (Coralville, IA, USA). DNA samples were diluted in 5X saline-sodium citrate (5XSSC) buffer.

### 2.2 Sample Selection and DNA Extraction

Nine fresh frozen tissue samples from six metastatic lymph node tissues of ESCC patients and three matched non-cancer oesophageal tissues (near the surgical section margin) were selected based on our previous findings on the detection of *FAM134B* mutations [8]. Ethical approval has been acquired for the use of these samples from human research ethics committee of Griffith University (GU Ref No: MED/19/08/HREC). Genomic DNA was extracted from fresh frozen ESCC tissue samples using all prep DNA/RNA mini kit (Qiagen, Hilder, Germany), following manufacturer's instructions. Briefly, the tissue samples were suspended in lysis buffer to disrupt and release the nucleic acids and proteins into the solution. Then, a digestion step was executed to remove the protein and RNA in the solution using proteinase and RNase enzymes, respectively. The digested proteins and RNA were removed by centrifuging the solution in a spin column. Then the purified DNA was eluted from the column in 100 µL of elution buffer. DNA quantification was performed using Nanodrop Spectrophotometer (BioLab, Ipswich, MA, USA) and purity was checked using 260/280 ratio. Concentration of DNA was noted in ng/µL and then stored at −20 °C until use.

### 2.3 Amplification of Target DNA Sequence

DNA copy number normalization was performed according to the procedure of our previous study [8]. To achieve the amplified amplicons of exon 4 of *FAM134B* gene, genomic DNA were amplified in a 10 μL reaction containing 5 μL of 2XSensiMix SYBR No-ROX master mix (Bioline, London, UK), 1 μL of each 10 picomole/μL forward and reverse primer, 1 μL of genomic DNA at 20–50 ng/μL and 2 μL of nuclease-free water. Thermal cycling was performed in a rotor Gene Q real-time PCR (Qiagen) using the following conditions: initial denaturation at 95 °C for 7 min followed by 40 cycles of 95 °C for 10 s (denaturation), 60 °C for 30 s (annealing), and 72 °C for 20 s (extension). Successful and specific PCR products were then purified using the manufacturer's protocols from the NucleoSpin Gel and PCR Clean-up kit (Macherey-Nagel, Bethlehem, PA, USA). The amplified PCR amplicon was electrophoresed through 1.5 % agarose gel (see Figures 2 A). The agarose gel encompassing the desired PCR amplicon was cut and dissolved in a buffer as well as centrifuged through a spin column to wash away impurities. The purified DNA was eluted in 20 μL of nuclease free water and quantified using a Nanodrop Spectrophotometer (BioLab, Ipswich, MA, USA) and then stored at −20 °C until use.

### 2.4 Electrochemical Detection of Mutation

All electrochemical measurements were performed on a CH1040C potentiostat (CH Instruments, USA) with the three-electrode system (gold working and counter electrodes, silver reference electrode) on each screen-printed gold electrode. Differential pulse voltammetric (DPV) experiments were conducted in 10 mM PBS solution containing 2.5 mM $[K_3Fe(CN)_6]$ and 2.5 mM $[K_4Fe(CN)_6]$ electrolyte solution. DPV signals were obtained with a potential step of 5 mV, pulse amplitude of 50 mV, pulse width of 50 ms, and pulse period of 100 ms. For synthetic DNA samples, 5 μL (diluted in SSC5X buffer to get 50 ng of DNA) sample was adsorbed on Au-SPE surface. For clinical samples analysis, 5 μL (diluted in SSC5X buffer to get 50 ng of DNA) were used for adsorption experiments. The electrodes were then washed three times with PBS prior to perform DPV measurements. The relative DPV current changes (i.e., $\%I_{Relative}$, percent difference of the DPV signals generated for DNA sample ($I_{Sample}$) with respect to the baseline current ($I_{Baseline}$)) due to the adsorption of DNA samples were then measured by using Eq. 1.

$$\%I_{Relative} = \frac{\%I_{Baseline} - \%I_{Sample}}{\%I_{Baseline}} \times 100 \quad (1)$$

### 2.5 Validation of Results Using HRM Curve Analysis and Sanger Sequencing

To validate the electrochemistry based detection of *FAM134B* mutation status, we have used HRM curve analysis by amplifying target sequences on the Rotor-Gene Q detection system (Qiagen). The exons 4 of *FAM134B* gene was amplified in 10 μL reactions mixture containing 5 μL of 2Xsensimix HRM master, 1 μL of 30ng/μL genomic DNA, 2 μL nuclease free water and 1 μL of each *FAM134B* forward and reverse primer. The thermal cycling protocol was carried out using the following conditions: Denaturation at 98 °C for 4 minutes followed by 40 cycles of 98 °C for 5 seconds, 64.5 °C for 15 seconds (annealing) and at 72 °C for 15 seconds (extensions). A negative (no template) control was included in each PCR run. The melt curve data was generated by increasing the temperature from 65 °C to 85 °C for all assays, with temperature increase rate of 0.05 °C/seconds and recording fluorescence. Each mutant allele had its own distinctive melting curve while compared to the wild-type allele. HRM results were interpreted as mutant when both replicates showed a variant compared to wild type.

Additionally, the accuracy of the electrochemical analysis was confirmed with our recently reported Sanger sequencing of *FAM134B* mutation [8]. Sanger sequencing was performed and analyzed using a 3730xl Capillary sequencer (Applied Biosystems) under standardized cycling PCR conditions in the Australian Genome Research Facility (AGRF, Brisbane).

## 3 Results and Discussion

### 3.1 Principle of Mutation Detection Electrochemical Assay

Scheme 1 illustrates the principle of the method. Briefly, genomic DNA was extracted from frozen tissue samples of ESCC. A PCR amplification step was then performed to achieve the amplified amplicons comprising the exon 4 of *FAM134B* gene. Subsequently, a purification step of PCR product was accomplished to obtain purified dsDNA amplicons. These purified ds-DNA were then directly adsorbed on the unmodified gold electrode (AU-SPE) surface. The amount of the adsorbed ds-DNA amplicons were detected by DPV in the presence of a small redox active $[Fe(CN)_6]^{3-/4-}$ group. Unlike conventional redox system (e.g., $[Ru(NH_3)_6]^{3+}/[Fe(CN)_6]^{3-}$), the $[Fe(CN)_6]^{3-/4-}$ alone can be used to quantify the adsorbed DNA on an electrode surface.[24–30] The use of the adsorbed DNA to retard the access of the $[Fe(CN)_6]^{3-/4-}$ system to the electrode surface require a special consideration to achieve reliably. It needs a partial blocking (i.e., adsorption) of the electrode (but not too much blocking) so that the different amount of adsorbed DNA with different levels of mutation can be discerned. This is because there is only a finite amount of effective surface and having the large amount of adsorbed DNA could completely block

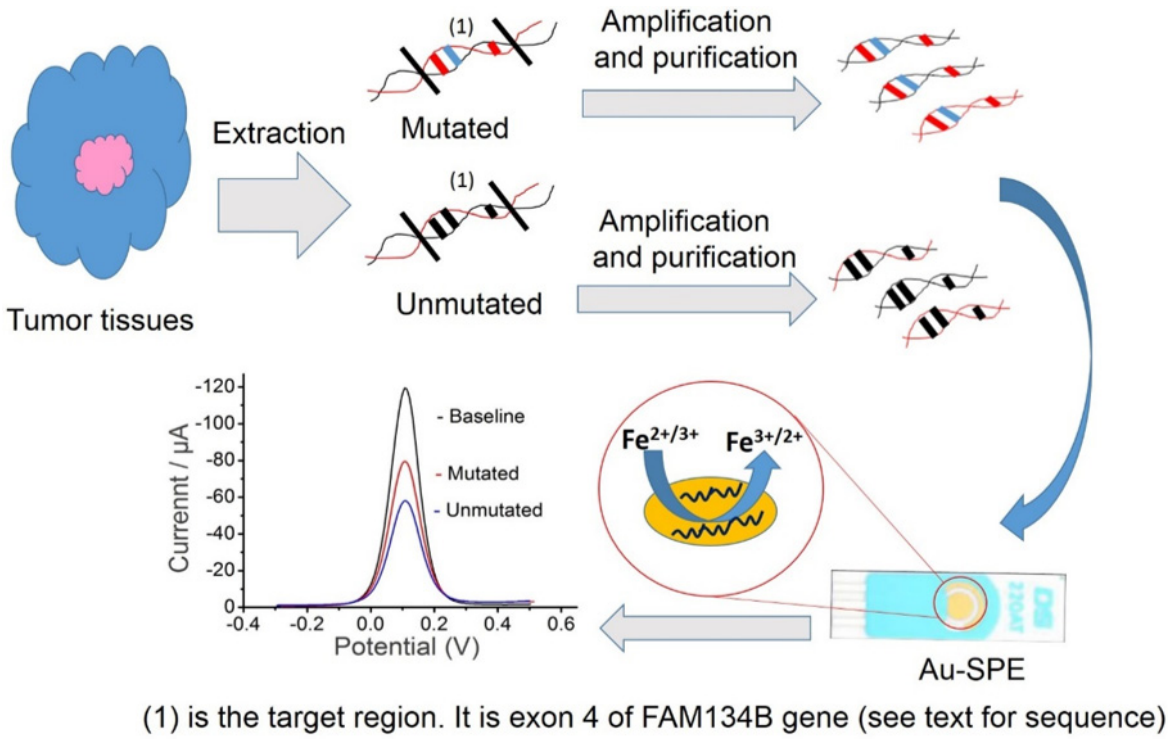


Scheme 1. Schematic of Gold-DNA adsorption based mutation detection assay. The adsorption of ds-DNA on Au-SPE repulse $[Fe(CN)_6]^{3-}$ molecules from accessing electrode surface, providing a significate DPV signal. Inset, typical differential pulse voltammetric signals showing the nonmutated DNA that produces lower DPV currents in comparison to mutated DNA.

the $[Fe(CN)_6]^{3-/4-}$ redox system from accessing the electrode surface, resulting undetectable signal difference between mutated and unmutated DNA samples. Under the condition of partially blocked surface, $[Fe(CN)_6]^{3-/4-}$ system has sufficient access to the electrode surface to generate a detectable current. Since gold-DNA affinity interactions follows the trend A > C > G > T, the mutated DNA (e.g., deletion of A) sequence leads to a lower level of adsorbed DNA on the electrode in comparison to the nonmutated sequence, providing high Faradaic current due to the less coulombic repulsion between $[Fe(CN)_6]^{3-}$ and less amount of negatively charged surface bound-DNA. Therefore, the level of current generated by the $[Fe(CN)_6]^{4-/3-}$ system should have a clear correlation with the mutation level. It is important to note that this direct adsorption approach will not be affected by the non-specific adsorption of non-target species. This is because highly purified PCR product, diluted in high salt-buffer will be used.

### 3.2 Synthetic Sample Design and Analysis

*FAM134B* gene encodes a cis-Golgi transmembrane protein that controls its expression patterns and regulates apoptosis in gastrointestinal carcinomas and neurological diseases [4–8,31,32]. More recently, we have reported 37 mutations in different exons of *FAM134B* gene and its significant DNA copy number variations in ESCC tissues [8]. We have also shown that the exon 4 containing a length of 329 bases is a frequent mutational hotspot of the *FAM134B* gene in metastatic lymph node tissues in ESCC patients suggesting its potential role in the pathogenesis and progression of ESCC [8]. In order to execute our approach, the exon 4 of *FAM134B* gene was selected as a target analyte. Therefore, we designed synthetic samples containing different mutation sites within exon 4 of *FAM134B* gene which originally mimicked the PCR-processed mutated (four samples) and unmutated (control sample) DNA regions (i.e., SDM-1, A deletion; SDM-2, AA deletion; SDM-3, AA deletion + CT > GG, and SDM-4, AA deletion + CT > GG + G > A. For details, see Table 1 in supporting information). As outlined above, the analytical functionality of the current method rely on the partial adsorption of target DNA on the electrode surface. To get the optimal conditions for achieving the best analytical performance of the method, we optimized the experimental parameters, such as amount of the target DNA and adsorption time using wild type (control DNA) and mutated DNA (SDM2) samples. As shown in Figure S1, 60 min and 90 min adsorption times provided significant difference ($\Delta i_r$, see calculation details in the caption of Figure S1) between the relative DPV currents for control DNA and SDM2 samples. We then optimised the DNA concentration and found that 10 and 20 ng/µL concentration provided significant difference the relative DPV current for the two DNA. Although 90 min

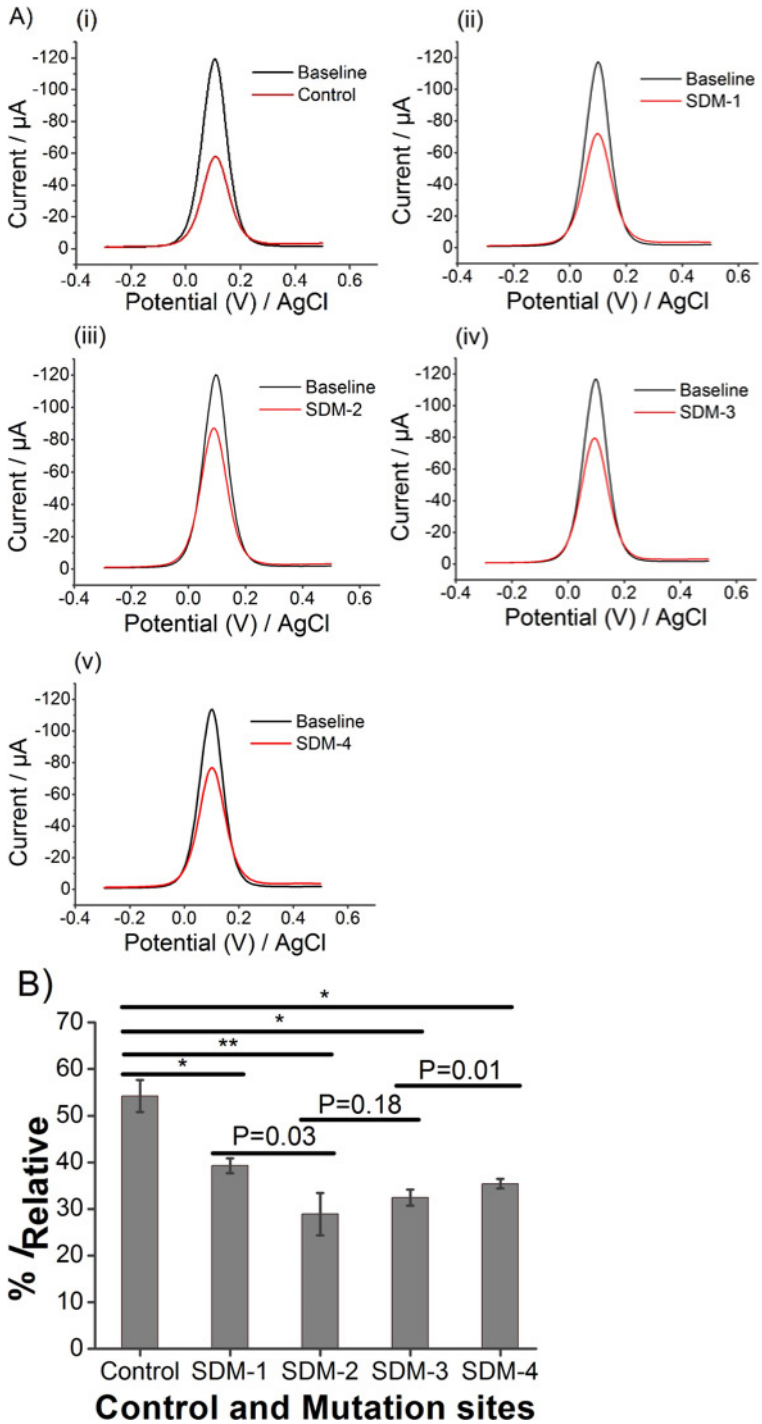


Fig. 1. (A) Differential pulse voltammetric current changes with respect to the designated mutation sites. B). Right, Relative current changes for detecting *FAM134B* point mutations for the synthetic sample containing 1 (A deletion), 2 (AA deletion), 3 (AA deletion, CT > GG) and 4 (AA deletion, CT > GG, G > A) mutation sites and control DNA. Each data point represents the average of three repeat trails, and error bars represent the standard deviation of measurements (% RSD = < 5.0 %; for $n$ = 3). Statistical significance were determined by pairwise comparison between 2 conditions using student t-test. *, $p = 0.005$ to 0.05 and **, $p = 0.0005$ to 0.005..

adsorption time and 20 ng/µL sample concentration provided slightly higher difference between the relative DPV current for control DNA and SDM2 samples than the 60 min time and 10 ng/ µL concentration, we have selected the later as the optimal conditions (to get sufficient adsorption at optimal time and concentration).

Under optimized conditions, four known mutated and their non-mutated matched synthetic samples were examined [8]. We observed different level of relative current changes (with respect to the baseline current) for all these synthetic samples indicating that the relative current changes is a function of the mutation levels present in the target sample. In SDM-1 sample containing a single A deletion, we found approximately 39 % relative current changes in comparison to that of control DNA (i.e., % $I_{Relative}$ = 39 *versus* 54 %) (Figure 1B). Two A bases deletion from the DNA sequence (i.e., in SDM-2 sample) further reduced the relative current changes to 28 % compared to SDM-1 sample. This is because the additional A base deletion resulted a lower level of adsorbed

DNA on the electrode surface (i.e., higher DPV current and hence lower % $I_{Relative}$). The sample that contains two A deletion and CT bases substituted by GG bases (SDM-3 sample), resulted in a 32% relative current reduction. It implies that the adsorbed DNA on the electrode surface is slightly higher than that for the SDM-2 case. This difference could be explained by the fact that GG bases have a stronger affinity interaction towards gold as compared to the CT bases (i.e., lower DPV current and hence higher % $I_{Relative}$). The SDM-4 sample offers about 35% relative current changes - again slightly higher than that of the SDM-3 sample. This could be due to the additional G > A changes in the sequence. Since A has the strongest adsorption affinities toward gold, the amount of adsorbed SDM-4 sample on the electrode surface would be a bit higher that of the SDM-3 sample, leading to a relatively lower DPV current (i.e., higher % $I_{Relative}$). These data clearly demonstrate that our assay is sensitive to detect different level of mutation in the target sequence. A similar level of detection sensitivity was achieved previously for DNA methylation detection using gold-DNA affinity interaction [24, 26]. The inter-assay relative standard deviations (%RSD) was found to be less than <5.0%, indicating a good assay reproducibility. Importantly, unlike existing electrochemical or conventional methods, our method detects the mutation status of DNA molecules with different mutation landscapes by simply monitoring their direct adsorption on an unmodified gold electrode in less than 1.5 h (excludes sample preprocessing time). This time is much higher than that of the currently reported chip-based [33] and a portable battery-operated electrochemical device [34] based assays. However, the devices and electrodes used in these assays are not commercially available, and are limited by the surface functionalizations for mutation detection. In contrast, our method is based on commercially available screen-printed electrodes and avoids surface functionalization step. Furthermore, the analytical performance of our method is either comparable or much better than many of the currently reported electrochemical methods for point mutations [35–46]. For example, our method is much faster than the recently reported electrochemical detection of *KRAS* point mutation in pancreatic cancer samples [36].

### 3.3 Clinical Sample Analysis and Validation

To demonstrate the potential clinical applications of our assay, we challenged our electrochemical assay to DNA samples extracted from six lymph node with metastatic ESCC and three matched non-cancer oesophageal tissue samples. We found an excellent consistency between our assay and previously reported Sanger sequencing and HRM curve analysis results on *FAM134B* mutations in exon 4 [8]. In our assay, we found about 52% relative current changes in the non-tumour (control) tissues, whereas six ESCC tissue samples displayed variable relative current changes (28-36%) indicating lower adsorption of DNA occurred on the electrode surface (Figure 2). As can be seen in Figure 2 and Figure S2 in supporting information, we achieved roughly 36% relative current changes for P1 sample which might be due to mutations present in the sequence, resulting in a low amount of adsorbed DNA on the electrode surface (Figure 2 and Figure S2 in supporting information). HRM curve analysis also identified this variant which is evident by differential melting of the variants in comparison with the WT sequence in the normalized melting curve. (Figure S3A(i) in supporting information). This was further evident by plotting the rate of change in fluorescence per unit of change in temperature on the *y* axis to create a derivative plot (Figurer S3 A(i′) in supporting information). Furthermore, Sanger sequencing data [8] confirmed c.660G > A, c.546-56delA, c.672 + 26delT mutations in P1 samples (Table 2 in supporting information). P2 samples demonstrated about 30% relative current changes indicating mutations. Analogous findings were also noted with HRM curve Analysis. Sanger sequencing data confirmed that this sample contains c.660G > A, c.546-64delA and c.546-56delA mutations. The additional reduction of the relative current changes (30% *versus* 36%) could be explained by the fact that an additional A deletion in this sample resulted a lower level of adsorbed DNA on the electrode surface (i.e., high DPV current and hence low % $I_{Relative}$) (Figures 2 and 3, Table 2 in supporting information). In a P3 sample, we found about 32% relative current changes, indicating relatively higher amount of adsorbed DNA on the electrode surface (i.e., lower DPV currents with respect to that of the P2 sample). This might be due to the nature of mutation (c.546-64delA, c.672 + 46-47delTG) as verified *via* HRM curve analysis and Sanger sequencing[8] (Figures S2, S3 and Table 2 in supporting information).

The level of relative current changes for P4 samples is almost similar to that of P1 sample, indicating that both samples contain identical mutation patterns for *FAM134B*. HRM curve analysis and Sanger sequencing were also supported these findings (Figures S2, S4, and Table 2 in supporting information). The P5 sample displayed about 28% relative current changes that might be occurred due to the presence of the following mutations in the target sequence: c.546-547CT > GG, c.660G > A, c546-64delA, c.546-56delA, and c.672 + 46-47delTG. Notably, this relative current changes is slightly lower that that obtained for the sample SDM-4. This can be explained by considering the fact that an additional deletion of c.672 + 46-47delTG in P5 sample results the lower amount of adsobed DNA on the electrode surface, leading to a high DPV currents (i.e., low % $I_{Relative}$) (Figures S2, S4, and Table 2 in supplementary information). For sample P6, we found about 29% relative current difference, which was due to the lower level of adsorbed DNA on the electrode surface (i.e. high DPV current). Indeed, this sample contains c.660G > A, c.546-56delA, c.672 + 26delT, c.672 + 46-47delTG mutations (Figure S2, S4, and Table 2 in supporting information). Unlike synthetic samples, the

  

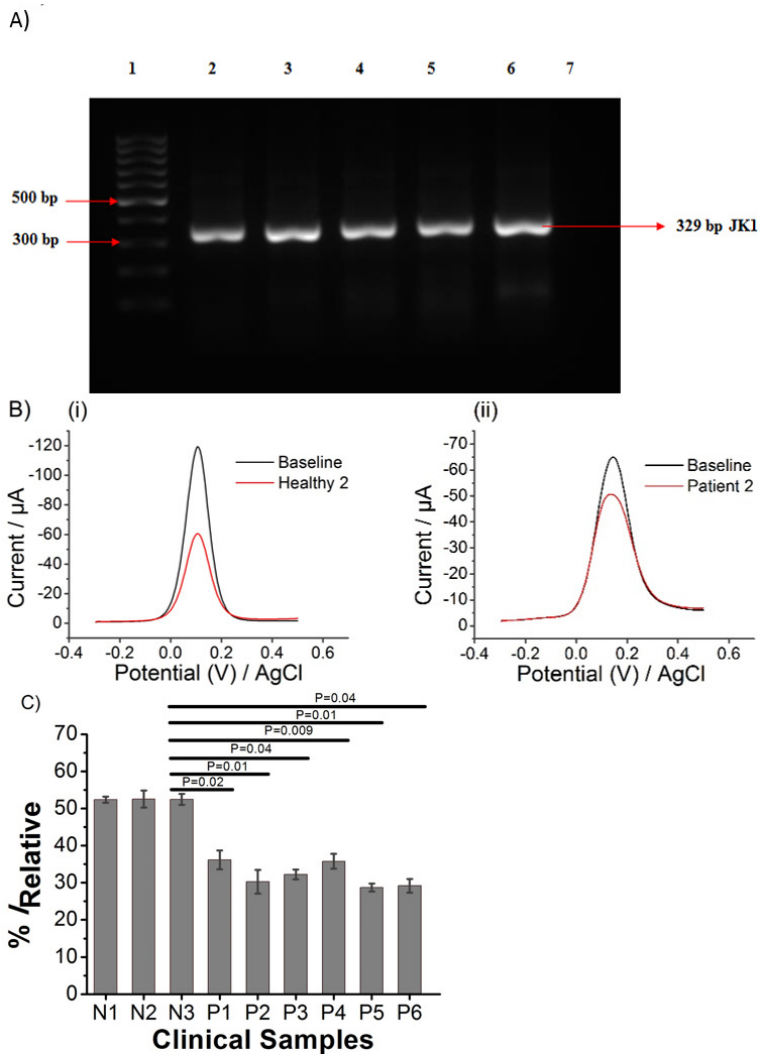


Fig. 2. (A) Representative amplified PCR products of exon-4 of *FAM134B* (JK1) in 1.5% agarose gel. *FAM134B* (JK1) were present in all the samples (1-6) except non template control (7). Hundred base pair DNA ladder used for comparison. (B) Representative differential pulse voltammetric current changes for detecting *FAM134B* point mutations in healthy and patients samples. (C) Relative current changes for detecting *FAM134B* point mutations for the three normal (N1, N2 and N3) and six (P1-P6) oesophageal cancer tissue samples. Each data point represents the average of three repeat trails, and error bars represent the standard deviation of measurements (%RSD = < 5.0%; for $n$ =3). Statistical significance were determined by pairwise comparison between 2 conditions using student t-test. *, $p$ = 0.005 to 0.05 and **, $p$ = 0.0005 to 0.005..

inter-assay %RSD for the clinical samples analysis was found to be <5.0%. These data imply that the electrochemical signal generated by our assay was able to distinguish the presence or the absence of mutations in samples collected from ESCC patients. Additionally, the validation of these results from previously reported HRM curve analysis and Sanger sequencing further suggest that our method may help in easy and cost effective detection of *FAM134B* gene mutations in cancer patients. However, further studies with large number of clinical cohorts are needed for the functional validation of our method.

Although there are many electrochemical methods successfully developed in detecting point mutations or SNPs, our method provides several unique advantages over these methodologies. First, we used direct adsorption of DNA samples on an unmodified gold electrode rather than the conventional biosensing approach of using recognition and transduction layers. This proposed technology substantially simplifies the detection method by avoiding the complicated chemistries underlying each step of the sensor fabrication. Second, it avoids the use of various enzymes (such as endonuclease [43], exonuclease [35] and *E. Coli* DNA ligase [36]), fluorescence tags [47], electrochemically active reporters such as methylene blue (MB) [12] and capture probes for target hybridization and detection, and thus provides relatively faster and easier platform for mutation analysis. Third, single-use screen-printed electrode is a well-known detector for inexpensive readout in electrochemistry. It is also worth noting that several gold nanoparticle (AuNPs)-based DNA mutation assays are currently available [48–50]. Although these methods allow naked eye detection and require no covalent modification of the DNA or AuNPs surfaces, most of them rely on the use of salt-induced aggregation [48], additional oligonucleotide strand as the linker [49] or magnetic isolation and hybridization [50] steps. In contrast, our current assay quantify the DNA mutation by simply monitoring their direct adsorption on an unmodified gold surface.

## 4 Conclusions

We have demonstrated a relatively simple and new electrochemical method for the detection of gene specific

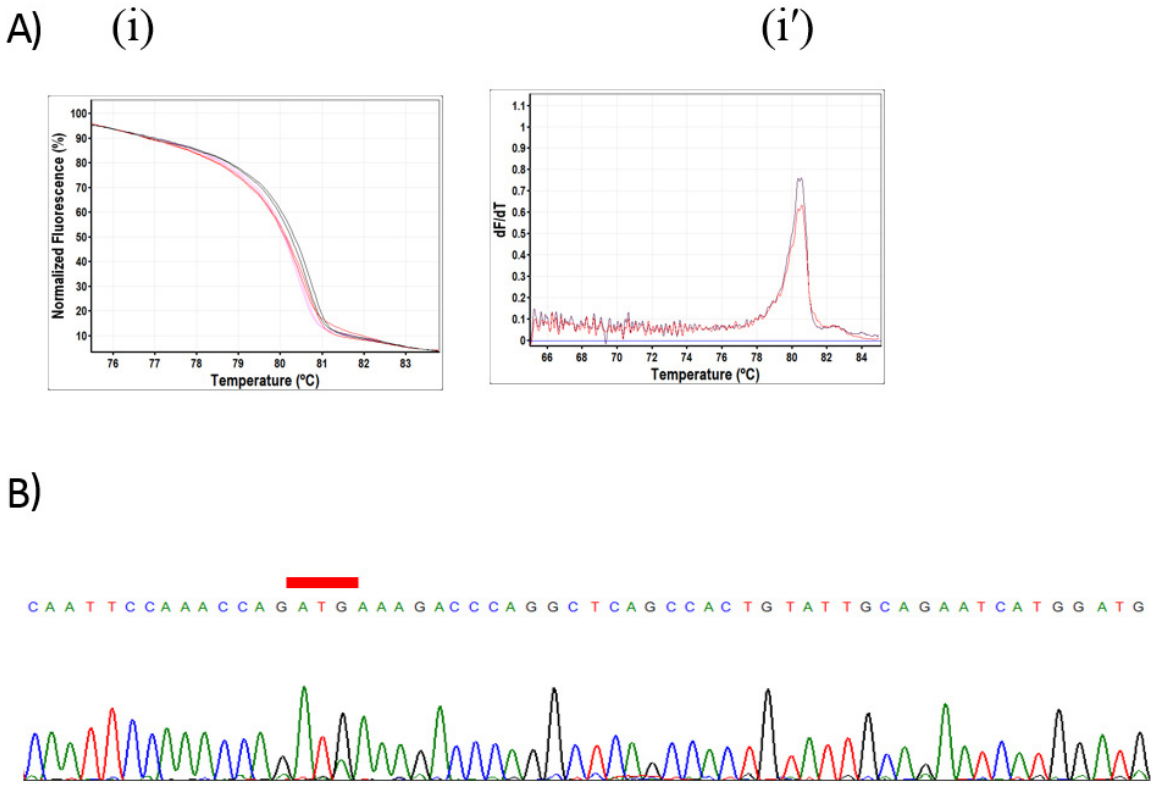


Fig. 3. (A) Representative differential melting properties of two healthy and patients DNA samples with variant amplicons of *FAM134B* exon 4 in the normalized melting curves. (i′) Differential melting curves of these variants were also evident by the derivative plots (B) Sanger sequencing confirms the presence of *FAM134B* point mutation.

mutations in PCR-amplified genomic DNA samples based on the different adsorption affinity of DNA nucleotides towards gold. The detection was achieved by the direct adsorption of two sequentially different PCR amplified mutated and unmutated DNA samples onto an unmodified gold electrode. Using this approach, we were able to detect mutations in 50 ng of target PCR-amplified product within 1.5 h with high reproducibility (% RSD = < 5.0) and specificity. We used the method to analyze a small panel of clinical samples from ESCC patients, and the results were validated with HRM curve analysis and sequencing. We anticipate that this method can potentially be applicable for point mutation detection in clinical diagnostics.

## Acknowledgements

This work was supported by the NHMRC CDF (APP1088966 to M.J.A.S.), Griffith University New Researcher Grant Scheme and HDR scholarships (GUIPRS and GUPRS scholarships to M.H.H., M.N.I. and F.I.) from the Griffith University.

## References

[1] D. Sidransky, *Nat. Rev. Cancer*, **2002**, *2*, 210–219.
[2] C. Greenman, P. Stephens, R. Smith, G. L. Dalgliesh, C. Hunter, G. Bignell, et al. *Nature*, **2007**, *446*, 153–158.
[3] L. Scheubert, R. Schmidt, D. Repsilber, M. Lustrek, G. Fuellen, *DNA Res.*, **2011**, *18*, 233–251.
[4] W. K. Tang, C. H. Chui, S. Fatima, S. H. Kok, K. C. Pak, T. M. Ou, et al. *Int. J. Mol. Med.*, **2007**, *19*, 915–923.
[5] K. Kasem, V. Gopalan, A. Salajegheh, C. T. Lu, R. A. Smith, A. K. Lam, *Exp. Cell Res.*, **2014**, *326*,166-173.
[6] F. Islam, V. Gopalan, R. Wahab, R. A. Smith, B. Qiao, A. K. Lam, *Mol. Carcinog.* **2016**, doi: 10.1002/mc.22488.
[7] I. Kurth, T. Pamminger, J. C. Hennings, D. Soehendra, A. K. Huebner, A. Rotthier, *Nat. Genet.*, **2009**, *41*, 1179–1181.
[8] M. H. Haque, V. Gopalan, K. W. Chan, M. J. A. Shiddiky, R. A. Smith, A. K. Lam, *Sci. Rep.*, **2016**, *6*, 29173.
[9] M. Grompe, *Nat. Genet.*, **1993**, *5*, 111–117.
[10] P. M. Holland, R. D. Abramson, R. Watson, D. H. Gelfand, *Proc. Natl. Acad. Sci. U. S. A.*, **1991**, *88*, 7276–7280.
[11] P. L. Ross, K. Lee, P. Belgrader, *Anal. Chem.*, **1997**, *69*, 4197–4202.
[12] S. O. Kelley, E. M. Boon, J. K. Barton, N. M. Jackson, M. G. Hill, *Nucleic Acids Res.*, **1999**, *27*, 4830–4837.
[13] E. M. Boon, D. M. Ceres, T. G. Drummond, M. G. Hill, J. K. Barton, *Nat. Biotechnol.*, **2000**, *18*, 1096–1100.
[14] E. L. Wong, J. J. Gooding, *Anal. Chem.*, **2006**, *78*, 2138–2144.
[15] M. Inouye, R. Ikeda, M. Takase, T. Tsuri, J. Chiba, *Proc. Natl. Acad. Sci. U. S. A.*, **2005**, *102*, 11606–11610.

[16] J. Wakai, A. Takagi, M. Nakayama, T. Miya, T. Miyahara, T. Iwanaga, S. Takenaka, Y. Ikeda, M. Amano, T. Urata, *Nucleic Acids Res.*, **2004**, *32*, e141.
[17] C. J. Yu, Y. Wan, H. Yowanto, J. Li, C. Tao, M. D. James, C. L. Tan, G. F. Blackburn, T. J. Meade, *J. Am. Chem. Soc.*, **2001**, *123*, 11155–11161.
[18] Y. Xiao, A. A. Lubin, B. R. Baker, K. W. Plaxco, A. J. Heeger, *Proc. Natl. Acad. Sci. U. S. A.*, **2006**, *103*, 16677–16680.
[19] A. A. Lubin, R. Y. Lai, B. R. Baker, A. J. Heeger, K. W. Plaxco, *Anal. Chem.*, **2006**, *78*, 5671–5677.
[20] K. J. Cash, A. J. Heeger, K. W. Plaxco, Y. Xiao, *Anal. Chem.*, **2009**, *81*, 656–661.
[21] S. Piana, A. Bilic, *J. Phys. Chem. B*, **2006**, *110*, 23467–23471.
[22] H. Kimura-Suda, D. Y. Petrovykh, M. J. Tarlov, L. J. Whitman, *J. Am. Chem. Soc.*, **2003**, *125*, 9014–9015.
[23] J. J. Storhoff, R. Elghanian, C. A. Mirkin, R. L. Letsinger, *Langmuir*, **2002**, *18*, 6666–6670.
[24] A, A. Sina, S. Howell, L. G. Carrascosa, S. Rauf, M. J. A. Shiddiky, M. Trau, *Chem. Commun.*, **2014**, *50*, 13153–13156.
[25] A. A. Sina, L. G. Carrascosa, R. Palanisamy, S. Rauf, M. J. A. Shiddiky, M. Trau, *Anal. Chem.*, **2014**, *21*, 10179–10185.
[26] K. M. Koo, A. A. I. Sina, L. G. Carrascosa, M. J. A. Shiddiky, M. Trau, *Analyst*, **2014**, *139*, 6178–6184.
[27] K. M. Koo, L. G. Carrascosa, M. J. A. Shiddiky, M. Trau, *Anal. Chem.*, **2016**, *88*, 6781–6788.
[28] K. M. Koo L. G. , Carrascosa, M. J. A. Shiddiky, M. Trau, *Anal Chem.*, **2016**, *88*, 2000–2005.
[29] J. Zhang, L. Wang, D. Pan, S. Song, C. Fan, *Chem. Commun.*, **2007**, *11*, 1154–1156.
[30] J. Das, K. B. Cederquist, A. A. Zaragoza, P. E. Lee, E. H. Sargent, S. O. Kelley, *Nat. Chem.*, **2012**, *4*, 642–648.
[31] K. Kasem, V. Gopalan, A. Salajegheh, C. T. Lu, R. A. Smith, A. K. Lam, *Exp. Mol. Pathol.*, **2014**, *97*, 31–36.
[32] K. Kasem, E. Sullivan, V. Gopalan, A. Salajegheh, R. A. Smith, A. K. Lam, *Exp. Mol. Pathol.*, **2014**, *97*, 99–104.
[33] J. Das, I. Ivanov, L. Montermini, J. Rak, E. H. Sargent, S. *O. Kelley*, *Nat. Chem.* **2015**, *7*, 569–575.
[34] J. A. MacLeod, A. C. Nemeth, W. C. Dicke, D. Wang, S. W. Manalili, J. C. Hannis, G. B. Collier, J. J. Drader, *Lab Chip* **2016**, *16*, 2513–2520.
[35] X. W. Xu, X. H. Weng, C. L. Wang, W. W. Lin, A. L. Liu, W. Chen, X. H. Lin, *Biosens. Bioelectron.*, **2016**, *80*, 411–417.
[36] C. Zhao, S. Yang, L. Lin, S. Weng, Q. Liu, A. Liu, X. Lin, *Sens. Actuator B-Chem.*, **2016**, *223*, 946–951.
[37] Y. Wu, R. Y. Lai, *Chem. Commun.*, **2013**, *49*, 3422–3424.
[38] D. Pu, H. Liang, F. Wei, D. Akin, Z. Feng, Q. Yan, et al. *Thorac. Cancer*, **2016**, *7*, 428–436.
[39] T. Garcia-Mendiola, V. Bayon-Pizarro A. , Zaulet, I. Fuentes, F. Pariente, F. Teixidor, C. Vinas, E. Lorenzo, *Chem. Sci.*, **2016**, (doi: 10.1039/C6SC01567 K).
[40] F. Li, Y. Xu, X. Yu, Z. Yu, H. Ji, Y. Song, H. Yan, G. Zhang, *Sens. Actuator B-Chem.*, **2016**, *234*, 648–657.
[41] R. P. Johnson, J. A. Richardson, T. Brown, P. N. Bartlett, *J. Am. Chem. Soc.*, **2012**, *134*, 14099–14107.
[42] E. Hamidi-Asl, J. Bakhsh Raoof, M. Saeid Hejazi, S. Sharifi, S. Mahdi Golabi, I. Palchetti, M. Mascini, *Electroanalysis*, **2015**, *27*, 1378–1386.
[43] C. Yang, B. Dou, J. Yang, R. Yuan, Y. Xiang, *Chem. Commun.*, **2016**, *52*, 8707–8710
[44] G. Liu, Y. Lin, *J. Am. Chem. Soc.*, **2007**, *129*, 10394–10401.
[45] F. Lucarelli, G. Marrazza, M. Mascini, *Biosens. Bioelectron.*, **2005**, *20*, 2001–2009.
[46] P. O. Wang, X. Li, Z. Dai, X. Zou, X. Han, *Sen. Actuator B-Chem.*, **2014**, *201*, 222-227.
[47] D. D. L. Bowtell, *Nat. Genet.* **1999**, *21*, 25–32.
[48] H. Li, L. J. Rothberg, *J. Am. Chem. Soc.* **2004**, *126*, 10958–10961.
[49] W. Xu, X. Xue, T. Li, H. Zeng, X. Liu, *Angew. Chem. Int. Ed.* **2009**, *48*, 6849–6852.
[50] P. Valentini, R. Fiammengo, S. Sabella, M. Gariboldi, G. Maiorano, R. Cingolani, P. R. Pompa, *ACS Nano* **2013**, *7*, 5530–5538.

Received: January 19, 2017
Accepted: February 1, 2017
Published online on ■■ ■■, 0000

# FULL PAPER

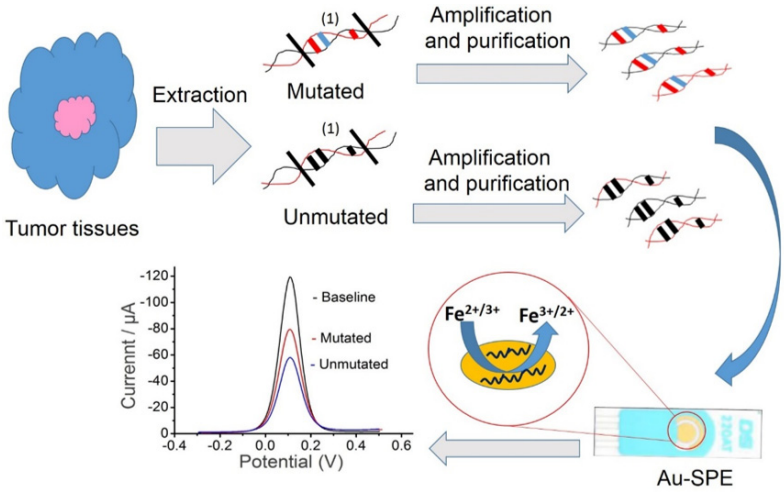


(1) is the target region. It is exon 4 of FAM134B gene (see text for sequence)

*M. H. Haque, M. N. Islam, F. Islam, V. Gopalan*, N.-T. Nguyen, A. K. Lam*, M. J. A. Shiddiky**

**Electronic Supporting Information (SI)**

**For**

# Electrochemical Detection of FAM134B Mutations in Oesophageal Cancer Based on DNA-Gold Affinity Interactions

*Md. Hakimul Haque, Md Nazmul Islam, Farhadul Islam, Vinod Gopalan, Nam-Trung Nguyen, Alfred K. Lam, Muhammad J. A. Shiddiky*

## Primer Design

Primer were designed for detecting *FAM134B (JK1)* mutation and copy number changes were designed based on GenBank accession number for variant 1 NM_001034850 and for variant 2 NM_019000 as well as for a control gene, *HBD* (GenBank accession number NM_000519) using Primer3 version 0.4.0 (http://frodo.wi.mit.edu/primer3). All primers were analyzed for specificity using Primer Blast (http://www.ncbi.nlm.nih.gov/tools/primer-blast) and Primer Premier program version 5 (Premier Biosoft, Palo Alto, CA, USA) to check for primer parameters like GC content, annealing temperature of primer (Tm) and to forecast any possible mismatching, primer dimmer or hairpin formation. Primers for *FAM134B (JK1)* gene were designed within the intronic regions on either side of the exon of interest to ensure coverage of the entire exon 4 to amplify and direct sequencing both isoforms of the gene for screening of mutation in ESCC. Synthetic DNA mutations (SDM) were designed based on mimicking PCR products. The primer pairs were obtained from Integrated DNA technologies (Coralville, IA, USA). The list of chosen primer sets are summarized in Table S1.

**Table 1.** List of the oligonucleotide sequences used in this study. The synthetic DNA mutations in the intron (black colour) and exon-4 (blue colour) of *FAM134B (JK1)* interest are highlighted in red colour. Each mutations and control in synthetic DNA represent mutated and unmutated samples obtained after PCR of *FAM134B* gene.

| Target genes | Oligonucleotide Sequences (5'--3′) |
|---|---|
| *FAM134B*-F | CCAGAGGGTGTGGCCAACAGTAG |
| *FAM134B*-R | TGGAGAAATCTGACAAGCTG |
| *HBD*-F | CAGCATCAGGAGTGGACAGA |
| *HBD*-R | CTCGGCGGCACCCAC |
| SDM-1 | CCAGAGGGTGTGGCCAACAGTAGATGCTCAATAAATATTTGCCAAAGC C-TAAAT<br>GTTGAATGAATCATCCAAAGTTCAGTAGTATTTTTTTTCTTTTTGTCTCTTTAGCTG<br>GGAAGTTATCAATTCCAAACCAGATGAAAGACCCAGGCTCAGCCACTGTATTGCA<br>GAATCATGGATGAATTTCAGCATATTTCTTCAAGAAATGTCTCTTTTTAAACAGCA<br>GAGCCCTGGCAAGGCAAGTTTTCCAGTAAAGGAGTATGTTTTAAAATGTTCAGTTA<br>CTTGGAAACAAAT GAACTAACCTATTTTATCAGCTTGTCAGATTTCTCCA |
| SDM-2 | CCAGAGGGTGTGGCCAACAGTAGATGCTCAATAAATATTTGCCAAAGC C-TAA-T<br>GTTGAATGAATCATCCAAAGTTCAGTAGTATTTTTTTTCTTTTTGTCTCTTTAGCTG<br>GGAAGTTATCAATTCCAAACCAGATGAAAGACCCAGGCTCAGCCACTGTATTGCA<br>GAATCATGGATGAATTTCAGCATATTTCTTCAAGAAATGTCTCTTTTTAAACAGCA<br>GAGCCCTGGCAAGGCAAGTTTTCCAGTAAAGGAGTATGTTTTAAAATGTTCAGTTA<br>CTTGGAAACAAAT GAACTAACCTATTTTATCAGCTTGTCAGATTTCTCCA |
| SDM-3 | CCAGAGGGTGTGGCCAACAGTAGATGCTCAATAAATATTTGCCAAAGC C-TAA-T<br>GTTGAATGAATCATCCAAAGTTCAGTAGTATTTTTTTTCTTTTTGTCTCTTTAGGGG<br>GGAAGTTATCAATTCCAAACCAGATGAAAGACCCAGGCTCAGCCACTGTATTGCA<br>GAATCATGGATGAATTTCAGCATATTTCTTCAAGAAATGTCTCTTTTTAAACAGCA<br>GAGCCCTGGCAAGGCAAGTTTTCCAGTAAAGGAGTATGTTTTAAAATGTTCAGTTA<br>CTTGGAAACAAAT GAACTAACCTATTTTATCAGCTTGTCAGATTTCTCCA |
| SDM-4 | CCAGAGGGTGTGGCCAACAGTAGATGCTCAATAAATATTTGCCAAAGC C-TAA-T<br>GTTGAATGAATCATCCAAAGTTCAGTAGTATTTTTTTTCTTTTTGTCTCTTTAGGGG<br>GGAAGTTATCAATTCCAAACCAGATGAAAGACCCAGGCTCAGCCACTGTATTGCA<br>GAATCATGGATGAATTTCAGCATATTTCTTCAAGAAATGTCTCTTTTTAAACAGCA<br>AAGCCCTGGCAAGGCAAGTTTTCCAGTAAAGGAGTATGTTTTAAAATGTTCAGTTA<br>CTTGGAAACAAAT GAACTAACCTATTTTATCAGCTTGTCAGATTTCTCCA |
| Control DNA | CCAGAGGGTGTGGCCAACAGTAGATGCTCAATAAATATTTGCCAAAGCCATAAAT<br>GTTGAATGAATCATCCAAAGTTCAGTAGTATTTTTTTTCTTTTTGTCTCTTTAGCTG<br>GGAAGTTATCAATTCCAAACCAGATGAAAGACCCAGGCTCAGCCACTGTATTGCA<br>GAATCATGGATGAATTTCAGCATATTTCTTCAAGAAATGTCTCTTTTTAAACAGCA<br>GAGCCCTGGCAAGGCAAGTTTTCCAGTAAAGGAGTATGTTTTAAAATGTTCAGTTA<br>CTTGGAAACAAAT GAACTAACCTATTTTATCAGCTTGTCAGATTTCTCCA |

**Table 2.** List of the patient samples with mutation sites of FAM134B gene in ESCC.

| Name of clinical samples | Mutation Sites in the exon-4 of FAM134B gene |
|---|---|
| Patient 1 | c.660G>A, c.546-56delA, c.672+26delT |
| Patient 2 | c.660G>A, c.546-64delA, c.546-56delA |
| Patient 3 | c.546-64delA, c.672+46-47delTG |
| Patient 4 | c.660G>A, c.546-56delA, c.672+26delT |
| Patient 5 | c.546-547CT>GG, c.660G>A, c546-64delA,c.546-56delA, c.672+46-47delTG |
| Patient 6 | c.660G>A, c.546-56delA, c.672+26delT, c.672+46-47delTG |

**Optimisation of the operating parameters**

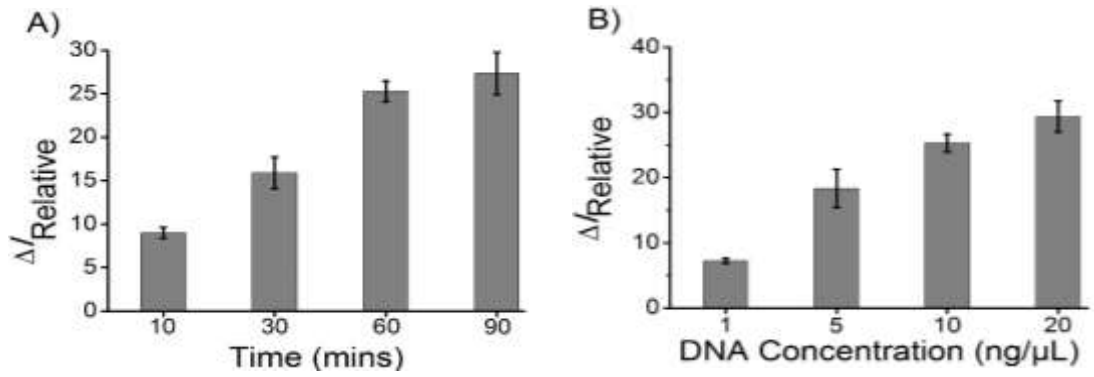


**Fig. S1.** Optimisation of the operating parameters for the adsorption of wild type (control DNA) and SDM2 (2A detection) samples at (A) different time (DNA concentration, 10 ng/μL; pH of the SSC buffer 7.0) and (B) different concentration (adsorption time, 60 min; pH of the SSC buffer 7.4). Each bar represents the average of three separate trials (n = 3). Error bars represent the standard deviation of measurements (%RSD = <5% for n = 3). Current difference ($\Delta i$r) is calculated using the equation, $\Delta i_r = \%i_{r,\text{control DNA}} - \%i_{r,\text{SDM2}}$, where $\%i_{r,\text{control DNA}}$ and $\%i_{r,\text{SDM2}}$ are the relative DPV signals for the control and SDM2 samples, respectively.

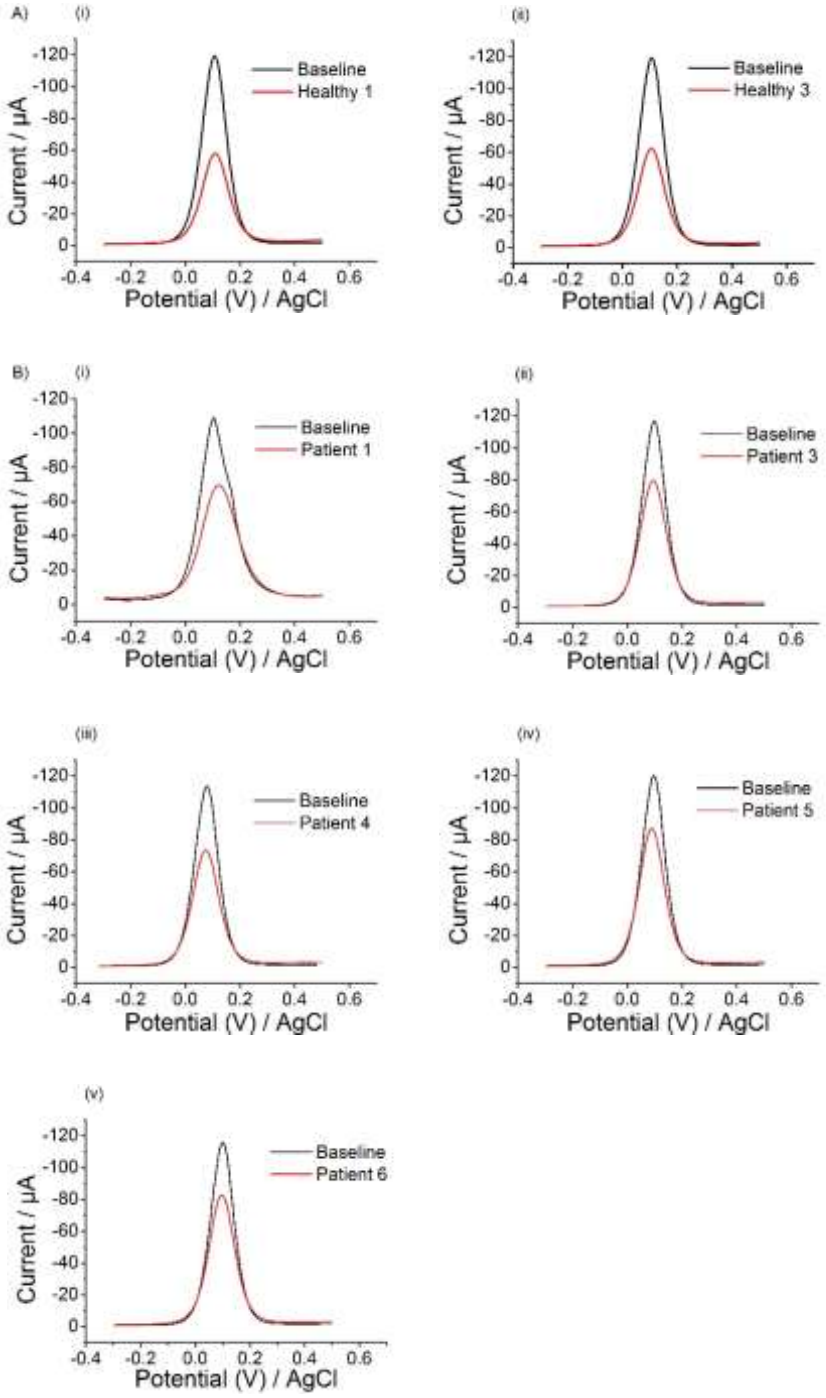


**Fig. S2A.** (i-ii) Representative differential pulse voltammetric current changes for detecting FAM134B point mutations in two healthy samples. **2B.** (i-v) differential pulse voltammetric current changes for detecting FAM134B point mutations forfive (P1, P3-P6) oesophageal cancer tissue samples. Each data point represents the average of three repeat trails, and error bars represent the standard deviation of measurements (%RSD = <5.0% for *n* =3).

A) (i) (i′)

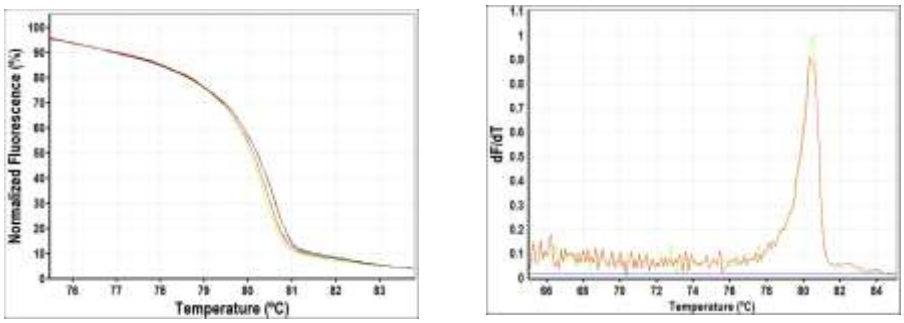


(ii) (ii′)

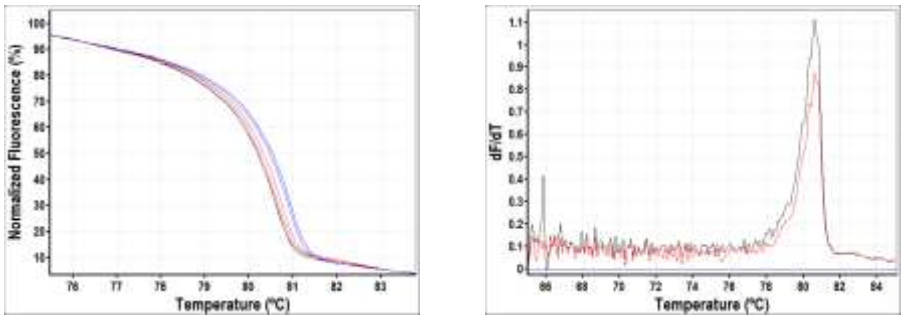


B) (i)

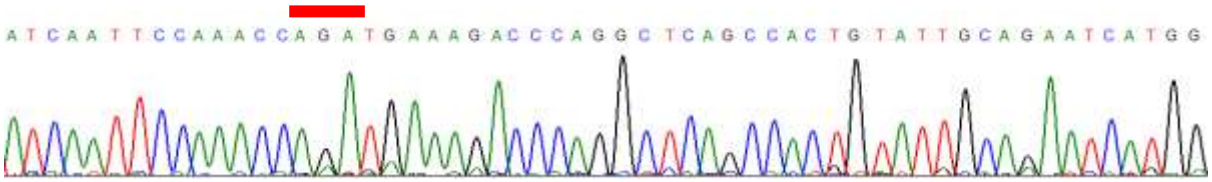


(ii)

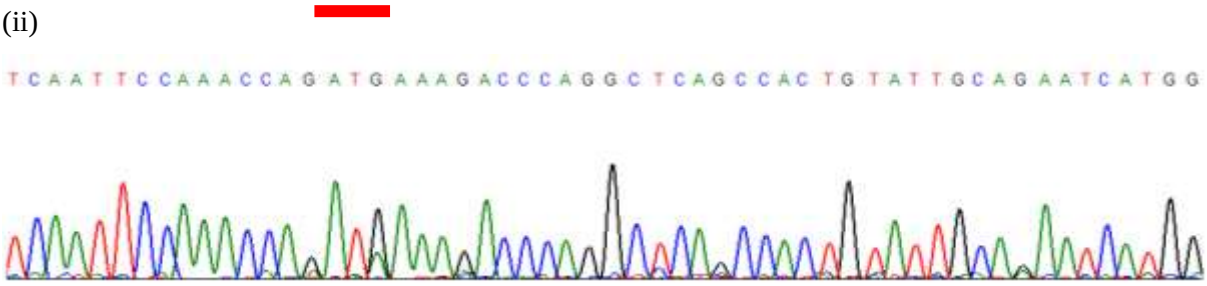


**Fig. S3A**. (i-ii) Representative differential melting properties of healthy and patients DNA samples (P1 and P3) with variant amplicons of FAM134Bexon 4 in the normalized melting curves. (i′-ii′)Differential melting curves of these variants were also evident by the derivative plotsB). **3B.** (i-ii)Sanger sequencing confirms the presence of FAM134B point mutation in patients DNA samples (P1 and P3).

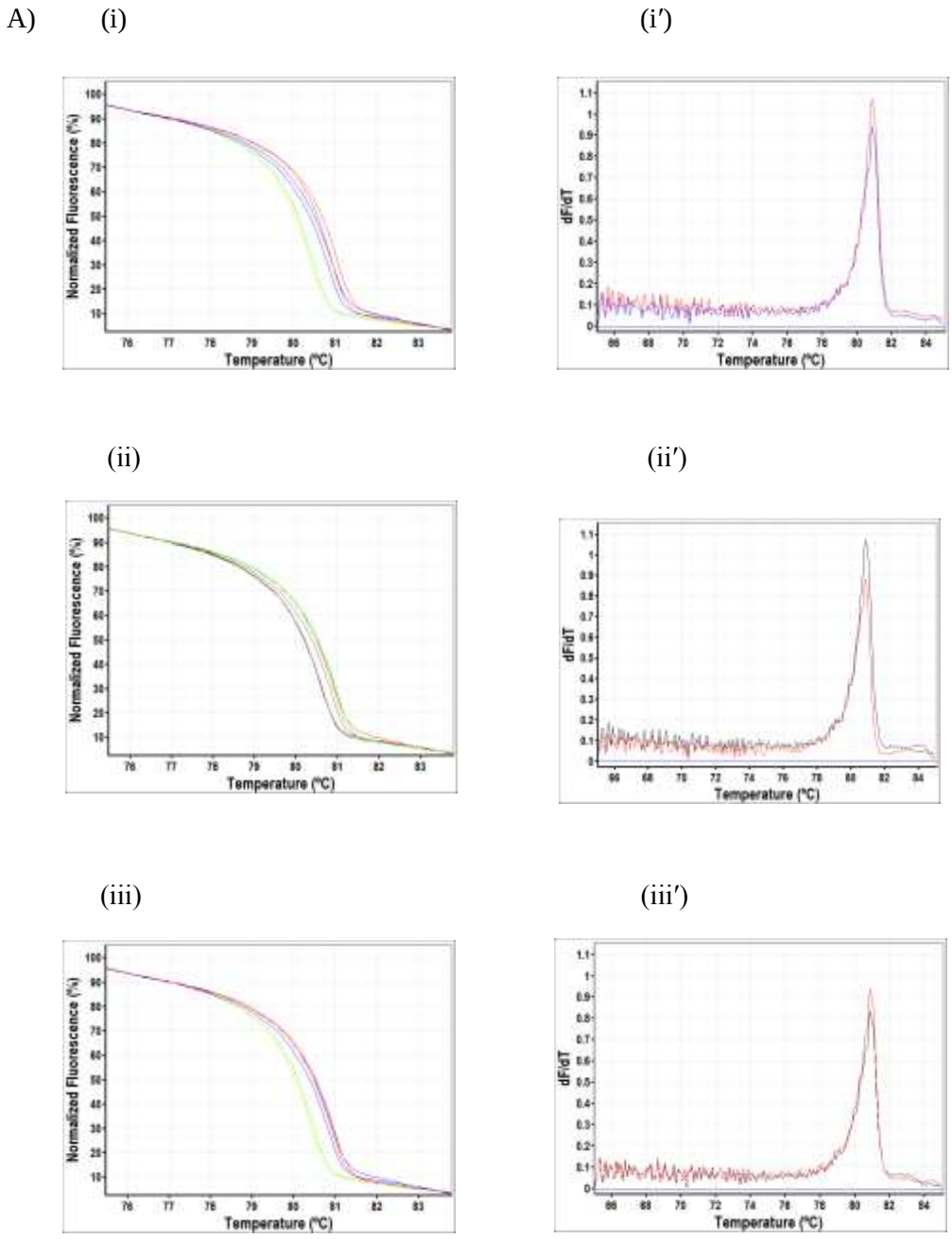


**Fig. S4A.** (i-iii) Representative differential melting properties of healthy and patients DNA samples (P4-P6) with variant amplicons of FAM134Bexon 4 in the normalized melting curves. (i′-iii′)Differential melting curves of these variants were also evident by the derivative plots.

(B)

(i)

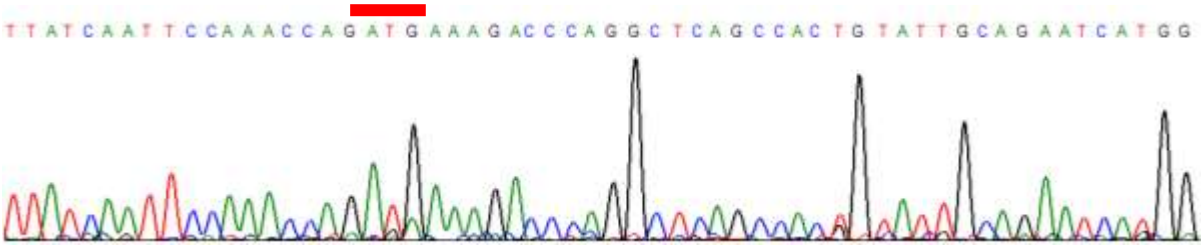


(ii)

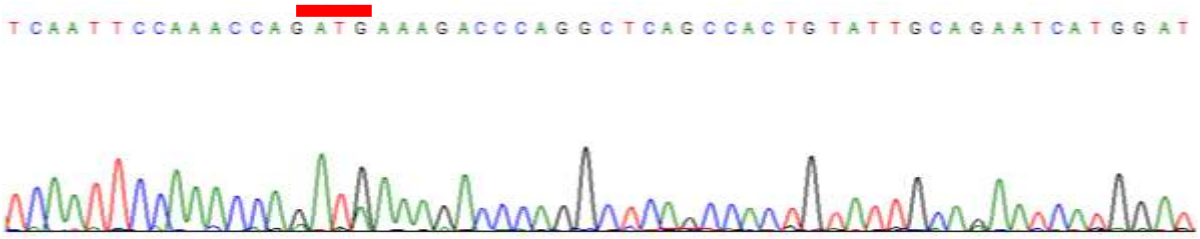


(iii)

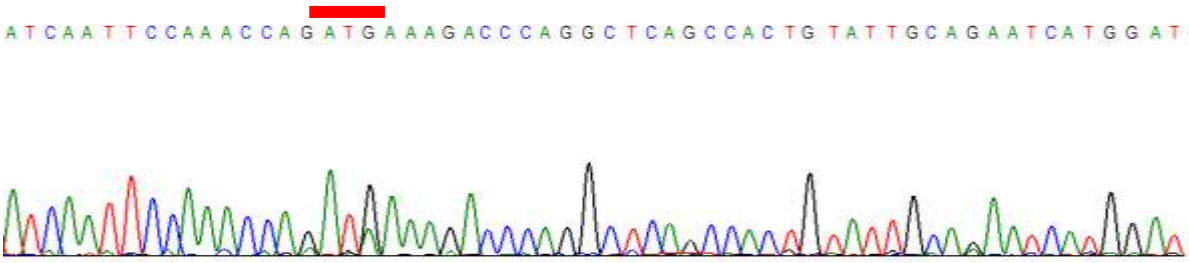


**Fig. S4B.** (i-iii)Sanger sequencing confirms the presence of FAM134B point mutation in patients DNA samples (P4-P6).

# Chapter 6

# Nanotechnological approaches for regional methylation of *FAM134B* gene and its clinical application in ESCC

Chapter 6 is included as it appears in Biosensor and Bioelectronics (2016).

# Introduction

A simple and inexpensive electrochemical method is developed for detecting regional DNA methylation using direct adsorption of bisulfite-treated and PCR amplified DNA sequences onto graphene-modified screen-printed carbon electrode (g-SPCE). In recent years it has been demonstrated that the nature of adsorption affinity of unmodified DNA towards graphene is finely governed by the composition of DNA bases and strictly follows the trend: guanine (G)> adenine (A)> thymine (T)> cytosine (C). However, no one has ever used this direct adsorption process as a tool for the detection of DNA methylation at a single CpG level of resolution. This is the first report on a simple electrochemical method for the detection of DNA methylation on bisulphite-treated samples using base dependent affinity interaction of DNA bases with graphene. The amount of the adsorbed DNA on graphene-modified screen-printed carbon electrode was quantified by differential pulse voltammetry (DPV) in the presence of the $[Fe(CN)_6]^{3-/4-}$ system. The coulombic repulsion between $Fe(CN)_6^{3-}$ and negatively charged DNA (adsorbed) on the electrode surface enables distinguishing guanine-enriched methylated (strongly adsorbed) DNA samples from the adenine-enriched unmethylated (relatively less adsorbed) samples at a single CpG level of resolution. To demonstrate the applicability of the method, we targeted DNA sequences containing eleven potentially methylated CpG sites located within a small region of *FAM134B* promoter gene. The methylation status of this gene region has already been highlighted as a potential biomarker in oesophageal and colorectal cancers. We believe that the simplicity, high specificity and sensitivity along with the ability to detect single CpG methylation make our method potentially attractive for future diagnostic applications.

Biosensors and Bioelectronics 87 (2017) 615–621

Contents lists available at ScienceDirect

Biosensors and Bioelectronics

journal homepage: www.elsevier.com/locate/bios

# Detection of regional DNA methylation using DNA-graphene affinity interactions

Md. Hakimul Haque [a,b], Vinod Gopalan [a,*], Sharda Yadav [b,c], Md Nazmul Islam [b,c], Ehsan Eftekhari [c,d], Qin Li [c,d], Laura G. Carrascosa [e], Nam-Trung Nguyen [c], Alfred K. Lam [a,*], Muhammad J.A. Shiddiky [b,c,**]

[a] Cancer Molecular Pathology Laboratory in School of Medicine, Menzies Health Institute Queensland, Griffith University, Gold Coast Campus, Australia
[b] School of Natural Sciences, Griffith University, Nathan Campus, QLD 4111, Australia
[c] Queensland Micro and Nanotechnology Centre, Griffith University, Nathan Campus, QLD 4111, Australia
[d] School of Engineering, Griffith University, Nathan, QLD 4111, Australia
[e] The University of Queensland, Brisbane, QLD 4072, Australia

ARTICLE INFO

*Article history:*
Received 3 June 2016
Received in revised form
29 August 2016
Accepted 4 September 2016
Available online 5 September 2016

*Keywords:*
DNA methylation
Regional methylation
Electrochemical detection
Graphene-DNA base interaction
Disposable screen-printed electrode

ABSTRACT

We report a new method for the detection of regional DNA methylation using base-dependent affinity interaction (*i.e.*, adsorption) of DNA with graphene. Due to the strongest adsorption affinity of guanine bases towards graphene, bisulfite-treated guanine-enriched methylated DNA leads to a larger amount of the adsorbed DNA on the graphene-modified electrodes in comparison to the adenine-enriched unmethylated DNA. The level of the methylation is quantified by monitoring the differential pulse voltammetric current as a function of the adsorbed DNA. The assay is sensitive to distinguish methylated and unmethylated DNA sequences at single CpG resolution by differentiating changes in DNA methylation as low as 5%. Furthermore, this method has been used to detect methylation levels in a collection of DNA samples taken from oesophageal cancer tissues.



## 1. Introduction

DNA methylation is a cell-type specific epigenetic marker, essential for controlling gene expression via transcriptional regulation, silencing of repetitive DNA and genomic imprinting (Jones and Takai, 2001; Wu and Zhang, 2010). Current advances in DNA methylation research have suggested that different types of cancers appear to have distinct DNA methylation levels at selected regions (*i.e.*, regional methylation), which are responsible for their various responses to treatment (Taleat et al., 2015; Zhang et al., 2015). For example, regional methylation plays a fundamental role in the initiation and progression of oesophageal squamous cell carcinoma (ESCC) by inactivating transcription and loss of gene function (Chang et al., 2002; Delpu et al., 2013; Wong et al., 2006, 2003). Also, DNA methylation based biomarker has proven to be used alone or in combination with other diagnostic methods in cancer (Delpu et al., 2013). Thus, detection of methylation in targeted cancer specific genes could have diagnostic and prognostic implications in human cancers.

Over the past several decades, a number of conventional molecular biology approaches, including-bisulfite sequencing, MS-PCR, mass spectrometry and fluorescence based methods have been extensively used to measure the level of DNA methylation in cancers (Herman et al., 1996; Cao and Zhang, 2012; Zhang et al., 2011, 2015; Plongthongkum et al., 2014; Taleat et al., 2015). These approaches employed sequencing, mass spectrometric or fluorescence readouts to differentiate between methylated and unmethylated sequences. They are relatively robust but are limited by the costly instruments, DNA fragmentation, chimeric product generation, fluorescent labels and long analysis time. Furthermore, these methods are limited by the background fluorescence interference as well as to high labour and bioinformatics costs.

In the recent years, much attention has been focused on developing inexpensive and faster detection strategies based on colorimetry, electrochemistry, Raman scattering readouts and surface plasmon resonance (Carrascosa et al., 2014; Kato et al., 2011, 2008; Koo et al., 2014b; Kurita et al., 2012; Taleat et al., 2015; Wang et al., 2016; Wee, 2015a, 2015b; Zhang et al., 2015). While all these methods have many advantages, their sensor fabrication procedure and data deconvolution methods are rather complicated due to the involvement of complex surface functionalisation steps or coupling chemistry (Carrascosa et al., 2014; Kato et al.,

* Corresponding authors.
** Corresponding author at: School of Natural Sciences, Griffith University, Nathan Campus, QLD 4111, Australia.
*E-mail addresses:* v.gopalan@griffith.edu.au (V. Gopalan), a.lam@griffith.edu.au (A.K. Lam), m.shiddiky@griffith.edu.au (M.J.A. Shiddiky).

http://dx.doi.org/10.1016/j.bios.2016.09.016
0956-5663/

2011, 2008; Koo et al., 2014b; Kurita et al., 2012; Taleat et al., 2015; Wang et al., 2016; Wee, 2015a, 2015b; Zhang et al., 2015). Therefore, a simple and inexpensive method that could simplify the detection method by avoiding the complicated chemistry underlying each step of the sensor fabrication represents an appealing alternative to alleviate some of these issues.

More recently, we have reported a simple method for quantifying DNA methylation using different adsorption affinity of DNA bases onto an unmodified gold substrate (Koo et al., 2014a; Sina et al., 2014a, 2014b). Similar to gold substrate, graphene (Varghese et al., 2009) and graphene oxide (Wu et al., 2011) have been reported as promising substrates for adsorbing nucleobases and nucleosides. Over the past few years, several fundamental studies have been carried out to explore the nature of the direct interaction (*i.e.,* adsorption) of nucleobases and nucleosides onto the graphene and graphene oxide surface (Gowtham et al., 2007; Varghese et al., 2009; Wu et al., 2011). These studies have suggested that the physisorption between individual nucleobases and the graphene (*i.e.*, adsorption on graphene) is controlled by the polarisabilities of the individual nucleobases. Among all nucleobases, guanine and adenine with their five- and six-membered rings possess the largest polarisabilities, whereas other bases with only six-membered rings exhibit lower polarisabilities. Additionally, guanines with its double-bonded oxygen atom possess a larger polarisability than adenine. Since the van der Wall (vdW) energy is directly proportional to the interacting nucleobases, Gowtham et al. (2007) and Varghese et al. (2009) have proposed that vdW interaction is indeed the main driving force for the adsorption of nucleobases onto the graphene and follows the adsorption trend as guanine (G) > adenine (A) > thymine (T) > cytosine (C). Because this interaction is base (*i.e.*, sequence) dependent and bisulfite conversion generates two DNA sequences with different base compositions, bisulfite-converted two DNA sequences should give different adsorption patterns on graphene surface. To date, there is no other method that uses the graphene-DNA affinity interaction to quantify DNA methylation.

Herein, we report a simple and inexpensive method for detecting regional DNA methylation using direct adsorption of bisulfite-treated and PCR amplified DNA sequences onto graphene-modified screen-printed carbon electrode (g-SPCE). In this approach, following the bisulfite conversion and asymmetric PCR amplifications steps, the amplified products was directly adsorbed on g-SPCE. The relative adsorption of the amplified products was then detected *via* differential pulse voltammetry (DPV) in the presence of the $[Fe(CN)_6]^{3-/4-}$ redox system. We first optimised the adsorption parameters (*i.e.*, adsorption time, pH of the solution, etc) to achieve optimal analytical performance of the method. Then, we applied this method to detect *FAM134B* promoter gene methylation in a panel of ESCC cell lines and patient samples derived from oesophageal squamous cell carcinoma. Finally, we established a correlation between promoter hypermethylation and *FAM134B* gene expression levels.

## 2. Experimental

### 2.1. Materials

All reagents were of analytical grade and purchased from Sigma Aldrich (St Louis, MO, USA). UltraPureTM DNase/RNase-free distilled water (Invitrogen, Carlsbad, CA, USA) was used throughout the experiments. Jurkat 100% methylated genomic DNA was purchased from New England Biolabs (Ipswich, MA, USA). Two oesophageal squamous cell carcinoma (ESCC) cell lines, HKESC-1 and HKESC-4, were kindly gifted from Department of Pathology, University of Hong Kong. Another ESCC cell line- KYSE-510 was purchased from Leibniz Institute DSMZ (German collection of microorganisms and cell cultures). All these cell lines were grown in minimum essential medium alpha (MEMα growth medium, Gibco (ThermFisher scientific, Waltham, MA, USA) medium with non-essential amino acids supplemented with 10% fetal bovine serum (FBS, Gibco), 100 μg/mL penicillin (Gibco) and 100 unit/mL streptomycin (Gibco) in a humidified cell culture incubator containing 5% $CO_2$ at 37 °C. Graphene-modified screen-printed carbon electrodes (g-SPCE, 110GPH) were acquired from Dropsens (Spain).

### 2.2. Clinical samples

Surgically resected fresh tissue samples (cancer and matched non-cancer) from eight ESCC patients were used for this study. Histopathological confirmation of carcinoma was made prior to DNA isolation. All ESCC patients selected in this study were free from radio/chemotherapy and were matched with gender (all male) and clinical staging (stage III & IV). Mean age group of the patients were 65±14, ranging from 45 to 74 years. Ethical approval has been obtained for the use of these samples (GU Ref no: MED/19/08/HREC). The selected samples were sectioned using a cryostat (Leica CM 1850 UV, Wetzlar, Germany) and stained by haematoxylin and eosin.

### 2.3. Genomic DNA extraction

HKESC-1, HKESC-4 and KYSE-510 ESCC cell lines were grown in minimum essential medium alpha (MEMα growth medium, Gibco (ThermoFisher scientific, Waltham, MA, USA) medium with non-essential amino acids supplemented with 10% fetal bovine serum (FBS, Gibco), 100 μg/mL penicillin (Gibco) and 100 unit/mL streptomycin (Gibco) in a humidified cell culture incubator containing 5% $CO_2$ at 37 °C. Genomic DNA was extracted and purified from $10^5$ cell plates of the aforesaid cell lines and clinical samples using DNeasy blood and tissue kit (Qiagen Pty. Ltd., Venlo, Netherlands) following manufacturer's instructions. Briefly, after harvesting, appropriate number of cells were suspended in phosphate buffer solutions. A digestion step was executed to remove the protein and RNA in the solution via proteinase and RNase enzymes, respectively. Then, cell samples were suspended in lysis buffer to disrupt and release the nucleic acids and proteins into the solution. The digested proteins and RNA were removed by centrifuging the solution in a spin column. The purified DNA was eluted from the column in 100 μL of elution buffer and stored at −20 °C. The whole genomic amplified (WGA) DNA samples was prepared through amplifying about 50 ng genomic DNA using REPLI-g whole genome amplification kit (Qiagen Pty. Ltd., Venlo, Netherlands) according to manufacturer's instructions. DNA quantification was achieved via Nanodrop Spectrophotometer (BioLab, Ipswich, MA, USA) and purity was measured using 260/280 ratio. Concentration of DNA was noted in ng/μL and then stored at −20 °C until use.

### 2.4. Bisulphite treatment

MethylEasy™ Xceed kit (Human Genetic Signatures Pty. Ltd., NSW, Australia) was used to perform bisulphite conversion as per the manufacturer instruction. Briefly, 500 ng of DNA were incubated with 150 mM NaOH solution at 37 °C for 15 min followed by treatment with sodium bisulphite at 80 °C for 45 min. Then bisulphite-treated DNA solution was purified using the protocol from MethylEasy™ Xceed kit. DNA quantification and purity was checked *via* Nanodrop Spectrophotometer (BioLab, Ipswich, MA, USA). Concentration of bisulphite treated DNA was noted in ng/μL and then stored at −20 °C until use.

### 2.5. Normalization of DNA copy number

In order to normalize the DNA copy number from each DNA source, the relative amount of *FAM134B (JK1)* genes in bisulphite treated cell and WGA DNA samples were determined by real-time amplification of the house keeping *HBD* gene using the Rotor-Gene Q detection system (Qiagen, Hilden, Germany) and performing comparative analysis of Ct (*i.e.* the fractional PCR cycle number at which the reporter fluorescence is greater than the threshold). qRT-PCR was performed in a total volume of 10 μL reaction mixture comprising 5 μL of 2XSensiMix SYBR No-ROX master mix (Bioline, London, UK), 1 μL of each 250 nM primer, 1 μL of equal concentrated target cell and WGA DNA samples with 2 μL of nuclease-free water. Thermal cycling programs encompassed initial denaturation and activate the hot start DNA polymerase in one cycle of 7 min at 95 °C followed by 40 cycles of 10 s at 95 °C (denaturation), 30 s at 60 °C (annealing) and 20 s at 72 °C (extension).

### 2.6. Asymmetric PCR

Asymmetric PCR of the bisulphite treated DNA was carried out using AmpliTaq Gold 360 master mix (ThermoFisher scientific, Waltham, MA USA) to generate ss-DNA amplicons. Asymmetric PCR was performed by suing 60 μL reaction mixture comprising 30 μL of AmpliTaq Gold 360 master mix, 1 μL of 125 nM forward primer and 375 nm reverse primer (see Table S1), 1 μL of 50 ng bisulphite treated DNA and 28 μL of nuclease-free water. PCR cycling program was performed under the following conditions: 95 °C for 10 min followed by 49 cycles of 30 s at 95 °C (denaturation), 30 s at 61 °C (annealing) and 20 s at 72 °C (extension).

### 2.7. Methylation specific-high resolution melting (MS-HRM) curve analysis

MS-HRM was performed according to the modified versions of the previously published procedure (Wojdacz and Dobrovic, 2007). Briefly, HRM curve analysis was carried out on the Rotor-Gene Q detection system (Qiagen) using the Rotor-Gene ScreenClust Software. PCR was performed in a 10 μL total volume containing 5 μL of 2Xsensimix HRM master mix, 1 μL of 20 ng/μL bisulfite modified genomic DNA, 2 μL RNase free water and 1 μL of each primer. The thermal profile comprised 15 min at 95 °C, followed by 50 cycles of 30 s at 95 °C, 30 s at 61 °C and 20 s at 72 °C. High resolution melting analyses were carried out at temperature ramping from 70 to 95 °C. The normalization of melting curve were performed following the previous procedure (Wojdacz and Dobrovic, 2007).

### 2.8. Electrochemical measurements of DNA methylation

All electrochemical measurements were performed on a CH1040C potentiostat (CH Instruments, Bee Cave, TX, USA) with the three-electrode system printed on a ceramic substrate (length 33 × width 10 × height 0.5) mm. In the three-electrode system, working (diameter =4 mm), counter and reference electrodes were graphene/carbon, carbon, and silver-modified electrodes. Differential pulse voltammetry experiments were conducted in 10 mM phosphate buffered saline (PBS) solution containing 2.5 mM $[K_3Fe(CN)_6]$ and 2.5 mM $[K_4Fe(CN)_6]$ electrolyte solution. DPV signals were obtained with a potential step of 5 mV, pulse amplitude of 50 mV, pulse width of 50 ms, and pulse period of 100 ms. For synthetic DNA samples, 8 μL (diluted in SSC5X buffer to get 100 nM of DNA) sample was adsorbed on g-SPCE surface. For cell lines and clinical samples analysis, 10 times-diluted amplified products (*i.e.*, 20 μL of amplified DNA spiked in 200 μL of SSC5X buffer) were used for adsorption experiments. The electrodes were then washed three times with PBS prior to perform DPV measurements. The relative DPV current changes (*i.e.*, $\%I_{Relative}$, percent difference of the DPV signals generated for DNA sample ($I_{Sample}$) with respect to the baseline current ($I_{Baseline}$)) due to the adsorption of DNA samples were then measured by using Eq. 1. The difference in relative DPV signals between unmethylated and methylated DNA was calculated by using Eq. (2).

$$\%I_{Relative} = \frac{I_{Baseline} - I_{Sample}}{I_{Baseline}} \times 100 \quad (1)$$

$$\Delta I_{\mathrm{Relative}} = \%I_{Relative,M} - \%I_{Relative,\ \mathrm{UM}} \quad (2)$$

where $\%I_{Relative,\ \mathrm{M}}$ and $\%I_{Relative,\ \mathrm{UM}}$ are the relative DPV signals for the methylated, and unmethylated samples, respectively.

### 2.9. Fourier Transform Infrared Spectroscopy and UV–Vis Experiments

Fourier Transform Infrared Spectroscopy (FTIR) spectra were collected on a Perkin-Elmer Spectrum 100 with a resolution of 4 $cm^{-1}$ in absorption mode. A baseline correction was applied after the measurement. The measurements were performed for a bare graphene-modified and DNA/graphene-modified working electrode. UV–vis absorption spectra were measured on Agilent 8453 UV–Vis spectrometer. The UV–vis measurements were done in aqueous solution.

## 3. Results and discussion

### 3.1. Principle

Fig. 1 illustrates the principle of the method. Briefly, ds-DNAs were first extracted from the cancer cell lines. A bisulfite conversion step was then performed to convert unmethylated cytosines in ds-DNA (double stranded DNA) into uracils while methylated cytosines remain unchanged. In a subsequent asymmetric PCR amplification step, all ds-DNA were converted to ss-DNA (single stranded DNA) amplicons. In this step, cytosines in the complementary strand will be copied to guanines and uracils to adenines resulting in methylated sample into guanine-enriched and unmethylated into adenine-enriched ss-DNA. These samples were then directly adsorbed on the g-SPCE surface. The DNA-attached g-SPCE surfaces were characterised by FTIR analysis. The interaction between graphene and DNA sequences has also been tested in solution phase *via* UV–Vis spectrometry (for details see text and Fig. S1 in Supplementary Material). The adsorbed ss-DNA amplicons were detected by differential pulse voltammetry (DPV) in the presence of a small redox active $[Fe(CN)_6]^{3-/4-}$ group. Previously, we (Koo et al., 2014a; Sina et al., 2014a, 2014b) and Zhang et al. (2007) have shown that unlike conventional redox system (*e.g.*, $[Ru(NH_3)_6]^{3+}$/$[Fe(CN)_6]^{3-}$) (Das et al., 2012), the $[Fe(CN)_6]^{3-/4-}$ alone is sufficient for quantifying surface-bound sequences reliably. As outlined by Zhang et al. (2007), the process follows an electron transfer kinetics-based mechanism, where density of the adsorbed DNA sequences at the electrode surface should be sufficiently low (*i.e.*, partial blocking). Under this condition, the columbic repulsion between the surface-bound ss-DNA and $[Fe(CN)_6]^{3-}$ is not strong enough to fully repel $[Fe(CN)_6]^{3-}$molecules from accessing the surface. Therefore, it generates a significant DPV signal which is lower than that of the un-modified electrode (*i.e.*, before ss-DNA adsorption) (Koo et al., 2014a; Sina et al., 2014a, 2014b). In the current method, since the adsorption strength of DNA bases towards graphene vary as G > A > T > C, the guanine-enriched methylated DNA leads to a

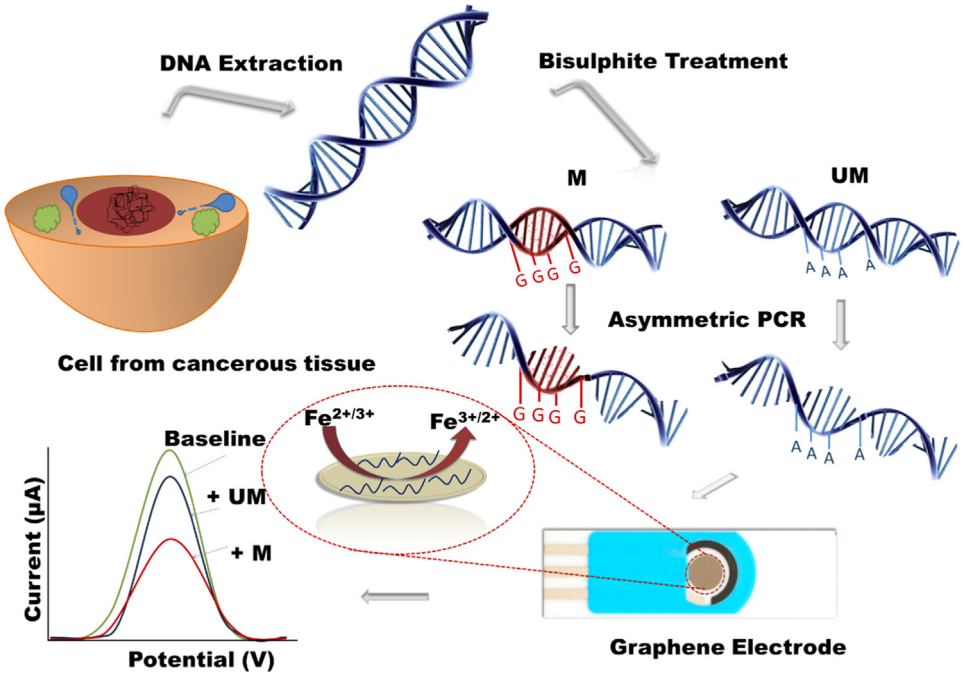


**Fig. 1.** Schematic of graphene-DNA adsorption based methylation assay. The adsorption of ss-DNA on g-SPCE repulse $[Fe(CN)_6]^{3-}$ molecules from accessing electrode surface, providing a significate DPV signal. Inset, typical differential pulse voltammetric signals showing the guanine-enriched methylated DNA that produces lower DPV currents in comparison to the adenine-enriched unmethylated DNA.

larger level of adsorbed DNA on the electrodes in comparison to the adenine-enriched unmethylated DNA. Hence, as schematically shown in Fig. 1, methylated DNA results in a smaller DPV current (*i.e.*, larger relative current change, $\%I_{Relative}$).

We have first explored the oncogenic properties and altered expression of *FAM134B (JK1)* gene in oesophageal squamous cell carcinoma (Tang et al., 2007). Also, *FAM134B* has been reported to have roles in pathogenesis as well as prediction of prognosis of other gastrointestinal cancer, namely colorectal cancer (Kasem et al., 2014). Most current approaches detect DNA methylation in oesophageal cancers via methylation specific PCR amplification process (Kuroki et al., 2003; Long et al., 2007). In this proof-of-concept study, we have used graphene-DNA affinity interaction for detecting gene-specific DNA methylation in *FAM134B*. Firstly, the *FAM134B* promoter region containing 11 CpG sites located within a length of 60 bases was chosen as a target DNA. In order to further validate our approach, we have designed synthetic samples containing 0, 1, 5 and 11 CpG sites within the promoter region of *FAM134B* gene which mimic the bisulfite treated and asymmetric PCR processed methylated and unmethylated DNA regions (See Table S1, Supplementary Material).

One of the key considerations of the current method is that there is only a finite amount of electrode area and we should have the right amount of adsorbed DNA on the electrode surface so that the extent of methylation makes discernible signal difference. Therefore, we first optimised adsorption time and pH of the solution to achieve optimal amount of adsorbed DNA on the electrode surface so that the affinities of the DNA with different amounts of methylation can be discerned. Relative current differences ($\Delta I_{Relative,}$ see Experimental) between the 100 nM methylated (11 CpG) and unmethylated (0 CpG) DNA samples were measured. As seen in Fig. S2, an adsorption time of only 1 min is sufficient to generate a significant $\Delta I_{Relative}$ value. The maximum $\Delta I_{Relative}$ was found at 2 min, which was rapidly decreased with increasing adsorption time. Long adsorption time ($>10$ min) would lead to large amount of adsorbed DNA (*i.e.*, complete block of the surface) on electrode surface. This results in a similar level of columbic repulsion between the surface-bound DNA and $[Fe(CN)_6]^{3-}$ for both the methylated and unmethylated cases, providing two DPV signals with almost identical magnitudes leading to a small $\Delta I_{Relative}$ changes.

We then evaluated the pH-dependent $\Delta I_{Relative}$ changes by varying the pH of the solution from 3.0 to 9.5 (Fig. S3). Clearly, both methylated and unmethylated DNA samples could be distinguished at all the pH examined. The optimal $\Delta I_{Relative}$ value was found at pH 7.4. This can be explained by the fact that negative charge of the phosphate backbone of DNA at this pH is optimal to hinder the graphene-DNA interaction for both methylated and unmethylated samples while still allowing the methylated DNA with higher guanine contents to be interacted strongly. At the lower pH, the N3 position of the cytosines in methylated and unmethylated sequences can be protonated ($pKa=4.2$) (Wu et al., 2011). This may contribute to reduce the Van-der Wall interaction (*i.e.*, electrostatic repulsion) between targets sequences and graphene surface, and thus result in a lower adsorption, leading to higher DPV currents (*i.e.*, lower $\Delta I_{Relative}$ changes). At the higher pH, the electrostatic interaction (adsorption) between graphene and DNA sequences is very strong, which significantly contribute to facilitate their adsorption on graphene-modified surfaces (*i.e.*, both targets reach to the saturation level within a very short time giving a reduced $\Delta I_{Relative}$ value).

The main advantage of gold standard sequencing-bisulphite based method is that they can detect DNA methylation with single-base resolution. To evaluate the feasibility of our assay for detecting a minimum number of CpG methylation, four synthetic DNA samples containing 0, 1, 5 and 11 CpG sites were tested (as outlined above and in Table S1, Supplementary Material). Fig. 2 shows that the decrease of the relative current changes is a function of the number of CpG cites. This is due to the increase of the guanine contents with increasing methylated CpG sites in the target sequence. The level of relative adsorption pattern of methylated CpG sites agreeably implies the high specificity of our assay for effective detection of DNA methylation at a single CpG level of resolution.

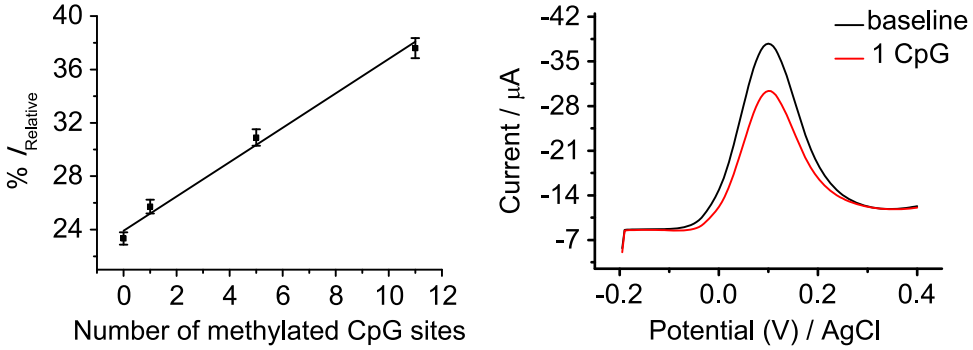


**Fig. 2.** Left, differential pulse voltammetric current changes with respect to the designated CpG sites. Right, typical DPV signal for the sample containing 1 CpG site and its corresponding background signal. Each data point represents the average of three repeat trails, and error bars represent the standard deviation of measurements (% RSD = < 5% for $n=3$).

Since tissue samples from patients with cancer usually contain a mixture of methylated and unmethylated DNA, accurate quantification of heterogeneous DNA methylation pattern is significant for detection and prediction of various clinicopathological parameters in cancers. It is therefore important to detect the degree of methylation in a high background of unmethylated DNA samples. To evaluate the assay performance for detecting heterogeneous DNA methylation pattern, we analysed the dependence of the relative current changes on various degree of methylation. The samples were prepared by mixing synthetic standards of methylated and unmethylated DNA sequences to get 0%, 5%, 25%, 50%, 75%, 95% and 100% methylation, Fig. 3. The relative current changes ($\%I_{Relative}$) increases with increasing levels of methylation, probably due to the increasing guanine contents in the target DNA sequences (*i.e.*, low DPV current and thus the higher $\%I_{Relative}$). The linear regression equation was y ($\%I_{Relative}$) = 2.3193x + 20.77 (C) with a correlation coefficient ($r^2$) of 0.9921. A methylation change as low as 5% could be detected from 100 nM of DNA. These data was much better than our previous gold-DNA based approach (Koo et al., 2014a; Sina et al., 2014a, 2014b) and was of comparable to recent approaches (Carrascosa et al., 2014; Koo et al., 2014b; Wang et al., 2016; Wee, 2015a, 2015b), and clearly demonstrate that our approach is both specific and sensitive in detecting methylated DNA in the nanogram regime.

To test the applicability of our assay for detecting methylation level of *FAM134B* promoter gene, DNA samples derived from three ESSC cell lines were tested, Fig. 4A. A fully unmethylated whole genome amplified DNA was used as an internal standard. For avoiding any PCR bias, as outlined in our previously reported *methylsorb* assay (Koo et al., 2014a; Sina et al., 2014a, 2014b), we normalized the gene copy number prior to PCR amplification (see Experimental for details). As expected, for all the three cancer cell lines and WGA samples, significant relative current changes were observed indicating the presence of different degree of methylation. Importantly, two of the cell-derived samples (*i.e.,* KYSE-510 and HKESC-1) resulted in a large relative current changes when compared to that of the unmethylated WGA (*e.g.*, $\Delta I_{Relative}$ between KYSE-510 cell lines and unmethylated WGA was found to be ~14.6%), indicating DNA sequence derived from KYSE-510 and HKESC-1 cell lines could be hypermethylated at *FAM134B* promoter gene. These data clearly indicate that the proposed assay may be a useful alternative for detecting *FAM134B* promoter gene methylation in cell-derived samples.

To further demonstrate the applicability of our method in analysing clinical samples, we extended our assay to analyse six tissue DNA samples derived from patients with primary

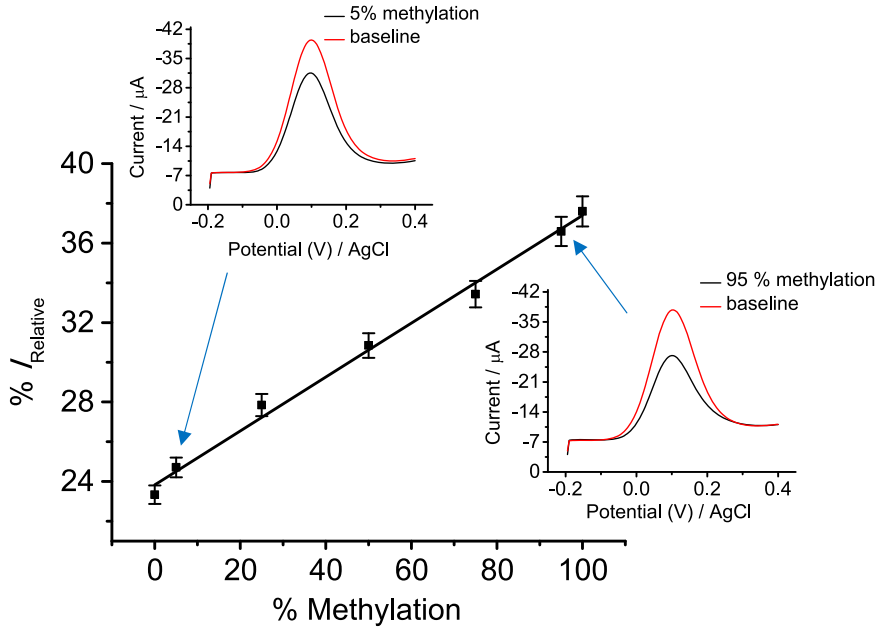


**Fig. 3.** Differential pulse voltammetric current changes with respect to the designated methylation level. Inset, typical DPV signals for the sample containing 5% (left, top) and 95% (right, bottom) and their corresponding background signals. Each data point represents the average of three repeat trails, and error bars represent the standard deviation of measurements (%RSD = < 5% for $n=3$).

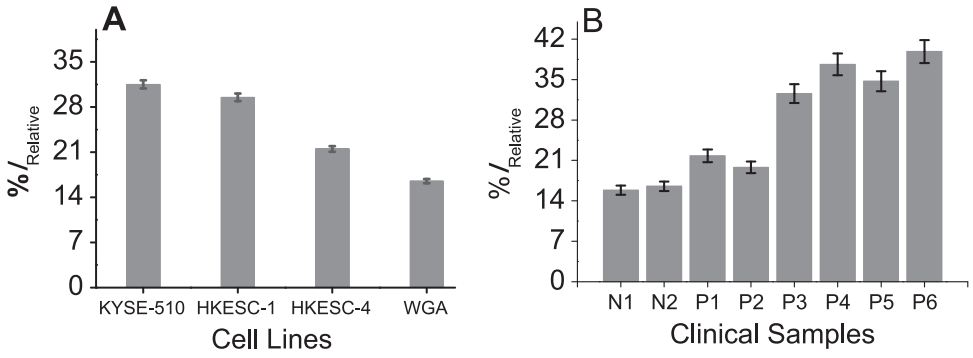


**Fig. 4.** Relative current changes for detecting *FAM134B* promoter region in (**A**) three oesophageal cancer cell lines and unmethylated, and (**B**) two normal (N1 and N2) and six (P1–P6) oesophageal cancer tissue samples. Each data point represents the average of three repeat trails, and error bars represent the standard deviation of measurements (% RSD = < 5% for $n=3$).

oesophageal squamous cell carcinoma. Two oesophageal non-cancerous tissue DNA samples were also used as a control (see Experimental for details). Fig. 4B indicates that all samples showed different degree of methylation. The level of relative current changes with respect to that of the WGA obtained for two normal samples clearly show that these two samples are unmethylated. Also by comparing the level of relative current changes found in cell lines (Fig. 4A), we can estimate that four DNA samples derived from P3, P4, P5 and P6 cancer patients were highly methylated, while P1 and P2 samples were partially methylated (*i.e.*, low methylation) at *FAM134B* promoter gene. We then validated our assay performance with well-known MS-HRM curve analysis. As can be seen in Fig. S5, WGA and N1 samples have almost similar methylation level. Also the P6 sample has relatively higher methylation level compare to that of the P2 sample. These data are in-line with our adsorption based data.

Previously, it has been reported that gene silencing due to promoter hypermethylation play a fundamental role in pathogenesis of oesophageal squamous cell carcinoma (Wong et al., 2006). To evaluate whether the promoter hypermethylation of the *FAM134B* gene is linked with oesophageal cancer development, the *FAM134B* mRNA expression in all studied samples were examined *via* qRT-PCR (see Fig. S4 and experimental details in Supplementary Material). While our assay have showed higher level of methylation (*i.e.*, aberrant promoter hypermethylation) of the *FAM134B* gene in four primary cancer patients (P3, P4, P5 and P6 in Fig. 4B), the mRNA expression study revealed under-expression in three of these DNA samples (P4, P5 and P6, Fig. S4 in Supplementary Material). Furthermore, mRNA over-expression was found in three patient samples (P1, P2, P3), indicating that the associated CpG region could be unmethylated or partially methylated. In our assay, we have noted that the levels of methylation for P1 and P2 samples are slightly higher than those of WGA (see Fig. 4A) and normal samples (N1 and N2 in Fig. 4B), indicating that these two samples (P1 and P2) could be partially methylated, and is in good agreement with RNA-expression data. In contrast, P3 sample showed significantly higher methylation levels than normal and WGA samples. This outcome suggests that this region could be hypermethylated, in disagreement with our mRNA expression data. The electrochemical data presented here clearly suggests that there is a relationship between promoter methylation level and mRNA expression of *FAM134B* gene in oesophageal squamous cell carcinoma, and support the accuracy of our assay. Although an in-depth study is needed to fully evaluate and validate clinical utility of the method, the analytical performance of the assay in its current form suggests the high feasibility of our assay in clinical sample analysis.

## 4. Conclusion

We have developed a simple and new method for the quantification of gene-associated DNA methylation using affinity interaction between DNA bases and graphene. The method is based on the different adsorption affinity of DNA nucleotides towards graphene-modified electrodes. The detection was achieved by the direct adsorption of two sequentially different DNA samples (bisulphite-treated and PCR amplified sequences representing methylated and unmethylated DNA) onto a graphene-modified electrode, which avoids multiple modifications and functionalisation steps involved in conventional assays. Furthermore, it avoids the need for sequencing analysis. Most importantly, we have tested the feasibility of our assay to detect methylation target of *FAM134B* promoter gene in a panel of ESCC cell lines and clinical samples from ESCC patients. We anticipated that our assay might be able to detect global hypomethylation since the methylated and unmethylated DNA-base changes of bisulphite-treated genomes entails a large number of CpG sites, which might generate a marked adsorption difference between fully methylated and partially methylated samples. In addition, our assay could be viably useful in clinical diagnostics because of its potential for accurate detection of epigenetic biomarker.

## Acknowledgement

This work was supported by the NHMRC CDF (APP1088966 to M.J.A.S.), Griffith University New Researcher Grant Scheme and higher degree research scholarships (GUIPRS and GUPRS scholarships to M.H.H., S.Y. and M.N.I.) from the Griffith University, Australia.

## Appendix A. Supporting information

Supplementary data associated with this article can be found in the online version at http://dx.doi.org/10.1016/j.bios.2016.09.016.

## References

Cao, A., Zhang, C.Y., 2012. Anal. Chem. 84, 6199–6205.
Carrascosa, L.G., Sina, A.A., Palanisamy, R., Sepulveda, B., Otte, M.A., Rauf, S., Shiddiky, M.J.A., Trau, M., 2014. Chem. Commun. 50, 3585–3588.
Chang, H.W., Chow, V., Lam, K.Y., Wei, W.I., Yuen, A., 2002. Cancer 94, 386–392.
Das, J., Cederquist, K.B., Zaragoza, A.A., Lee, P.E., Sargent, E.H., Kelley, S.O., 2012. Nat. Chem. 4, 642–648.
Delpu, Y., Cordelier, P., Cho, W.C., Torrisani, J., 2013. Int. J. Mol. Sci. 14, 15029–15058.
Gowtham, S., Scheicher, R.H., Ahuja, R., Pandey, R., Karna, S.P., 2007. Phys. Rev. B., 76 (article number 033401).

Herman, J.G., Graff, J.R., Myöhänen, S., Nelkin, B.D., Baylin, S.B., 1996. Proc. Natl. Acad. Sci. USA 93, 9821–9826.
Jones, P.A., Takai, D., 2001. Science 293, 1068–1070.
Kasem, K., Gopalan, V., Salajegheh, A., Lu, C.T., Smith, R.A., Lam, A.K.Y., 2014. Exp. Cell Res 326, 166–173.
Kato, D., Goto, K., Fujii, S.-i, Takatsu, A., Hirono, S., Niwa, O., 2011. Anal. Chem. 83, 7595–7599.
Kato, D., Sekioka, N., Ueda, A., Kurita, R., Hirono, S., Suzuki, K., Niwa, O., 2008. J. Am. Chem. Soc. 130, 3716–3717.
Koo, K.M., Sina, A.A., Carrascosa, L.G., Shiddiky, M.J.A., Trau, M., 2014a. Analyst 139, 6178–6184.
Koo, K.M., Wee, E.J., Rauf, S., Shiddiky, M.J.A., Trau, M., 2014b. Biosens. Bioelectron. 56, 278–285.
Kurita, R., Arai, K., Nakamoto, K., Kato, D., Niwa, O., 2012. Anal. Chem. 84, 1799–1803.
Kuroki, T., Trapasso, F., Yendamuri, S., Matsuyama, A., Alder, H., Mori, M., Croce, C. M., 2003. Clin. Cancer Res. 9, 1441–1445.
Long, C., Yin, B., Lu, Q., Zhou, X., Hu, J., Yang, Y., Yu, F., Yuan, Y., 2007. Cancer Invest 25, 685–690.
Plongthongkum, N., Diep, D.H., Zhang, K., 2014. Nat. Rev. Genet. 15, 647–661.
Sina, A.A., Howell, S., Carrascosa, L.G., Rauf, S., Shiddiky, M.J., Trau, M., 2014a. Chem. Commun. 50, 13153–13156.
Sina, A.A.I., Carrascosa, L.G., Palanisamy, R., Rauf, S., Shiddiky, M.J.A., Trau, M., 2014b. Anal. Chem. 86, 10179–10185.
Taleat, Z., Mathwig, K., Sudhölter, E.J.R., Rassaei, L., 2015. Trac- Trends Anal. Chem. 66, 80–89.
Tang, W.K., Chui, C.H., Fatima, S., Kok, S.H., Pak, K.C., Ou, T.M., Hui, K.S., Wong, M.M., Wong, J., Law, S., Tsao, S.W., Lam, K.Y., Beh, P.S., Srivastava, G., Chan, A.S., Ho, K. P., Tang, J.C., 2007. Int. J. Mol. Med. 19, 915–923.
Varghese, N., Mogera, U., Govindaraj, A., Das, A., Maiti, P.K., Sood, A.K., Rao, C.N.R., 2009. ChemPhysChem 10, 206–210.
Wang, Y., Wee, E.J.H., Trau, M., 2016. Chem. Commun. 52, 3560–3563.
Wee, E.J., Rauf, S., Shiddiky, M.J.A., Dobrovic, A., Trau, M., 2015a. Clin. Chem. 61, 163–171.
Wee, E.J.H., Ha Ngo, T., Trau, M., 2015b. Sci. Rep. 5 (article number 15028).
Wojdacz, T.K., Dobrovic, A., 2007. Nucleic Acids Res. 35, e41.
Wong, M.L., Tao, Q., Fu, L., Wong, K.Y., Qiu, G.H., Law, F.B., Tin, P.C., Cheung, W.L., Lee, P.Y., Tang, J.C., Tsao, G.S., Lam, K.Y., Law, S., Wong, J., Srivastava, G., 2006. Int. J. Oncol. 28, 767–773.
Wong, T.S., Man, M.W., Lam, A.K., Wei, W.I., Kwong, Y.L., Yuen, A.P., 2003. Eur. J. Cancer 39, 1881–1887.
Wu, M., Kempaiah, R., Huang, P.-J.J., Maheshwari, V., Liu, J., 2011. Langmuir 27, 2731–2738.
Wu, S.C., Zhang, Y., 2010. Nat. Rev. Mol. Cell. Biol. 11, 607–620.
Zhang, J., Wang, L., Pan, D., Song, S., Fan, C., 2007. DNA hybridization “turns on” electrocatalysis at gold electrodes. Chem. Commun. 11, 1154–1156.
Zhang, J.J., Zhang, L., Zhou, K., Ye, X., Liu, C., Zhang, L., Kang, J., Cai, C., 2011. Anal. Biochem 413, 164–170.
Zhang, L., Xu, Y.-Z., Xiao, X.-F., Chen, J., Zhou, X.-Q., Zhu, W.-Y., Dai, Z., Zou, X.-Y., 2015. Trac-Trends Anal. Chem. 72, 114–122.

Supplementary material

*for*

**Detection of Regional DNA Methylation Using DNA-Graphene Affinity Interactions**

Md. Hakimul Haque,[a] Vinod Gopalan,[a]* Sharda Yadav,[b,c] Md Nazmul Islam,[b,c] Ehsan Eftekhari,[c,d] Qin Li,[c,d] Laura G. Carrascosa,[e] Nam-Trung Nguyen,[c] Alfred K. Lam,[a]* Muhammad J. A. Shiddiky [b,c]*

## Fourier Transform Infrared Spectroscopy and UV-Vis Experiments

Figure S1(a) shows the FTIR spectrum of DNA absorbed on graphene electrode, along with the bare graphene electrode and DNA for comparison. In all samples, a broad absorption peak ranging from 3600 to 3000 $cm^{-1}$ was observed which corresponds to the stretching of O–H bonds. After DNA adsorption, we observed a FT-IR spectra band changes generated from interaction of DNA and graphene surface. It should be highlighted that there is a distinctive, broad peak between 1200 $cm^{-1}$ and 1500 $cm^{-1}$ were characteristic signatures of C-N and C-H bonds in nucleic acids (Dovbeshko et al. 2002). DNA adsorption on graphene electrode surface resulted in absorbance change at band positions of 2850, 1670, 1050 $cm^{-1}$ characteristic of C-H, C=O and C-O bonds. The above result suggests that the DNA is well-bound to the surface of graphene electrode. This correlates with the observed UV–visible results (Fig. S1(b)). The UV-vis spectrum of graphene exhibits two characteristic adsorption peaks, at 250 nm and 300 nm corresponding to C–C and C=O bonds, respectively. The characteristic adsorption peak of DNA observed at ~256 nm is in agreement with other report (Tiwari et al. 2013). In the case of DNA absorbed on graphene surface, the absorption spectrum appears to be dominated by the DNA's characteristics, while the broadening of the 260 nm peak and the small shoulder at 300 nm reveals the presence if graphene. Overall, the

spectral analysis confirms that the DNA strands are well bound to the surface of the graphene electrode.

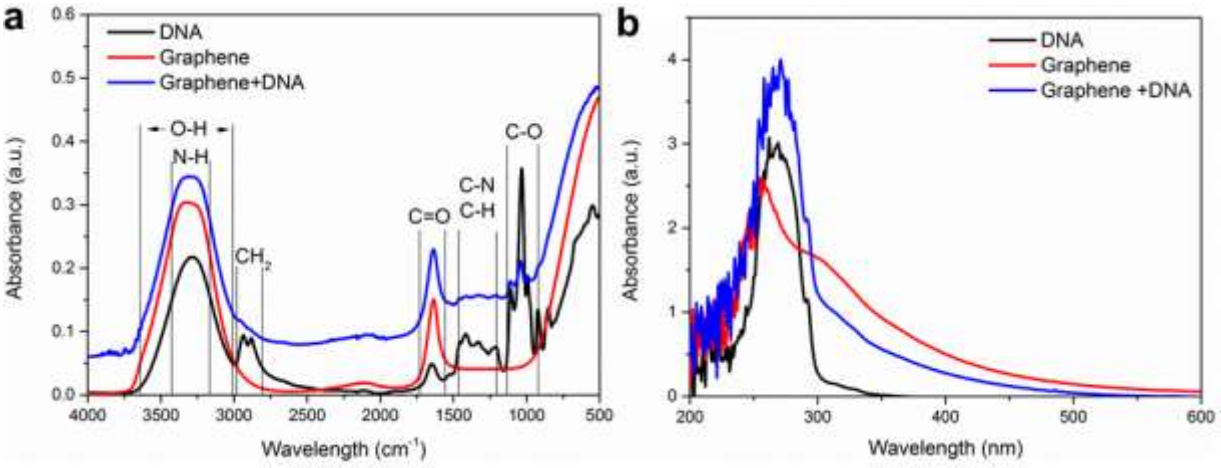


**Fig. S1 (a)** FTIR spectra of DNA, graphene electrode and DNA absorbed on graphene electrode **(b)** UV–vis absorption spectrum of DNA, graphene electrode and DNA absorbed on graphene electrode in aqueous solution.

**Primer design.**

Primer were designed for detecting *FAM134B (JK1)* promotor methylation based on promoter region of GenBank accession number for variant 1 NM_019000 and for a control gene, *Haemoglobin delta (HBD)* (GenBank accession number NM_000519) using primer designing and search tool (http://bisearch.enzim.hu/). All primers were analysed for specificity using oligonucleotide properties calculator (http://biotools.nubic.northwestern.edu/OligoCalc.html) to check for primer parameters like GC content, annealing temperature of primer (Tm) and to forecast any possible mismatching, primer dimmer or hairpin formation. Synthetic DNA methylations were deigned based on mimicking the bisulphite treated and asymmetric PCR processed. The primer pairs were

obtained from Integrated DNA technologies (Coralville, IA, USA). The list of chosen primer sets are summarized in Table S1.

**Table S1.** List of the oligonucleotide sequences used in this study. The eleven potentially methylate CpG sites in the *FAM134B (JK1)* promoter region of interest are highlighted in red colour. The G/A base changes in synthetic DNA representing methylated and unmethylated samples that would be obtained after bisulphite treatment and asymmetric PCR of *FAM134B* gene are highlighted with green and orange colour.

| **Target genes** | **Oligonucleotide Sequences (5'--3′)** |
|---|---|
| *FAM134B* promotor region (Chr5: 16617106) | TCGGCGGCACCCACACCCAGGCGCGCCCGCGCGCGCCCGGCCCCGT |
| *FAM134B*-F | AGAGGTTTTTTAGGAATTTAGAGTTTTT |
| *FAM134B*-R | CCATCTTCAACTATACTTCCAAACAAA |
| *HBD*-F | CAGCATCAGGAGTGGACAGA |
| *HBD*-R | CTCGGCGGCACCCAC |
| Synthetic DNA-1 (11 methylated CpG sites) | AC**G**AAACC**G**AAC**G**C**G**C**G**C**G**AAC**G**C**G**CCTAAATATAAATACC**G**CC**G**A |
| Synthetic DNA-2 (5 methylated CpG sites) | AC**A**AAACC**G**AAC**A**C**G**C**A**C**G**C**A**AAC**G**C**A**CCTAAATATAAATACC**G**CC**A**A |
| Synthetic DNA-3 (1 methylated CpG sites) | AC**G**AAACC**A**AAC**A**C**A**C**A**C**A**C**A**AAC**A**C**A**CCTAAATATAAATACC**A**CC**A**A |
| Synthetic DNA-4 (0 methylated CpG sites) | AC**A**AAACC**A**AAC**A**C**A**C**A**C**A**C**A**AAC**A**C**A**CCTAAATATAAATACC**A**CC |

**Optimization of the adsorption time**

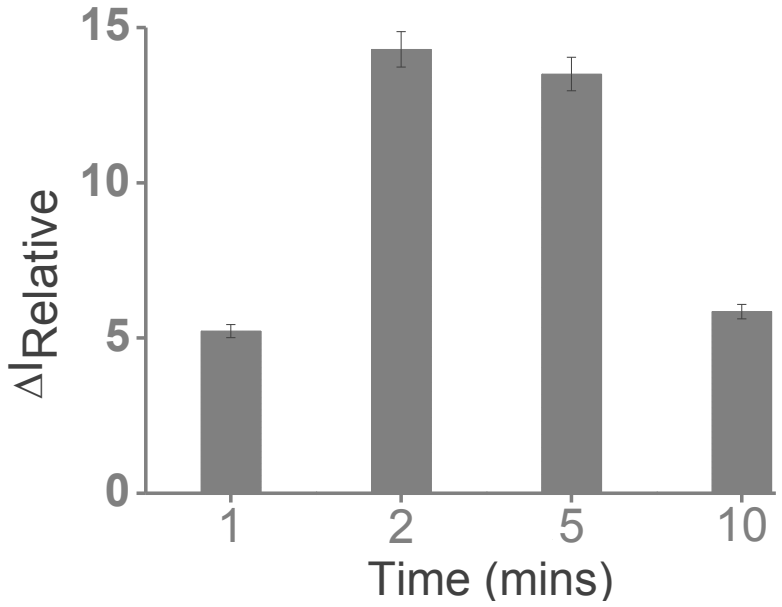


**Fig S2.** Mean values of the relative DPV signals between 100 nM unmethylated (0 CpG) and 100 nM methylated (11 CpG) DNA sequences at designated adsorption time at pH 7.4 Each data point represents the average of three repeat trails, and error bars represent the standard deviation of measurements (%RSD = <5% for $n$ = 3).

**Optimization of the solution pH**

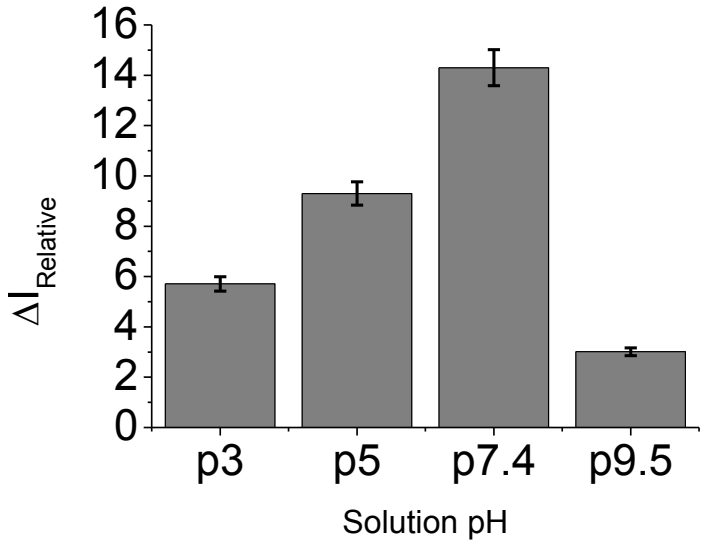


**Fig S3.** Mean values of the relative DPV signals between 100 nM unmethylated (0 CpG) and 100 nM methylated (11 CpG) DNA sequences at designated pH at 2 min of adsorption. Each data point represents the average of three repeat trails, and error bars represent the standard deviation of measurements (%RSD = <5% for $n$ = 3).

**Correlation between promoter hypermethylation and FAM134B gene expression**

To evaluate whether the promoter hypermethylation of the *FAM134B* gene linked with ESCC development, the *FAM134B* mRNA expression of *FAM134B* promotor region in all tested ESCC primary cancers and matched noncancerous tissue were studied *via* qRT-PCR. RNA extraction, cDNA conversion and qRT-PCR studies have been done as described below -

**(i) RNA extraction from tissue samples.** The selected samples were sectioned using a cryostat (Leica CM 1850 UV, Wetzlar, Germany) and stained by haematoxylin and eosin. To confirm the presence of non-cancer and cancerous tissues for RNA extraction, light microscopic examination of the tissues has been performed by the author (AKL). RNA was then extracted using the protocol from all prep DNA/RNA mini kit (Qiagen, Hilden, NRW, Germany). As outlined above for DNA extraction, quantification of extracted RNA was measured via Nanodrop Spectrophotometer (BioLab, Ipswich, MA, USA) and purity was checked by the same instrument using 260/280 ratio. Concentration of RNA is noted in ng/μL and stored at -80$^{O}$C until assayed.

**cDNA conversion.** Reverse transcription reactions were performed using 1 μg total RNA in a final reaction volume of 20 μL. cDNA conversion was achieved using the manufacturer's instructions from miScript Reverse Transcription kit (Qiagen, Hilden, NRW, Germany). In order to inactivation of reverse transcriptase mix, 1 μg of total RNA and master mix were incubated for 60 minutes at 37ºC and then heated up for 5 min at 95ºC. Each cDNA sample was diluted to 30ng/μL for providing uniformly concentrated sample of RNA for qRT-PCR. Samples were stored at -20ºC.

**Primer design.** The primer sets for amplification of FAM134B (JK1) (GenBank accession number for variant 1 NM_001034850 and for variant 2 NM_019000), and GAPDH (GenBank accession number NM_002046) genes were designed using Primer3 version 0.4.0 (http://frodo.wi.mit.edu/primer3/). The primer sets for FAM134B were 5′-TGACCGACCCAGTGAGGA-3 and 5′-GGGCAAACCAAGGCTTAA-3′ with an amplicon of 106 bp and for a reference gene, 5'-TGCACCACCAACTGCTTAGC-3' and 5'-GGCATGGACTGTGGTCATGAG-3' with an amplicon of 88 bp for GAPDH were selected.

**qRT-PCR.** qRT-PCR was performed in a total volume of 10 μL reaction mixture comprising 5 μL of 2XSensiMix SYBR® No-ROX master mix (Bioline, London, UK), 1 μL of each10 picomole/ μL primer, 1 μL of cDNA/ genomic DNA at 20-50 ng/μL and 2 μL of nuclease-free water. Assays were accomplished in duplicate and a non-template control was included in all the experiment. The results of the quantitative real-time polymerase change reaction were analysed using methods published previously (Gopalan et al. 2010)

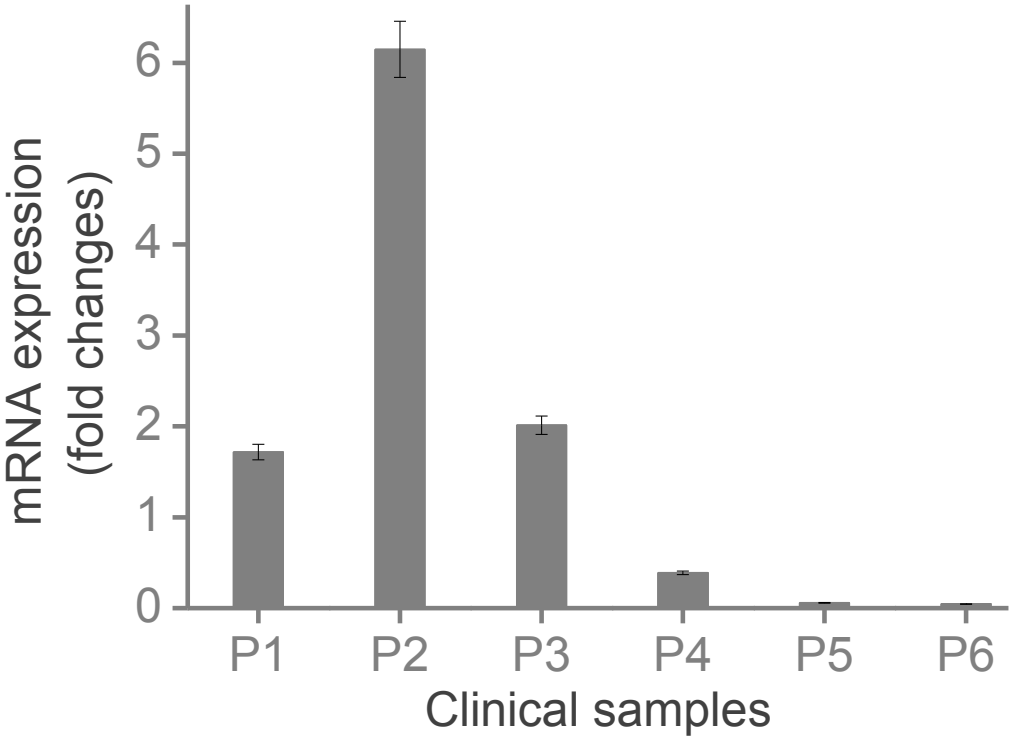


**Fig. S4** Altered mRNA expression level of *FAM134B* gene in different clinical samples of primary oesophageal cancer patients. Each data point represents the average of three repeat trails, and error bars represent the standard deviation of measurements (%RSD = <5% for *n* = 3).

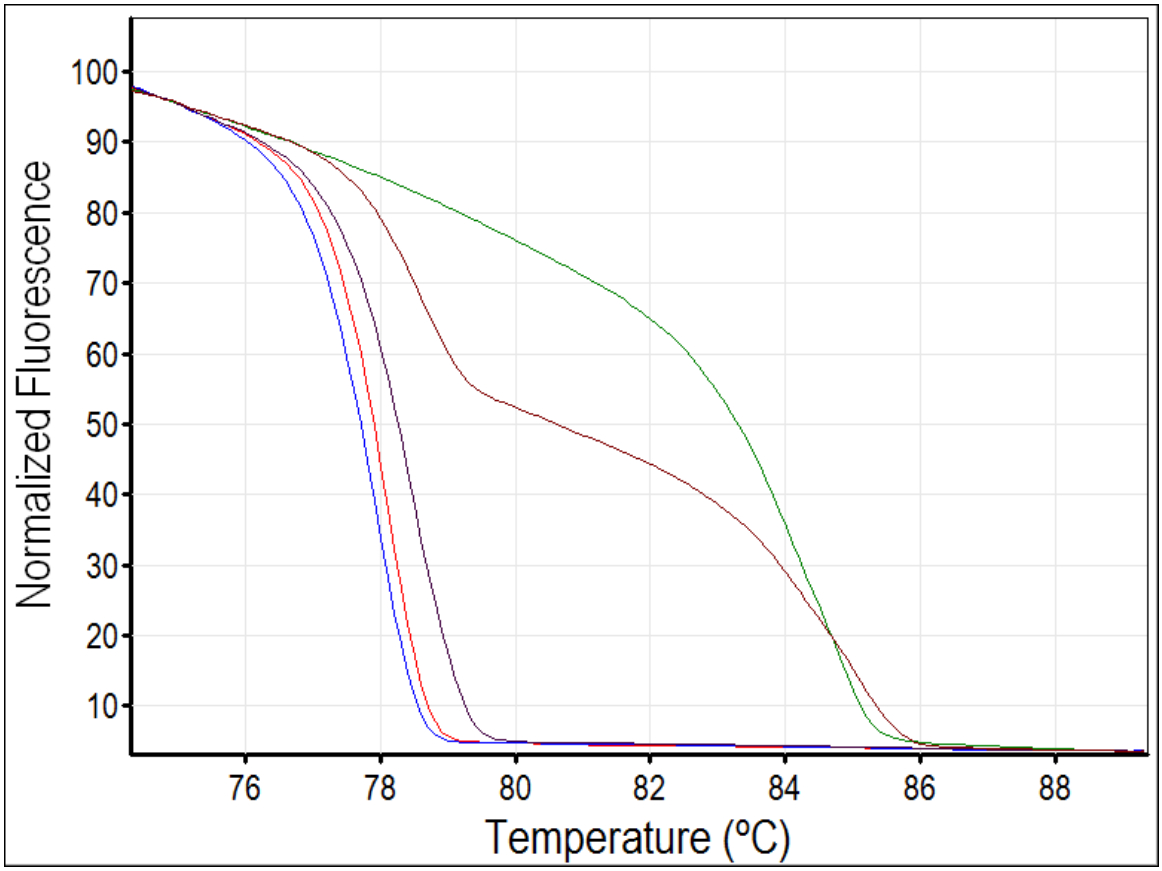


Fig. S5 The MS-HRM analysis of FAM134B gene promoter region in ESCC. MS-HRM curves for 100% methylated Zurkat (green) and fully unmethylated (0% methylation) WGA (blue) along with two patients (P6, maroon); P2, dark maroon) and one normal (N1, Red) samples.

## References

Dovbeshko, GI., Chegel, VI., Gridina, N. Y., Repnytska, O. P., Shirshov, Y. M., Tryndiak V. P., Todor, I. M., Solyanik, G. I, 2002. Biopolymers 67, 470-486.

Gopalan, V., Smith, R.A., Nassiri, M.R., Yasuda, K., Salajegheh, A., Kim, S.Y., Ho, Y.H., Weinstein, S., Tang, J.C., Lam, A.K., 2010. Hum. Pathol. 41, 1009-1015

Tiwari, J. N., Nath, K., Kumar, S., Tiwari, R. N., Kemp, K. C., et al., 2013. *Nat. Commun. 4*, Article number 3221, DOI:10.1038/ncomms3221

# Chapter 7

## Quantification of gene-specific DNA methylation in oesophageal cancer via electrochemistry

Chapter 7 is included as it appears in Analytica Chimica Acta (2017)

# Introduction

A relatively simple, fast and inexpensive electrochemical method is depicted for detecting gene-specific DNA methylation using direct adsorption of bisulfite-treated and PCR amplified DNA sequences onto the unmodified screen-printed gold electrode (SPE-Au). Previously, we demonstrated the use of direct adsorption of bisulfite treated and asymmetric PCR-amplified DNA sequences onto an unmodified gold electrode (without the use of complementary capture probe and hybridization steps) to quantify the level of DNA methylation present in the sequence via measuring the total adsorbed DNA onto the electrode surface. While these assays are relatively simple, it follows an electron transfer kinetic-based mechanism, where the density of the DNA sequences at the electrode surface should be sufficiently low. Additionally, the risk of false-positive responses at low concentration of target is well known when using a detection technique based on attenuation of the interfacial electron transfer reaction of a redox process (*i.e.*, "signal-off" approach). In order to avoid this complexity, in the current study, we explored whether simply monitoring the total charge generated by the electrostatically-attached $[Ru(NH_3)_6]^{3+}$ onto the adsorbed DNA could report on the degree of DNA methylation present in target DNA sequence, where generated total redox charge is the function of adsorbed sequences on the electrode surface. To demonstrate the applicability of the method we analysed the various degree of methylation in cancer cell lines (n=3) and fresh tissues samples from patients (n=8) with oesophageal squamous cell carcinoma containing eleven potentially methylated CpG sites located in the *FAM134B* promoter gene. We believe that the simplicity, high accuracy and sensitivity along with the ability to detect heterogeneous CpG methylation level in clinical samples make our method potentially attractive for future diagnostic applications.

Analytica Chimica Acta xxx (2017) 1–10

Contents lists available at ScienceDirect

Analytica Chimica Acta

journal homepage: www.elsevier.com/locate/aca

# Quantification of gene-specific DNA methylation in oesophageal cancer via electrochemistry

Md. Hakimul Haque [a, b], Vinod Gopalan [a, *], Md. Nazmul Islam [b, c], Mostafa Kamal Masud [b, d], Ripon Bhattacharjee [b, c], Md. Shahriar Al Hossain [d], Nam-Trung Nguyen [c], Alfred K. Lam [a, **], Muhammad J.A. Shiddiky [b, c, ***]

[a] Cancer Molecular Pathology Laboratory in Menzies Health Institute Queensland, Griffith University and School of Medicine, Gold Coast, QLD 4222, Australia
[b] School of Natural Sciences, Griffith University, Nathan Campus, Nathan, QLD 4111, Australia
[c] Queensland Micro- and Nanotechnology Centre (QMNC), Griffith University, Nathan Campus, Nathan, QLD 4111, Australia
[d] Institute for Superconducting and Electronic Materials, Australian Institute for Innovative Materials, University of Wollongong, NSW 2519, Australia

## HIGHLIGHTS

- A method for gene-specific DNA methylation in oesophageal cancer is described.
- Affinity interaction between DNA bases and gold is used to distinguish methylated and unmethylated sequences.
- The methylation level is quantified by measuring saturated amount of redox molecules in the surface-attached DNAs.
- The method is sensitive to detect 10% methylation differences.
- The assay is applied to analyze and validate various degree of methylation in cell lines and fresh tissues samples.
- The method is validated with methylation specific-high resolution melting curve analysis and Sanger sequencing methods.

## GRAPHICAL ABSTRACT

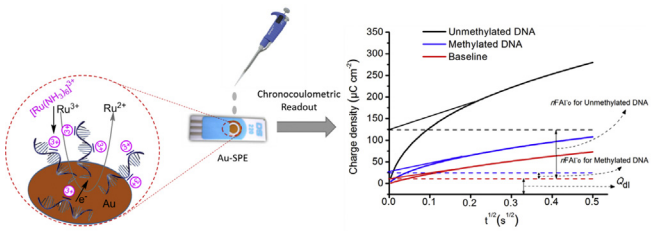


## ARTICLE INFO

*Article history:*
Received 20 January 2017
Received in revised form
10 April 2017
Accepted 10 April 2017
Available online xxx

*Keywords:*
DNA methylation

## ABSTRACT

Development of simple and inexpensive method for the analysis of gene-specific DNA methylation is important for the diagnosis and prognosis of patients with cancer. Herein, we report a relatively simple and inexpensive electrochemical method for the sensitive and selective detection of gene-specific DNA methylation in oesophageal cancer. The underlying principle of the method relies on the affinity interaction between DNA bases and unmodified gold electrode. Since the affinity trend of DNA bases towards the gold surface follows as adenine (A) > cytosine (C) > guanine (G)> thymine (T), a relatively larger amount of bisulfite-treated adenine-enriched unmethylated DNA adsorbs on the screen-printed gold electrodes (SPE-Au) in comparison to the guanine-enriched methylated sample. The methylation levels were (*i.e.*, different level of surface attached DNA molecules due to the base dependent differential

* Corresponding author.
** Corresponding author.
*** Corresponding author. School of Natural Sciences, Griffith University, Nathan Campus, Nathan, QLD 4111, Australia.
*E-mail addresses:* v.gopalan@griffith.edu.au (V. Gopalan), a.lam@griffith.edu.au (A.K. Lam), m.shiddiky@griffith.edu.au (M.J.A. Shiddiky).

http://dx.doi.org/10.1016/j.aca.2017.04.034

Gene-specific methylation
Electrochemical detection
Chronocoulometry
Oesophageal squamous cell carcinoma

adsorption pattern) quantified by measuring saturated amount of charge-compensating $[Ru(NH_3)_6]^{3+}$ molecules in the surface-attached DNAs by chronocoulometry as redox charge of the $[Ru(NH_3)_6]^{3+}$ molecules quantitatively reflects the amount of the adsorbed DNA confined at the electrode surface. The assay could successfully distinguish methylated and unmethylated DNA sequences at single CpG resolution and as low as 10% differences in DNA methylation. In addition, the assay showed fairly good reproducibility (% RSD= <5%) with better sensitivity and specificity by analysing various levels of methylation in two cell lines and eight fresh tissues samples from patients with oesophageal squamous cell carcinoma. Finally, the method was validated with methylation specific-high resolution melting curve analysis and Sanger sequencing methods.



## 1. Introduction

DNA methylation is one of the clinically relevant epigenetic biomarkers that regulates gene expression *via* controlling transcriptional alteration, genomic stability, X chromosome inactivation, genomic imprinting and mammalian cell development [1]. Recent studies on epigenetic research demonstrate that aberrant DNA methylation plays a critical role in the pathophysiology of human cancers including oesophageal squamous cell carcinoma (ESCC) [2,3]. For example, gene-specific promoter hypermethylation is an important driver in the development and progression of many human cancers *via* transcriptional inactivation and suppressing of gene function [4–8]. More recently, it has also been demonstrated that DNA methylation can be used as tumour-specific therapeutic targets in ESCC [2]. Therefore, sensitive and specific profiling of gene-specific DNA methylation in ESCC could have potential implication for prediction of prognosis as well as therapy response monitoring in clinical settings.

Until recently, gene-specific DNA methylation in ESCC is generally detected *via* methylation specific PCR approaches along with bisulfite sequencing [9,10]. Over the past several decades, a variety of molecular biological approaches including methylation-sensitive single nucleotide-primer extension, methylight, methylation-sensitive high resolution melting, enzyme-linked immunosorbent assay (ELISA) based methylation assays, mass spectroscopy and fluorescence readout based methods have been conspicuously exploited to quantify the level of the DNA methylation in many human cancers [11–16]. However, most of these approaches are relatively simpler and robust but typically require large sample volumes, sophisticated instruments, multi-step procedures, hazardous radiolabeling, complex fabrication, expensive antibodies, etc. Furthermore, these assays are affected by multiple external controls for quantitative analysis, background fluorescence interference, high labour and bioinformatics costs which limit their use in routine clinical applications.

In recent years, much attention has been focused on the development of sensitive, specific, relatively simple and inexpensive method for the analysis of DNA methylation using electrochemistry, colorimetry, surface plasmon resonance and Raman scattering readouts [17–22]. While most of these readout methods have their own merits and demerits, electrochemical readout offers additional advantages in clinical diagnostics applications due to their relatively higher sensitivity and specificity, cost-effectiveness and compatibility with the miniaturization [23–25]. In these assays, sensor requires a surface-attached capture probe to hybridize the complementary target sequence, and to form duplex DNA that intercalatively bind with a redox-active transition-metal cations (e.g., $[Ru(NH_3)_6]^{3+}$) for the generation of electrochemical signals [26–29]. As described in many conventional electrochemical assays [30–33], the saturated amount of charge-compensation $[Ru(NH_3)_6]^{3+}$ complex (RuHex) on the electrode surface is electrochemically determined, which is directly proportional to the number of negatively charged phosphate residues and thereby the surface density of the target DNA.

Previously, we demonstrated the use of direct adsorption of bisulfite treated and asymmetric PCR-amplified DNA sequences onto an unmodified gold electrode (without the use of complementary capture probe and hybridization step) to quantify the level of DNA methylation present in the sequence *via* measuring the total adsorbed DNA on to the electrode surface [34,35]. Since the adsorption (*i.e.*, physisorption) trend of the DNA bases to gold surfaces follows as adenine (A) > cytosine (C) > guanine (G)> thymine (T) [36,37], two DNA sequences with different methylation patterns (*i.e.*, bisulfite treated adenine-enriched unmethylated and guanine-enriched methylated DNA sequences) should have different adsorption affinity towards gold surface. Indeed, a relatively large amount of unmethylated DNA was adsorbed on the gold electrode in comparison to the methylated DNA. In this system, we showed that monitoring the Faradaic current generated by the $[Fe(CN)_6]^{3-/4-}$ system alone could be used for the interrogation of DNA methylation level present in the bisulfite treated samples [34,35]. While this assay is relatively simple, it follows an electron transfer kinetic-based mechanism, where density of the DNA sequences at the electrode surface should be sufficiently low [31]. Additionally, the risk of false-positive responses at low concentration of target is well known when using a detection technique based on attenuation of the interfacial electron transfer reaction of a redox process (i.e., “signal-off” approach).

In order to avoid this complexity, in the current study, we explored whether simply monitoring the total charge generated by the electrostatically-attached RuHex onto the adsorbed DNA could report on the level of DNA methylation present in the samples, where generated total redox charge is the function of adsorbed DNA sequences on the electrode surface [26–29]. Since in this “signal-on” approach, the charge of the RuHex complex qualitatively reflects the amount of the adsorbed DNA at the electrode surface [30], the electrochemical signal generated by the chronocoulometric (CC) interrogation of DNA-bound RuHex will give the level of methylation present in the amplified samples. It is also important to note that unlike RuHex based conventional methods [30], the current method detects DNA methylation by simply monitoring the adsorbed target DNA on an unmodified SPE-Au electrode. Since we use direct adsorption of target DNA on an unmodified electrode rather than the conventional biosensing approach of using recognition and transduction layers, this method substantially simplifies the detection system by avoiding the complicated chemistries underlying each step of the sensor fabrication.

In this method, we first optimized the adsorption parameters (*i.e.*, adsorption time, pH of the solution, and concentration of DNA) for the direct adsorption of target DNA onto the unmodified SPE-Au surface. Then, we detected the level of promoter methylation present in *FAM134B* gene in a panel of ESCC cell lines and tissue



Please cite this article in press as: Md.Hakimul-g.H. Haque, et al., Quantification of gene-specific DNA methylation in oesophageal cancer via electrochemistry, Analytica Chimica Acta (2017), http://dx.doi.org/10.1016/j.aca.2017.04.034

samples derived from patients with ESSC. We also validated the results with methylation specific-high resolution melting (MS-HRM) curve analysis and Sanger sequencing.

## 2. Experimental

### 2.1. Genomic DNA preparation

All reagents and chemicals were analytical grade and purchased from Sigma Aldrich (St Louis, MO, USA) unless otherwise noted. UltraPure DNase/RNase-free distilled water was obtained from Invitrogen (Carlsbad, CA, USA). Whole genome amplification DNA was prepared according to the manufacture's protocol from REPLI-g whole genome amplification kit (Qiagen, Hilden, Germany). Two ESCC cell lines (HKESC-1 and HKESC-4) were kindly provided from our collaborative research group [38,39]. Another ESCC cell line, KYSE-510 was purchased from Leibniz Institute DSMZ (German collection of microorganisms and cell cultures). 100% methylated Jurkat genomic DNA was obtained from New England Biolabs (Ipswich, MA, USA). Eight fresh frozen tissue samples from patients with ESCC and two non-neoplastic oesophageal tissues (as controls) were recruited for this study. Ethical approval was taken from the Griffith University human research ethics committee for the use of these samples (GU Ref Nos: MED/19/08/HREC and MSC/17/10/HREC). After histopathological confirmation, genomic DNA was purified from all ESCC tissue samples with all prep DNA/RNA mini kit (Qiagen, Hilden, Germany), according to the manufacturer's protocols. Blood and cell culture DNA mini kit (Qiagen, Hilden, Germany) was used for the purification of DNA from ESCC cell lines. All patients had not received pre-operative were free from radio/chemotherapy, matched with gender (all male) and clinical staging (stage III & IV). Mean age group of the patients was 65 ± 14 ranging from 45 to 74 years. Screen-printed gold electrodes were acquired from Dropsens (Spain).

### 2.2. Bisulfite modification

Bisulfite conversion and purification of the genomic DNA was performed with MethylEasy Xceed kit (Human Genetic Signatures Pty. Ltd., NSW, Australia) as recommended by the manufacturer. DNA quantification and purity was checked *via* Nanodrop Spectrophotometer (BioLab, Ipswich, MA, USA). Concentration of bisulfite treated DNA was noted in ng/μL and then stored at −20 °C until use. Approximately 500 ng genomic DNA from each samples was the starting amount for the bisulfite treatment.

### 2.3. DNA quantification

The DNA copy number normalization of *FAM134B (JK1)* genes in bisulfite treated cell and WGA DNA samples were analyzed by the Rotor-Gene Q PCR detection system (Qiagen, Hilden, Germany). qRT-PCR was performed in a total volume of 10 μL reaction mixture containing 5 μL of 2XSensiMix SYBR No-ROX master mix (Bioline, London, UK), 1 μL of each 250 nM primer, and 1 μL of equal concentrated target cell and WGA DNA samples with 2 μL of nuclease-free water. Thermal cycling programs encompassed initial denaturation and activate the hot start DNA polymerase in one cycle of 7 min at 95 °C followed by 40 cycles of 10 s at 95 °C (denaturation), 30 s at 60 °C (annealing) and 20 s at 72 °C (extension).

### 2.4. Asymmetric PCR

Asymmetric PCR of the bisulfite treated DNA was carried out using AmpliTaq Gold 360 master mix (ThermFisher scientific, Waltham, MA USA) to generate ss-DNA amplicons. Asymmetric PCR was performed by using 60 μL reaction mixtures comprising 30 μL of AmpliTaq Gold 360 master mix, 1 μL of 125 nM forward primer and 375 nm reverse primer, 1 μL of 30 ng bisulfite treated DNA and 28 μL of nuclease-free water. PCR cycling programs was performed under the following conditions: 95 °C for 10 min followed by 49 cycles of 30 s at 95 °C (denaturation), 30 s at 61 °C (annealing) and 20 s at 72 °C (extension).

### 2.5. Determination of the surface area of the electrodes

Screen-printed electrode with the three-electrode system printed on a ceramic substrate (length 33 × width 10 × height 0.5 mm) was purchased from Dropsens (Spain). In the three-electrode system, working (SPE-Au, diameter = 4 mm), counter and reference electrodes were gold, platinum, and silver-modified electrodes, respectively. The effective working area of the electrodes were determined under cyclic voltammetric conditions for the one-electron reduction of $K_3[Fe(CN)_6]$ [2.0 mM in water (0.5 M KCl)] and use of the Randles-Sevcik eqn (1),

$$i_p = \left(269 \times 10^5\right) n^{3/2} A D^{1/2} C \nu^{1/2} \quad (1)$$

where $i_p$ is the peak current (A), $n$ is the number of electrons transferred ($Fe^{3+} \rightarrow Fe^{2+}$, $n = 1$), $A$ is the effective area of the electrode ($cm^2$), $D$ is the diffusion coefficient of $[Fe(CN)_6]^{3-}$ (taken to be $7.60 \times 10^{-5} cm^2 s^{-1}$), $C$ is the concentration (mol $cm^{-3}$), $\nu$ is the scan rate ($Vs^{-1}$).

### 2.6. Electrochemical measurements of DNA methylation

All electrochemical measurements were performed on a CH1040C potentiostat (CH Instruments, TX, USA). Cyclic voltammetric (CV) experiments were performed in 10 mM PBS solution containing 2 mM $[K_3Fe(CN)_6]$ electrolyte solution. Chronocoulometric readouts were obtained in 10 mM tris buffer (pH 7.4) in the presence and absence of 50 μM RuHex with a potential step of 5 mV and pulse width of 250 ms, and sample interval of 2 ms. For synthetic DNA samples, 5 μL (diluted in SSC5X buffer to get 100 nM of DNA) sample was adsorbed on SPE-Au surface. For clinical samples analysis, 5 μL (diluted in SSC5X buffer to get 50 ng of DNA) were used for adsorption experiments. The electrodes were then washed three times with PBS prior to perform CC readouts. The total charge ($Q$/C) flowing through the DNA-attached electrode comprising both Faradaic (redox) and non-Faradaic (capacitive) charges at a time $t$ can be expressed by the integrated Cottrell equation [30],

$$Q = \frac{2nFA_0^{1/2} C_0^* t^{1/2}}{\pi^{1/2}} + Q_{dl} + nFA\Gamma_0 \quad (2)$$

where $n$ is number of electrons involved in electrode reaction, $F$ is Faraday constant (C/equivalent), $A$ is the electrode area ($cm^2$), $D_o$ is the diffusion coefficient ($cm^2/s$), $C_o^*$ *is the* bulk concentration (mol/$cm^2$), $Q_{dl}$ the capacitive charge (C), $\Gamma_0$ is designates the surface excess and represents the amount of RuHex confined near the electrode surface. CC curves were constructed by plotting the charge flowing through the DNA-attached electrode versus square-root of time ($t^{1/2}/s^{1/2}$) in the presence and absence RuHex. $Q$ and $Q_{dl}$ were estimated from the intercept of these two curves at $t = 0$. The redox charge corresponding to RuHex electrostatically bound to the surface-attached DNA ($Q_{target}$) was calculated using Eq. (3).

$$Q_{target} = Q - Q_{dl} \quad (3)$$

The redox charge difference ($\Delta Q$) in CC signals between



Please cite this article in press as: Md.Hakimul-g.H. Haque, et al., Quantification of gene-specific DNA methylation in oesophageal cancer via electrochemistry, Analytica Chimica Acta (2017), http://dx.doi.org/10.1016/j.aca.2017.04.034

unmethylated and methylated was estimated using Eq. (4).

$$\text{Charge difference}(\Delta Q) = Q_{total,unmethylated} - Q_{total,methylated} \quad (4)$$

where $Q_{total,methylated}$ and $Q_{total,unmethylated}$ are the CC signals estimated for the methylated and unmethylated samples respectively.

### 2.7. Methylation specific-high resolution melting (MS-HRM) curve analysis

MS-HRM was carried out based on the modified versions of the previously published procedure [13]. Briefly, HRM curve analysis was demonstrated on the Rotor-Gene Q detection system (Qiagen) using the Rotor-Gene ScreenClust Software. PCR was performed in a 10 μL total volume containing 5 μL of 2Xsensimix HRM master mix, 1 μL of 20 ng/μL bisulfite modified genomic DNA, 2 μL RNase free water and 1 μL of each primer. The thermal profile comprised 15 min at 95 °C, followed by 50 cycles of 30 s at 95 °C, 30 s at 61 °C and 20 s at 72 °C. HRM analyses were carried out at temperature ramping from 70 to 95 °C. The normalization of melting curve was performed as previously reported [40].

### 2.8. Sanger sequencing

To further confirm the methylation status of FAM134B promoter region, we employed Sanger sequencing analysis. The purified DNA was mixed with the primer (12 ng of DNA + 1 μL of 10 pmol primer in 12 μL of $H_2O$) sequence using the Big Dye Terminator (BDT) chemistry Version 3.1 (Applied Biosystems). Sanger sequencing was performed and analyzed using a 3730xl Capillary sequencer (Applied Biosystems) under standardised cycling PCR conditions in the Australian Genome Research Facility (AGRF, Brisbane).

### 2.9. Statistical analysis

Statistical analyses were performed *via* pairwise comparisons between two conditions using student's t-test. Significance level of the tests was taken at $p < 0.05$.

## 3. Results and discussion

### 3.1. Principle of the quantification of gene-specific DNA methylation assay

We first extracted double stranded (ds)-DNA from the cancer cell lines and clinical tissue samples from ESCC patients to demonstrate the working principle of the method. We performed a bisulfite conversion step for converting unmethylated cytosines in ds-DNA into uracils while methylated cytosines remain unchanged. Then, an asymmetric PCR amplification step was performed to convert all ds-DNA into ss-DNA amplicon. In this step, cytosines in the complementary strand would be copied into guanines and uracils into adenines resulting guanine-enriched methylated and adenine-enriched unmethylated samples. The samples were then directly adsorbed on a SPE-Au electrode surface. The adsorbed ss-DNA samples were detected by CC interrogation in presence of an electroactive complex RuHex. Here, RuHex cations act as the signaling molecule that binds to the anionic phosphate of DNA strands in a stoichiometric manner [41]. Previous studies have clearly showed that redox charge of RuHex quantitatively indicates the amount of DNA strands localized at the electrode surface [13,41,42]. In the present method, since the adsorption strength of DNA bases towards gold surface follows as A > C > G > T, adenine-enriched unmethylated DNA leads to a higher level of adsorbed DNA on the gold electrode surface in comparison to guanine-enriched methylated DNA, resulting in a significant difference in CC signals for unmethylated and methylated targets. This base-dependent adsorption process can be explained by the conventional physisorption mechanism, where DNA bases adopt a flat conformation that allow maximum overlapping of electronic densities [36]. The strongest adsorption strength of adenine could be due to the formation of an additional chemical bond between the amino group of adenine and a gold atom [43]. As schematically presented in Fig. 1, methylated DNA results in a relatively low level of CC charges (*i.e.*, a significant charge density/$\mu Ccm^{-2}$) in comparison to that of the unmethylated DNA.

### 3.2. Synthetic sample design

Recent studies suggested that alterations in *FAM134B* gene have a significant impact in gastrointestinal carcinomas and neurological diseases *via* regulating its expression patterns and cellular autophagy [44–47]. It has also been reported that *FAM134B* is mutated in metastatic lymph node tissues and its DNA copy number is significantly alterated in oesophageal squamous cell carcinoma tissues [44]. In this proof-of-concept study, we have used gold-DNA affinity interaction for detecting gene-specific DNA methylation in *FAM134B* promoter region containing designated CpG sites located within a length of 48 bases. In order to execute our approach, we have designed synthetic samples containing 0, 1, 5 and 11 CpG sites within the promoter region of *FAM134B* gene which mimic the bisulfite treated and asymmetric PCR processed methylated and unmethylated DNA regions.

### 3.3. Assay optimization

The extent of the adsorption of the target DNA on unmodified SPE-Au depends on the adsorption condition such as adsorption time, solution pH and amount of DNA. We first optimized the adsorption time (5–40 min) of target DNA samples by measuring the redox charge differences between the 10 ng/μL synthetic methylated (11 CpG) and unmethylated (0 CpG) DNA in a solution of pH 7. As depicted in Fig. 2A, the maximum level of difference in charge densities between methylated and unmethylated samples was achieved at 5 min of adsorption time and gradually decreased with increasing time. At >20 min of the adsorption time, the difference in charge densities is minimum. This can be explained by the fact that longer adsorption time led to the saturation of the electrode surface with the methylated and unmethylated samples, causing a similar level of the surface confined redox process (*i.e.*, RuHex localized at electrode) in CC for both the methylated and unmethylated cases providing two CC signals with almost identical magnitudes. Therefore, 5 min of the adsorption time was chosen for all subsequent experiments.

We further investigated the effect of DNA concentration (2.5–40 ng/μL) on the change of the charge densities between the methylated and unmethylated DNA samples onto a SPE-Au in a solution of pH 7 for 5 min of adsorption. As seen in Fig. 2B, a significant change in charge densities (80.24) between methylated and unmethylated samples was found at the DNA concentration of 5 ng/μL. The maximum redox charge density difference i.e., 95.54 was achieved using 10 ng/μL of DNA between these two samples. This is related to the increasing level of adsorbed DNA (i.e., larger RuHex redox probes) on the electrode surface with increasing concentrations. At >20 ng/μL DNA concentration, a sharp decrease in the charge densities changes was observed. For example, 40 ng/



Please cite this article in press as: Md.Hakimul-g.H. Haque, et al., Quantification of gene-specific DNA methylation in oesophageal cancer via electrochemistry, Analytica Chimica Acta (2017), http://dx.doi.org/10.1016/j.aca.2017.04.034

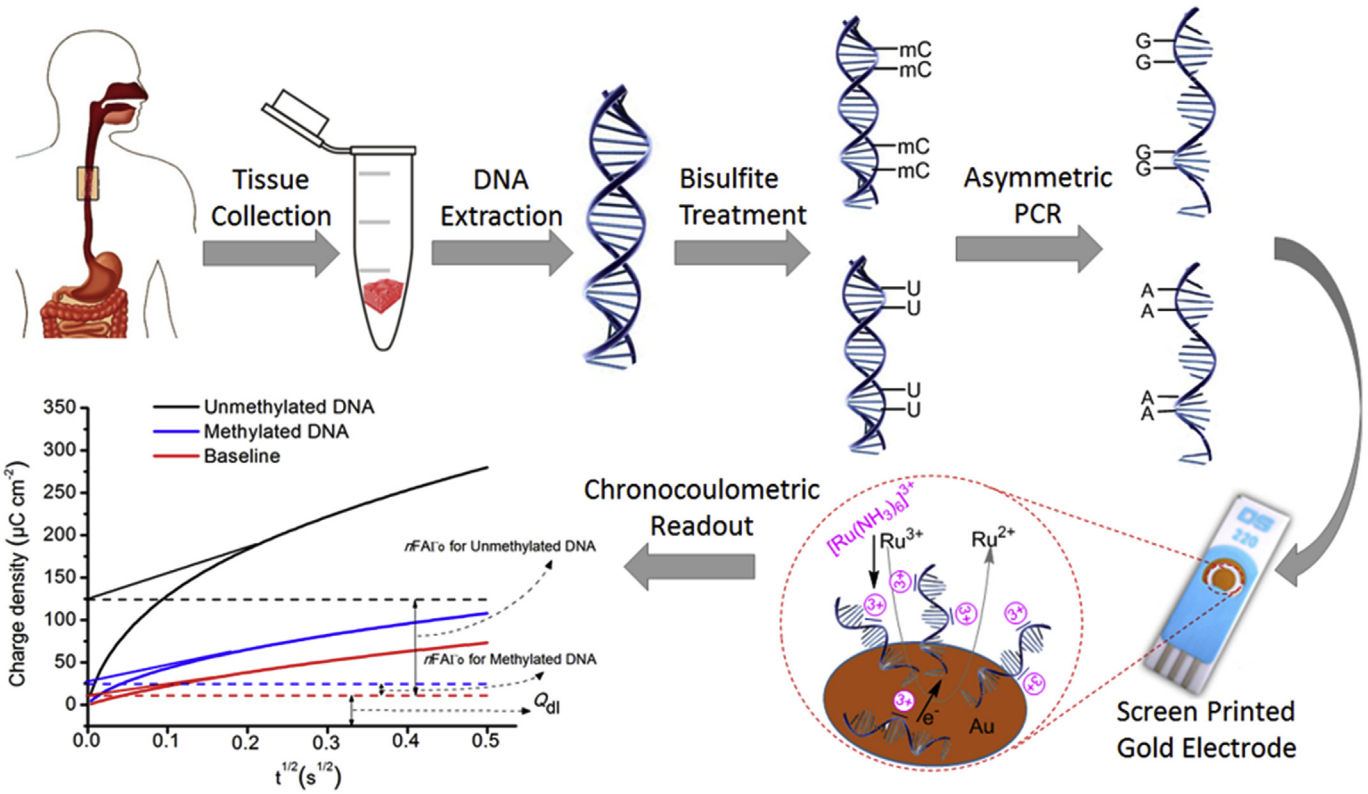


**Fig. 1.** Principle of the quantification of gene-specific DNA methylation assay. The adenine-enriched unmethylated ss-DNA adsorbs relatively larger amount on SPE-Au electrode in compare to that of the guanine-enriched methylated ss-DNA. A significant electrochemical signals were generated by the CC interrogation of DNA-bound $Ru(NH_3)_6]^{3+}$ complexes. Inset, typical CC signals showing the adenine-enriched unmethylated DNA that produces higher CC charge in comparison to guanine-enriched methylated DNA.

μL of DNA concentration resulted the charge densities changes of 40.34 between methylated and unmethylated samples. These findings clearly indicate that the amount of DNA at >10 ng/μL offers almost similar level of CC signals for both the methylated and unmethylated sequences. This can be explained by the fact that saturation of both sequences on the electrode surface was achieved within 5 min of adsorption at higher DNA concentrations which eventually leads to a similar level of redox charge densities. Thus, 10 ng/μL of DNA concentration was selected as an optimal concentration for all subsequent experiments. We then estimated the effect of the pH of the solution on the adsorption of target DNA by varying the pH of the solution from 3.0 to 9.5. Fig. 2C clearly showed that the redox charge density changes between methylated and unmethylated DNA samples were found to be 35.25 at pH 3.0. The optimal charge density changes 95.55 was achieved at neutral pH (*i.e.*, 7), whereas at > pH = 7.0, a gradual decrease in charge density changes was recorded. These results clearly showed that pH of the buffer solution influence the competition between DNA and gold electrostatic forces (i.e., inherent interaction between DNA bases and gold electrodes). At neutral pH, negative charge of the phosphate backbone of DNA is optimal to hinder the adsorption of methylated samples while still allowing the unmethylated DNA with higher adenine contents to be adsorbed strongly. At basic pH, the gold surface would be more negatively charged and electrostatic repulsion with the negatively-charged phosphate backbone of DNA could reduce overall DNA adsorption. On the other hand, at the lower pH (3), cytosines and adenine in the target sequences would be protonated which could facilitate faster adsorption for methylated and unmethylated samples resulting saturation of both targets on the gold surface within a very short time leading to a reduced level of charge density changes. Therefore, we selected pH 7 as an optimal pH for our assay.

### 3.4. Synthetic sample analysis

To evaluate the applicability of our approach for the detection of various level of CpG methylation within the promoter region of *FAM134B* gene, four synthetic DNA samples containing 0, 1, 5 and 11 CpG sites were examined. Fig. 3 shows that the decrease of the redox charge densities is a function of the number of CpG cites. This is due to the decrease of the adenine contents with increasing methylated CpG sites in the target sequence (i.e., low level of adsorbed DNA leading to the lowering of the charge densities). The linear regression equation was estimated to be y (charge, $\mu Ccm^{-2}$) = −8.2926 (number of CpG sites) + 103.9 with the correlation coefficient ($R^2$) of 0.9999. The level of redox charge responses showed in Fig. 3 clearly indicates that our assay can effectively detect DNA methylation at a single CpG level of resolution. For these studies, the relative standard deviation (%RSD) over three independent experiments was found to be <5%. A similar result has also been reported previously based on gold-DNA [34] and graphene-DNA [40] affinity interaction based approaches. We have also checked the stability of the DNA-attached SPE-Au electrodes by using six independent electrodes at four day interval over 20 days. The electrodes were modified with synthetic DNA containing 11 CpG sites, and stored at 25 $^{O}$C. Each electrode was used in each interval (data not shown). The electrode-to-electrode reproducibility (*i.e.*, % RSD) was found to be <6% (for $n = 6$), indicating the good stability of the sensor with good analytical reproducibility.

### 3.5. Heterogonous sample analysis

Heterogeneous methylation can arise as a mixture of fully



Please cite this article in press as: Md.Hakimul-g.H. Haque, et al., Quantification of gene-specific DNA methylation in oesophageal cancer via electrochemistry, Analytica Chimica Acta (2017), http://dx.doi.org/10.1016/j.aca.2017.04.034

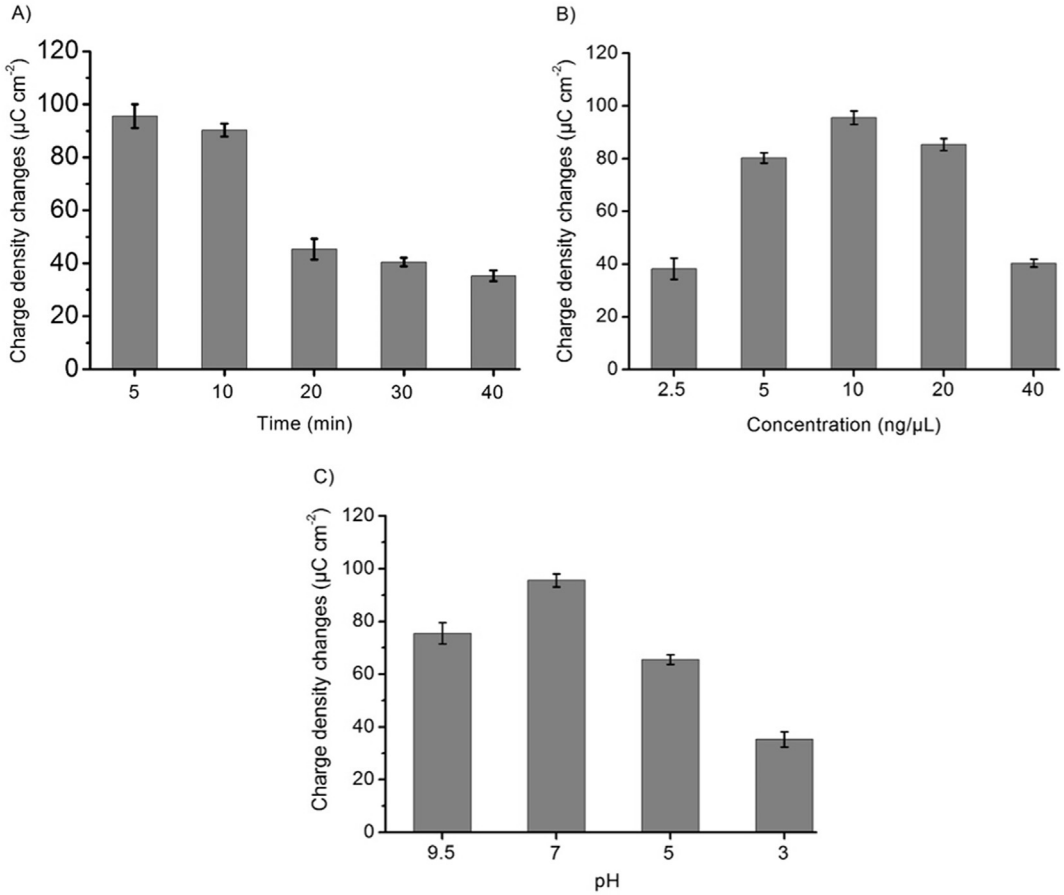


**Fig. 2.** The charge difference between the adsorption of unmethylated (0 CpG) and methylated (11 CpG) DNA sequences at different (A) time (B) concentration and (C) pH of the solution. Each data point (A–C) represents the average of three repeat trails, and error bars represent the standard deviation of measurements (%RSD = <5%, for $n = 3$).

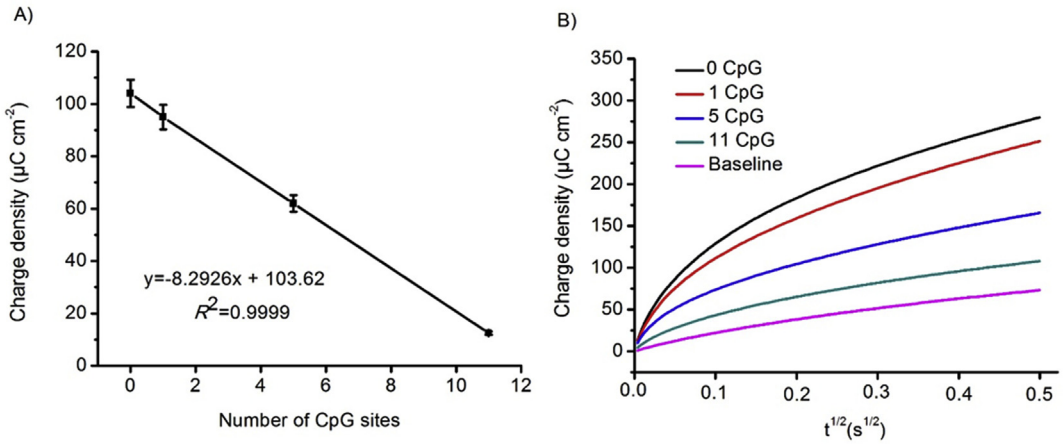


**Fig. 3.** (A) Plot for charge density versus number of CpG sites (0, 1, 5, 11 CpG). (B) Their corresponding CC curves and a typical background signal. Each data point represents the average of three repeat trails, and error bars represent the standard deviation of measurements (%RSD = <5%, for $n = 3$).

methylated and unmethylated DNA in varying proportions in tissue samples from cancer patients [48]. A heterogeneous mixture of cancer cells may contain both fully unmethylated and methylated DNA like imprinted gene *H19* [49]. Accurate quantification of heterogeneous DNA methylation pattern plays critical role for the detection and prediction of clinical prognosis in human cancers [48]. It is therefore important to screen the degree of methylation pattern in a high background of unmethylated DNA samples. To evaluate the assay performance for detecting heterogeneous DNA methylation pattern, we analyzed the dependence of the CC responses on various degree of methylation. The samples were made by mixing synthetic standards of methylated and unmethylated DNA sequences to get 0%, 10%, 25%, 50%, 75%, 90% and 100% methylation, Fig. 4. The total change densities decrease with



Please cite this article in press as: Md.Hakimul-g.H. Haque, et al., Quantification of gene-specific DNA methylation in oesophageal cancer via electrochemistry, Analytica Chimica Acta (2017), http://dx.doi.org/10.1016/j.aca.2017.04.034

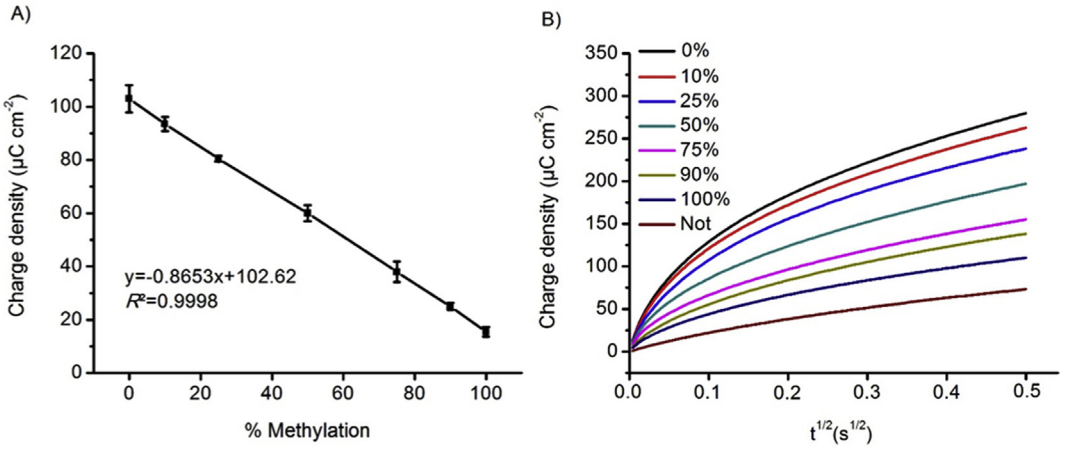


**Fig. 4.** (A) Plot for charge density versus designated degree of methylation (i.e., sample containing 0%, 10%, 25%, 50%, 75%, 90% and 100%). (B) Their corresponding CC curves and a typical background signal. Each data point represents the average of three repeat trails, and error bars represent the standard deviation of measurements (%RSD = <5% for $n = 3$).

increasing levels of methylation, probably due to the increasing adenine contents in the target DNA sequences. The linear regression equation was found to be y (charge, $\mu Ccm^{-2}$) = −0.8653 (% methylation) + 102.6 with a correlation coefficient ($R^2$) of 0.9998. A methylation change as low as 10% could be detected from 10 ng/μL of DNA. This data clearly demonstrate that our approach is sensitive enough in detecting methylated DNA in the nanogram regime. It is important to note that this level of data was much better than the findings of our previous gold-DNA based approach [34,35], and was also comparable to recent approaches [18–22].

### 3.6. Gene-specific methylation detection and validation in cell line and clinical sample

To demonstrate a complex biological application, we applied our assay to detect the methylation status at the eleven CpG sites of the targeted *FAM134B* promoter which have been reported to be methylated in ESCC [40]. Purified DNA amplicons obtained from whole genome amplification and Jurkat DNA was used as fully unmethylated DNA and 100% methylated control, respectively. For avoiding any PCR bias, we quantified the gene copy number prior to PCR amplification [34,35]. Purified genomic DNA samples generated from three ESSC cell lines were then amplified asymmetrically (see agarose gel electrophoresis image in Fig. 5A) and analyzed using our approach under the optimized conditions. As indicated in Fig. 5B and C, significant redox charge responses were observed in three cancer cell lines, unmethylated WGA, and 100% methylated Jurkat DNA samples signifying the presence of different percentage of methylation. When compared to that of the fully unmethylated WGA and 100% methylated Jurkat DNA samples, the level of the total redox charges obtained for the DNA sequences derived from HKESC-4, KYSE-510 and HKESC-1 cell lines indicated that HKESC-4 is partially and other two could be highly methylated (i.e., hypermethylated) at *FAM134B* promoter gene. The %RSD over three independent experiments in quantifying DNA methylation from these cell line samples analysis was found to be <5%. These data were validated with MS-HRM curve analysis and Sanger sequencing. As can be seen in Fig. S1, MS-HRM curve analysis showed that DNA samples derived from HKESC-4 is partially methylated while KYSE-510 and HKESC-1 DNA samples are hypermethylated. Moreover, Sanger sequencing also confirmed the different methylation level in WGA, Jurkat DNA and different ESCC cell lines sample (Figs. S2 and 3). These data clearly indicate that the proposed assay could be a useful alternative for detecting *FAM134B* promoter gene methylation in cell-derived samples.

To further demonstrate the potential utility of our method in analysing clinical samples, we extended our assay to analyze eight tissue DNA samples derived from patients with primary ESCC. Two oesophageal non-cancerous tissue DNA samples were also used as control (see Experimental for details). As indicated in Fig. 5D, all samples showed different degree of methylation. The level of total redox charge of two normal samples clearly showed that these two samples were unmethylated in comparison to that of the WGA and Jurkat DNA samples. Similarly, by comparing the level of total redox charges found for WGA and Jurkat DNA samples (Fig. 5C), we can estimate that four DNA samples derived from P5, P6, P7 and P8 cancer patients were relatively highly methylated, while P1, P2, P3 and P4 samples were partially methylated (i.e., low methylation) at *FAM134B* promoter gene. We then validated our assay performance with well-known MS-HRM curve analysis and Sanger sequencing. As can be seen in Figs. S1B and C, MS-HRM curve analysis identified almost similar methylation level in WGA, N1 and N2 samples. Also, P5, P6, P7 and P8 cancer patients were highly methylated with respect to that of P1, P2, P3 and P4 samples. Sanger sequencing also confirmed that P5, P6, P7 and P8 samples were relatively highly methylated (see typical sequencing data in Figs. S2–S4). Moreover, %RSD over three independent experiments in quantifying DNA methylation from clinical samples analysis were found to be <5%. These data clearly indicated that CC signals generated by our assay were able to quantify different degree of DNA methylation in ESCC tissue samples. Also, our assay is highly reproducible with greater sensitivity and specificity without costly fluorescence labels used in many of current methylation detection techniques [50–52]. In addition, validation studies with MS-HRM curve analysis and Sanger sequencing further suggested that our assay could detect DNA methylation in easy and inexpensive way from cancer patients.

Our method offers several advantages over current methodologies. First, the method involves the direct adsorption of target DNA onto an unmodified electrode rather than the conventional biosensing approach of using recognition and transduction layers, and hence it substantially simplifies the detection method by avoiding the use of complicated chemistries underlying each step of the sensor fabrication. It also avoids the use of capture probe as well as hybridization step. Second, it circumvents the need for the use of radioactive labels, methylation-sensitive restriction enzymes,



Please cite this article in press as: Md.Hakimul-g.H. Haque, et al., Quantification of gene-specific DNA methylation in oesophageal cancer via electrochemistry, Analytica Chimica Acta (2017), http://dx.doi.org/10.1016/j.aca.2017.04.034

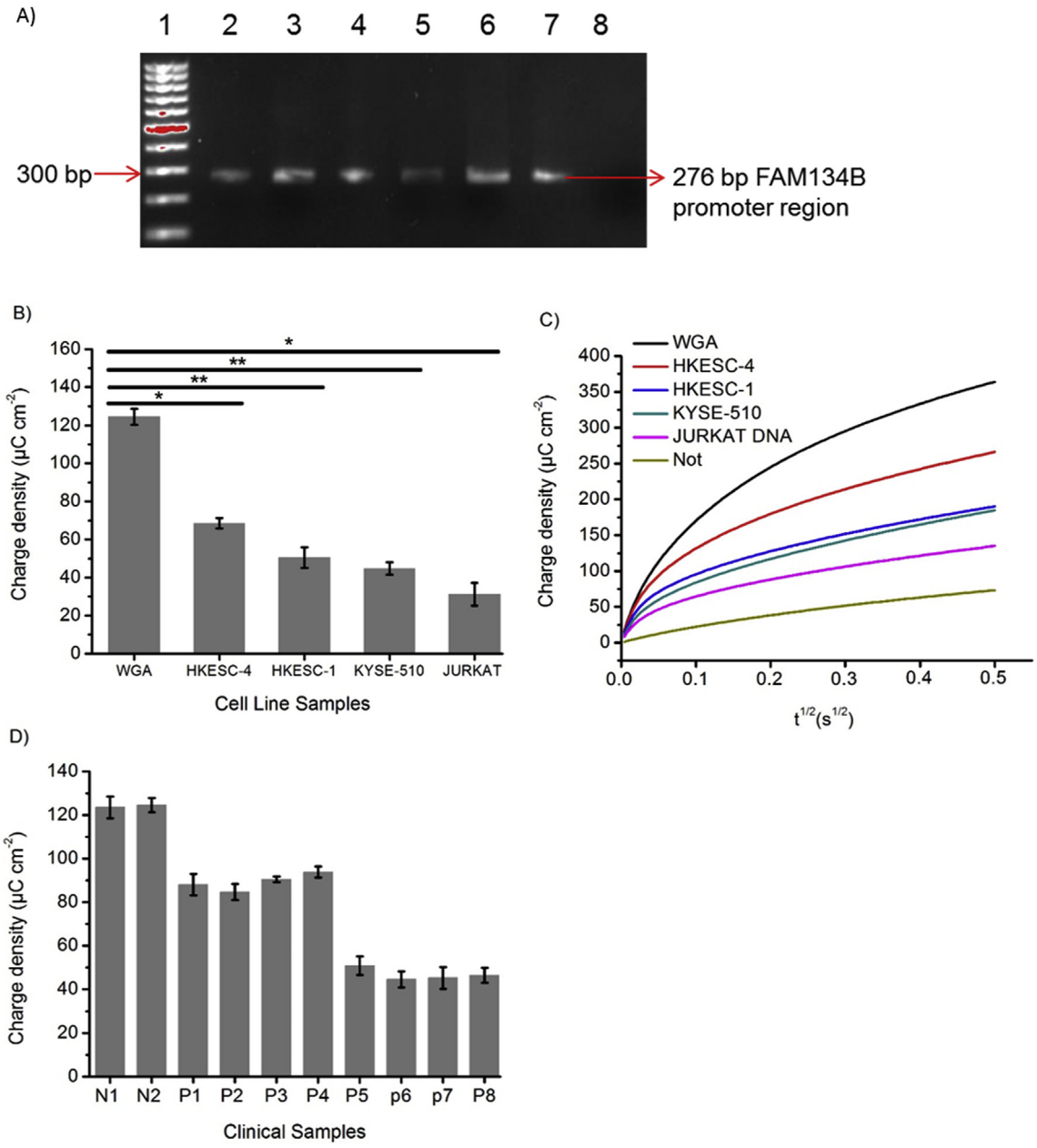


**Fig. 5.** (A) Representative images for amplified PCR products of FAM134B promoter region in 1.5% agarose gel. FAM134B were present in all the samples (2–7) except non template control (8). Hundred base pairs DNA ladder is used for comparison. (B) CC charges for detecting *FAM134B* promoter region in three oesophageal cancer cell lines, a fully unmethylated WGA, and a 100% methylated Jurkat DNA samples. (C) CC curves for detecting *FAM134B* promoter region in three oesophageal cancer cell lines, a fully unmethylated WGA, and a 100% methylated Jurkat DNA samples. (D) CC charges for detecting *FAM134B* promoter region two normal (N1 and N2) and eight (P1-P8) oesophageal cancer tissue samples. Each data point represents the average of three repeat trails, and error bars represent the standard deviation of measurements (%RSD = <5%, for $n = 3$). Statistical significance was determined by pairwise comparison between 2 conditions using student t-test. *, $p = 0.005$ to 0.05 and **, $p = 0.0005$ to 0.005.

antibodies, and sequencing analysis. Third, the use of commercially available and disposable SPE-Au (containing a three-electrode system) successfully eliminates the utilization of typical electrochemical cells, counter and reference electrodes thereby offering a relatively inexpensive (~USD $5 per SPE-Au) platform for DNA methylation detection. Moreover, the use of SPE-Au potentially avoids the usual time-consuming cleaning steps associated with conventional electrodes making the analysis much faster. Fourth, the detection step of our proposed assay can take only ten min in total (excluding bisulfite treatment and asymmetric PCR steps) to achieve electrochemical readout, which is considerably faster than many recent electrochemical DNA methylation assays [13,29,40].

## 4. Conclusion

We have reported a simple and new method for the quantification of targeted *FAM134B* gene-associated DNA methylation *via* the different adsorption affinity interaction of DNA bases with gold. The detection was achieved by simply monitoring their direct adsorption of bisulfite-treated and PCR amplified sequences onto a SPE-Au. The adsorption of the DNA sequence representing methylated and unmethylated was then quantified *via* CC interrogation of the DNA-bound RuHex complexes. Most importantly, our developed assay can successfully quantify *FAM134B* promoter methylation at varying level in a panel of ESCC cell lines and clinical



Please cite this article in press as: Md.Hakimul-g.H. Haque, et al., Quantification of gene-specific DNA methylation in oesophageal cancer via electrochemistry, Analytica Chimica Acta (2017), http://dx.doi.org/10.1016/j.aca.2017.04.034

samples from ESCC patients. The analytical performance of our method has shown a good agreement with the data obtained using MS-HRM analysis and Sanger sequencing. We anticipated that our approach could be potentially useful for the detection of epigenetic biomarker in both clinical diagnostics and research.

## Acknowledgements

This work was supported by the NHMRC CDF (APP1088966 to M.J.A.S.) and higher degree research scholarships (GUIPRS and GUPRS scholarships to M.H.H., M.N.I. and R.B.) from the Griffith University.

## Appendix A. Supplementary data

Supplementary data related to this article can be found at http://dx.doi.org/10.1016/j.aca.2017.04.034.

## References

[1] K.D. Robertson, P.A. Jones, Methylation: past, present and future directions, carcinogenesis 21 (2000) 461–467.
[2] K. Ma, B. Cao, M. Guo, The detective, prognostic, and predictive value of DNA methylation in human esophageal squamous cell carcinoma, Clin. Epigenetics 8 (2016) 43.
[3] I.Y. Kuo, J.M. Chang, S.S. Jiang, C.H. Chen, I.S. Chang, B.S. Sheu, P.J. Lu, W.L. Chang, W.W. Lai, Y.C. Wang, Prognostic CpG methylation biomarkers identified by methylation array in esophageal squamous cell carcinoma patients, Int. J. Med. Sci. 11 (2014) 779–787.
[4] H.W. Chang, V. Chow, K.Y. Lam, W.I. Wei, A. Yuen, Loss of E-cadherin expression resulting from promoter hypermethylation in oral tongue carcinoma and its prognostic significance, Cancer 94 (2002) 386–392.
[5] Y. Delpu, P. Cordelier, W.C. Cho, J. Torrisani, DNA methylation and cancer diagnosis, 2013, Int. J. Mol. Sci. 14 (2013) 15029–15058.
[6] T.S. Wong, M.W. Man, A.K. Lam, W.I. Wei, Y.L. Kwong, A.P. Yuen, The study of p16 and 15 gene methylation in head and neck squamous cell carcinoma and their quantitative evaluation in plasma by real-time PCR, Eur. J. Cancer 39 (2003) 1881–1887.
[7] M.L. Wong, Q. Tao, L. Fu, K.Y. Wong, G.H. Qiu, F.B. Law, P.C. Tin, W.L. Cheung, P.Y. Lee, J.C. Tang, G.S. Tsao, K.Y. Lam, S. Law, J. Wong, G. Srivastava, Aberrant promoter hypermethylation and silencing of the critical 3p21 tumour suppressor gene, RASSF1A, in Chinese oesophageal squamous cell carcinoma, Int. J. Oncol. 28 (2006) 767–773.
[8] A.W. Chai, A.K. Cheung, W. Dai, J.M. Ko, J.C. Ip, K.W. Chan, D.L. Kwong, W.T. Ng, A.W. Lee, R.K. Ngan, C.C. Yau, S.Y. Tung, V.H. Lee, A.K. Lam, S. Pillai, S. Law, M.L. Lung, Metastasis-suppressing NID2, an epigenetically-silenced gene, in the pathogenesis of nasopharyngeal carcinoma and esophageal squamous cell carcinoma, Oncotarget 7 (2016) 78859–78871.
[9] T. Kuroki, F. Trapasso, S. Yendamuri, A. Matsuyama, H. Alder, M. Mori, C.M. Croce, Promoter hypermethylation of RASSF1A in esophageal squamous cell carcinoma, Clin. Cancer Res. 9 (2003) 1441–1445.
[10] C. Long, B. Yin, Q. Lu, X. Zhou, J. Hu, Y. Yang, F. Yu, Y. Yuan, Promoter hypermethylation of the RUNX3 gene in esophageal squamous cell carcinoma, Cancer Invest 25 (2007) 685–690.
[11] M.L. Gonzalgo, P.A. Jones, Rapid quantitation of methylation differences at specific sites using methylation-sensitive single nucleotide primer extension (Ms-SNuPE), Nucleic Acids Res. 25 (1997) 2529–2531.
[12] C.A. Eads, K.D. Danenberg, K. Kawakami, L.B. Saltz, C. Blake, D. Shibata, P.V. Danenberg, P.W. Laird, MethyLight: a high-throughput assay to measure DNA methylation, Nucleic Acids Res. 28 (2000) E32.
[13] T.K. Wojdacz, A. Dobrovic, Methylation-sensitive high resolution melting (MS-HRM): a new approach for sensitive and high-throughput assessment of methylation, Nucleic Acids Res. 35 (2007) e41.
[14] M.N. Islam, S. Yadav, M.H. Haque, M. Ahmed, F. Islam, M.S.Al Hossain, V. Gopalan, A.K. Lam, N.T. Nguyen, M.J.A. Shiddiky, Optical biosensing strategies for DNA methylation analysis, Biosens. Bioelectron. (2016), http://dx.doi.org/10.1016/j.bios.2016.10.034.
[15] S. Kurdyukov, M. Bullock, DNA methylation analysis: choosing the right method, Biology 5 (2016) 3.
[16] D. Kato, K. Goto, S. Fujii, A. Takatsu, S. Hirono, O. Niwa, Electrochemical DNA methylation detection for enzymatically digested CpG oligonucleotides, Anal. Chem. 83 (2011) 7595–7599.
[17] D. Kato, N. Sekioka, A. Ueda, R. Kurita, S. Hirono, K. Suzuki, O. Niwa, A nanocarbon film electrode as a platform for exploring DNA methylation, J. Am. Chem. Soc. 130 (2008) 3716–3717.
[18] L.G. Carrascosa, A.A. Sina, R. Palanisamy, B. Sepulveda, M.A. Otte, S. Rauf, M.J.A. Shiddiky, M. Trau, Molecular inversion probe-based SPR biosensing for specific, label-free and real-time detection of regional DNA methylation, Chem. Commun. 50 (2014) 3585–3588.
[19] K.M. Koo, E.J. Wee, S. Rauf, M.J.A. Shiddiky, M. Trau, Microdevices for detecting locus-specific DNA methylation at CpG resolution, Biosens. Bioelectron. 56 (2014) 278–285.
[20] E.J.H. Wee, T. HaNgo, M. Trau, A simple bridging flocculation assay for rapid, sensitive and stringent detection of gene specific DNA methylation, Sci. Rep. 5 (2015) 15028.
[21] E.J.H. Wee, S. Rauf, M.J.A. Shiddiky, A. Dobrovic, M. Trau, DNA ligase-based strategy for quantifying heterogeneous DNA methylation without sequencing, Clin. Chem. 61 (2015) 163–171.
[22] Y. Wang, E.J.H. Wee, M. Trau, Accurate and sensitive total genomic DNA methylation analysis from sub-nanogram input with embedded SERS nanotags, Chem. Commun. 52 (2016) 3560–3563.
[23] E.L. Wong, J.J. Gooding, The electrochemical monitoring of the perturbation of charge transfer through DNA by cisplatin, J. Am. Chem. Soc. 129 (2007) 8950–8951.
[24] M. Labib, E.H. Sargent, S.O. Kelley, Electrochemical methods for the analysis of clinically relevant biomolecules, Chem. Rev. 116 (2016) 9001–9090.
[25] S.M. Choi, D.M. Kim, O.S. Jung, Y.B. Shim, A disposable chronocoulometric sensor for heavy metal ions using a diaminoterthiophene-modified electrode doped with graphene oxide, Anal. Chim. Acta 892 (2015) 77–84.
[26] G.L. Wang, L.Y. Zhou, H.Q. Luo, N.B. Li, Electrochemical strategy for sensing DNA methylation and DNA methyltransferase activity, Anal. Chim. Acta 768 (2013) 76–81.
[27] J. Ji, Y. Liu, W. Wei, Y. Zhang, S. Liu, Quantitation of DNA methyltransferase activity via chronocoulometry in combination with rolling chain amplification, Biosens. Bioelectron. 85 (2016) 25–31.
[28] S. Sato, M. Tsueda, Y. Kanezaki, S. Takenaka, Detection of an aberrant methylation of CDH4 gene in PCR product by ferrocenylnaphthalene diimide-based electrochemical hybridization assay, Anal. Chim. Acta 715 (2012) 42–48.
[29] H. Zhang, Y. Yang, H. Dong, C. Cai, A superstructure-based electrochemical assay for signal-amplified detection of DNA methyltransferase activity, Biosens. Bioelectron. 86 (2016) 927–932.
[30] A.B. Steel, T.M. Herne, M.J. Tarlov, Electrochemical quantitation of DNA immobilized on gold, Anal. Chem. 70 (1998) 4670–4677.
[31] J. Zhang, S. Song, L. Wang, D. Pan, C. Fan, A gold nanoparticle-based chronocoulometric DNA sensor for amplified detection of DNA, Nat. Protoc. 2 (2007) 2888–2895.
[32] E.L. Wong, J.J. Gooding, A selective electrochemical DNA biosensor, Anal. Chem. 78 (2006) 2138–2144.
[33] M.J.A. Shiddiky, A.A. Torriero, Z. Zeng, L. Spiccia, A.M. Bond, Highly selective and sensitive DNA assay based on electrocatalytic oxidation of ferrocene bearing zinc(II)-cyclen complexes with diethylamine, J. Am. Chem. Soc. 132 (2010) 10053–10063.
[34] A.A. Sina, S. Howell, L.G. Carrascosa, S. Rauf, M.J.A. Shiddiky, M. Trau, eMethylsorb: electrochemical quantification of DNA methylation at CpG resolution using DNA-gold affinity interactions, Chem. Commun. 50 (2014) 13153–13156.
[35] K.M. Koo, A.A. Sina, L.G. Carrascosa, M.J.A. Shiddiky, M. Trau, eMethylsorb: rapid quantification of DNA methylation in cancer cells on screen-printed gold electrodes, Analyst 139 (2014) 6178–6184.
[36] H. Kimura-Suda, D.Y. Petrovykh, M.J. Tarlov, L.J. Whitman, Base-dependent competitive adsorption of single-stranded DNA on gold, J. Am. Chem. Soc. 125 (2003) 9014–9015.
[37] J.J. Storhoff, R. Elghanian, C.A. Mirkin, R.L. Letsinger, Sequence-dependent stability of DNA-modified gold nanoparticles, Langmuir 18 (2002) 6666–6670.
[38] Y. Hu, K.Y. Lam, T.S. Wan, W. Fang, E.S. Ma, L.C. Chan, G. Srivastava, Establishment and characterization of HKESC-1, a new cancer cell line from human esophageal squamous cell carcinoma, Cancer Genet. Cytogenet 118 (2000) 112–120.
[39] L.C. Cheung, J.C. Tang, P.Y. Lee, L. Hu, X.Y. Guan, W.K. Tang, G. Srivastava, J. Wong, J.M. Luk, S. Law, Establishment and characterization of a new xenograft-derived human esophageal squamous cell carcinoma cell line HKESC-4 of Chinese origin, Cancer Genet. Cytogenet 178 (2007) 17–25.
[40] M.H. Haque, V. Gopalan, S. Yadav, M.N. Islam, E. Eftekhari, Q. Li, L.G. Carrascosa, N.T. Nguyen, A.K. Lam, M.J.A. Shiddiky, Detection of regional DNA methylation using DNA-graphene affinity interactions, Biosens. Bioelectron. 87 (2016) 615–621.
[41] J. Zhang, S. Song, L. Zhang, L. Wang, H. Wu, D. Pan, C. Fan, Sequence-specific detection of femtomolar DNA via a chronocoulometric DNA sensor (CDS): effects of nanoparticle-mediated amplification and nanoscale control of DNA assembly at electrodes, J. Am. Chem. Soc. 128 (2006) 8575–8580.
[42] P.S. Ho, C.A. Frederick, D. Saal, A.H. Wang, A. Rich, The interactions of ruthenium hexaammine with Z-DNA: crystal structure of a Ru(NH3)6+3 salt of d(CGCGCG) at 1.2 A resolution, J. Biomol. Struct. Dyn. 4 (1987) 521–534.
[43] S. Piana, A. Bilic, The nature of the adsorption of nucleobases on the gold [111] surface, J. Phys. Chem. B 110 (2006) 23467–23471.
[44] M.H. Haque, V. Gopalan, K.W. Chan, M.J.A. Shiddiky, R.A. Smith, A.K. Lam, Identification of novel FAM134B (JK1) mutations in oesophageal squamous cell carcinoma, Sci. Rep. 6 (2016) 29173.
[45] W.K. Tang, C.H. Chui, S. Fatima, S.H. Kok, K.C. Pak, T.M. Ou, K.S. Hui, M.M. Wong, J. Wong, S. Law, S.W. Tsao, K.Y. Lam, P.S. Beh, G. Srivastava, A.S. Chan, K.P. Ho, J.C. Tang, Oncogenic properties of a novel gene JK-1 located in chromosome 5p and its overexpression in human esophageal squamous



Please cite this article in press as: Md.Hakimul-g.H. Haque, et al., Quantification of gene-specific DNA methylation in oesophageal cancer via electrochemistry, Analytica Chimica Acta (2017), http://dx.doi.org/10.1016/j.aca.2017.04.034

cell carcinoma, Int. J. Mol. Med. 19 (2007) 915–923.
[46] K. Kasem, V. Gopalan, A. Salajegheh, C.T. Lu, R.A. Smith, A.K.Y. Lam, The roles of JK-1(FAM134B) expressions in colorectal cancer, Exp. Cell Res. 326 (2014) 166–173.
[47] F. Islam, V. Gopalan, R. Wahab, R.A. Smith, B. Qiao, A.K. Lam, Stage dependent expression and tumor suppressive function of FAM134B (JK1) in colon cancer, Mol. Carcinog. 56 (2016) 238–249.
[48] T. Mikeska, I.L. Candiloro, A. Dobrovic, The implications of heterogeneous DNA methylation for the accurate quantification of methylation, Epigenomics 2 (2010) 561–573.
[49] A. Kerjean, J.M. Dupont, C. Vasseur, D. Le Tessier, L. Cuisset, A. Pàldi, P. Jouannet, M. Jeanpierre, Establishment of the paternal methylation imprint of the human H19 and MEST/PEG1 genes during spermatogenesis, Hum. Mol. Genet. 9 (2000) 2183–2187.
[50] V.J. Bailey, H. Easwaran, Y. Zhang, E.S. Griffiths, A. Belinsky, J.G. Herman, S.B. Baylin, H.E. Carraway, T.H. Wang, MS-qFRET: a quantum dot-based method for analysis of DNA methylation, Genome Res. 19 (2009) 1455–1461.
[51] I. Van der Auwera, W. Yu, L. Suo, L. Van Neste, P. van Dam, E.A. Van Marck, P. Pauwels, P.B. Vermeulen, L.Y. Dirix, S.J. Van Laere, Array-based DNA methylation profiling for breast cancer subtype discrimination, PLoS One 5 (2010) e12616.
[52] J. Zhang, B. Xing, J. Song, F. Zhang, C. Nie, L. Jiao, L. Liu, F. Lv, S. Wang, Associated analysis of DNA methylation for cancer detection using CCP-based FRET Technique, Anal. Chem. 86 (2014) 346–350.



Please cite this article in press as: Md.Hakimul-g.H. Haque, et al., Quantification of gene-specific DNA methylation in oesophageal cancer via electrochemistry, Analytica Chimica Acta (2017), http://dx.doi.org/10.1016/j.aca.2017.04.034

*Supplementary data*

***for***

# Quantification of Gene-specific DNA Methylation in Oesophageal Cancer via Electrochemistry

Md. Hakimul Haque[ab], Vinod Gopalan[a*], Md. Nazmul Islam[b], Mostafa Kamal Masud[b,c], Ripon Bhattacharjee [b], Md Shahriar Al Hossain[c], Nam-Trung Nguyen[b], Alfred K. Lam[a*], and Muhammad J. A. Shiddiky[b*]

**Table 1**

List of the primer sequences used in this study. The CpG sites in methylated and unmethylated samples are highlighted with green and orange colour.

| **Target genes** | **Oligonucleotide Sequences (5'--3′)** |
|---|---|
| *FAM134B*-F | AGAGGTTTTTTAGGAATTTAGAGTTTTT |
| *FAM134B*-R | CCATCTTCAACTATACTTCCAAACAAA |
| *HBD*-F | CAGCATCAGGAGTGGACAGA |
| *HBD*-R | CTCGGCGGCACCCAC |
| 11 CpG sites | ACGAAACCGAACGCGCGCGCGAACGCGCCTAAATATAAATACCGCCGA |
| 5 CpG sites | ACAAAACCGAACACGCACGCAAACGCACCTAAATATAAATACCGCCAA |
| 1 CpG sites | ACGAAACCAAACACACACACACAAACACACCTAAATATAAATACCACCAA |
| O CpG sites | ACAAAACCAAACACACACACACAAACACACCTAAATATAAATACCACCAA |

**Methylation Specific High Resolution Melting Curve Analysis (MS-HRM)**

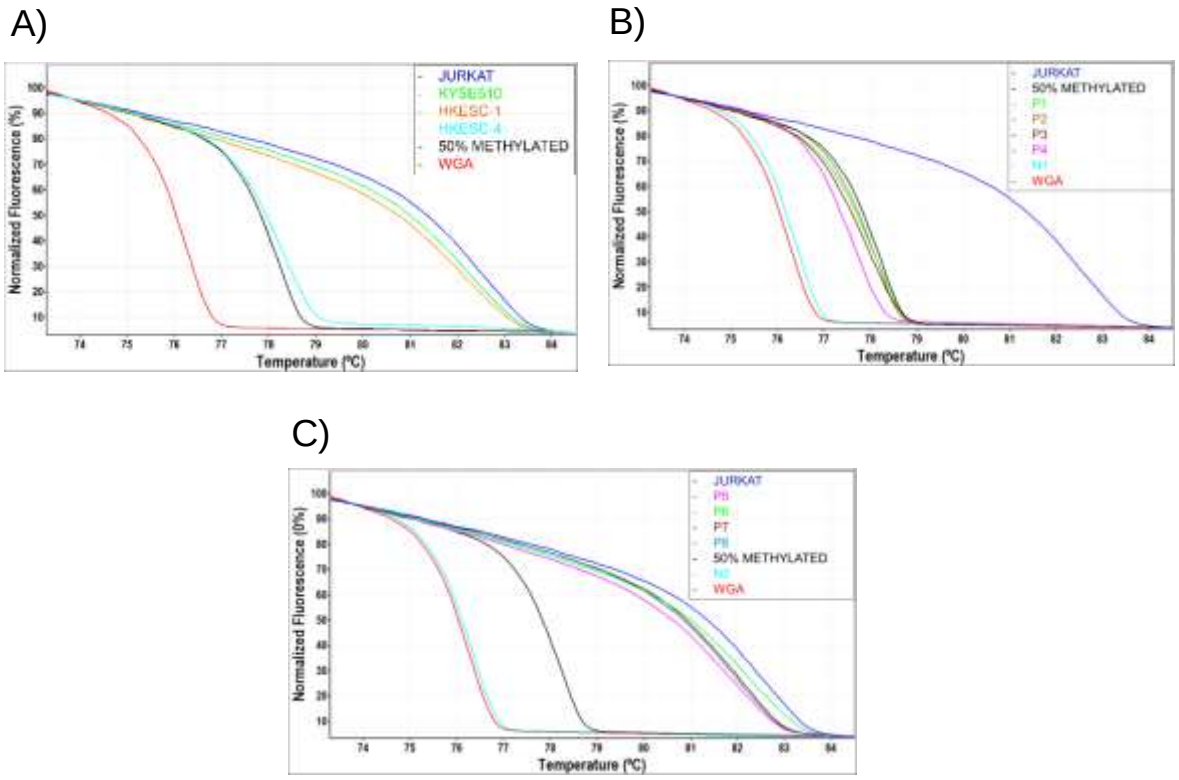


**Fig. S1.** The MS-HRM curve analysis for DNA methylation detection of *FAM134B* gene promoter region in ESCC. Representative MS-HRM curves for 100% methylated Jurkat, fully unmethylated (0%) WGA and diluted 50% methylated standards along with (A) three ESCC cell lines (KYSE-510, HKESC-1 and HKESC-4), (B) four patient (P1, P2, P3, and P4) and one normal samples (N1), and (C) four patient (P5, P6, P7, and P8) and one normal sample (N2).

**Sanger sequencing analysis**

a)

Jurkat DNA

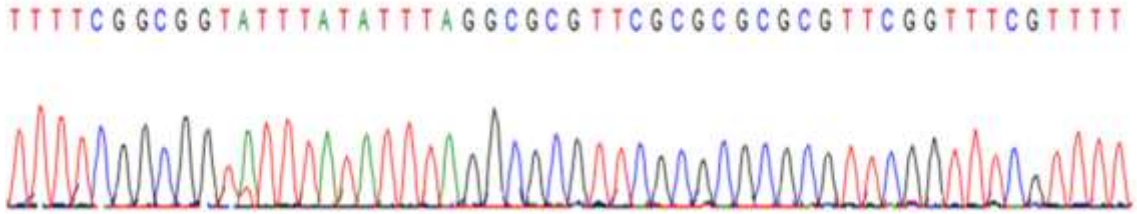

b)

WGA DNA

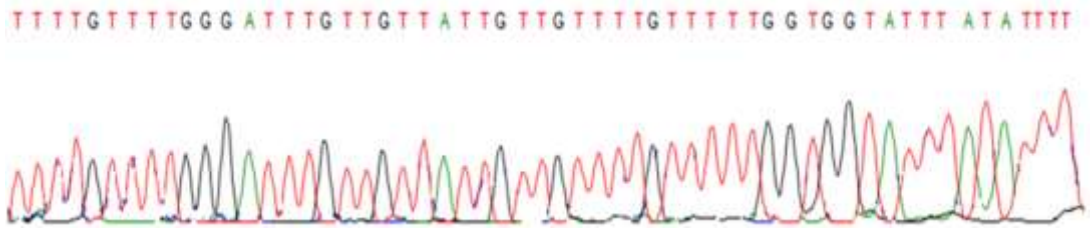

**Fig. S2.** Representative Sanger sequencing analysis for 100% methylated Jurkat and fully unmethylated (0%) WGA.

HKESC-1 DNA

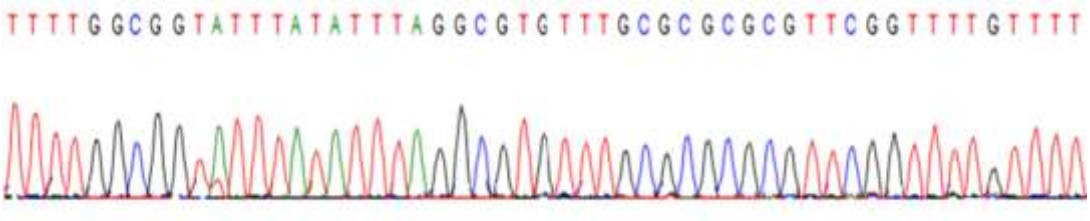


**Fig. S3**. Representative Sanger sequencing analysis for DNA methylation detection of *FAM134B* gene promoter region in HKESC cell lines of ESCC.

A)

P5 sample

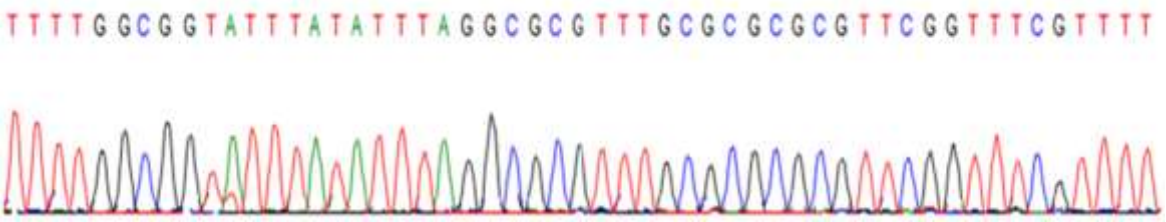


B)

P2 sample

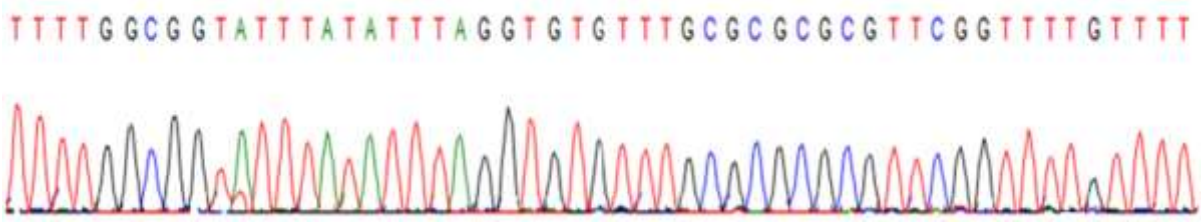


**Fig. S4.** Representative Sanger sequencing analysis for DNA methylation detection of *FAM134B* gene promoter region in P5 and P2 tissue samples of ESCC.

# Chapter 8

## Colorimetric and electrochemical quantification of global DNA methylation using methylcytosine specific antibody

Chapter 8 is included as it appears in Analyst (2017)

# Introduction

We developed a new method for quantifying global DNA methylation in an integrated approach consisting of both colorimetric and electrochemical methods. To develop a first pass screening, we first demonstrated a colorimetric method which enables the naked-eye detection of methylation. Initially, extracted, bislufite treated and denatured ssDNA was directly adsorbed onto an SPE-Au followed by the immuno-recognition of methylated region using HRP conjugated anti-mC antibody. Enzymatic oxidation of TMB resulted in a coloured complex which can be evaluated with naked-eye and quantified by measuring absorbance at 450nm. Next we developed an electrochemical method for quantifying global DNA methylation. Since, $TMB_{(ox)}$ is electrochemically active, detectable amount of amperometric current is observed at 150mV vs Ag pseudo-reference electrode on SPE-Au. Compared to exisiting related approaches, our assay has comparable specificity and reproducibility. Our method can sensitivily detect as low as 5% differences in methylation levels while analysing various levels of global DNA methylation in synthetic samples and cell lines. The method has further been successfully challenged in eight tissues samples collected from patients with ESCC. The methods developed here are highly sensitive, cost-effective and relatively rapid. Thus we believe that our assay will find its relevance as a low-cost and rapid methylation screening tools in clinical settings.

Analyst

PAPER

View Article Online
View Journal



Cite this: DOI: 10.1039/c7an00526a

# Colorimetric and electrochemical quantification of global DNA methylation using a methyl cytosine-specific antibody†

Md. Hakimul Haque,‡[a,b] Ripon Bhattacharjee,‡[b] Md. Nazmul Islam,[b] Vinod Gopalan,*[a] Nam-Trung Nguyen,[b] Alfred K. Lam*[a] and Muhammad J. A. Shiddiky*[b,c]

We report a simple colorimetric (naked-eye) and electrochemical method for the rapid, sensitive and specific quantification of global methylation levels using only 25 ng of input DNA. Our approach utilises a three-step strategy; (i) initial adsorption of the extracted, purified and denatured bisulfite-treated DNA on a screen-printed gold electrode (SPE-Au), (ii) immuno-recognition of methylated DNA using a horseradish peroxidase (HRP)-conjugated methylcytosine (HRP-5mC) antibody and (iii) subsequent colorimetric detection by the enzymatic oxidation of 3,3′,5,5′-tetramethylbenzidin (TMB)/$H_2O_2$ which generated a blue-coloured product in the presence of methylated DNA and HRP-5mC immunocomplex. As $TMB_{(ox)}$ is electroactive, it also produces detectable amperometric current at +150 mV *versus* a Ag pseudo-reference electrode (electrochemical detection). The assay could successfully differentiate 5-aza-2′-deoxycytidine drug-treated and untreated Jurkat DNA samples. It showed good reproducibility (relative standard deviation (% RSD) = <5%, for $n$ = 3) with fairly good sensitivity (as low as 5% difference in methylation levels) and specificity while analysing various levels of global DNA methylation in synthetic samples and cell lines. The method has also been tested for analysing the methylation level in fresh tissue samples collected from eight patients with oesophageal squamous cell carcinoma. We believe that this assay could be potentially useful as a low-cost alternative for genome-wide DNA methylation analysis in point-of-care applications.

Received 28th March 2017,
Accepted 25th April 2017

DOI: 10.1039/c7an00526a

rsc.li/analyst



## Introduction

Alterations in the DNA methylation landscape are one of the crucial and early events in the pathogenesis of many chronic diseases including cancers.[1] DNA methylation occurs predominantly in cytosine/guanine (CpG) dinucleotide areas located in the promoter regions of genes in mammals.[2] Human genome contains about 28 million CpG, 70–80% of which are methylated.[3,4] Both global hypomethylation (*i.e.*, gradual loss in methylation levels throughout the genome) and regional hypermethylation (*i.e.*, acquisition of increasing 5mC levels in gene promoters) are reportedly involved in cancer pathogenesis *via* dysregulation of various cellular pathways including chromatin modulation, genomic stability, transcription of proto-oncogenes, and activation of tumour suppressor genes.[5–9] For instance, several studies have demonstrated the strong correlation between global methylation with the progression of oesophageal squamous cell carcinoma (ESCC).[10–12] In ESCC, aberrant global methylation (mostly hypomethylation) was found to be involved in the silencing and alterations of several key genes associated with tumour progression such as cell cycle genes, DNA repair genes and genes responsible for Wnt and TGF-β signalling pathways.[10,11] Therefore, screening of DNA methylation across the genome can aid in the diagnosis, prognosis and therapeutics of cancer thereby enabling more personalized patient care.

Currently, the major challenges in DNA methylation biomarker discovery include obstacles in assay development, detection of patient specific methylation load, and varying sensitivity and specificity.[13] Until recently, several conventional methods have been developed to profile global methylation

[a]*Cancer Molecular Pathology laboratory in Menzies Health Institute Queensland, Griffith University and School of Medicine, Gold Coast, QLD 4222, Australia. E-mail: v.gopalan@griffith.edu.au, a.lam@griffith.edu.au*

[b]*School of Natural Sciences, Griffith University, Nathan Campus, Nathan, QLD 4111, Australia. E-mail: m.shiddiky@griffith.edu.au*

[c]*Queensland Micro- and Nanotechnology Centre (QMNC), Griffith University, Nathan Campus, Nathan, QLD 4111, Australia*

†Electronic supplementary information (ESI) available. See DOI: 10.1039/c7an00526a

‡Contributed equally.

including high performance liquid chromatography (HPLC),[14] mass spectrometry (MS),[15] and bisulfite modification of DNA followed by some form of sequencing.[16] While the analytical excellence of these methods is widely acknowledged, they are not suitable for methylation analysis in any decentralized settings where sophisticated and expensive laboratory-based equipment is lacking. Consequently, in recent years, extensive progress in nanobiotechnology and epigenetic fields has led to the development of a number of biosensing strategies for methylation analysis which mostly rely on optical and electrochemical readouts.[17,18]

A common approach in the methylation detection techniques is the use of affinity capture molecules such as methyl CpG-binding domain (MBD) proteins along with array hybridization and next generation sequencing (NGS).[19] MBD have also been used for developing optical and electrochemical readouts for quantifying methylation levels both at the regional and global scale.[20–23] However, it has been reported that a restriction enzyme is commonly required in the MBD based assay to avoid the non-specific bindings.[18] Additionally, MBD cannot effectively bind single stranded DNA (ssDNA) and are only specific for a selected portion of CpG regions.[24] The methylcytosine (5mC) antibody, in contrast, can recognise and bind 5mC in any CpG region (*i.e.*, sequence specificity is not required) allowing the relatively easy quantification of methylation events in the genome.[24,25] Hence, the 5mC antibody has been employed in several methylation assays based on SPR,[26] electrochemistry[21] and electrochemiluminescence[27] readouts. Also, most of these approaches commonly use restriction enzymes and other complicated steps associated with sensor fabrication.

Herein, we have introduced, as a proof-of-concept, a relatively simple methylation assay to detect global DNA methylation. In this method, extracted genomic DNA was first bisulfite treated and denatured at 95 °C. The resultant ssDNA was directly adsorbed onto an unmodified disposable screen-printed electrode (SPE-Au) followed by the immuno-recognition of the methylated region using the HRP-5mC antibody. Then, in the presence of 3,3′,5,5′-tetramethylbenzidin (TMB)/$H_2O_2$, the enzymatic oxidation of TMB resulted in a blue-coloured complex which enabled the colorimetric quantification (naked-eye) of global methylation. In addition to a colorimetric readout, using the electrochemical properties of $TMB_{(ox)}$, genome-wide methylation is also detected *via* the chronoamperometric method. Finally, the method was developed for quantifying methylation in ESCC cell lines and clinical samples. While most of the existing methods require highly sophisticated instruments, the colorimetric (naked eye) and electrochemical detection based approaches described here rely on the significantly simplified sensor design and use of minimal and inexpensive equipment for the analysis of global DNA methylation which could be applicable for resource-poor diagnostic settings. As the healthcare sector becomes increasingly decentralized, we believe that our method has high translational potential in the next generation point-of-care platform for screening human diseases.

# Experimental

### Reagents and chemicals

Unless otherwise noted, all reagents and chemicals were analytical grade and purchased from Sigma Aldrich (Sydney, NSW, Australia). UltraPure DNase/RNase-free distilled water was obtained from Invitrogen (Carlsbad, CA, USA). Screen-printed gold electrodes (SPE-Au, diameter = 4 mm) were acquired from Dropsens (Llanera, Asturias, Spain). TMB substrate solutions were purchased from Thermo Fisher Scientific Australia Pty Ltd (Scoresby, VIC, Australia). The methylcytosine antibody and HRP conjugation kit were purchased from Abcam (Melbourne, VIC, Australia).

### Preparation of genomic DNA

Eight fresh frozen tissue samples from patients with ESCC and two matched non-neoplastic oesophageal mucosae (as controls) were recruited for this study. For the use of these samples, ethical approval was taken from the Griffith University human research ethics committee (GU Ref no.: MED/19/08/HREC and MSC/17/10/HREC). After histopathological confirmation, genomic DNA was isolated and purified from all these tissues using a DNA/RNA mini kit which is specifically designed for both DNA and RNA purification from fresh tissues (Qiagen, Hilden, Germany). Also, two ESCC cell lines (HKESC-1 and HKESC-4) were provided by our research group.[28,29] Another ESCC cell line, KYSE-510, was purchased from Leibniz Institute DSMZ (German collection of microorganisms and cell cultures). A blood and cell culture DNA mini kit (Qiagen, Hilden, Germany) was used for the purification of DNA from these ESCC cell lines.

Whole genome amplification DNA was constructed using the protocol of the REPLI-g whole genome amplification kit (Qiagen) and purified using the protocol of the DNeasy Blood and Tissue kit (Qiagen). The highly methylated genomic DNA (M-WGA) was prepared following the manufacturer's instruction of New England BioLabs (Ipswich, MA, USA). The methylation conversion efficiency of SssI-treated DNA was examined using a methylation sensitive HpaII restriction enzyme (data not shown). Jurkat (100% methylated) and 5-aza-2′-deoxycytidine (5-Aza)-treated Jurkat genomic DNA samples were purchased from New England BioLab.

### Bisulfite modification

Approximately 500 ng of the extracted genomic DNA from each sample was taken for bisulfite treatment. Bisulfite treatment and purification of the extracted genomic DNA were done by using the MethylEasy Xceed kit (Human Genetic Signatures Pty. Ltd, NSW, Australia) following the manufacturer's protocols. This treatment converts unmethylated cytosines to uracils while methylated cytosines remain unchanged. A Nanodrop spectrophotometer (BioLabs, Ipswich, MA, USA) was used for quantifying the purity of DNA. The concentration of bisulfite treated DNA was noted in ng $\mu L^{-1}$ and then stored at −20 °C until use.

### Conjugation of 5mC antibody

The 5mC monoclonal antibody was conjugated with HRP by the HRP conjugation kit (Abcam) according to the manufacturer's instructions. Briefly, 1.0 μL of a modifier reagent was mixed gently with the 10 μL of 5mC antibody (1.0 mg $mL^{-1}$). Then, the 5mC antibody with a modifier mixture was added directly to the lyophilized HRP mixture and resuspended two times by pipetting. The complex was then kept overnight in the dark at room temperature to facilitate the conjugation of the antibody with HRP. After the incubation, 1.0 μL quencher reagent was mixed gently into the solution. The conjugated antibody (*i.e.*, HRP-5mC) solution was stored at 4 °C.

### Determination of the surface area of the electrodes

The effective areas of the SPE-Au were determined by the measurement of the peak current obtained as a function of the scan rate under cyclic voltammetric conditions for the one-electron reduction of $[Fe(CN)_6]^{3-}$ [2.0 mM in PBS (0.5 M KCl)] and by using the Randles–Sevcik equation (eqn (1)),[30,31]

$$i_p = (2.69 \times 10^5)\, n^{3/2} A D^{1/2} C \nu^{1/2} \quad (1)$$

where, $i_p$ is the peak current (A), $n$ is the number of electrons transferred ($Fe^{3+} \rightarrow Fe^{2+}$, $n = 1$), $A$ is the effective area of the electrode ($cm^2$), $D$ is the diffusion coefficient of $[Fe(CN)_6]^{3-}$ (taken to be $7.60 \times 10^{-5}$ $cm^2$ $s^{-1}$), $C$ is the concentration (mol $cm^{-3}$), and $\nu$ is the scan rate (V $s^{-1}$).

### Chronoamperometric and colorimetric detection of global DNA methylation

Bisulfite-treated DNA samples were denatured at 95 °C for 10 min to form ssDNA and then, gradually cooled to room temperature for subsequent experiments. For DNA sample analysis, 5.0 μL denatured ssDNA samples were diluted in 5× sodium saline citrate (SSC) buffer to get 25 ng of DNA. Then, 5.0 μL of each denatured DNA sample were directly dropped onto a clean SPE-Au and allowed to adsorb for 10 min. The electrodes were then washed three times with 10 mM phosphate buffered saline (PBS) at a pH of 7.4. After air drying of the electrode, 10 ng $\mu L^{-1}$ of HRP-5mC antibody was placed onto the electrode surface and incubated for 30 min at room temperature with gentle shaking (unless otherwise stated) to facilitate the binding of the antibody with ssDNA. Then, the electrode was again washed three times with 10 mM PBS to remove all unbound HRP-5mC antibody. Finally, 50 μL of TMB substrate solution was added onto the gold electrode surface and incubated for 15 min in the dark. The color change was visually observed. For quantitative measurements of color change, 2.0 μL of hydrochloric acid solution (2.0 M HCl) was added, and absorbance readings were recorded at 450 nm using a spectrophotometer (SpectraMax). To perform electrochemical measurements, a CH1040C potentiostat (CH Instruments, TX, USA) was used. Chronoamperometric measurements were conducted in the presence of 50 μL of the complex onto the SPE-Au surface with a potential of +150 mV. The current levels generated at 60 s were used for quantitative measurement.

## Results and discussion

### Assay principle

The assay protocol for analysing genome-wide DNA methylation in ESCC is schematically depicted in Fig. 1. In this study, a methylation specific antibody was used to selectively recognise the methylated cytosine in the ssDNA sequence. Briefly, genomic DNA samples were extracted and purified from ESCC cells and tissues (see the Experimental section for details). They were then bisulfite treated and denatured (at 95 °C for 10 min) to generate ssDNA. Previously, we[32,33] and other researchers[34] have successfully demonstrated that due to the sequence specific (A > C > G > T) affinity of DNA towards the gold surface, ssDNA can be adsorbed on an unmodified gold electrode. Thus, the denatured ssDNA samples were directly adsorbed on the SPE-Au for 10 min. The HRP-5mC antibody was then incubated for 30 min on the SPE-Au for recognizing methylated DNA. After removing the unbound HRP-5mC antibody *via* a washing step, TMB substrate solution was added on the electrode surface. $HRP/H_2O_2$ catalyses the oxidation of TMB that generates a blue-coloured complex, which turns yellow after the addition of an acid solution to the reaction media. This yellow product has been recognized as a two-electron oxidation product (diimine) which is stable in the acid solution. The intensity of the coloured product is directly proportional to the amount of the captured HRP-5mC antibody, which is, in turn, proportional to the level of methylation in the sample. As TMB is electroactive, the amount of enzymatically generated $TMB_{(ox)}$ was chronoamperometrically measured by applying the potential of +150 mV at SPE-Au.

### Assay optimization and minimizing nonspecific adsorption of HRP-5mC antibody

The level of adsorption of the target DNA on an unmodified SPE-Au relies on the adsorption time, pH in the solution and the amount of DNA. Previously, these parameters have been optimized for the electrochemical detection of gene specific DNA methylation and RNA based biomarkers in cancer.[32–35] In this assay, unless otherwise stated, 25 ng of target DNA diluted in 5× SSC (pH 7.4) was adsorbed on the SPE-Au for 10 min. The analytical performance of the assay is also dependent on the amount of 5mC antibody. Therefore, we optimized the concentration of the HRP-5mC antibody. To perform this, a series of HRP-5mC antibody concentrations such as 5, 10, 25, 50 and 100 ng $\mu L^{-1}$ were tested by chronoamperometric measurement. As can be seen in Fig. S1,† relatively high current densities resulted for all concentrations except 5 ng $\mu L^{-1}$. Notably, the current density for the 10 ng $\mu L^{-1}$ antibody concentration was almost similar to that obtained for >10 ng $\mu L^{-1}$ concentration, and thus 10 ng $\mu L^{-1}$ was selected as the optimal concentration for the described assay.

To check the nonspecific adsorption of the HRP-5mC antibody onto the surface of the unmodified SPE-Au electrode, 10 ng $\mu L^{-1}$ HRP-5mC antibody was directly placed onto the gold electrode surface and incubated for 30 min at room temperature with gentle shaking. Then, the electrode was washed three

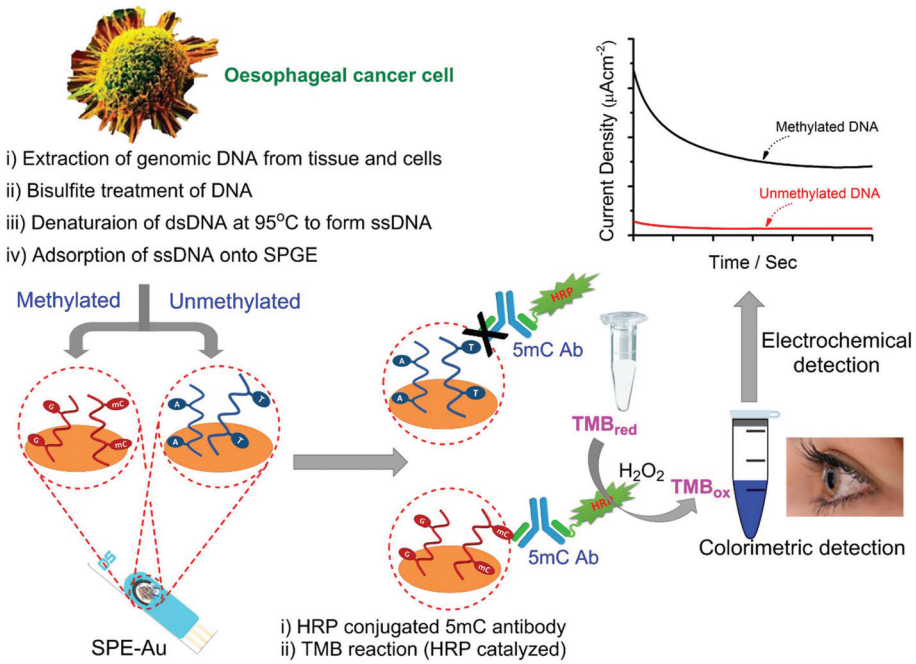


**Fig. 1** Schematic of the global DNA methylation detection assay. Initially, the bisulfite-treated and denatured ssDNA was adsorbed onto a SPE-Au surface followed by immunorecognition of methylated DNA using the HRP-5mC antibody. Subsequent detection of the genomic DNA methylation pattern was performed through coupling reaction of HRP with the TMB/$H_2O_2$ complex on the SPE-Au surface *via* naked-eye, UV-vis and chronoamperometry. Inset: Typical chronoamperometric signals showing the methylated DNA that produces higher amperometric currents in comparison with unmethylated DNA.

times with 10 mM PBS. 50 μL of the TMB substrate solution was added onto the gold electrode surface and incubated in the dark at room temperature for 15 min. The level of chronoamperometric current and naked-eye visualization color (Fig. S2†) suggests that the nonspecific adsorption of the HRP-5mC antibody is negligible. Notably, these data are almost identical to that obtained for U-WGA (fully unmethylated) samples.

### Heterogeneous sample design and analysis

Global DNA methylation plays a crucial role in the pathogenesis of ESCC by altering the expression of different genes. It was reported that the heterogeneity of DNA methylation at the genomic scale has a significant impact on the progression of ESCC.[36] The accurate quantification of heterogeneous genome-wide DNA methylation could have significant implications for the prediction of clinical prognosis in human cancers.[37] Thus, it is important to quantify the different graded DNA methylations in a high background of unmethylated DNA samples. To examine the heterogeneity at the genome-wide DNA methylation level, we first constructed the designated proportions of methylated and unmethylated samples using Jurkat (100% methylated; used as positive control samples) and unmethylated whole genome amplified (U-WGA; used as negative control samples) DNA. A series of heterogeneous samples were then prepared by mixing the Jurkat and U-WGA DNA sequences to get 0%, 5%, 10%, 25%, 50%, 75%, and 100% methylated samples and they were analysed *via* our colorimetric and electrochemical assays under optimized conditions (Fig. 2).

In the colorimetric method, due to the interaction between HRP-5mC and TMB substrate solution, a coloured complex was produced which is related to the level of methylation. As expected, the fully methylated positive control samples (Jurkat) gave a strong blue coloured complex compared to the negative control samples (0% methylated; U-WGA). The color intensity was increased (Fig. 2B, from right to left) with the increasing percentage of methylation. This can be explained by the fact that with an increasing number of methylated CpG sites, the amount of HRP-5mC increased leading to a higher concentration of the enzymatically generated diimine complex (*i.e.*, high intensity). Notably, the color observed from 5% methylated samples (light blue) could be easily distinguished from U-WGA (light purple) (Fig. 2B) thereby demonstrating that our assay can detect as low as 5% methylation by naked-eye evaluation. After stopping the enzymatic oxidation of TMB substrate solution with an acid, the subtle colour changes derived from heterogeneous samples were further quantified by absorbance (Abs) measurements *via* UV-vis at the wavelength of 450 nm. As shown in Fig. 2A, the linear regression equation was estimated to be $y$ (Abs@450 nm) = 0.0081 (% methylation) + 0.09928 with a correlation coefficient ($R^2$) of 0.94424. The minimum detectable Abs was found in 5% methylated samples. The positive control (Abs@450 nm = 0.80) consistently produced an Abs of at least 5-times higher than that of U-WGA (Abs@450 nm = 0.095) while detectable Abs differences

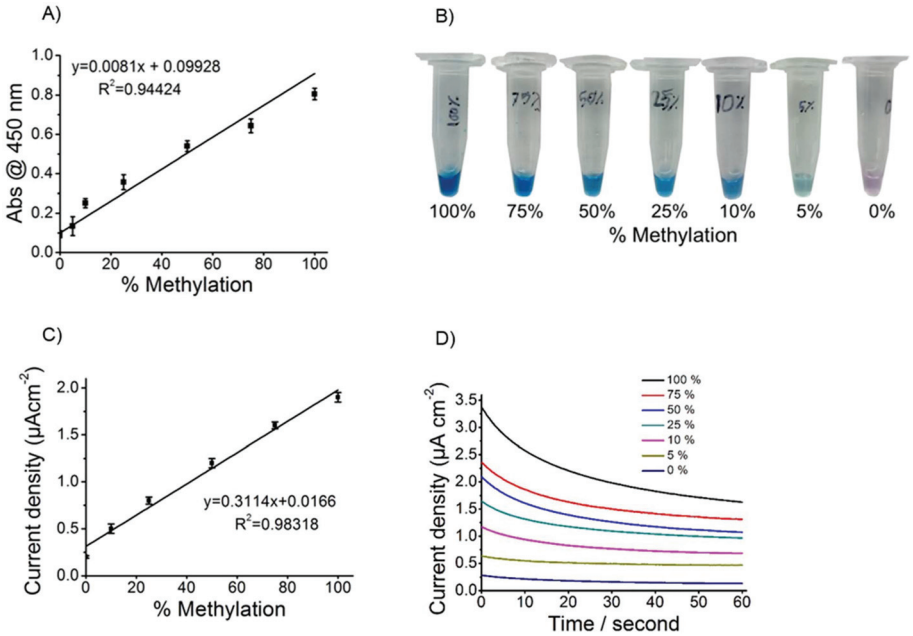


**Fig. 2** Calibration plots obtained for the mean values of (A) absorbance (UV-vis) and (C) chronoamperometric current density for the heterogeneous sample containing 0%, 5%, 10%, 25%, 50%, 75%, 90% and 100% methylation. (B) and (D) show the corresponding photos and chronoamperograms respectively. Each data point in (A) and (C) represents the average of three repeated trails, and error bars represent the standard deviation of measurements (%RSD = <5%, for $n$ = 3).

exist among the heterogeneous samples containing 5%, 10%, 25%, 50% and 75% methylated DNA. These data clearly show that the colorimetric assay is highly specific for quantifying global DNA methylation in heterogeneous samples.

To check electrochemical quantification, the chronoamperometric current density for the heterogeneous sample containing designated 0%, 5%, 10%, 25%, 50%, 75%, and 100% methylated levels was measured. As can be seen in Fig. 2D, significant differences in the current density were observed for all these samples. The linear regression equation was estimated to be $y$ (current density, μA cm$^{-2}$) = 0.3114 (% methylation) + 0.0166 with a correlation coefficient ($R^2$) of 0.98318 (Fig. 2C). Similar to colorimetric measurements (shown in Fig. 2A and B), a methylation change as low as 5% could be detected from 25 ng input DNA. These findings clearly showed that our approach is highly sensitive to detect global DNA methylation in a low amount of starting DNA. It is worth noting that our findings are comparable to the recent approaches.[23,38] In addition, our approach is highly comparable to different traditional methods such as HPLC (Kuo *et al.*, 1980)[39] and MS methods.[15] While these conventional methods consider all cytosines across the genome to quantify methylation, our approach only screens the methylated CpG sites for quantifying global methylation.

### Assay validation using a demethylating agent

To further validate the analytical performances of our assay, we applied our approach for analysing the status of global DNA methylation in human cancer cells before and after treatment with the demethylating drug, 5-Aza. For this, 5-Aza-treated and untreated Jurkat, highly methylated (M-WGA) and unmethylated (U-WGA) genomic DNA samples were used for the methylation analysis using naked-eye, UV-vis and chronoamperometric readouts (Fig. 3). In our assay, distinct colour intensity differences were observed between 5-Aza treated DNA and other control DNA samples (*i.e.*, M-WGA Jurkat and U-WGA samples) during the naked-eye observation (Fig. 3B). As expected, the relative Abs data obtained for the M-WGA and 100% methylated Jurkat DNA samples are significantly higher than that of 5-Aza-treated and U-WGA samples. The amperometric current density for the M-WGA and 100% methylated Jurkat DNA samples is also higher than that of 5-Aza-treated and U-WGA (2.35 and 1.90 μA cm$^{-2}$ *versus* 0.50 and 0.20 μA cm$^{-2}$ respectively) samples (Fig. 3C). These data clearly demonstrate that our assay could differentiate 5-Aza-treated and untreated Jurkat DNA samples and distinguish between M-WGA and U-WGA samples. These results are consistent with the previous findings,[40] suggesting the potential application of our method in tracking patient response to demethylating drug treatment.

### Cancer cell line sample analysis

To demonstrate our assay in a complex biological application, we have challenged our colorimetric and electrochemical methods for detecting genome-wide DNA methylation in the ESCC cell line (HKESC-4, KYSE-510 and HKESC-1) samples. To perform the analysis, genomic DNA extracted from cell lines was bisulfite treated and denatured to form ssDNA. As seen in Fig. 4A, Abs values obtained for the three ESCC cell lines and Jurkat DNA were significantly higher in comparison with

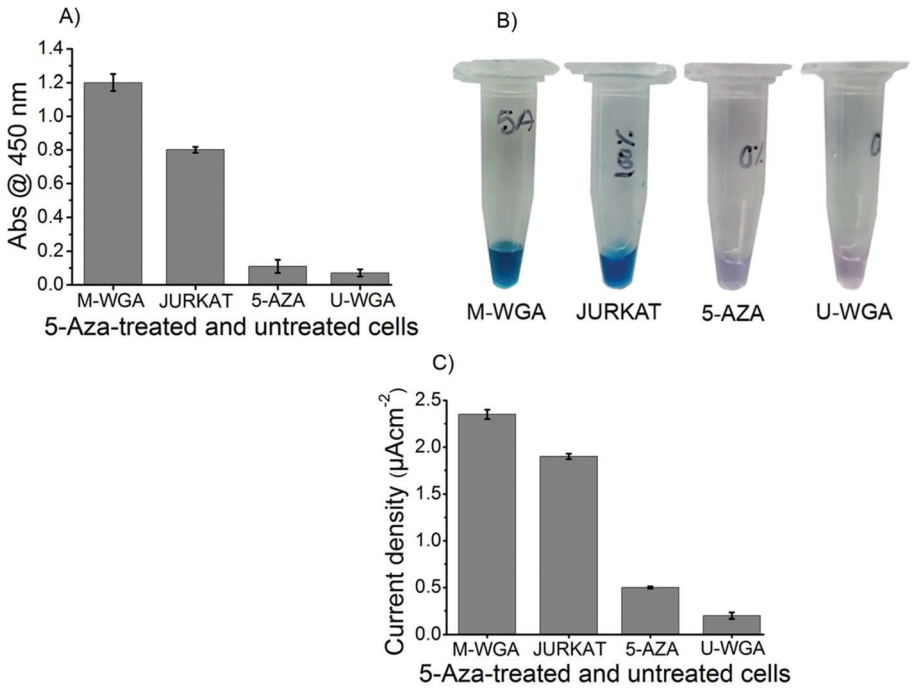


**Fig. 3** Mean values of (A) absorbance (UV-vis) and (C) chronoamperometric current density for the highly methylated genomic DNA (M-WGA), before and after 5-Aza drug-treated (*i.e.*, Jurkat and 5-Aza) and U-WGA samples. (B) Shows representative photos for the naked-eye detection. Each data point in (A) and (C) represents the average of three repeated trails, and error bars represent the standard deviation of measurements (%RSD = <5%, for $n$ = 3).

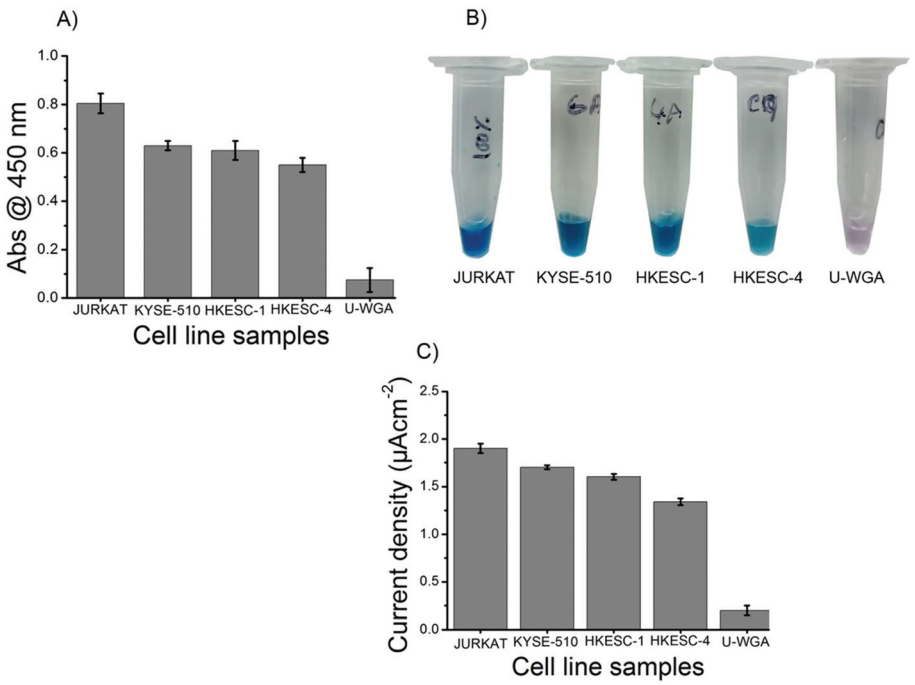


**Fig. 4** Mean values of (A) absorbance (UV-vis) and (C) chronoamperometric current density for the ESCC cell lines (KYSE-510, HKESC-1, HKESC-4), Jurkat and U-WGA samples. (B) Shows representative photos for the naked-eye detection. Each data point in (A) and (C) represents the average of three repeated trails, and error bars represent the standard deviation of measurements (%RSD = <5%, for $n$ = 3).

U-WGA samples indicating the presence of a different level of methylation in the cancer cell lines. As can be seen in the picture (Fig. 4B), these differences can also be easily distinguished by naked-eye examination. Furthermore, the chronoamperometric readout of these samples (Fig. 4C) also gives a similar trend of the methylation level where cell line samples showed a considerably higher current density compared to that of the negative control. Overall, these findings indicate that genomic DNAs from KYSE-510 and HKESC-1 cells contain a high level of methylation (*i.e.*, hypermethylation) as compared to that of the HKESC-1 (*i.e.*, partially methylated). These data demonstrated that our assay could act as an effective alternative method for detecting global DNA methylation in cell-derived samples.

### Clinical sample analysis

To further demonstrate the clinical application of our assay, we analysed the global DNA methylation levels in eight tissue samples from patients with metastatic ESCC. Two non-neoplastic mucosae were used as the controls. As seen in Fig. 5A, the naked-eye detection can easily distinguish the different levels of methylation present in the cancer samples when compared to the controls. By comparing the Abs level using UV-vis experiment, we can also easily estimate that cancer DNA samples obtained from P1, P3, P4, P6, P7 and P8 were highly methylated at the genomic scale, and P2 and P5 were partially methylated when compared to non-neoplastic control samples (Fig. 5B). We also tested these samples using the chronoamperometric approach and found that our data were in good agreement with those obtained from colorimetric studies (both naked-eye and Abs measurements). Current density data revealed that P1, P3, P4, P6, P7 and P8 were highly methylated at the genomic scale when compared to P2, P5 and non-neoplastic samples (Fig. 5C). Furthermore, the interassay variation was found to be less than 5% (%RSD = <5%, for $n$ = 3), indicating the good reproducibility of our assay. These data clearly indicate that the current density generated from our approach is able to quantify the global methylation level in tissue samples from patients with ESCC. In comparison with the MBD-based flow cytometry[41] or the oxygen channelling assay,[42] our assay has similar analytical performance in detecting global DNA methylation while the analysis time is relatively faster.

### Potential application of our assay

In comparison with the many existing approaches for quantifying global methylation, our assay offers several unique features which could underpin the possibility of providing relatively rapid diagnostic results in resource-poor settings. First, the assay is suitable for both colorimetric (naked eye) evaluation and electrochemical quantification where naked eye evaluation could be used as a first-pass screening of a large amount of samples (a method capable of giving a yes/no answer is particularly important when a large sample screening is necessary within a very short time) and the subsequent electrochemical readout can be used for quantifying the level of methylation present in each sample. Second, the assay is relatively rapid (it eliminates the asymmetric PCR step; the disposable nature of the SPE-Au also avoids a complicated cleaning procedure associated with conventional disk electrode-based sensors). Third, our assay is cost-effective due to the use of the highly inexpensive disposable SPE-Au (AUD $4/electrode). It is note-

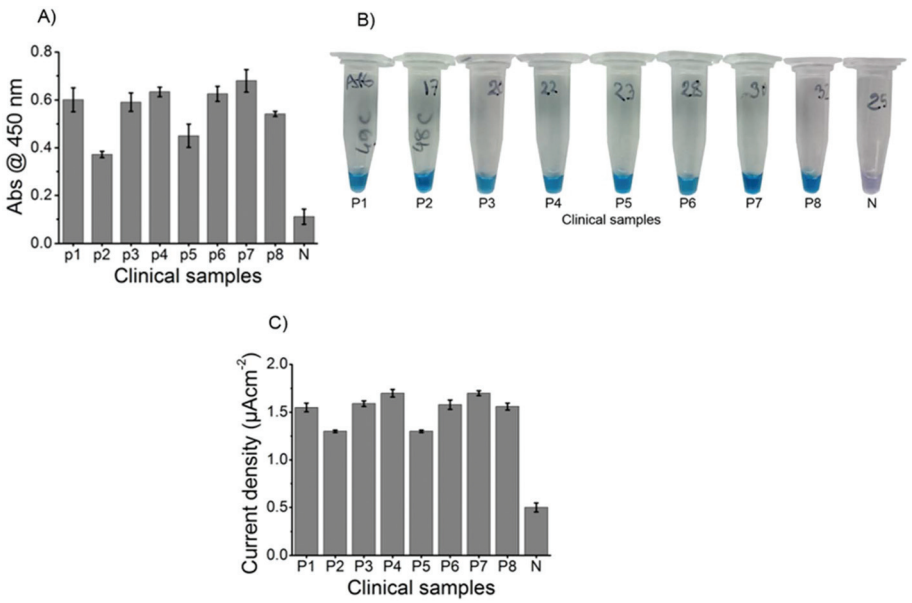


**Fig. 5** Mean values of (A) absorbance (UV-vis) and (C) chronoamperometric current density for the one normal (N) and eight (P1–P8) oesophageal cancer tissue samples. (B) Shows representative photos for the naked-eye detection. Each data point in (A) and (C) represents the average of three repeated trails, and error bars represent the standard deviation of measurements (%RSD = <5%, for $n$ = 3).

worthy that the assay significantly reduces the cost and time without affecting the sensitivity of the assay (it can quantify as low as 5% methylation differences from complex heterogeneous samples). Fourth, the approach has extensively simplified sensor design as it employs direct adsorption of the target ssDNA on an unmodified SPE-Au without the use of a capture probe based hybridization protocol. Taken together, these distinct features including the minimal equipment benefits of the colorimetric sensor along with the versatility and sensitivity of the electrochemical method offer a promising possibility towards the point-of-care screening of methylation in resource-limited settings.

## Conclusions

We have developed a relatively simple naked-eye colorimetric and electrochemical method based on the direct conjugation of denatured DNA (without PCR) and immunorecognition of the methylated cytosine on the SPE-Au. The amperometric detection was found to be more effective and sensitive in comparison with the colorimetric detection system. The assay was sensitive to as low as 5% differences in global DNA methylation with good reproducibility (% RSD = <5%, $n$ = 3) from 25 ng DNA in 90 min. We successfully applied the assay to quantify the global DNA methylation in a panel of ESCC cells and clinical samples collected from patients with ESCC. We have also demonstrated the potential application of our method in de-methylating drug therapy monitoring in clinical diagnostics and research. In addition, our assays are not limited to global DNA methylation. This method could be applied to develop a variety of assays by selecting the specific antibodies in the immune-recognition step for the detection of various DNA-biomarkers (*e.g.*, autoimmune diseases[43] and HPV 16 E6[44]). We anticipate that the combined use of colorimetry and electrochemical readouts could be used as a low-cost and functional detection method for the analysis of global DNA methylation in many diseases including cancer.

## Acknowledgements

This work was supported by the NHMRC CDF (APP1088966 to M. J. A. S.) and higher degree research scholarships (GUIPRS and GUPRS) to M. H. H., R. B. and M. N. I. from the Griffith University.

## Notes and references

1 K. D. Robertson, *Nat. Rev. Genet.*, 2005, **6**(8), 597–610.
2 S. Ledoux, J. Nalbantoglu and N. R. Cashman, *Brain Res. Mol. Brain Res.*, 1994, **24**, 1–4.
3 M. Ehrlich, M. A. Gama-Sosa, L. H. Huang, R. M. Midgett, K. C. Kuo, R. A. McCune and C. Gehrke, *Nucleic Acids Res.*, 1982, **10**(8), 2709–2721.
4 R. Lister, M. Pelizzola, R. H. Dowen, R. D. Hawkins, G. Hon, J. Tonti-Filippini, J. R. Nery, L. Lee, Z. Ye, Q. M. Ngo, L. Edsall, J. Antosiewicz-Bourget, R. Stewart, V. Ruotti, A. H. Millar, J. A. Thomson, B. Ren and J. R. Ecker, *Nature*, 2009, **462**(7271), 315–322.
5 A. Aggerholm, P. Guldberg, M. Hokland and P. Hokland, *Cancer Res.*, 1999, **59**(2), 436–441.
6 M. Ehrlich, *Oncogene*, 2002, **21**(35), 5400.
7 M. Kulis and M. Esteller, *Adv. Genet.*, 2010, **70**(10), 27–56.
8 S. B. Baylin, M. Esteller, M. R. Rountree, K. E. Bachman, K. Schuebel and J. G. Herman, *Hum. Mol. Genet.*, 2001, **10**(7), 687–692.
9 R. J. Klose and A. P. Bird, *Trends Biochem. Sci.*, 2006, **31**(2), 89–97.
10 T. D. Ahrens, M. Werner and S. Lassmann, *Cell Tissue Res.*, 2014, **356**(3), 643–655.
11 K. Ma, B. Cao and M. Guo, *Clin. Epigenet.*, 2016, **8**(1), 43.
12 X. Li, F. Zhou, C. Jiang, Y. Wang, F. Lu, N. Yang, N. Wang, H. Yang, Y. Zheng and J. Zhang, *PLoS One*, 2014, **9**(7), e103162.
13 S. Jain, T. K. Wojdacz and Y. H. Su, *Expert Rev. Mol. Diagn.*, 2013, **13**(3), 283–294.
14 K. C. Kuo, R. A. McCune, C. W. Gehrke, R. Midgett and M. Ehrlich, *Nucleic Acids Res.*, 1980, **8**(20), 4763–4776.
15 J. Singer, W. C. Schnute, J. E. Shively, C. W. Todd and A. D. Riggs, *Anal. Biochem.*, 1979, **94**(2), 297–301.
16 P. W. Laird, *Hum. Mol. Genet.*, 2005, **14**, R65–R76.
17 T. Hossain, G. Mahmudunnabi, M. K. Masud, M. N. Islam, L. Ooi, K. Konstantinov, M. S. A. Hossain, B. Martinac, G. Alici, N.-T. Nguyen and M. J. A. Shiddiky, *Biosens. Bioelectron.*, 2017, **94**, 63–73.
18 M. N. Islam, S. Yadav, M. H. Haque, A. Munaz, F. Islam, M. S. A. Hossain, V. Gopalan, A. K. Lam, N.-T. Nguyen and M. J. A. Shiddiky, *Biosens. Bioelectron.*, 2017, **92**, 668–678.
19 S. S. Nair, M. W. Coolen, C. Stirzaker, J. Z. Song, A. L. Statham, D. Strbenac, M. D. Robinson and S. J. Clark, *Epigenetics*, 2011, **6**(1), 34–44.
20 S. Pan, J. Xu, Y. Shu, F. Wang, W. Xia, Q. Ding, T. Xu, C. Zhao, M. Zhang, P. Huang and S. Lu, *Biosens. Bioelectron.*, 2010, **26**(2), 850–853.
21 H. Yin, B. Sun, Y. Zhou, M. Wang, Z. Xu, Z. Fu and S. Ai, *Biosens. Bioelectron.*, 2014, **51**, 103–108.
22 Y. Wang, E. J. Wee and M. Trau, *Chem. Commun.*, 2015, **51**(54), 10953–10956.
23 E. J. Wee, T. H. Ngo and M. Trau, *Clin. Epigenet.*, 2015, **7**, 65.
24 T. Kurinomaru and R. Kurita, *Anal. Methods*, 2017, **9**(10), 1537–1549.
25 M. Weber, J. J. Davies, D. Wittig, E. J. Oakeley, M. Haase and W. L. Lam, *Nat. Genet.*, 2005, **37**(8), 853–862.
26 R. Kurita, H. Yanagisawa, K. Yoshioka and O. Niwa, *Biosens. Bioelectron.*, 2015, **70**, 366–371.
27 R. Kurita and O. Niwa, *Anal. Chem.*, 2012, **84**(17), 7533–7538.
28 Y. Hu, K. Y. Lam, T. S. Wan, W. Fang, E. S. Ma, L. C. Chan and G. Srivastava, *Cancer Genet. Cytogenet.*., 2000, **118**, 112–120.

 

29 L. C. Cheung, J. C. Tang, P. Y. Lee, L. Hu, X. Y. Guan, W. K. Tang, G. Srivastava, J. Wong, J. M. Luk and S. Law, *Cancer Genet. Cytogenet.*, 2007, **178**, 17–25.
30 M. J. A. Shiddiky, A. A. Torriero, C. Zhao, I. Burgar, G. Kennedy and A. M. Bond, *J. Am. Chem. Soc.*, 2009, **131**(23), 7976–7989.
31 A. J. Bard and L. R. Faulkner, *Electrochemical Methods*, John Wiley & Sons, New York, 1980, pp. 199–206.
32 K. M. Koo, A. A. I. Sina, L. G. Carrascosa, M. J. A. Shiddiky and M. Trau, *Analyst*, 2014, **139**, 6178–6184.
33 A. A. Sina, L. G. Carrascosa, R. Palanisamy, S. Rauf, M. J. A. Shiddiky and M. Trau, *Anal. Chem.*, 2014b, **21**, 10179–10185.
34 R. Y. Zhang, D. W. Pang, Z. L. Zhang, J. W. Yan, J. L. Yao, Z. Q. Tian, B. W. Mao and S. G. Sun, *J. Phys. Chem. B*, 2002, **106**(43), 11233–11239.
35 K. M. Koo, L. G. Carrascosa, M. J. A. Shiddiky and M. Trau, *Anal. Chem.*, 2016a, **88**, 2000–2005; K. M. Koo, L. G. Carrascosa, M. J. A. Shiddiky and M. Trau, *Anal. Chem.*, 2016b, **88**, 6781–6788.
36 J. J. Hao, D. C. Lin, H. Q. Dinh, A. Mayakonda, Y. Y. Jiang, C. Chang, Y. Jiang, C. C. Lu, Z. Z. Shi, X. Xu, Y. Zhang, Y. Cai, J. W. Wang, Q. M. Zhan, W. Q. Wei, B. P. Berman, M. R. Wang and H. P. Koeffler, *Nat. Genet.*, 2016, **48**(12), 1500–1507.
37 T. Mikeska, I. L. Candiloro and A. Dobrovic, *Epigenomics*, 2010, **2**(4), 561–573.
38 Y. Wang, E. J. H. Wee and M. Trau, *Chem. Commun.*, 2016, **52**, 3560–3563.
39 K. C. Kuo, R. A. McCune, C. W. Gehrke, R. Midgett and M. Ehrlich, *Nucleic Acids Res.*, 1980, **8**(20), 4763–4776.
40 M. Bibikova, J. Le, B. Barnes, S. Saedinia-Melnyk, L. Zhou, R. Shen and K. L. Gunderson, *Epigenomics*, 2009, **1**(1), 177–200.
41 S. R. Corrie, P. Sova, Q. Feng, T. Blair, N. B. Kiviat and M. Trau, *Analyst*, 2011, **136**(4), 688–691.
42 E. J. Wee and M. Trau, *Chem. Commun.*, 2014, **50**(74), 10894–10896.
43 M. B. Uccellini, P. Busto, M. Debatis, A. Marshak-Rothstein and G. A. Viglianti, *Immunol. Lett.*, 2012, **143**(1), 85–91.
44 S. Ding, S. Y. Qian, Y. Zhang, W. Wu, G. Lu, Y. Lu, X. Feng, L. Li and P. Shen, *Sci. Rep.*, 2015, **5**, 13686.

Supporting Information (SI)

*for*

# Colorimetric and electrochemical quantification of global DNA methylation using methyl cytosine-specific antibody

Md. Hakimul Haque[+ab], Ripon Bhattacharjee[+b], Md. Nazmul Islam[b], Vinod Gopalan[a*], Nam-Trung Nguyen[b], Alfred K. Lam[a*], and Muhammad J. A. Shiddiky[b*]

## Optimization of the HRP-conjugated mC antibody concentration

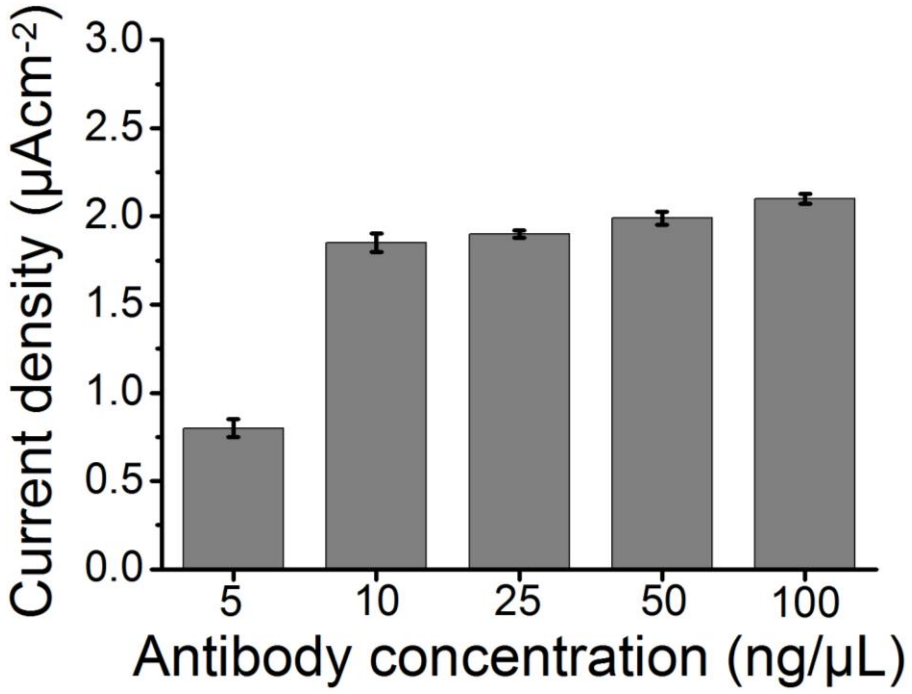


**Fig. S1.** Optimisation of antibody concentration. Mean values chronoamperometric current density for 25 ng Jurkat DNA using different the amount of HRP-conjugated mC antibody. Each data point represent the average of three repeat trails, and error bars represent the standard deviation of measurements (%RSD = <5%, for $n$ = 3).

**Nonspecific adsorption of the HRP-conjugated mC antibody onto the unmodified SPE-Au electrode**

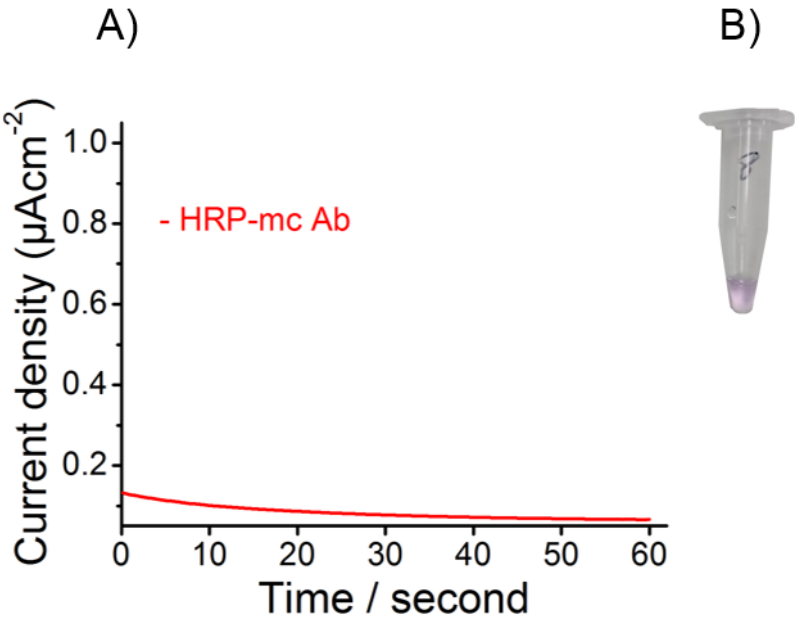


**Fig. S2.** (A) Chronoamperometric current response obtained for the unmodified SPE-Au electrode (without presence of the surface-confined bisulfite-treated and denatured ssDNA). SPCEfor the HRP-5mC antibody. (B) Shows representative photos for the naked-eye detection. This experiment clearly shows that the nonspecific adsorption of the HRP-conjugated mC antibody onto the SPE-Au electrode surface is negligible.

# Chapter 9

## Summary and Conclusions

# Chapter 9: Summary and Conclusions

Chromosomal copy number changes can guide to activation of oncogenes and inactivation of tumour suppressor genes in human cancers (Hanahan and Weinberg, 2000). In the previous study, *FAM134B* copy number alterations were found as a frequent incident in colorectal adenoma and adenocarcinoma. Our group have also observed the mRNA expression of *FAM134B* on a large number of tissue samples from patients with colorectal tumours. The results showed that mRNA was notably lower in colorectal cancer than in normal and benign tumour groups (Kasem and Lam, 2010). Colon cancer cell line demonstrated significantly lower levels of FAM134B mRNA expression compared to non cancer colonic epithelial cell line (Kasem et al., 2014b). They also found the high expression levels of *FAM134B* in colorectal adenoma implying that *FAM134B* play roles in the initial stages in tumour progression (Kasem et al., 2014c). On the other hand, the low expression levels of *FAM134B* in colorectal adenocarcinomas indicating that *FAM134B* acts as a tumour suppressor gene in colorectal adenocarcinoma (Kasem et al., 2014c). Studies on *FAM134B* gene have also reported its role in degenerative neurological diseases (Davidson et al., 2012; Kong et al., 2011; Kurth, 2010; Kurth et al., 2009). We have previously studied the roles of this gene by analysing the RNA expression in oesophageal cancer and presentation in a mouse model (Tang et al., 2007). Until now, this is the first study to investigate *FAM134B* copy number change in a large cohort of oesophageal squamous cell carcinoma. In this research, it has been observed that oesophageal squamous cell carcinomas have higher *FAM134B* copy number than non-neoplastic tissue. It implied that *FAM134B* copy number change is also a common event in ESCC.

The higher copy number of *FAM134B* in cancer compared to non-neoplastic tissue was found in this study. It indicates that it may play a vital role in the pathogenesis of ESCC, possibly performing with other oncogenic mutations. Gene amplification was one of the major genomic aberrations and a frequent mechanism for oncogene overexpression as well as for activating proto-oncogenes (Lam, 2000). It was believed that the amplified DNA might comprise some key genes whose expression provided a selective force for tumour development (Kitagawa et al., 1991). As cancer develops, amplification of *FAM134B* may occur simply as a side effect of other mutations associated with the progression. Consequently, regional amplification of 5p might cause extra copies of *FAM134B* in the tumour cells, and eventually, an

overexpression of *FAM134B*. *FAM134B* up-regulation might induce or contribute to tumour formation, a rapid growth of tumour cells, unscheduled cell proliferation and malignancy through an interaction of FAM134B and another candidate gene(s). It is likely that amplification of *FAM134B* offers a direct growth advantage to tumours and occurs as part of the overall progression of the disease. Hence, our present study showed that an amplification of *FAM134B* might be relevant to the pathogenesis and progression of ESCC. This study also revealed loss of *FAM134B* copies relative to control tissue which might associate with other genetic events, such as chromosome deletion and/or hypermethylation of the *FAM134B* promoter (Lehrbach et al., 2003).The percentage of *FAM134B* copy number gain and loss are more or less similar in this study implying that this gene might act as both oncogene and tumour suppressor in the progression of oesophageal squamous cell carcinoma. This research has also observed the correlations between *FAM134B* copy number alterations and the clinicopathological parameters of the ESCC patients including the sex, age, exact site, stage, TNM stage and status of tumours. Indeed, the DNA copy number of *FAM134B* in the cancer population was found to have no significant relationship with the age, size, grade, lymph node metastasis, survival status, histological subtypes or TNM staging of the oesophageal squamous cell carcinomas. In this study, *FAM134B* copy number gain was common in patients with stage II (24%) and stage III (64%) ESCC. Tang et al. also reported *FAM134B* overexpression was common in patients with stage II (5/9, 56%) and stage III ESCC (4/9, 44%) (Tang et al., 2007). This research also showed more amplification in lymph node metastasis which is almost similar to the findings of Tang et al (Tang et al., 2007). In contrast, FAM134B gene copy number changes were highly associated with pathological staging (TNM) of colorectal adenocarcinomas. More deletions in the *FAM134B* gene were noticed in higher T (tumour) and N (lymph node) stage. However, the same trend is also found in M stage (metastasis). This may indicate that *FAM134B* gene may have a vital role in preventing tumour growth and local spread to lymph nodes as chromosomal instability is an early event in colorectal carcinogenesis. So, *FAM134B* copy number alterations may be relevant to tumour invasiveness and metastasis in ESCC.

Till now, this is the first study to examine *FAM134B* expression in a large cohort of oesophagal squamous cell carcinoma. The current study shows that *FAM134B* is overexpressed in 49% of ESCC tissue samples while 47% (26/55) revealed downregulation of *FAM134B* when compared to matched non-neoplastic tissues which are almost similar to the findings of Tang et al (Tang et al., 2007).

Altered mRNA expression levels of *FAM134B* is consistent with previous reports on *FAM134B* DNA copy number changes suggesting its potential role in the progression of ESCC. For example, an overexpression of the nuclear factor cyclin D1 has been commonly showed in ESCC cell lines and tumour samples from ESCC (Doki et al., 1997) and it may provide growth advantage and enhance tumorigenesis in ESCC (Lam, 2000). Additionally, an overexpression of a signal transducer, ras, has been suggested to be related to a higher proliferative state of ESCC cancer cells when compared with their corresponding normal cells (Lam, 2000).

This is the first systematic study to investigate possible mutations in FAM134B gene in oesophageal squamous cell carcinoma. Previous studies by Kurth et al. illustrated that the human FAM134B protein contains 497 amino acids (Kurth et al., 2009). Bioinformatic analysis revealed that the N-terminal half of FAM134B has 2 unusually long hydrophobic segments of about 35 amino acids each that are separated by a hydrophilic loop of about 60 amino acids. This structure is similar to that of reticulon proteins that shape the curvature of endoplasmic reticulum membranes. FAM134B mutations are found over the entire coding sequence and are prone to loss-of-function mutations.Until now, the five homozygous mutations accounted such as three are nonsense mutations, one is a frameshift mutation, and one is a splice-site mutation (Kurth et al., 2009; Davidson et al., 2012; Murphy et al., 2012). Previously, Kurth et al. have depicted a homozygous mutation in the splice donor consensus site of intron 7 of the gene (Kurth et al., 2009). In this study, oesophageal squamous cell carcinoma with mutations detected on HRM using *FAM134B* gene primer which is located in Exon 7 of the gene. After HRM analysis of possible mutations, samples of ESCC cases in each group (wildtype, heterozygous mutations and homozygous mutation) were selected for Sanger sequencing. All the *FAM134B* mutations (N=4) were found in lymph node metastasis cases. Tang et al. reported that about 44% (4/9) and 56% (5/9) of the tissue specimens showed regional lymph node metastases (N1) and no regional lymph node metastases (N0), respectively. *FAM134B* overexpression may be occurred due to mutation of this site. Therefore, overexpression of *FAM134B* in ESCC tumour cells could be a potential prognostic marker for determining regional lymph node metastatic potential of tumours.

Although the other mutation detected on HRM is not an amino acid changing mutation, it is possible for a non-amino acid changing variation to affect gene expression by changing from a codon which has more tRNAs available to one where

there are fewer tRNAs, which could slow down the process of gene expression, thereby affecting tumour behaviour. Another possibility is that this mutation alters a miRNA binding site, which would influence tumour behaviour by altering the transcriptional and post-transcriptional regulation of gene expression. It is also possible that the presence of the HRM variations actually equates to the presence of another variant close by or it might be a sign of higher mutation rates in the gene. Such mutations may well be loss-of-function mutations and be the causative agents behind the associations seen with clinicopathological features and patient survival. Therefore further research should concentrate on functional impact of a *FAM134B* mutation in oesophageal squamous cell carcinoma to reveal out its more functional interaction site and post-translational modifications which will help in understanding of the complete depiction of the molecular and genetic basis of this in cell and cancer biology.

We have demonstrated a relatively simple and new electrochemical method for the detection of gene-specific mutations in PCR-amplified genomic DNA samples based on the different adsorption affinity of DNA nucleotides towards gold. The detection was achieved by the direct adsorption of two sequentially different PCR amplified mutated and unmutated DNA samples onto an unmodified gold electrode. Using this approach, we were able to detect mutations in 50 ng of target PCR-amplified product within 1.5h with high reproducibility (% RSD = <5.0) and specificity. We used the method to analyse a small panel of clinical samples from ESCC patients, and the results were validated with HRM curve analysis and sequencing. We anticipate that this method can potentially be applicable for point mutation detection in clinical diagnostics.

We have developed a simple and new method for the quantification of gene-associated DNA methylation using affinity interaction between DNA bases and graphene. The method is based on the different adsorption affinity of DNA nucleotides towards graphene-modified electrodes. The detection was achieved by the direct adsorption of two sequentially different DNA samples (bisulfite-treated and PCR amplified sequences representing methylated and unmethylated DNA) onto a graphene-modified electrode, which avoids multiple modifications and functionalization steps involved in conventional assays. Furthermore, it avoids the need for sequencing analysis. Most importantly, we have tested the feasibility of our assay to detect methylation target of *FAM134B* promoter gene in a panel of ESCC cell lines and clinical samples from ESCC patients. We anticipated that our assay might be able to detect global hypomethylation since the methylated and unmethylated DNA-base

changes of bisulfite treated genomes entail a large number of CpG sites, which might generate a marked adsorption difference between fully methylated and partially methylated samples. In addition, our assay could be viably useful in clinical diagnostics because of its potential for accurate detection of the epigenetic biomarker.

We have reported a simple and new method for the quantification of targeted *FAM134B* gene-associated DNA methylation *via* the different adsorption affinity interaction of DNA bases with gold. The detection was achieved by the direct adsorption of bisulfite-treated and PCR amplified sequences onto an SPE-Au. The adsorption of the DNA sequence representing methylated and unmethylated was then quantified *via* CC interrogation of the DNA-bound RuHex complexes. Our method offers several advantages over current methodologies. First, our assay does not involve any conventional recognition and transduction biosensing, time-consuming electrode surface modification and does not require any complex data analysis. Second, it avoids the need of using capture probe, hybridization, and surface treatment steps (and associated underlying chemistries). Third, it circumvents the need for the use of radioactive labels, methylation-sensitive restriction enzymes, antibodies, and sequencing analysis, which are most commonly used in existing methodologies (Gebhard et al., 2006; Wang et al., 2013; Ji et al., 2016; Sato et al., 2012). Fourth, our current assay can quantify DNA methylation by simply monitoring their direct adsorption using single-use disposable SPE-Au. Most importantly, our developed assay can successfully quantify *FAM134B* promoter methylation at a varying level in a panel of ESCC cell lines and clinical samples from ESCC patients. The analytical performance of our method has shown a good agreement with the data obtained using MS-HRM analysis and Sanger sequencing. We anticipate that the approach reported here could be potentially useful for the detection of an epigenetic biomarker in both clinical diagnostics and research.

Finally, We have developed a relatively simple naked-eye colorimetric and electrochemical methods based on direct conjugation of denatured DNA (without PCR) and immunorecognition of the methylated cytosine on SPE-Au. The detection was achieved by the catalytic reaction of HRP with TMB/$H_2O_2$ complex onto SPE-Au surface *via* chronoamperometry and colorimetry (naked-eye detection). In this study, amperometric analysis was found to be more effective and sensitive approach in comparison to the UV-vis detection system. We successfully applied the assay to quantify the global DNA methylation in a panel of ESCC cells and clinical samples

collected from patients with ESCC. The assay was sensitive to as low as 5% differences in global DNA methylation with good reproducibility (% RSD= <5%) from 25ng DNA input using 90 minutes. Also, the assay described here could be potentially useful in tracking of the global DNA methylation in de-methylating drug therapy monitoring in clinical diagnostics and research. In addition, our assays are not confined to global DNA methylation and a variety of assay can be developed by altering the specific antibodies in the immune-recognition step for detection of DNA-based biomarkers in clinical samples. We anticipate that the combined use of colorimetry and SPGE based electrochemical readout could be used as a model and low cost POC device for the analysis of global DNA methylation in chronic diseases.

In conclusion, this thesis has demonstrated the potential role of FAM134B in the oesophageal squamouse cell carcinoma *via* exhibiting its altered copy number and expression at mRNA and protein level. Based upon copy number study, we can conclude thst this gene might act as both oncogene and tumor suppressor in the progression of ESCC. This research identified some novel mutations in tissue samples of patients with ESCC. The altered expression patterns and copy number changes of *FAM134B* in ESCCs which might be regulated by these mutation changes in *FAM134B*. In this study, we observed a strong association of FAM134B mutations with metastatic lymph node tissues in ESCC indicating its use as a potential predictor for metastasis in ESCCs. Also, the mutation detection *via* electrochemical methods was successful distinguishing single point mutation in DNA from oesophageal cancer implying its potential application in point mutation detection in clinical diagnostics. This study also developed a simple and new method for the quantification of gene-associated DNA methylation using affinity interaction between DNA bases and graphene. We anticipated that our assay might be able to detect global hypomethylation. In addition, we have reported a simple and new method for the quantification of targeted *FAM134B* gene-associated DNA methylation *via* the different adsorption affinity interaction of DNA bases with gold. Our developed assay can successfully quantify *FAM134B* promoter methylation at varying level in a panel of ESCC cell lines and clinical samples from ESCC patients. Finally, we developed a new method for quantifying global DNA methylation in an integrated approach consisting of both colorimetric and electrochemical methods. We anticipated that our approach could be potentially useful as low-cost alternative for the detection of epigenetic biomarker in both clinical diagnostics and research.

# References

Davidson G, Murphy S, Polke J, Laura M, Salih M, Muntoni F, Blake J, Brandner S, Davies N, Horvath R, Price S, Donaghy M, Roberts M, Foulds N, Ramdharry G, Soler D, Lunn M, Manji H, Davis M, Houlden H, Reilly M. Frequency of mutations in the genes associated with hereditary sensory and autonomic neuropathy in a UK cohort. J Neurol. 2012 ;259:1673-1685.

Doki T, Imoto M, Han EKH, Sgambato A and Weinstein IB. Increased expression of the p27KIP1 protein in human esophageal cancer cell lines that over-express cyclin D1. Carcinogenesis. 1997;18:1139-48.

Gebhard C, Schwarzfischer L, Pham TH, Andreesen R, Mackensen A, Rehli M. Rapid and sensitive detection of CpG-methylation using methyl-binding (MB)-PCR. Nucleic Acids Res. 2006 Jul 5;34(11):e82.

Hanahan D, Weinberg RA. The hallmarks of cancer. Cell. 2000;100:57-70.

Ji J, Liu Y, Wei W, Zhang Y, Liu S. Quantitation of DNA methyltransferase activity via chronocoulometry in combination with rolling chain amplification. Biosens Bioelectron. 2016;85:25-31.

Kasem K, Gopalan V, Salajegheh A, Lu CT, Smith RA, Lam AK. The roles of JK-1 (FAM134B) expressions in colorectal cancer. Exp Cell Res. 2014b;326:166-173.

Kasem K, Lam A. Analysis of a novel JK-1 gene expression in benign and malignant colorectal tumors. Virchows Arch. 2010;457:165.

Kasem K, Sullivan E, Gopalan V, Salajegheh A, Smith RA, Lam AK. JK1 (FAM134B) represses cell migration in colon cancer: a functional study of a novel gene. Exp Mol Pathol. 2014c;97:99-104.

Kitagawa Y, Ueda M, Ando N, Shinozawa Y, Shimizu N and Abe O. Significance of int-2/hst-1 coamplification as a prognostic factor in patients with esophageal squamous carcinoma. Cancer Res. 1991;51:1504-08.

Kong M, Kim Y, Lee C. A strong synergistic epistasis between FAM134B and TNFRSF19 on the susceptibility to vascular dementia. Psychiatr Genet. 2011;21:37-41.

Kurth I, Pamminger T, Hennings JC, Soehendra D, Huebner AK, Rotthier A, Baets J, Senderek J, Topaloglu H, Farrell SA, Nürnberg G, Nürnberg P, De Jonghe P, Gal A, Kaether C, Timmerman V, Hübner CA. Mutations in FAM134B, encoding a newly identified Golgi protein, cause severe sensory and autonomic neuropathy. Nat Genet. 2009;41:1179-81.

Kurth I. Hereditary Sensory and Autonomic Neuropathy Type II. 2010 [updated 2015 Feb 19]. In: Pagon RA, Adam MP, Ardinger HH, Wallace SE, Amemiya A,Bean LJH, Bird TD, Dolan CR, Fong CT, Smith RJH, Stephens K, editors.GeneReviews® [Internet].

Lam AK. Molecular biology of esophageal squamous cell carcinoma. Crit Rev Oncol Hematol. 2000;33:71-90.

Lehrbach DM, Nita ME, Cecconello I. Molecular aspects of esophageal squamous cell carcinoma carcinogenesis. Arq Gastroenterol. 2003;40:256-61.

Murphy SM, Davidson GL, Brandner S, Houlden H, Reilly MM. Mutation in FAM134B causing severe hereditary sensory neuropathy. J Neurol Neurosurg Psychiatry. 2012;83:119-20.

Sato S, Tsueda M, Kanezaki Y, Takenaka S. Detection of an aberrant methylation of CDH4 gene in PCR product by ferrocenylnaphthalene diimide-based electrochemical hybridization assay. Anal Chim Acta. 2012 ;715:42-48.

Tang WK, Chui CH, Fatima S, Kok SH, Pak KC, Ou TM, Hui KS, Wong MM, Wong J, Law S, Tsao SW, Lam KY, Beh PS, Srivastava G, Chan AS, Ho KP, Tang JC. Oncogenic properties of a novel gene JK-1 located in chromosome 5p and its overexpression in human esophageal squamous cell carcinoma. Int J Mol Med. 2007;19:915-23.

Wang GL, Zhou LY, Luo HQ, Li NB. Electrochemical strategy for sensing DNA methylation and DNA methyltransferase activity. Anal Chim Acta. 2013;768:76-81.

# Appendix

## DNA extraction and purification protocol

Fresh frozen tissue samples were sectioned into 10µm slices for DNA and RNA extraction. The DNA extraction and purification protocol are described below:

1. The tissue samples were disrupt and homogenise using pipette, then suspended in lysis buffer to disrupt and release the nucleic acids and proteins into the solution.
2. Then, a digestion step was performed to remove the protein and RNA in the solution using proteinase and RNase enzymes, respectively.
3. The digested proteins and RNA were removed by centrifuging the solution in a spin column.
4. Washing buffer was then added to the spin coloumn and centrifuge for 30 second at 12000 rpm.
5. Another washing buffer was poured on the spin coloumn and again centrifuge for 30 second at 12000 rpm.
6. Then the purified DNA was eluted from the column in 100 µL of elution buffer.
7. DNA quantification was performed using Nanodrop Spectrophotometer (BioLab, Ipswich, MA, USA) and purity was checked using 260/280 ratio.

## RNA extraction and purification protocol

1. Using a pipette, the tissue samples were disrupt and homogenise in the lysis buffer. To homogenise, the pipette was repetitively suck up and released the RNA/DNA and protein in to the solutions.
2. The lysate was centrifuged at maximum speed. Thye supernatant was carefully removed and transfer by pipetting into the another spin column placed in a two ml collection tube.
3. Then another centrifugal step was performed centrifuge for 30s at >10000 rpm aand collect the flow throw.
4. About 600 ul of 100% ethanol was added to the flow-through and Mix well by pipetting.
5. Then, Different washing steps was done and finaazaly eluted the RNA with elution or RNAase/DNAse free water.
6. RNA quantification was done using nanodrop Spectrophotometer. For checking the purity, 260/280 ratio was used.